POLITECNICO DI MILANO
PhD Program in Bioengineering

Technologies and methods for treatment geometry optimization in radiation therapy with accelerated particles

Tutor: Prof. Antonio PEDOTTI
Supervisor: Prof. Guido BARONI
Coordinator: Prof. Maria Gabriella SIGNORINI

PhD Thesis by:
Andrea PELLA
738496
XXIV cycle

Academic years 2009/2011

Acknowledgments

I am sincerely thankful to my supervisor, Professor Guido Baroni, whose guidance enabled me to reach this result.
I also would like to thank Doctor Marco Riboldi for his support during the PhD program.
My personal regards to all of those that collaborated with me during the completion of this work, particularly: Doctor Raffaella Cambria, Eng. Barbara Tagaste, Doctor Ahmad Esmaili Torshabi, Eng. Matteo Seregni, Eng. Giovanni Fattori.

Index

Summary

Among possible strategies for tumor control, benefits of radiation therapy (RT) are recognized and proved. In conventional RT patients are treated with high energy X-ray (photons). Reasons to use RT can be both curative or palliative, or it can be used as concomitant treatment or consequent to other interventions, like surgery or chemotherapy. Theoretically, supposing an high setup control in delivering radiations, the majority of the tumors could be at least controlled with RT.

Beside photon RT, the number of facilities able to offer a treatment with accelerated particles is nowadays worldwide increasing. Studies on accelerated particles for RT started in 50's in United States. Only in 70's first treatments were performed. Nowadays around 70.000 patients have received this kind of treatment. This number is designated to increase because of the availability of new facilities, because of technological improvement in dose delivery techniques, and of setup control procedures. There are several differences between RT with photons and accelerated particles. These differences are both in the technology for beams production and in the modality of interaction with the biological matter, which also affect the biological effects. The attenuation of dose distribution in case of RT with photons is exponentially decreasing in the irradiated body. This means that the higher amount of energy is released in proximal areas, whereas in depth the dose profile is attenuated. Particles, on the contrary, release relatively low energy in proximal areas (when their energy is high) and the maximum of the energy is released in a precise depth. This behavior, typical of particles, is

called Bragg peak. The depth of the Bragg peak depends by different factors: density of the body, presence of oxygen, energy and velocity of particles.
Thanks to the physical properties of particles, their use in RT results indicated to treat deep tumors. Bragg peak allows to release the higher energy ideally in a point, saving entrance pathways and tissues around this area. More than one Bragg peak can be combined to obtain profiles of uniform dose distribution in the treatment volume. There are mainly two different methods to obtain the so called Spread Bragg peaks (SOBP): the first one is passive (that is, one energy spill, use of range shifters to compensate the depth) and the second one is active (that is, sum of different spills by tuning accelerator parameters).
Reasons that justify the use of particles in RT, and a comparison between hadrons and photons, are described in the thesis. Even if this different behavior in dose distribution can be intended as a potential advantage, since the therapeutic dose is concentrated in the tumor mass saving healthy tissues, there are different reasons why RT with accelerated particles is proved to be a valuable treatment technique. If compared with photons, particles are affected by a lower lateral scattering effects. Moreover, particles have an higher radiobiological effectiveness (RBE). RBE is an index defined as the effectiveness of absorbed doses of radiation delivered by different types of radiation. It increases the more the particles density increases (defined by the linear energy transfer, LET). LET depends by several factors such as charge and particles velocity. The increased efficiency can be evidenced in the effects of particles on cells and tissues, where the number of cell killed in tumor mass is maximum. Photons and particles differs also in how they react in presence of oxygen: X-ray are affected by an higher sensitivity in presence of oxygen. On the contrary, in RT with particles in hypoxic conditions an increment of RBE effects can be noticed. Moreover, in vitro studies have proved X-rays to have stimulating effects in angiogenesis. Possible secondary issues like metastasis are not negligible in this case.
The most common particles used in RT are protons and carbon ions. The vantage of protons is that their mass allows the use of relatively small accelerators. Carbon ions beam is characterized by an RBE index of 1 at the entrance of the field and 3-4 in correspondence of Bragg peak. Nevertheless, readers should be awarded that other ion species have been tested and are now under investigation. Indeed, due to their interesting and advantageous RBE, carbon ions are currently recognized as the best compromise in clinical activity.
Since particles have mass and charge, magnets can be used to focus and steer the beam line. It is possible to focalize the beam in spots of millimetric diameter. Moreover, the beam can be deflected using scanning magnets, placed before the gantries.
This potentialities, combined with the Bragg peak behavior, give enormous potentialities in geometrical selectivity of dose delivery systems. These aspects are even more relevant, if we consider tumors difficult to reach, or because of the presence of organs at risk in the neighborhood or because their deep position in the body.
RT with particles is a relatively new technique, and research is active in different fields. Studies are conducted on the effects of different ion species on tissues and cells. Delivery systems are also investigated. Technology improvements are critical. Smaller and more compact accelerators could surely have a positive influence on cost - effectiveness ratio, leading to the diffusion of new facilities able to perform this treatment. Dose delivery techniques can open new frontiers in organ motion management during irradiation. The idea to perform tumor tracking on line, in case of not negligible organ motion effects incrementing therapeutic effects, is challenging but stimulating. How to save healthy tissues surrounding the tumor mass remains an open issue, and tools and software aimed at estimating the current tumor position could play an important role.
Cost - effectiveness ratio in RT with particles has been debated deeply in scientific community. Even if studies in Japan and Germany has demonstrates that RT with particles is indicated as

the best solution for different types of tumor (radio-resistant tumors, pediatric tumors just as examples), money required for facilities building and maintenance are huge (around hundred million of Euros). This aspect is indeed one of the main reasons why only few centers nowadays can offer this type of treatment. Indeed, if the use of protons requires a cyclotron, carbon ions requires much more complex and expensive synchrotrons. Differences between these machines are significant. A cyclotron is a moderately compact device able to accelerate charged particles using potential difference of alternating voltage. A perpendicular magnetic field drives the particles many times in the accelerating potentials until they are spilled out the cyclotron. A synchrotron is an accelerator that is mainly composed by 3 parts: sources and linear accelerator, a circular accelerator (synchrotron), an exit line. Ions are generated from plasma of radioactive sources and pulled into the linear accelerator, that provides the first ramp of energy. Then, particles are injected in the synchrotron, that pushes particles to the desired energy. Beam is extracted in the exit line, and sent to the treatment rooms. Synchrotrons are bigger than cyclotron and more expensive, but they can accelerate a great number of ions, and the number of energies available increases. One of the advantages in the case of synchrotron facilities is that it is possible to accelerate both protons and ions, while it is impossible to accelerate ions using a cyclotron.
High technology is rapidly improving also in systems devoted to patient positioning and setup control before and during the irradiation. These systems must guarantee an adequate accuracy in repositioning. Recent researches claim that 33 centers are nowadays running and treating patients with protons and 5 with protons and carbon ions. In Europe, only two centers are now treating patients using a synchrotron. The first one is in Germany (HIT, Heidelberg). The second one is in Italy, Pavia. The National Center for Oncological Hadrontherapy (Centro Nazionale di Adroterapia Oncologica, CNAO) started to treat patients on September 22nd 2011.

Section I

CNAO will be the first Center in Italy able to offer a treatment with protons and carbon ions. It was ideated as a center for clinical activity and research. CNAO is a no profit organization (Foundation) created with the financial law 2001, and designed by TERA Foundation.
At the end of 2003 CNAO Foundation acquired the project and hired the design group. Today CNAO Foundation has ended the commissioning of the high technology and first treatments have been started. CNAO has identified seven groups of diseases that are considered at high priority: lung tumors, liver tumors, sarcomas, head and neck tumors, eye tumors, central nervous system lesions and pediatric tumors. Even if the first trials will be performed with protons, at steady state CNAO will devote 80% of the time to ions and the remaining 20% to protons. The Center will play an important role both in National territory and in International scenario. Actually, projects and collaborations are active with several Institutions and facilities.
CNAO is proprietary of a custom designed synchrotron. The synchrotron, 24 meters diameter, was dimensioned to best reach energies for clinical activities. It is able to accelerate proton and carbon ions to a maximum energy of 400MeV/u (corresponding to 27 cm penetration depth in water).
Regarding dose delivery techniques, CNAO employs an active spot-scanning system. Two orthogonal magnetic fields are used to scan the beam in planes parallel to its direction. Magnets are designed to allow scanning of square slices of 20 x 20 cm. Depth is varied directly by adjusting the beam energy. The smallest step of penetration range achievable is 0.2 mm. The synchrotron allows variation of the energy at each spill, meaning that every second it is possible to irradiate a layer at a different depth. Scanning magnets, sensors to measure position and intensity of the beam, and control systems are incorporated in the nozzle.
The Center is equipped with three treatment rooms. Two of them have an horizontal fixed beam, while one of them has two fixed lines, one horizontal and one vertical.

The workflow and logistic were designed to optimize efficiency. Each of the treatment rooms has a dedicated preparatory room where the patient is immobilized on a dedicated transport system. There are two different tools available for patient positioning and immobilization: a carbon couch and a chair. Their use depend by the district of interest. Head and neck cases will be mainly irradiated with the chair, while extra-cranial districts with the carbon couch.
The use of image guidance systems is surely a promising option for setup check and control. Obviously, all the systems used in conventional RT have to be optimized for particle therapy case. The Politecnico di Milano collaborates with CNAO in developing all the patient setup procedures. The Institution has participated as consultant and supervisor in selection, control and installation and it was responsible for the commissioning of these systems. Moreover, it was required to provide technical tutorials to CNAO personnel about the use of these high technology systems.
As previously introduced, procedures were designed to match state of the art technologies for accurate, automatic patient management. Multiple technological solutions were evaluated in a first stage, taking into account setup accuracy and patient throughput optimization as specific goals. The selected solutions are widely described and treated in the thesis.
As a modern center for RT, CNAO can count on at least three subsystems dedicated to patient positioning and set up control: an in-room imaging system (patient verification system, PVS), an optical tracking device for real time patient monitoring (optical tracking system, OTS) and an high precision robotic arm for patient positioning (patient positioning system, PPS). A detailed description of solutions adopted in CNAO is reported in the text. Briefly, the PVS installed is a stereoscopic X-ray imaging device suspended from the ceiling, that can rotate around the vertical axis according to the treatment table position. Both X-ray tubes and flat panels are deployed only during imaging, when the tubes pivot whereas the flat panels slide into position. PVS is installed in room 1 and room 3. No PVS is installed in room 2 (the one with two beam lines) because of the presence of the vertical nozzle. A different design has to be taken into account, and feasibility studies are going on. The PPS is a 6DOF robotic pantograph featuring a mechanical accuracy below ±0.3 mm and ±0.1°. The OTS is a three cameras system able to localize passive markers and laser spots within 0.5 mm in a 3x2x2 m volume.
After systems installation, an external company performed a set of measurements in all the treatment rooms, in order to check the accuracy claimed in the contract between the vendor and the Center. CNAO required a more comprehensive set of measurements, aimed at evaluating the accuracy and reproducibility of the systems during movements. Politecnico di Milano and CNAO personnel carried out a protocol aimed at testing those specifications. As mentioned, PPS is required to have a positioning accuracy within 0.3 mm. Different set up conditions were considered. In a first trial, aimed at testing the accuracy of the pantograph, we glued different sockets on the surface of the carbon couch and the treatment chair. In a second trial an additional weight was added on the transport systems. We operated in this way to test two different situations: we wanted to simulate the presence of a patience; we wanted to test the correctness of compensation adopted by the PPS.
A Leica laser tracker featuring 0.1 mm\m accuracy was used to track these control points.
A reference position was set to the PPS controller and recorded by means of the laser tracker. The only requirements in this operation was to match one of the control points in the nominal room isocenter. Then, different operators moved the PPS, imposing different sets of rotations and translations. All the markers were again recorded by means of the laser tracker. Off line data were exported in Matlab (The MathWorks, Inc), and roto-translations were applied to the reference position, according to what was performed in the bunkers. Two sets of marker coordinates were available at this point: a first one concerning a nominal, calculated position. The second one concerning a measured position, as seen by the laser tracker in treatment

rooms. Differences between these two sets were evaluated and statistical analysis was performed.
Even if a great number of acquisitions were recorded during the installation and the fine tuning of the systems, only those measurements related to the last version of the software and hardware are considered in the thesis.
During acceptance tests, we acquired in each room 20 random positions with carbon couch and 20 positions with treatment chair. For each treatment tool 10 positions were recorded without an additional weight and 10 measurements with an additional weight.
The first set of results presented in the thesis regards the isocentricity in random rotations. The importance of an high accuracy in isocentric rotations is critical because that one is the point where the therapeutic dose is focused. An high geometric accuracy allows to follow medical indications and save normal tissues around the tumor mass. Results obtained both in dynamic and static measurements proved that is possible to reach an accuracy within specification during isocentric rotations. This measurements were intended as preliminary if compared to tests of combined rotations and translations.
3D errors measured by Politecnico and CNAO personnel after measurement campaigns in room 1,2 and 3 are shown in the thesis. Excluding few out of nominal, we obtained results below the threshold in all the considered conditions. Mean 3D errors (and maximum values) for couch without load were: 0.16 [mm] (0.33 [mm]); 0.20 [mm] (0.35 [mm]); 0.12 [mm] (0.24 [mm]) for room1, 2, 3, respectively. With an additional load they were: 0.17 [mm] (0.27 [mm]); 0.16 [mm] (0.44 [mm]); 0.09 [mm] (0.24 [mm]) for room1, 2, 3, respectively. Mean 3D errors (and maximum values) for chair without load were: 0.24 [mm] (0.49 [mm]); 0.15 [mm] (0.32 [mm]); 0.13 [mm] (0.47 [mm]) for room1, 2, 3, respectively. With an additional load we observed: 0.32 [mm] (1.29 [mm]); 0.19 [mm] (0.50 [mm]); 0.17 [mm] (0.39 [mm]) for room1, 2, 3, respectively.
To evaluate and quantify PPS performance in terms of accuracy in all the rooms, a statistical comparison was necessary. Even if we recorded values below critical threshold in all the rooms, we observed a better performance of the carbon couch in room3, and of treatment chair in room1.
The analysis of PPS accuracy and of its integration with other in room systems was completed with a benchmark with the OTS. To evaluate the consistency of these two different systems, we prepared a protocol where a head phantom fitted with 4 passive markers was placed on the PPS. The PPS was then moved in 6DOF within a ±5 mm and ±3° range from isocenter and the final position was measured with the OTS. Results shown in the thesis demonstrate that is possible to reach sub-millimetric accuracy in repositioning with an adequate integration between different systems.
Also PVS accuracy in rotation and linear displacements of tubes and flat panels was considered in acceptance protocols. In principle, the setup chosen was the same used for PPS testing. Several sockets were applied to the moving parts of the cylinder and registered by a Leica laser tracker (0.01 mm\m accuracy). Two sets of acquisitions were performed: the first one was intended to quantify the errors in PVS rotations, the second one to quantify the errors in repositioning of flat panels and X-ray tubes during their deployment (linear repetitions). All the measurements were found to be below threshold. Moreover, a last quality assurance test was performed. We firstly aligned a radio-opaque object at the isocenter. This tool is usually utilized by medical physicists for laser cross calibration verification. Then, we acquired Xray images with the PVS. Imaging software (Verisuite, Medcom) allows to display on screen the center of the flat panels, that correspond to the projection of the isocenter supposing tubes correctly calibrated. We evaluated the distance of this point from the top of the custom tool, to verify the consistency between different tools.

Last, to investigate the compliance of the systems with patient's safety, here intended as speed of the PPS, acceleration of the PPS and breaking distance after pressing the emergency buttons, tables and graphs are reported in appendixes of the thesis.

Section II

As introduced in the previous section, CNAO uses beam scanning, a methodology applied in the majority of the centers. This technique allows to better conform the dose distribution, planning energy spills and operating on scanning magnets. If compared with beam scattering systems, the main advantage is that it is possible to plan the best dose distribution for each patient, without the use of collimators or wedges for geometry compensations. A major issue is represented by the need of high precision in setup control and dose delivery systems. This difficulty depends mainly by geometrical inaccuracies in target definition during setup procedures. Generally, safety margins are added to the nominal target volume, in order to minimize errors. Moreover, as described before, particles therapy implicitly requires the support of accurate methods for image guidance. We can argue that potential errors and inaccuracies are relatively less relevant in static tumors than in tumors affected by organ motion. In fact, the last check before irradiation is based on X-ray projections, and then on bone anatomy. Bone anatomy represents for static tumors a valuable reference for medical doctors and physicists evaluations. Possible causes of misalignments can be introduced by different aspects, like shrinkage effects of the tumor mass, but again they can be evaluated by medical doctors with diagnostic analysis during the treatment. The scenario is more challenging when tumor mass is affected by not negligible effects of organ motion (OM). OM can seriously affect the outcome of the treatment and it can be difficult to manage. An example of this effect is represented by lung cancer case. In lung cancer treatments, normal physiological breathing induces in tissues (and consequently in the tumor mass) not negligible displacements. In RT with particles, errors in target identification result in over or under dosage in planned structures. Consequently, we have to deal with two potential disadvantages: operators can release no therapeutic dose in healthy tissues but also a no uniform dose distribution inside the lesion. These issues in lung tumor treatments are evident. Actually, even if adequate safety margins can minimize uncertainties caused by small movements (dealing with an unwanted inclusion of healthy tissue in the treatment volume), with larger movements appropriate irradiation strategies have to be taken into account. In lung treatments different approaches have been debated. The use of anesthesia is, in principle, a possible solution to stabilize the physiological movements. Nobody uses this technique because it results invasively, and also because a complete treatment session last usually weeks. A first realistic solution is to ask the patient to hold the breathing (or force an interruption in breathing with mechanical respirators) during deep inspiration. In this way the physiological movement is somehow freezed, allowing to irradiate in a steady setup. However, variations in pulmonary compression and tension of muscles can affect stability and reproducibility. A diffuse technique is the so called gating. The patient is asked to breath normally. During the maximal expiration phases the patient is irradiated. During the other phases the irradiation is interrupted. Maximal expiration is considered as the most stable condition during breathing. It is obvious that this method requires the operators to monitor the breathing phase both during planning (a 4D CT is required) and during treatment sessions. In order to perform gating, different dedicated tools are available. These tools are usually placed on the abdomen of the patient, providing an information of the current breathing phase. One of the disadvantages in gating is that treatment time increases. Long sessions do not represent just an issue of optimization of machine duty cycle, they can also results in unwanted effects like not negligible baseline shifts in respiratory patterns. Main reasons are related to patient's body adjustment in immobilization tools or a general relax of muscles.

Another solution to manage OM in the case of lung cancer is to compensate its effect operating on the beam line during all the respiratory phases: that is the tumor tracking. In this case the direction of the beam, always active, is corrected phase by phase to mitigate the OM effect. This is an interesting approach (less beam and delivery time, high efficiency) but extremely challenging (it requires an estimation of a correction vector to follow the tumor mass, processing external signals characteristic of the surface of the patient). If we consider particle therapy, this solution does not present issues in latency of beam steering. Steering magnet system is faster than respiratory movements. This is not the case of RT with photons, where the corrections have to be imposed directly to the accelerator.
Nowadays, only Cyberknife® Synchrony® performs tumor tracking. Cyberknife® is a commercial device for RT treatments with photons. The system is composed by a couch, two Xray tubes (and related flat panels), an optical tracking system and a linear accelerator mounted on a robotic arm featuring 6 DoF. Once the patient is prepared and immobilized on the treatment couch, X-ray double projections are acquired, to identify metallic clips surgically placed nearby the tumor mass. In the meantime, the optical tracking system records the traces of three external surrogates placed on patient's body. These couples of external – internal coordinates are used to build a correlation model. Then, the treatment can start. The predictive model is used to provide a feedback to the robotic arm and to adjust consequently the position of the accelerator. During treatment, at predefined intervals, new X-ray images are acquired to check and update the correlation model. The system takes into account a delay dues to mechanical inertia of the robotic arm (around 200 ms).
Even considering the possible limitations, the use of models able to estimate the position of a lesion, processing data from external surrogates represents a promising goal also in RT with particles. They could play an important role both during treatment planning (in order to make it more robust) and during treatment, where the use of active beam scanning allows tumor tracking in a faster way, and potentially with much more advantages, than with photons.

Section III
Among possible strategies for respiratory motion mitigation, the correlation of tumor motion trajectory observed in 4D imaging with optically detected surface surrogates represent a promising approach for real-time target position estimation.
This section describes experimental activities on correlation models. It is subdivided as follow:

a. Materials and methods: state model , artificial neural networks and fuzzy logic.
b. Results of a benchmark study of alternative models vs. Cyberknife® Synchrony®.
c. Improvements in predictors and results of new approach in performances vs. Cyberknife® Synchrony®.
d. Design of a breathing phantom for model validation.
e. Use of artificial neural networks in real time (phantom study)
f. Integration of models and hardware for active beam scanning (tumor tracking). GSI experimental session 1 and 2.

a. Materials and methods for predictive models: state model , artificial neural networks and fuzzy logic.
Georgetown University Medical Center (Washington, DC) made available on line a database of Cyberknife® patient data. We restricted this database to 86 patients (339 treatment fractions), as no indication concerning the treatment site was available for the other cases, or because log-files were incomplete. In between this group, we analyze the performance of Synchrony® respiratory tracking in terms of residual tracking errors measured with X-ray imaging during treatment. Two groups were then extracted, 10 worst cases and 10 control cases randomly

selected among the population. The worst cases were defined as those fractions exhibiting the largest average tracking errors, as stored in the log files.
We firstly investigated, among the scenario of mathematical predictors, the best approach. We selected three different approaches: a linear \ quadratic correlation (state model), artificial neural networks and fuzzy logic. the choice was justified by the fact that these models are, in different ways, able to estimate a signal processing an arbitrary number of inputs, they have generalization capabilities, they can be trained and updated with theoretically no limitations. Moreover, neural networks and fuzzy logic allow the operator to tune architecture and parameters in ideally infinitive ways. To summarize, selected models featured:
• linear/quadratic correlation with implicit modeling of inhale/exhale variations. Such model is meant to represent a basic mathematical description of the regression curves that correlate the motion of external surrogates with internal tumor motion.
• artificial neural networks (ANN) to correlate multiple external variables through non linear transfer functions.
• fuzzy logic approach based on iterative data clustering and membership functions.

b. Results of a benchmark study of alternative models vs Cyberknife® Synchrony®
Models were tested and benchmarked vs. the Cyberknife® Synchrony® module in terms of residuals targeting errors.
Non parametric statistical analysis (Friedman test) applied to worst cases shows a significant difference among the implemented strategies (p-value <1.5·10-10). A post-hoc comparison (Dunn test) indicates that the state model has the worst performance, whereas the output of Cyberknife® Synchrony®, of the ANN-based and fuzzy logic algorithms are comparable at 99% confidence. Concerning the dataset of worst patients, the error reduction at 95% confidence of models in respect to Synchrony® was calculated at 0.55% for the State Model, 8.69% and 13.47 for ANNs and Fuzzy logic, respectively. Comparable results were highlighted for all strategies on the control cases, as confirmed by statistical non parametric tests (Friedman).
c. Improvements in predictors and results of new approach in models vs. Cyberknife® Synchrony®
Different methods required different optimization approaches. It is important to point out that predictive models are not adopted in clinical use in RT with particles. There is no evidence in literature about a best model in this application. A first study about improved models was conducted on the same Cyberknife® database, presented in the previous paragraphs.
Different data clustering approaches were studied due to their substantial effects on fuzzy modeler performance. A comparative investigation was performed on two fuzzy based and one neuro-fuzzy based inference systems with respect to Cyberknife®. Moreover, Due to the intrinsic inter-patient variability in fuzzy models performance, a model selectivity algorithm was proposed to select an adaptive fuzzy modeler on a case by case basis. an average 3D targeting increment (with respect to Synchrony) of 17.25 % for the control cases and a reduction of 24.8 % for the worst cases.
Artificial neural network approach was optimized by means of a more complex architecture, designed in C++ language. A non parametric statistical analysis (Wilcoxon ranksum test) was applied to control and worst cases and it returned *p-values* equal to 2.1066x10-5 and 0.0012 respectively, thus proving a statistically significant error reduction for the ANN-based method relative to the Synchrony® module. In conclusion, the proposed method allowed an average 3D targeting reduction (with respect to Synchrony®) of 17.84 % for the control cases and 23.15 % for the worst cases.

d. Design of a breathing phantom for model validation

Experimental validation of adaptive correlation models suffers from the lack of clinical database including appropriate description of tumor motion synchronized with external markers, thus forcing to rely on simulation and / or custom phantoms.

We designed a 4-dimensional (4D) breathing phantom, mimicking realistic respiratory motion and featuring simultaneous 3-D displacements of the external surface and of inner targets with variable phase and amplitude shifts. Motion in the first version of the phantom was driven by an electric motor (6-12 V, 1-4 A) with variable power supply voltage output for the tuning of breathing frequency. The mechanical coupling between the engine and the moving phantom was realized by means of a piston rod. The piston expanded a ribcage structure acting on two lateral and one frontal main ribs. The chest wall expansion was controlled by an elastic cover simulating the deformable skin surface, where external motion surrogates were attached. Motion of inner targets was provided by connecting targets to the driving piston and chest wall structures by means of variable and adjustable springs and elastic bands.

We tested our 4D phantom by means of an infrared optical tracking system equipped with 3 TV-cameras and capable of 3-D tracking 5-mm diameters passive markers at 70 Hz sampling rate. We placed 3 markers (2 laterals, 1 frontal) on the surface of the phantom and one in correspondence of the inner target. External marker motion was in the 2.2-6.1 mm range with variable phase shift depending on markers locations. 3D target displacements were up to 29.8 mm peak to peak, with significant hysteresis over multiple breathing cycles.

e. Use of artificial neural networks in real time (phantom study)

C++ application was installed on the OTS workstation in CNAO. It was then possible to use ANN based approach and the breathing phantom for real time studies.

The log file analysis of the phantom acquisitions showed that tumor position estimation took place consistently in real-time, except during the retraining of one or more ANNs. In these cases, the retrain procedure took, on average, a period of about 34 frames, corresponding to 0.57 seconds at the nominal acquisition frequency (60 Hz).

In order to quantify the tracking accuracy during three experimental acquisitions, 3D targeting errors are computed in correspondence to each acquired frame.

Median values (and interquartile range) of 3D errors were found to be 1.03 (0.99) [mm]; 1.01 (0.72) [mm]; 1.35 (0.66) [mm] in three separate acquisitions, respectively.

f. Integration of models and hardware for active beam scanning (tumor tracking). GSI experimental session 1 and 2.

The conclusive experimental activity presented in the thesis envisaged the integration of hardware and methods described in the previous paragraphs in the control logic of an active carbon ion beam. Our systems, here intended as the breathing phantom and the OTS, were moved to GSI, where two experimental sessions were conducted in collaboration with Moving Target group. A second version of the breathing phantom was built, according to the fact that the current version of the organ motion manager module at GSI can process only 2D translational movements of a moving target. Phantom repeatability of movements, as a feasibility study of the set up in terms of markers visibility were required as preliminary condition and was tested in Pavia.

The first experimental series, performed in July 2011 at GSI, aimed at establishing the communication between the OTS and the organ motion compensator (OMC).

For a proof-of-principle test the IR optical tracking system (OTS) were installed and connected to the therapy control system (TCS) at GSI to allow organ motion compensation by beam tracking. Phantom was equipped with GafChromic films and 4 pinpoint ionization chambers. During this first trial, the compensation parameters determined by the OTS were transmitted to the TCS via an analogue signal (National Instruments dedicated board) from which the

motion phase was determined in the TCS. Based on an offline created look-up table (LUT) this motion phase results into the required lateral motion compensation parameters.
The experimental series performed in July 2011 at GSI aimed at establishing the communication between the two systems were successful.
A second experimental session, performed in October 2011, was dedicated to the active tracking of the moving target, including in the protocol ANN based prediction with retraining capabilities. Even if the set up was the same of July, there were several differences in the approach, mainly in the communication between systems. First of all, correction vector was sent via UDP. UDP communication is theoretically faster than digital to analog converter and there is no need for a LUT or the NI board. Also the pinpoint holder was slightly improved, hosting 5 ionization chambers instead of 4.
Results of ANNs prediction errors, and about dosimetry were encouraging ad are presented in the thesis.

Conclusions
This thesis is composed by three main cores. The first one is focused on the use of accelerated particles in radiotherapy, the second on the management of organ motion effects and the last section is focused on the study of predictive models for tumor targeting, and their possible integration in a dose delivery system.
Protons and carbon ions are proved to be a valuable technique in cancer treatments. Potential advantages are represented by an high local control of the tumor and lower unwanted side effects. Moreover, this treatment is the only therapeutic solution for different types of tumors. High costs are the principal reason why this type of treatment is not largely diffused. Actually, in Europe only two facilities can offer this treatment. Dose distribution in depth requires an high accuracy and control in patient positioning and setup before and during irradiation. CNAO, the only facility in Italy able to perform radiotherapy with particles and carbon ions aims to provide a state of the art treatment. In this project, Politecnico di Milano has been involved in the selection of appropriate systems for patient positioning and in room setup control. The solutions adopted are described in the thesis. Installation of these systems last one year (2009). Hardware and software optimization required multiple checks and corrections. Measurements and integrations last two years (2010-2011), and they represent the result of a strong collaborations between institutions and suppliers. Today, CNAO is starting its clinical activity. Results of commissioning activities and measurements carried out during acceptance protocols are reported in the manuscript, supported by statistical analysis. They demonstrate that is possible to obtain sub-millimetric accuracy in patient repositioning. Integration of different systems was also successfully proved.
First treatments in CNAO will be devoted to static tumors. Even if difficulties in treatment planning optimization remain, dose delivery systems in radiotherapy with particles could offer enormous potentialities for tumor tracking when organ motion is not negligible. Organ motion management requires not only an accurate setup procedure, but also a description of the trajectory (magnitude of movements and phase) of the target volume. This is usually performed by means of correlation models between internal target and external surrogates. Predictive models for tumor tracking are nowadays used only in a commercial device (Cyberknife® Sinchrony®) utilized in radiotherapy with photons. Their use in radiotherapy with particles could open new scenarios in treatment planning optimization and in dose delivery. Different approaches are described in the thesis. Firstly, a benchmark of alternative methods (based on: linear \ quadratic correlation, artificial neural networks and fuzzy logic) vs. Cyberknife® Synchrony® was performed. Results put forward these models as a potentially valuable tool for tumor position estimation, given patient's surface surrogate information. In particular, the comparative study showed that complex models are required to predict tumor

motion over long time periods, showing better performances of neural networks and fuzzy logic if compared with linear \ quadratic correlation. A first tentative of optimization of neural networks and fuzzy logic approaches was performed. The aim in this case was to obtain better performances (in terms of 3D errors reduction) and to understand if it was possible to design an application able to run in CNAO hardware. A custom breathing phantom was built to supply the lack of clinical data. This phantom is able to mimic a realistic breathing, and it features an internal target that moves along an hysteretic trajectory in phase with the external ribcage. Results on phantom study demonstrate that neural networks can be not only integrated in CNAO hardware, but that they can be trained and updated with a clinical compatible time consumption. Of course the main limitation of this approach is that the phantom provides very simple movements and relatively small pattern variations. Moreover, predictor's architecture was very simple and not yet optimized. The use of an integrate system (phantom, optical tracking system with predictive capabilities) allowed us to validate our method in GSI, Germany. There, it was possible to test the possible integration of our systems in the steering logic of dose delivery. In this respect, result was successfully reached. Even if we observed remarkable performance of predictors during the second experimental session, retraining capabilities remain at this time a major issue. More experimental sessions will be dedicated to the search of a reliable estimator, and different methodologies have to be investigated. But the main goal, that was the active control of a carbon ion beam using a signal processed by a predicting model was reached..

Preface

During my Doctoral program, I have concentrated the most of my activities in the National Center for Oncological Hadrontherapy (Centro Nazionale di Adroterapia Oncologica, CNAO), Pavia. There, I was involved in the commissioning and testing of systems for patients' positioning and setup control, in the optimization of workflow, and also in supporting and tutoring CNAO personnel in the use of cited systems during first clinical sessions. In order to integrate these technological aspects with others more focused on research, I put attention also on treatment geometry optimization in radiation therapy, in particular working on external - internal correlation models for organ motion mitigation.

The first part of the thesis describes the rationale behind the use of accelerated particles in radiation therapy (Chapter I). The activities I was required to exploit in order to assure an adequate accuracy in patients' positioning and setup control before and during treatments are presented, after an extensive introduction of CNAO, in Chapter II. Consequently, as already mentioned, the first part of the thesis is focused mostly on technical aspects.

The second part of the thesis is dedicated to methods aimed at estimating the position of moving tumors processing surrogate signals of patients' surface. Implications, as the importance of this field of research, are recognized in the scientific community. An introduction to organ motion effects and to recent techniques for organ motion mitigation in radiation therapy are reported in Chapter III. Chapter IV is dedicated to the description of mathematical models for external - internal correlation and tumor tracking. This chapter includes a description of materials and methods and results obtained benchmarking selected approaches with a commercial device, and concludes presenting the integration of this method with the steering logic of an active scanning system for carbon ion treatments.

Finally, Chapter V reports general discussion and conclusions.

Chapter I

Introduction to radiation therapy with accelerated particles

We refer to the term cancer, or tumor, when in normal tissues there is an abnormal growth or proliferation of cells serving no physiological function. A wide variety of diseases can be included in this definition. When a malignant tumor grown and spreads cells throughout the body other tissues can be affected by disease (metastases).
Among possible strategies for tumor control, benefits of radiation therapy (RT) are recognized and proved. In conventional RT, patients are treated with high energy X-ray (photons). Reasons to use RT can be both curative or palliative, or it can be used as concomitant treatment or consequent to other interventions, like surgery (suitable when tumor is small and solid with no metastasis) or chemotherapy (use of drugs to stop proliferating cells). Theoretically, supposing an high setup control in delivering radiations, the majority of the tumors could be at least controlled with RT (Kraft 2002). If the dose is high enough, every tumor and thus group of cells can be killed with ionizing radiations. Obviously this approach is often impracticable, because it could led to unrecovered damages in healthy tissues. In RT there is always a tradeoff between costs and benefits. Tumor control is often halfway (see figure 1.1).

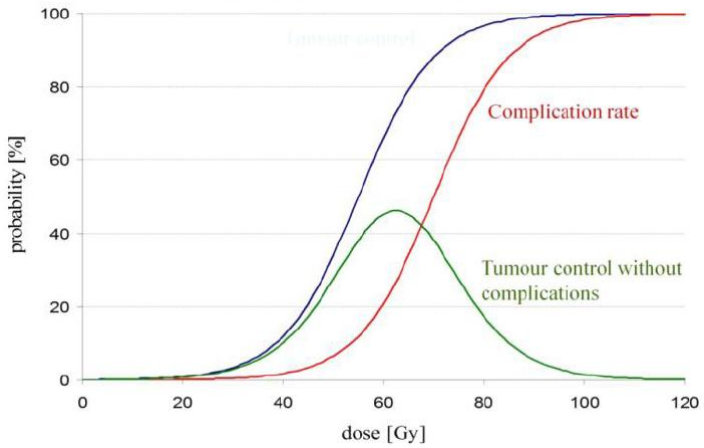

Figure 1.1 Schematic relation between tumor control probability (blue line), complication Rate (red line) and tumor control without complications (green line).

Beside photon RT, the number of facilities able to offer a treatment with accelerated particles is nowadays worldwide increasing. Studies on accelerated particles for RT applications started in 40's in United States (Wilson 1946). Only in 70's first treatments were performed. Nowadays around 70.000 patients have received this kind of treatment. This number is designated to increase because of the availability of new facilities, because of technological improvement in dose delivery techniques, and of setup control procedures.

Radiotherapy might eventually replace radical surgery in deeply situated anatomical locations. There are different advantages in this case: there is no need of long hospitalization, RT is not as much invasive as surgery, convalescence could be faster and obviously overall costs decrease.

There are several differences between RT with photons and accelerated particles. These differences are both in the technology for beams production and in the modality of interaction with the biological matter, which also affect the biological effects.

1.1 Differences in depth dose profile between photons and particles

Photon beams (usually called 'X-ray beams' by medical doctors) are characterized by an exponential absorption after a maximum which, for beams having a maximum energy of 8 MeV, is reached at a depth of 2-3 cm (Amaldi 2001). The attenuation of dose distribution in case of RT with photons is exponentially decreasing in the irradiated body. This means that the higher amount of energy is released in proximal areas, whereas in depth the dose profile is attenuated (Figure 1.2).

In clinical particle therapy is often called hadrontherapy. This term describes the many different techniques of RT which make use of fast non-elementary particles made of quarks: protons, neutrons and light nuclei of different species. Protons and Carbon ions are the hadrons used to locally control many types of tumors.

The effects of particles in a irradiated body were described over 100 years ago by William Bragg, a British physicist (Bragg 1903).

Particles release relatively low energy in proximal areas (when their energy is high) while the interaction probability to cause ionization increases as the velocity falls, thus the maximum of the energy is released in a precise depth, just before their coming to rest. By then, the depth-dose curves of proton and light ion beams are completely different from those of photons and neutrons, and dose depth profile is characterized by little scattering when penetrating in

matter and high dose near the end of their range. This behavior is described by the 'Bragg peak' (Figure 1.2). This particular dose profile is typical of particles, and the depth of the Bragg peak depends by different factors: density of the body, presence of oxygen, energy and velocity of particles.

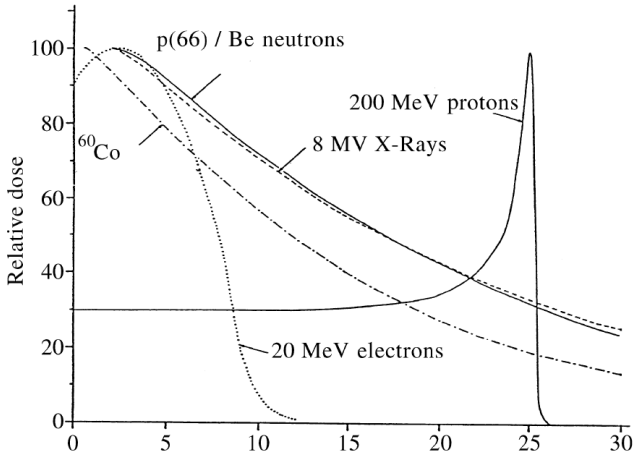

Figure 1.2. Depth-dose curves for photons (from a cobalt source and an 8MeV linear accelerator), neutrons and 200MeV protons. With protons, the highest dose is released near the end of their range giving rise to the `Bragg peak'. (Orecchia *et al* 1998)

This difference between photons and particles offers a number of theoretical advantages over conventional radiotherapy (Orecchia *et al* 1998). A lower energy in the entrance channel, with an higher peak in depth, allow to focus the dose deposition in depth, and save normal tissues (Figure 1.3).

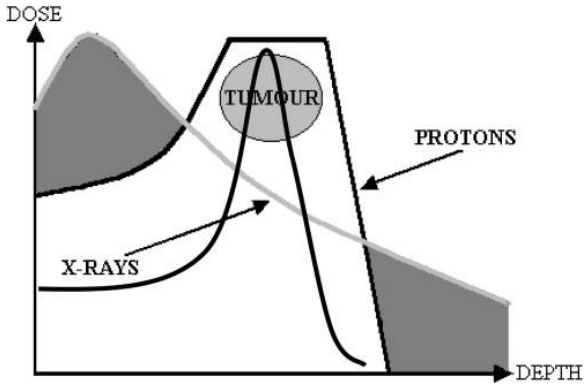

Figure 1.3. Schematic depth dose diagram of a proton beam Bragg peak, an extended Bragg peak and a megavoltage X-ray beam. The grey shaded areas indicate the extent of dose reduction within normal tissues situated proximal and distal to the tumor target. (Jones 2006)

Due to the unfavorable depth-dose distribution, that is very similar to that of photon beams, neutrons are becoming less interesting.
Protons and light ions are also advantageous in Intensity Modulated Hadron Therapy because of three physical properties:

- They deposit their maximum energy density in the Bragg peak at the end of their range, where they can produce severe damages to the cells while sparing both traversed and deeper located healthy tissues.
- They penetrate the patient practically without diffusion.
- Being charged, they can easily be formed as narrow focused and scanned pencil beams of variable penetration depth so that any part of a tumor can be accurately and rapidly irradiated.

As already mentioned, the depth of dose deposition depends by several factors but mostly by the beam energy (Figure 1.4). The limitations during planning phases under this point of view are related to the energies available.

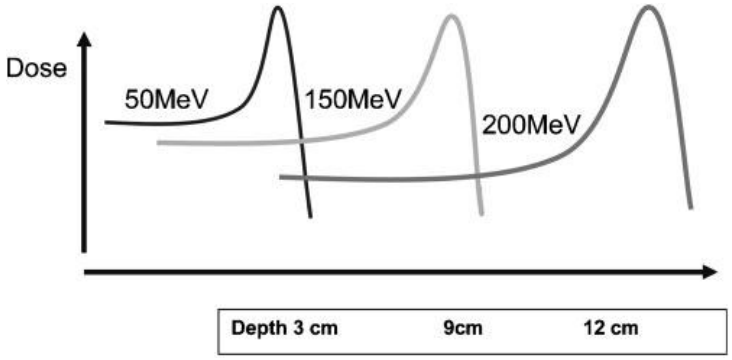

Figure 1.4. Approximate depth dose positions for protons of different energies. (Jones 2006)

Even if more data are required to exactly quantify the advantages, particle therapy should give a better tumor control. For example carbon beams of about 400 MeV/u are indicated for treatment of deep-seated tumors, which are radio-resistant both to X-rays and to protons. (Denekamp 1994; Koehler *et al* 1975; Essen *et al* 1985; Batterman *et al* 1981).

In order to selectively irradiate deep-seated tumors, in photon RT operators use multiple beams usually pointing to the geometrical centre of the target. These irradiation techniques are applied by machines containing linear accelerator rotating around a horizontal axis. Obviously a limiting factor is given by the amount of dose given to the healthy tissues. A solution is to conform the dose to the target, thus increasing the absorbed dose release inside the lesion. Conformal RT is the main goal of all recent developments in RT (Dearnaley *et al* 1999). *Intensity Modulated Radio-Therapy* (IMRT) makes use of 6-10 X-ray beams; the beams may be non-coplanar and their intensity is varied across the irradiation field by means of variable lamellar collimators (multileaf collimators) that are computer controlled. For planning the treatments codes for inverse planning have been developed.
Jones investigate the impact of particle therapy in these application. Inspection of axial views of three intersecting beams, as in Figure 1.5, shows the different dose distributions achievable. These figures can be normalized to give the same dose in the central region, with resulting lower peripheral doses for particles. The absence of dose in one direction beyond the target is striking and this arrangement may be used to reduce exposure to critical structures such as rectum, spinal cord and other organs at risk (Jones 2006).

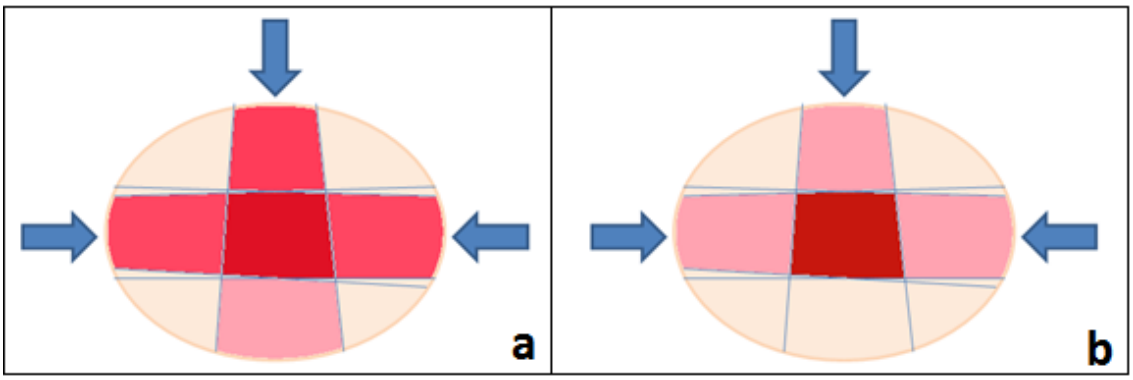

Figure 1.5. Axial views of simplified schematic dose distributions for three field coplanar techniques using X-rays (panel a) and particles (panel b). (arranged from Jones 2006).

1.2 Biological effects of particles

Biological effects are generally related to the absorbed dose, expressed in Gray (1 Gray=1 Joule/kg). The absorbed dose is not sufficient at describing the biological response because of the complexity of radiation-tissues interactions. Moreover, the same dose of different types of ionizing radiations do not produce the same effect.
The effects of light ions are qualitatively different from those produces by sparsely ionizing radiations as electrons, X-rays or photons. (Amaldi 2001). These lasts interact indirectly (dose is distributed homogeneously at cellular level) with DNA and produces repairable damages, while light ions produce multiple damage sites crossing the DNA of cells. In fact, charged particles cross the medium leaving structured tracks. Then, they are generally more appropriate where radio-resistance is an issue, and generally in those cases light ions overcome conventional and proton radiotherapy.

1.2.1 Ion species used in particle therapy

The most common particles used in RT are protons and carbon ions. Nevertheless, readers should be awarded that other ion species have been tested and are now under investigation (Figure 1.6).

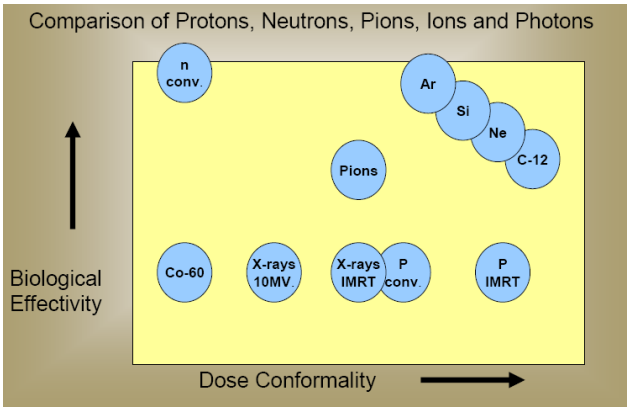

Figure 1.6. Dose conformability vs. biological effectiveness of different ion species (Hug and Debus 2008).

The vantage of protons is that their mass allows the use of relatively small accelerators.
They are characterized by a Bragg peak profile of depth dose, and so they present the same advantages in treating depth tumors saving tissues in the entrance channels. Their energy is lower (maximum 250 MeV), if compared with heavier ions (carbon ions have a max energy of 450 MeV), thus the RBE is lower.
Radiobiologists and radiotherapists have reached the conclusion that the optimal ions are found in the range Z = 3 - 6, i.e. between Lithium and Carbon (Amaldi 2001).
There are two main reasons for this.

- Low LET ions (<20KeV/ μm) could not be confined to the tumor tissues allowing a high conformability.
- When a particle beam is used to irradiate a body, the incoming ions fragment into lighter ones. These fragments are characterized by a lower charge: the main consequence is that they have a longer range if compared with original ions. The dose depth profile results in a combination of these effects, and the Bragg peak presents a tail, thus irradiating normal tissues.

1.2.2 Linear energy transfer

The energy transferred to materials when a ionizing particle crosses a body is referred as linear energy transfer (LET), and it is the average energy locally imparted to the medium per unit track length. LET is expressed in keV/micron (Zirkle *et al* 1952). Generally LET is meant to quantify the effects of radiations on irradiated body or tissue.

LET depends by several factors such as charge and particles velocity. From a biological point of view we generally distingue between:

- Low LET (<20 KeV/micron). Sparsely ionizing radiation with ionization distance higher than DNA diameter.
- High LET (50 -200 KeV/micron). Densely ionizing radiation with ionization distance comparable with DNA diameter.
- Very high LET (>1000 KeV/micron). Very densely ionizing radiation with ionization distance less than DNA diameter.

Photons are low LET ionizing radiations. Ionizations distances in this case are very spaced, and as already mentioned the majority of the damages can be repaired by normal mechanisms. The fractionation of the dose is a critical issue, and the radio-sensitivity depends from the type of irradiated cell, the cell phase, the presence of oxygen and other parameters. Moreover, studies have proved X-rays to have stimulating effects in angiogenesis (Sonveaux *et al* 2003). Possible secondary issues like metastasis are not negligible in this case.
An example of high LET radiation is offered by neutrons. Ionizing distances in this case are minimal, and damages cannot be repaired by normal cell mechanisms. Dose fractionation is not so relevant as in the case of photons, and the response to radiations is independent of cell phase and hypoxic conditions. Since the usual cellular repair mechanisms have little effect, there is no point in fractionating the dose in the 30 sessions as usually applied in conventional radiotherapy. This shortening of the treatment is an advantage, but the lack of repair may also induce late recurrences in the healthy tissues (Amaldi 2001).

1.2.3 Radiobiological Effectiveness

In order to compare the different radiation qualities an index has been proposes. The relative biological efficiency (RBE) is defined as the ratio of a reference species dose (generally X-rays) to investigated dose in order to achieve the same biological effect (Figure 1.7).

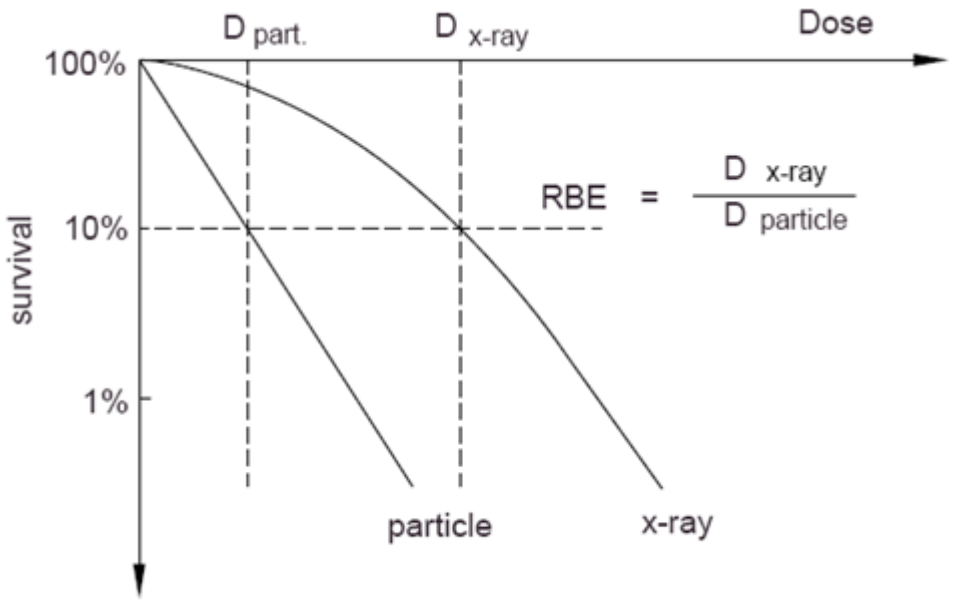

Figure 1.7. Definition of the relative biological effectiveness, illustrated for cell survival (Kraft 2002)

RBE depends on several factors.
RBE increases with increasing LET up to a maximum and then decreases (Barendsen 1968). This characteristic is depicted in figure 1.8. If very high LET values are applied, it is possible to observe a phenomena called 'overkill', and a rapid change in LET\RBE curve profile.

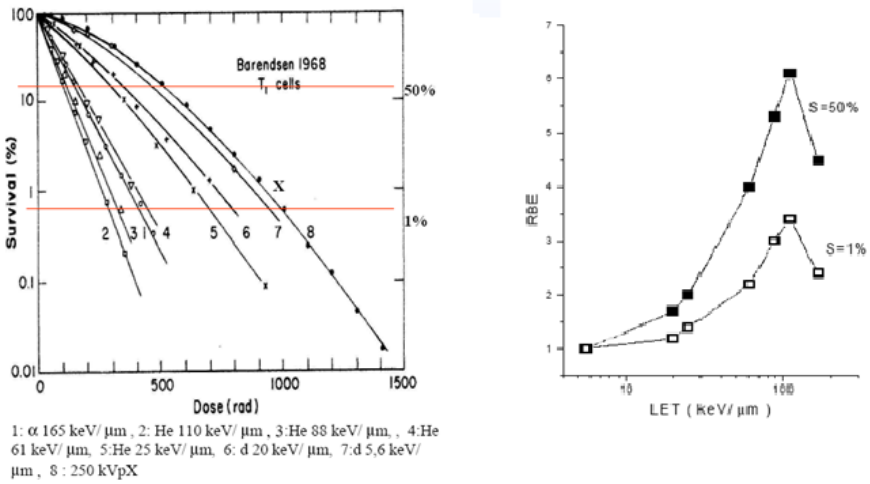

Figure 1-8. cell survival curves for different ion species and at different doses (left panel). LET vs. RBE correlation (right panel) (Barendsen 1968).

RBE depends on particle type, so there is not a single RBE- LET relationship for all the ions since maximum of ion effectiveness shifts towards higher LET values for heavier ions and height of the peak decreases for heavier ions. (Todd *et al* 1965, Deering and Rice1962, Skarsgard *et al* 1967, Kraft *et al* 1987, Belli *et al* 1989).
In figure 1.9 it is possible to notice that at a given LET the RBE for He ions is higher than that for the other ions. Accordingly to what already mentioned, The position of the maximum RBE shifts to higher LET values for heavier ions. This study was proposed by Furusawa *et al* (2000), performed with human salivary gland tumor cells irradiated with C, Ne or He particles, and LET values between 20-600 keV/mm.

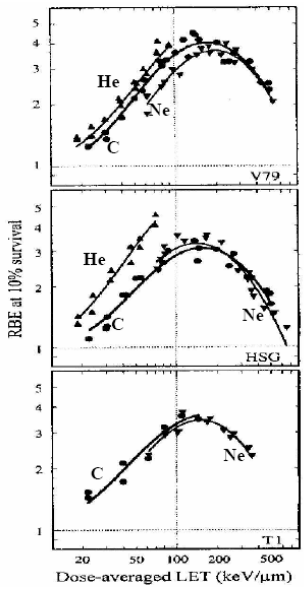

Figure 1.9. position of the maximum RBE vs. different LET values

The presence of Oxygen strongly influences the biological effect of X-rays (Figure 1.10). Thus, the definition of RBE is influenced by this factor since particles are less affected by oxygen concentration. In this situation it is necessary to define a new index, the Oxygen Enhancement Ratio(OER) as:
$OER = D_{hypoxic} / D_{aerated}$
Where D= dose for the same biological effect. In case of X-rays, OER has a value ~2.5-3.

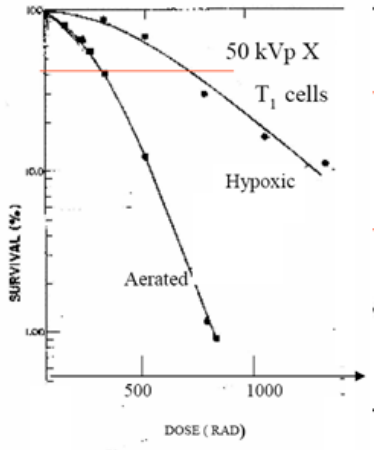

Figure 1.10. Effects of oxygen in cell survival curve (Todd 1964)

RBE is dose dependence. Because of the non-linearity of the X-ray curve, the RBE is not a constant value, unique for each ion specie in relation to photons.
RBE of a given radiation is greater at low doses, and decreases with increasing dose (Figure 1.11). Ideally, the two curves become parallel for high doses, and no differences can be noted. Obviously, very high doses may have no clinical application.

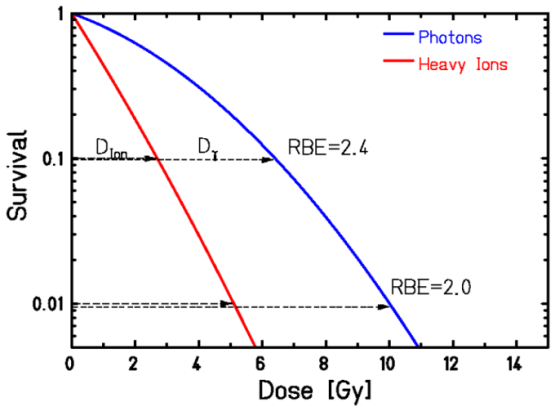

Figure 1.11. different RBE values can be obtained at different doses considering the same ion species (Scholtz 2008)

Finally, RBE depends also by other factors, like the fractionation effect (Blakely *et al* 1984) and cell repair capacity (Weyrather *et al* 1999). Readers can refer to literature for further details.

In conclusion, RBE depends on particle energy, dose, tissue, and others. As a consequence, for therapy which uses charged particles that are biologically more effective than photons (like carbons),physical doses must be corrected by the appropriate RBE's, in order to obtain homogenous distribution of effective dose in treatment volume.

$D_{effective} = D_{physical} \times RBE$

Assuming this relation, operators should be aware of the radiation effectiveness distribution in the medium, and correct the physical dose in order to obtain flat effective dose profiles. As example, an increase at the distal edge of RBE requires decrease of planned physical dose in that region (Figure 1.12).

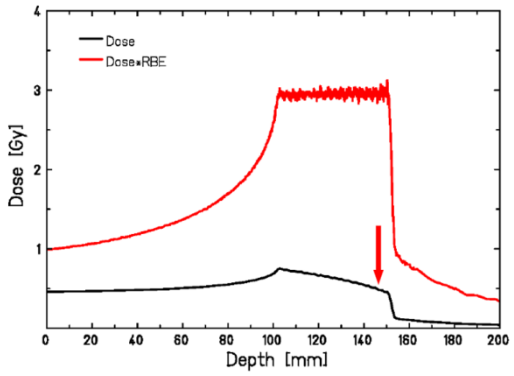

Figure 1.12. effective vs. physical dose. Physical dose is decreased in distal region in order to obtain a homogeneous distribution in effective dose (Scholtz 2008)

As seen, carbon ions beam is characterized by an advantageous RBE index of 1 at the entrance of the field and 3-4 in correspondence of Bragg peak. Indeed, due to their interesting and advantageous characteristics, carbon ions are currently recognized as the best compromise in clinical activity.

1.3 Dose delivery

A mono-energetic proton Bragg peak is not very useful for treating anything other than the smallest tumors. To make particles useful , we need to *spread out* the dose laterally and along the beam direction. The Bragg peak (see figure 1.13 b) can be spread out to achieve a plateau of uniform dose that covers a target (spread out Bragg peak, SOBP). To obtain a SOBP, beams of different energies have to be superimposed (Durante and Loeffler 2010).

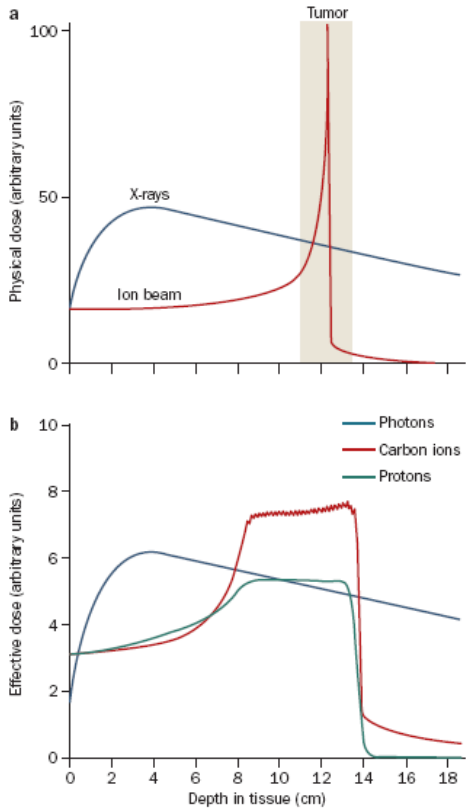

Figure 1.13. panel a: dose-depth profile for X-rays and carbon ions. Panel b: spread out Bragg peak obtained superimposing different beam energies. (Durante and Loeffler 2010).

Range-straggling broadens the individual Bragg curve and decreases the peak to plateau ratio. Only at the distal side of such extended or smeared-out Bragg peaks (SOBP) the natural decay is visible (Kraft 2002). In his study, Kraft compared the extended Bragg peaks of protons and carbon ions at different penetration depths (Figure 1.14).

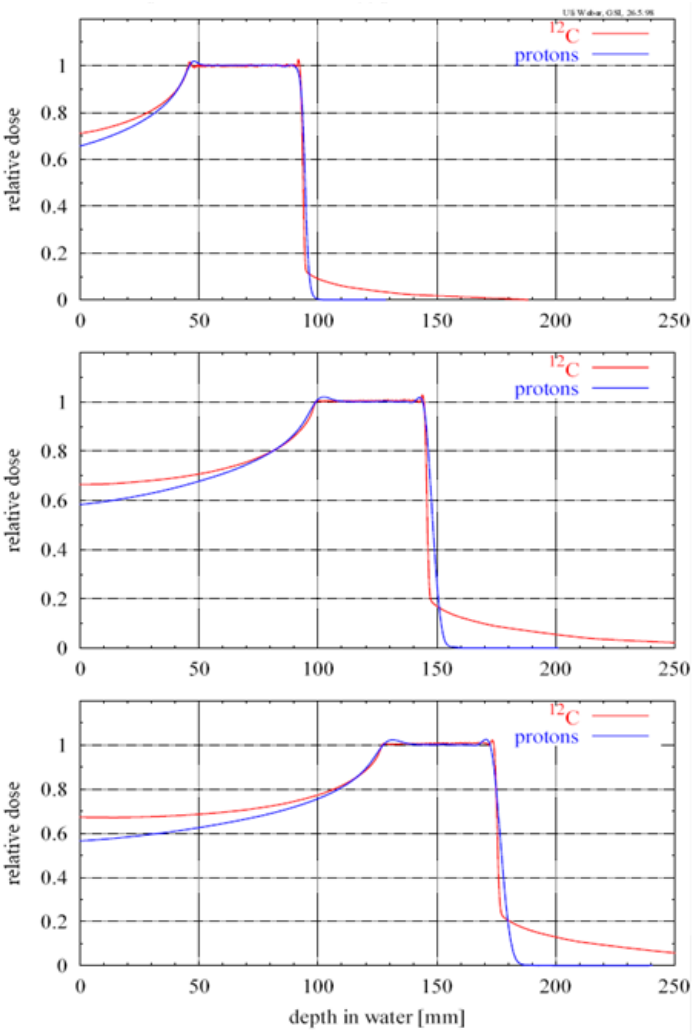

Figure 1.14. comparison of extended Bragg peaks for protons and carbon ions (Kraft 2002).

The author observed that differences between protons and carbon ions in the entrance channel as well as at the distal side are small. More important than the longitudinal straggling for therapy is the lateral scattering (see figure 1.15). In practical applications, a target in the proximity of a critical structure will not be treated in such a way that the beam stops in front of the critical site because of possible range uncertainties.

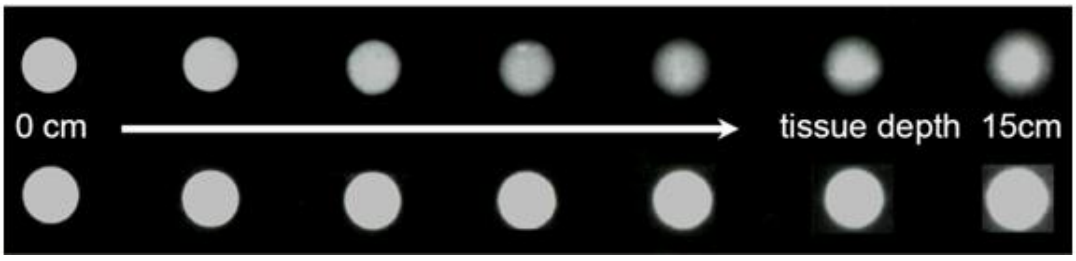

Figure 1.15. lateral scattering effects at different tissue depth. Upper spots: protons (200 MeV); lower box: carbon ions (300 MeV/u) (Hug and Debus 2008).

There are mainly two different methods to obtain the so called Spread Bragg peaks (SOBP): the first one through passive modulation (that is, one energy spill, use of range shifters of variable thickness to compensate the depth) and the second one is active modulation (that is, sum of different spills by tuning accelerator parameters).

1.3.1 Passive modulation

An extension of the dose in depth can be achieved with range shifter wheels and ridge filters (Figure 1.16). These two represent the main solution adopted in case of passive modulation for SOBP generation.

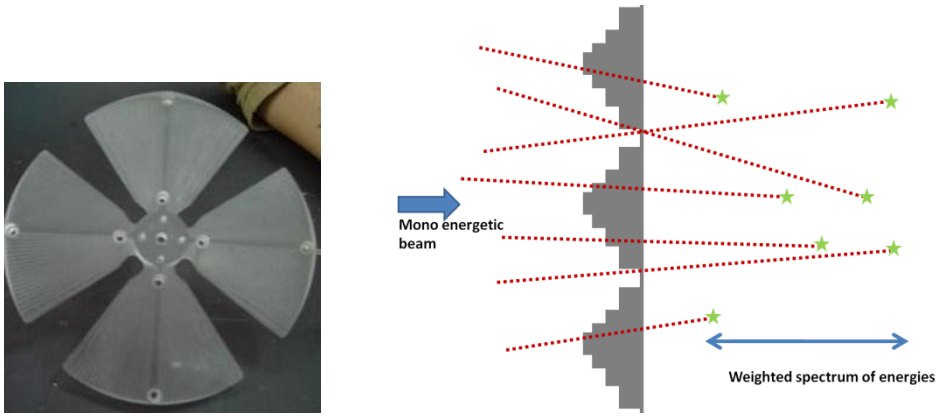

Figure 1.16. range shifter wheel (left) and ridge filters (right) for passive beam modulation.

The range shifter wheel is a rotating wheel (~3000 rpm) with varying thickness, while the ridge filter operates mechanically relative weighting of Bragg peaks determined by projected areas of ridge filter with different thicknesses.
Range shifter wheels are simple to produce, but as they are dynamic devices, they are difficult to use with beam delivery systems that are themselves dynamic. On the contrary, ridge filters are passive devices that can be used with all beam delivery systems. They are more difficult to produce if compared with range shifter wheels and must be very accurately aligned with the beam in order to ensure flat SOBP's.

In order to extend the dose laterally, the insertion of a scattering foil in the beam line can be used. A scattering foil is basically a thin metal plate used to disperse the beam. The function of the scattering foil is to flatten intensity over the field, broadening in Gaussian profile the beam. It is necessary to include a drift space to patient, required for beam to broaden to desired field size (typically 20cm). The use of this technique usually means very poor efficiency (very few particles contribute dose to target). However, they are characterized by a good penumbra after collimation. A single scatterer broadens the beam sufficiently for treatments requiring small fields.
For larger fields, a second scatterer is needed to ensure a uniform dose profile, and a combination of custom-made collimators and compensators in order to conform the dose to the target volume are required. Scattering foils can also be accomplished with a second composite and contoured scatterer (double scattering). If compared with the single scattering,

for similar drift space, larger field sizes have to be taken into account. They also present a better homogeneity of dose across field and better efficiency (many more particles contribute dose to target). One of the major disadvantages is that penumbra effects increase due to larger virtual source size.
In figure 1.17 is depicted an application of the presented strategies. The beam produced by the accelerator passes through a range shifter (A) (either a rotating wheel or a ridge filter) in order to spread the dose in depth. Then, dose is spread laterally by means of a scatterer foil (B), and collimate (C). A compensator is finally applied to maximize the geometrical conformity (D).

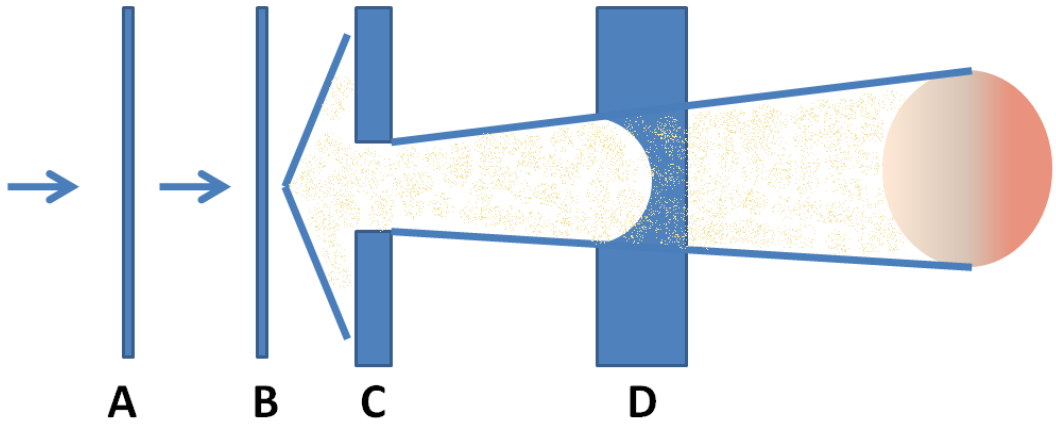

Figure 1.17. practical application scheme for passive beam modulation. A=range shifter; B=scatterer; C=collimator; D=compensator

1.3.2 Active modulation

Another way to extend the dose laterally is the so called 'wobbling'. An extension in lateral diffusion is obtained by the application of a continuously scanned, broad pencil beam, which overlaps enough to deliver a more homogenous dose over a defined field size.

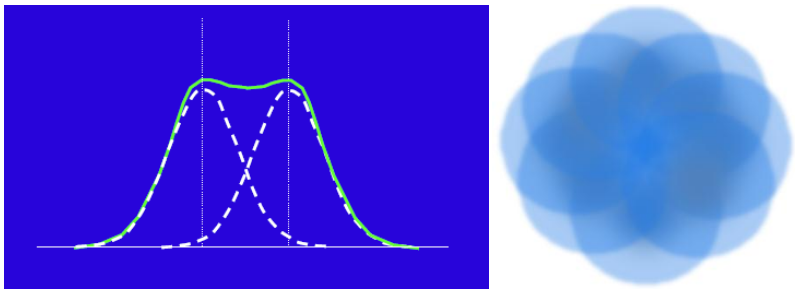

Figure 1.18. Wobbling effect (panel a) and combination of more peaks (panel b).

As depicted in figure 1.18, deliverable field size for a given flatness is function of radius of elemental beam and radius of wobbling. Wobbling has advantage of being able to deliver large fields, with poor penumbra effects. This strategy is difficult to synchronize with other movement parts, like range shifter wheels.

Since particles have mass and charge, magnets can be used to focus and steer the beam line. This potentialities, combined with the Bragg peak behavior, give enormous potentialities in geometrical selectivity of dose delivery systems. According to Bert and Durante (2011), mainly two treatment delivery options exist to shape the dose distribution to the patient: beam scattering (Chu *et al* 1993) and beam scanning (Haberer *et al* 1993, Pedroni *et al* 1995), each with active or passive energy modulation. Beam scanning is commonly referred as active spreading, or active scanning.

Active scanning, as with wobbling, utilizes the charge of the particles to magnetically scan pencil beams across the target. In contrast to wobbling, dose is confined to the target by actively steering the individual pencil beams such that only Bragg peaks that stop in the target volume are delivered. Scanning of beam is performed in depth through the use of Bragg peak specific energy modulation. Homogeneity and conformation of dose to target is achieved through mathematical optimization of weights of individual proton pencil beams. In this technique, no field specific hardware (collimators/compensators) is required (Figure 1.19).

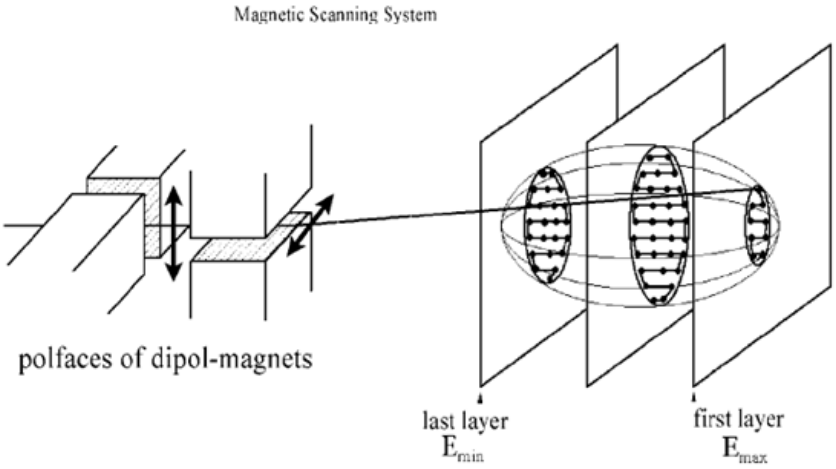

Figure 1.19. Schematic drawning of the intensity controlled magnetic scanning system. Target volume is dissected into layers of equal particle range that are covered by a net of picture points. The beam is guided along the imaginary line of picture points by two couples of fast magnets (Kraft 2002).

There are different approaches in dose delivery: the first one requires to leave the beam 'on' and steer the direction (like sliding painting). The second is a 'step and shoot' approach: once a voxel is irradiated, beam is turned off, the steering logic moved to another voxel to be irradiated and so on. There are also different delivery patterns for active scanning (see figure 1.20).

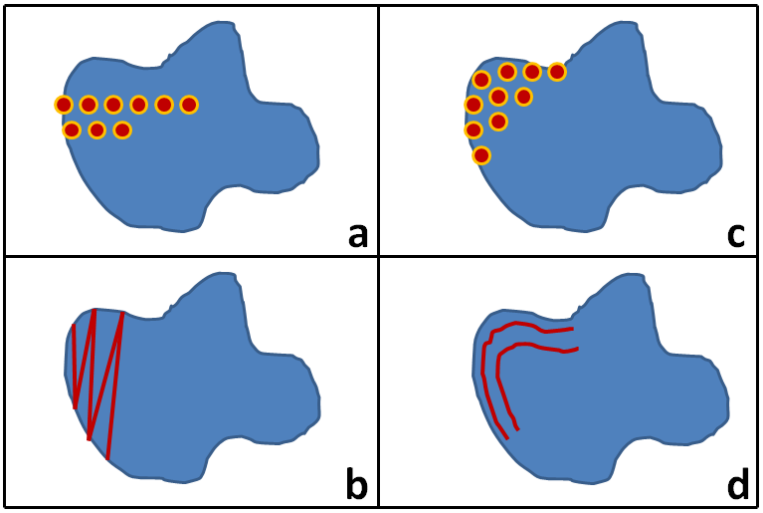

Figure 1.20. different approaches in dose delivery: a. spot scanning; b. optimized spot scanning; c. raster scanning; d. contoured scanning

In conclusion, there are different methods used in dose delivery, mainly dependent by the available hardware. Passive scanning approach is a mature technology and can offer different advantages, mainly related to a strong know how about hardware construction and optimization. Passive scanning is also insensible to small target movements. This last point is relevant in organ motion management.

Recent facilities generally delivered dose with active scanning techniques. Compared with passive, active scanning is implicitly more flexible. Moreover, there is no need for specific hardware, thus gantries are smaller. This last is a great advantage, since linear accelerators mounted on rotating gantries are standard equipment in conventional radiotherapy. To date, the requirement of gantries for proton and ion beam delivery is extending, due to the evident benefit in having more geometrical selectivity.

However, protons are heavier than electrons, and much larger magnets are therefore required for bending the proton beam onto the patient. Thus, for the foreseeable future particle gantries will always be larger than conventional linear accelerators (Figure 1.21).

Figure 1.21. different examples of rotating gantries. From left to right: a. a linear accelerator for conventional RT; b. the proton gantry at PSI; c. the first rotating gantry for protons and carbon ions at HIT; d. a scheme of the gantry installed at HIT.

1.4 Methods to accelerate particles

Nowadays there are two methods to accelerate particle for clinical use. The first one is through a cyclotron, the second using a synchrotron. A fully exhaustive and complete description of these modalities is not one of the aims of this thesis, considering the complexity of the problem. By then, an overview on functional principles is only provided in the following paragraphs.

1.4.1 Cyclotron

A cyclotron is a moderately compact device able to accelerate charged particles using potential difference of alternating voltage.
The cyclotron is a circular accelerator machine that makes use of the magnetic force.
The force acting on a particle (q=charge) inside a magnetic field (B), with constant velocity (v) is defined by:

$$\vec{F} = q\vec{v} \times \vec{B}$$

This relation is well know as Lorentz force. It is always perpendicular to the movement of the charged particle inside the field, so it is not affected by variations in kinetic energies but it affects only the direction of the movement. If $\vec{B}$ is aligned to the vertical axis, the followings are true:

- $\vec{v}$ is constant along an ideal vertical axes, and so it preserves the initial value.
- $\vec{v}$ changes direction during acceleration
- $\vec{F}$ is perpendicular to $\vec{v}$, so it is perpendicular to particle trajectory.

By then, a particle moves inside the magnetic field describing an elliptic trajectory (circular if the initial velocity along vertical axis is zero) (see Figure 1.22).

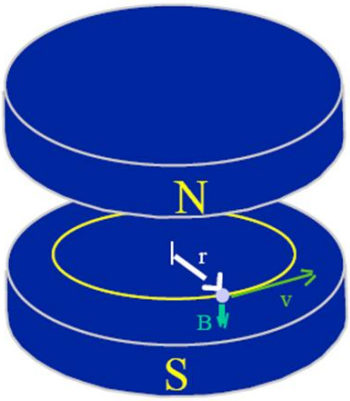

Figure 1.22. Descriptive scheme of particle motion in a magnetic field

A cyclotron is composed by two cavities (‘D’ or ‘Dee’ cavities) placed in a vacuum chamber one in front of the other. A perpendicular magnetic field is applied with two poles of a large magnet. The space between the ‘D’ cavities is called acceleration gap (Figure 1.23).

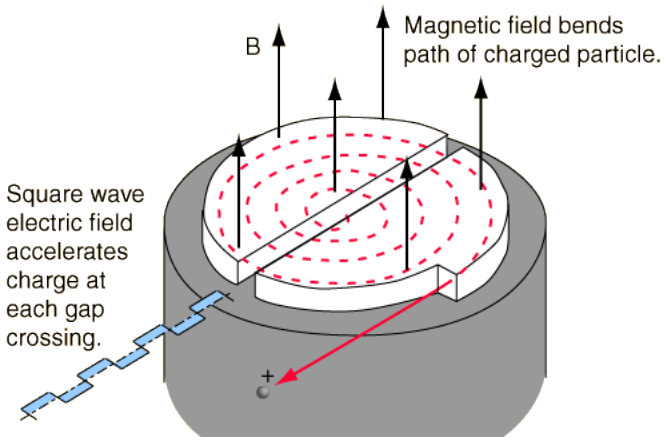

Figure 1.23. schematic design of a cyclotron and its functioning principles

In a cyclotron, 'D' cavities acts like electrodes, and they are responsible for the particles' energy ramp. An high-frequency alternating voltage is applied across the "D" electrodes, that alternately attracts and repels charged particles. It is necessary that the frequency used is phased to the one distinctive of the ion specie injected in the cyclotron. By then, particles injected near the center of the magnetic field increase in speed and energy when passing through the gap between the electrodes. The perpendicular magnetic field, combined with the increasing energy of the particles forces the particles to travel in a spiral path. The acceleration cycle follow a direction as depicted in figure 1.23.
Particles injected in the cyclotron are actracted by the negative 'D'. Applying an alternate wave between the two 'Dees' produce a boost of charge inside the gap. Every half period (that is, every time particles exit one D and entered into the other) the accelerating gap provide a ramp of acceleration. The more the particle is accelerated, the more its trajectory increase in diameter. This is one of the main limitations in producing high energies with a cyclotron.
Once energized, particles can be spilled out the cyclotron.

1.4.2 Synchrotron

The synchrotron is a circular accelerator. In a synchrotron, differently from a cyclotron, particles moves always on the same trajectory, defined by the mechanic of the machine. Obviously, these aspects require a different approach, both in the technology and in the functional principles.

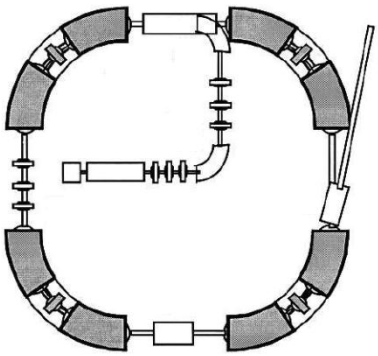

Figure 1.24. schematic design of a synchrotron.

From a technical point of view, a synchrotron is composed by different parts: sources and linear accelerator, a circular vacuum chamber (synchrotron), an exit line (Figure 1.24).
Ions are generated from plasma of radioactive sources and pulled into the linear accelerator, that provides the first ramp of energy. Then, beam is introduced in the synchrotron, where the energy is ramped up with radiofrequency cavities, whose frequency can be modulated in a wide range of values. When the energy matches the requirements, the beam is extracted in the exit line.
In order to focus and deflect the beam inside the vacuum chamber, the use of magnets is required. They are generally classified by the number of poles: dipoles (aimed at deflecting the beam in its orbit), quadrupoles (aimed at focalizing the beam inside the vacuum chamber) and sestupoles (aimed at increasing the tolerance in focalization systems).
In order to keep the beam on a constant trajectory and rise up its energy, the magnetic field has to be increased. Moreover, also the radiofrequency has to be increased at every cycle, according with beam energy (particles pulsation increase with magnetic field). If these quantities are not correctly tuned, it is impossible to accelerate particles.

Synchrotrons are bigger than cyclotron and more expensive, but they can accelerate a great number of ions, and the number of energies available increases. Cyclotrons produce beams characterized by a stable intensity. Beam energy on the contrary cannot be tuned easily, and filters and attenuators are generally required. In clinical activities cyclotrons are used to accelerate protons: technical requirements for accelerating heavier ion species like carbon ions would led to huge and very expensive magnets. For this porpoise, a synchrotron is the only realistic option. One of the advantages in the case of synchrotron facilities is that it is possible to accelerate both protons and ions, while it is impossible to accelerate ions using a cyclotron.
Another favorable aspect of synchrotrons compared with cyclotrons rely in the availability of a wider range of energies. In facts, it is possible to spill out the beam of the synchrotron tuning the number of cycles. This last is of particular relevance in clinical routine, where a fast modulation of beam energy allows to plan more accurately depth dose deposition in tissues.

1.5 Clinical indications for particle therapy

Different types of tumors can be treated with particles therapy. Some considerations valid for conventional RT are correct also for RT with particles. Obviously, The chance of tumor eradication with radiation depends on tumor-related factors, such as radio-sensitivity, volume, location and dissemination path, as well as factors related to the irradiation modality, such as the treatment plan and targeting accuracy (Orecchia *et al* 1998).
An increasing number of radiotherapy facilities around the world use beams of charged particles like protons or heavier ions like carbon (Sisterson 1999). One of the main reasons for this is the good physical selectivity of such beams and, in the case of carbon, negligible lateral scattering. Together with the techniques of active dose shaping by magnetic deflection, these physical properties offer a unique means of dose conformation, superior to conventional photon radiation (Kramer and Scholtz 2000).
Due to their particular interaction with the body, the main clinical indications for proton therapy are deep tumors, proximity of the target area to critical structures (where maximum selectivity of dose distribution is relevant), low tumor radio-sensitivity necessitating high-doses. Large tumors are, in particular, elective targets because with X-rays the surrounding tissues receive unavoidably a much larger dose (Amaldi 2001)
The National Institute for Radiological Sciences (NIRS) in Japan investigated the effect of therapy with carbon ions in a large cohort of patients. Their results indicate that carbon ion

therapy is particularly effective against a wide variety of irradiated tumors, against which photon therapy has reduced efficacy (Schultz and Tsujii 2007a, Tsujii *et al* 2007).
In a clinical trial based at GSI in Germany in 1997 (Shultz *et al* 2007b), 400 patients underwent to carbon ion RT. This study treated in particular tumors in the base of the skull or the brain. These type of tumors are very unresponsive to conventional radiotherapy, which necessitates irradiation with high tumor doses that result in severe morbidity (Durante and Loeffler 2010). The results of the clinical trial at GSI demonstrate that carbon ion RT is effective for the investigated cases.
Given the favorable tissue depth–dose distribution and the high effectiveness of cell killing, charged particles could be used for hypofractionated therapy.
It is trivial to claim particles should be preferred over photons, because to date there few data are made available and few facilities are able to offer this kind of treatments. However, results are promising, with high outcomes in those tumors particles are indicated as the best choice.
Staab *et al* (2011) in a recent study aimed at evaluating the effectiveness and safety of spot-scanning-based proton-radiotherapy (PT) for extracranial chordomas (ECC). 40 patients affected by chordoma of C-, T-, and L-spine and sacrum were treated between 1999–2006 at Paul Scherrer Institute (PSI) with proton therapy using spot-scanning.

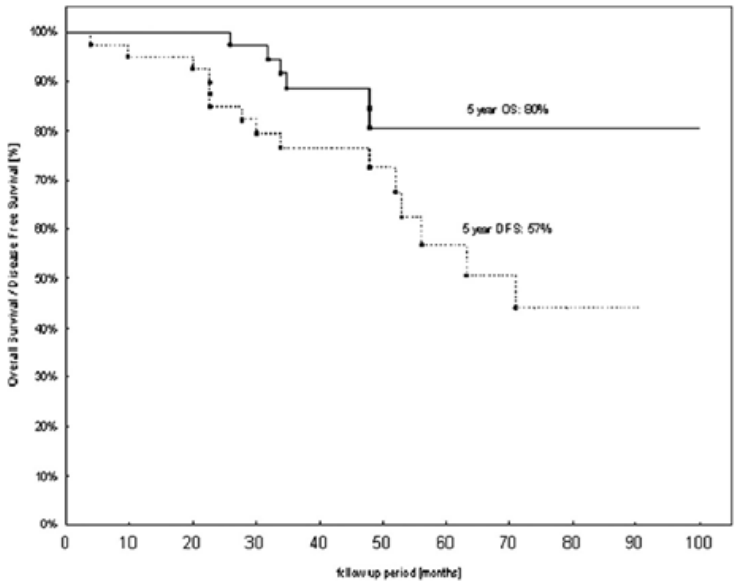

Figure 1.25. overall survival (OS) and disease-free survival (DFS) in 40 patients with external chordoma following spot-scanning based proton therapy. (Staab *et al* 2011)

Five-year results of this study indicate the safety and efficacy of spot-scanning-based PT for paraspinal tumors (figure 1.25). Actively scanned proton delivery achieves high rates of local tumor control in patients with extra-cranial chordomas even in view of large, unresectable disease (Staab *et al* 2011).
Recently the AIRO (Associazione Italiana Radioterapia Oncologica) reviewed an updating of the Italian tumor registries with the number of patients eligible to proton therapy in Italy (Zanetti *et al* 2002). The number of the patients eligible for proton therapy are reported in Table 1.1 (patients with elective indications) and Table 1.2 (patients to be included in clinical trials). Considering the data reported in the last survey of the Italian tumor registries (Zanetti *et al* 2002), about 25'000 new patients / year are affected by these tumors. Probably, only part of these cases could be treated with some clinical advantage considering the general condition of

the patients and the exclusion of cases with fairly advanced disease and distant metastases. According to Krengli and Orecchia (2004), about 10- 15%, i.e. 3'000-4'000 patients / year, could realistically benefit of ion therapy, which could be used as full treatment in the most radio-resistant tumors and as a boost after or prior to conventional radiotherapy in other cases (Table 1.3).

Tumours	New pts / year	No. eligible for protons	% eligible for protons
Uveal melanoma	310	310	100%
Chrodoma	46	45	100%
Chondrosarcoma (head, trunk)	90	90	100%
Meningioma (base of skull)	250	125	50%
Paranasal sinus	140	140	100%
Schwannoma of CNs	300	45	15%
Pituitary adenoma	750	75	10%
TOTAL	1885	830	44%

Table 1.1. number of Italian patients eligible for protontherapy.

Tumours	New pts / year	No. eligible for protons	% eligible for protons
Brain gliomas	2'600	520	20%
Brain metastases	1'000	100	10%
Head and neck tumours	6'780	1'017	15%
Unidff; Thyriod cancer	100	50	50%
NSCLCC	31'000	1'550	5%
Thymoma	110	11	10%
Esophageal carcinoma	2'840	142	5%
Biliary tract tumours	4'300	430	10%
Liver cancer	13'340	1'334	10%
Pancreatic carcinoma	9'050	1'810	20%
Cervic carcinoma	2'990	598	20%
Bladder carcinoma	16'950	1'695	10%
Prostate Carcinoma	22'390	5'582	25%
Pelvic recurrence	>500	>250	50%
Pediatric solid tumours	970	144	15%
AVMs	130	40	30%
Macular degeneration	?	?	
TOTAL	>114'490	>15'023	13%

Table 1.2. number of Italian patients eligible for protontherapy (clinical trials)

Tumours	New pts / year	No. eligible for carbon ions	% eligible for carbon ions
Salivary gland tumours	620	310	50
ENT mucosal melanoma	30	30	100%
Bone sarcoma		52	10%
Soft tissue sarcoma	520	136	10%
NSCLC	1360	1'550	5%
Hepatocellular carcinoma	31000	500	10%
Prostate carcinoma	22'330	1'116	5%
TOTAL	60'860	3'694	6%

Table 1.3. number of Italian patients eligible for carbon ion therapy.

1.6 Cost-effectiveness ratio

Cost - effectiveness ratio in RT with particles has been debated deeply in scientific community (Gademann 1994, Jones 2006, Lodge *et al* 2007), and this question has not been addressed univocally.

Even if studies in Japan and Germany have demonstrated that RT with particles is indicated as the best solution for different types of tumor (radio-resistant tumors, pediatric tumors just as examples), money required for facilities building and maintenance are huge (around hundred million of Euros). This aspect is indeed one of the main reasons why only few centers nowadays can offer this type of treatment. Indeed, if the use of protons requires a cyclotron, carbon ions requires much more complex and expensive synchrotrons. Differences between these machines are significant.

To date few clinical data are made available for quantitative considerations. Moreover, particular randomized comparative trials must be performed in order to unambiguously identify tumors for which particle therapy is superior to modern conventional radiotherapy. Even if is weird to discuss about money in applications that potentially save lives, the recent accumulation of evidences that radiotherapy with particles may be more effective than conventional radiotherapy in different tumor types put in light the need of a deep cost analysis, including long-term comparison with state of the art photon therapy.

Few years ago Orecchia *et al* (1998) reported that the average cost of cancer treatment is 15 000 DM ($8000) per patient, conventional radiotherapy costs 7000 DM ($3700) per patient, while an intensive course of chemotherapy, as applied in leukemia, for example, costs 60 000 DM ($24 000). Conformal X-ray therapy for prostate cancer costs, in Italy, the equivalent of 16 000-17 000 DM ($8500-9000). A course of particle therapy requires 20 000 DM ($10 500).

We can conclude that proton therapy, for example, is not more expensive than many of alternative therapies for tumor treatments.

Of course costs should be taken into account any advantage in terms of increased cure rate or reduction of acute and late complications rates will result in cost savings for salvage treatments. Another key point that surely need more investigations is the possibility, with particle therapy, to hypofractionate the dose, thus optimizing machine duty cycles. Moreover, it should be possible to combine boosts of conventional treatments with particle therapy sessions.

Jones (2006) has reported that Dr Neil Burnet in a personal communication has estimated from Swedish data that the proportion of total cancer care costs spent on radiotherapy would increase from the present 5% to 6% if 15% of all radiotherapy is given by protons (Ringborg *et al* 2003). This is likely to be cost effective in the long term because of the reduced side effects. Surely middle-long term follow up will provide in next years more data supporting the thesis that particle therapy has a positive cost effectiveness ratio. Other studies are addressed at needs and requirements for exploit more evidences about the effectiveness of particle therapy (Kraft and Kraft 2009).

1.7 Setup control in particle therapy

Advantages in radiotherapy with accelerated particles can be summarized as follow:

- Particles have an inverse dose profile, that allows to potentially concentrate a higher target dose, and lower to healthy tissues
- Millimeter – precision treatments
- High biological effectiveness in the target
- Relatively low biological effectiveness in the entrance channel
- Biological based treatment planning
- Low toxicity rate
- Good tumor control rate

In particular, particle therapy decreases the integrated dose, thus decreases the amount of healthy tissues irradiated. Moreover, it is a excellent tool for high dose radiotherapy. There are no evidences of unexpected acute or late toxicity due to the use of particles instead of photons. The incidence of toxicity is related to high dose escalation rather than the use of particles. To date the planned dose distribution and effectiveness have not been called into question by clinical results.

The future role of proton therapy, if compared with photons, is an high target dose coverage and the reduction of low moderate dose volumes. Moreover, the big conformability leads to a reduction of the irradiated volume, that means reduction of late effects and thus reduction of risk for inducing secondary malignancies.

The paradigm shifts in particle therapy equipment and facility design.

It should be evident that the potential advantages of particle therapy are stressed when used in combination with modern patient positioning systems, off-on line imaging, dose delivery systems well known in photon RT but optimized to the use of particles.

RT with particles is a relatively new technique, and research is active in different fields. Studies are conducted on the effects of different ion species on tissues and cells. Delivery systems are also investigated. Technology improvements are critical. Smaller and more compact accelerators could surely have a positive influence on cost - effectiveness ratio, leading to the diffusion of new facilities able to perform this treatment. Dose delivery techniques can open new frontiers in organ motion management during irradiation. The idea to perform tumor tracking on line, in case of not negligible organ motion effects incrementing therapeutic effects, is challenging but stimulating. How to save healthy tissues surrounding the tumor mass remains an open issue, and tools and software aimed at estimating the current tumor position could play an important role.

The main consideration regarding particle therapy is that high doses of radiation can be delivered to the target volume, while leaving surrounding tissues and organs at risk relatively untouched. However, this superior physical selectivity of particles could be inefficient if improved target definition and meticulous treatment planning techniques are not in use.

High technology is rapidly improving in systems devoted to patient positioning and setup control before and during the irradiation. These systems must guarantee an adequate accuracy in repositioning. Recent researches claim that 33 centers are nowadays running and treating patients with protons and 5 with protons and carbon ions (particle therapy coop group, on-line). In Europe, only two centers are now treating patients using a synchrotron. The first one is in Germany (HIT, Heidelberg). The second one is in Italy, Pavia. The National Center for Oncological Hadrontherapy (Centro Nazionale di Adroterapia Oncologica, CNAO) started to treat patients on September 22nd 2011.

A description of CNAO is reported in next chapter, focusing the attention of those systems devoted to patient positioning and setup control before and during treatment sessions.

Chapter II

The National Center for Oncological Hadrontherapy, CNAO

The National Center for Oncologic Hadrontherapy (Centro Nazionale di Adroterapia Oncologica, CNAO) is one of the first Centers in Italy able to offer a treatment with protons, and in next future it will be the first with carbon ions. In Europe only HIT, in Heidelberg (Germany) is nowadays treating patients with this technique. CNAO was ideated as a center for advanced clinical activity and research on accelerated particles. The Center is a no profit organization (Foundation) created with the financial law in 2001. It was designed by TERA Foundation. In 2003 CNAO Foundation acquired the project and hired the personnel and commenced the synchrotron design. Today CNAO Foundation has ended the commissioning of the high technology and first treatments have been started.

The Therapy with Hadronic Radiation Foundation (TERA), lead by U. Amaldi, was one of the founding Institutions. Other Institutions involved since the first stages were: the Italian National Institute of Nuclear Physics (INFN), the Universities of Milan and Pavia, the Politecnico di Milano University, and the Town of Pavia. Five major hospitals were also involved in the project.

In Table.2.1 all the participants in the projects (and their main responsibilities) are summarized.

Area	Institution	Main responsibilities
National	INFN	Co-direction; technical support; formation
	Town of Pavia	Authorizations
	University of Milano	Medical coordination; formation
	Politecnico of Milano	Patient positioning; radioprotection
	University of Pavia	Power supplies; betatron; electrical implants
	Province of Pavia	Logistics
	University of Torino	Dose delivery; treatment planning system
International	CERN	Magnets; dipoles; diagnostics
	GSI	Linear accelerator; special parts
	LPSC	Optics; betatron; low level RF; control system
	NIRS	Medical formation and activity

Table 2.1. The list of participants in CNAO projects and their main responsibilities.

Even if CNAO is equipped with state of the art diagnostic machines, the facility is not foreseen for middle-long term hospitalization. CNAO is equipped with a proprietary synchrotron. The design of the CNAO accelerator (synchrotron and beam transport lines) was developed by the European Counsel for Nuclear Research within the framework of the Proton-Ion Medical Machine Study from 1996 to 1999. The realization of the CNAO began in September 2002 with the final design of the high technology part. The two ion sources (each capable of producing protons and carbon ions) are operative, and the first beam was emitted on May 31, 2007. At the moment, carbon ion beam is under commissioning, while protons are ready for clinical use. The year 2008 was devoted to completion of high-technology installation and beam commissioning.
The final design appears as depicted in figure 1.1.

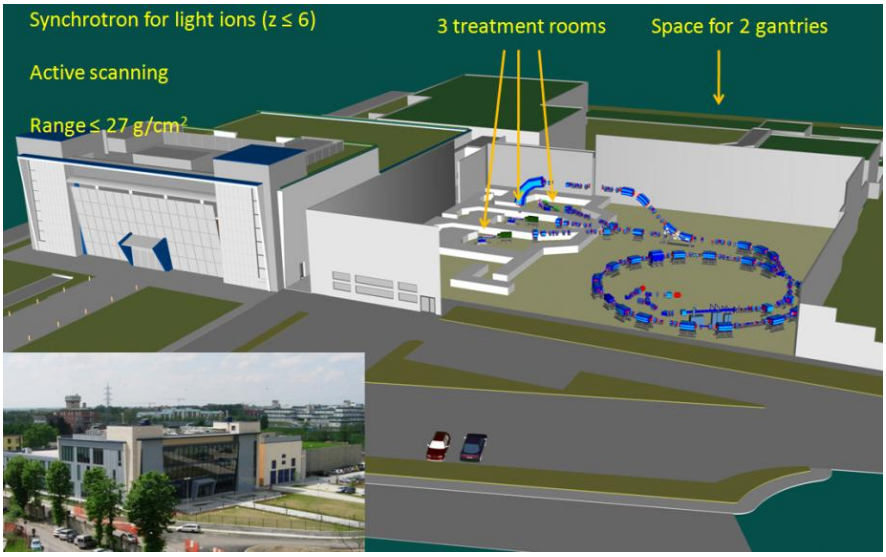

Figure 2.1. Final design of CNAO. In lower box a recent picture of the facility.

2.1 Current status and foreseen activities

At steady state, 80 % of the treatments will be performed with Carbon ion beam, while the other 20 % with protons. In this first phases of clinical activity, only protons are delivered. CNAO was built with two major missions: the first one is, obviously, clinical activity. The second one is research. These aspects are very close one to the other. Even if the benefits of particles in oncologic treatments are well established, clinical indications could be better defined for such a new therapy, and especially in a new facility like CNAO is. It is also important for readers to keep in mind that at this time CNAO is not certificate by European community (that is, it is not CE certified). As a consequence, at least in these first stages, selected patients are awarded to be included in a experimental clinical trial. Patient selection and recruitment is done under the responsibility of Medical Direction.

There are worldwide few facilities able to perform RT with particles. In order to optimize logistics, transparency and to play a relevant role in the international scenario, CNAO is working to connect the center to the international network of particle facilities and cooperative groups, and to share information about inclusion criteria in patient recruitment. This last would allow different facilities to share database and discuss about new standard. Collaborations with other institutions are frequently discussed and nowadays they include most of the major centers in Europe (HIT, Heidelberg; MedAustron, Wien; ETOILE project, ARCHADE project and Philips University of Marburg). All these initiatives impact not only on international visibility but also on the availability of a common database and a better treatment follow up. Patient recruitment is consequently wider because they could belong to foreign countries. Actually, waiting for CNAO to be fully operative, patients eligible for particle therapy are asked to moved in other facilities, with relevant costs for the Italian healthy system.

CNAO will manage not only exclusively treatments with particles but it will also perform boosts after conventional RT with photons.

At steady state the working volume will be 150 patient \ day. This number is obviously lower than the number of eligible patients. CNAO has identified seven groups of diseases that are considered at high priority: lung tumors, liver tumors, sarcomas, head and neck tumors, eye tumors, central nervous system lesions and pediatric tumors.

This list should not be intended as a static condition imposed by the Center. Different cases will be accurately evaluated by clinicians. However, the main goal was to concentrate the efforts and beam time on those pathologies particles are proved to be effective.

CNAO is also a Center for research activities. An additional beam line is foreseen for research purposes. Moreover, a work package of an European project (ULICE) is devoted to the feasibility study of a rotating gantry for carbon ions. Other foreseen research activities are correlated to the use of different ion species (like oxygen) and activities on dose delivery systems, in order to allow active tumor tracking.

The first treatment started September 22nd and now it is ended. Three patients are undergoing treatments with protons in these days (November 2011).

CNAO personnel is going on working on commissioning of carbon ion beam. In the meantime treatments with protons will continue: in 2012 CNAO foreseen to treat 170 patients. Next steps have been recently indicated by CNAO management, and they regard: the conclusion and the certification of protocol with protons (December 2012); pre-clinical activities with carbon ion beam (to be concluded in July 2012) and first treatments with carbon ion beam (October 2012).

2.2 Workflow analysis

CNAO is a facility for diagnosis and treatment. CNAO is equipped with state of the art diagnostic machines, but as already mentioned, there is no service for long recoveries. CNAO requires every patient to repeat all the diagnostic examinations. This condition is mainly required by medical doctors and it is justified by the effort to standardize processes. The list of diagnostic machines actually available in CNAO comprehend:

- 1 4D CT (Siemens SOMATOM Sensation Open)
- 1 CT/PET (Siemens BIOGRAPH 6 TruePoint)
- 1 MR (Siemens MAGNETOM Verio)

This operational choice allows operators to focus on the treatment planning, treatment sessions and to the workflow optimization. A general scheme of the entire process is reported in figure 2.2.

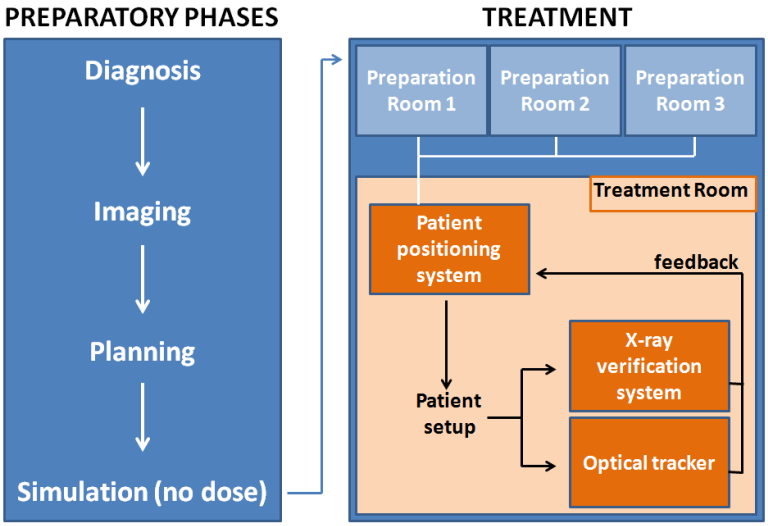

Figure 2.2. Scheme of the process: from diagnosis to treatment.

A workflow analysis has been performed and has shown that the facility will be able to deliver more than 18,000 treatment sessions per year at steady state. Particle therapy, and especially carbon ion RT, has shown a consistent trend toward hypofractionation. This is mainly due to the evidence that ions do not have a shoulder in the dose-survival curve, which correspond to the main reason why conventionally 1.8-2 Gy / fraction are delivered in conventional RT.
The design of the facility has specifically addressed this issue, and dedicated (computer-aided) positioning rooms have been built. Patients are positioned and immobilized on dedicated treatment tools (carbon couch or chair) outside the treatment room and then carried into the treatment rooms on a transport system, thus realizing an evident workflow optimization.
Treatment couches or chairs are docked to a state one of-the art, 6 degrees of freedom, patient positioning system. It is important to point out that a modern center for RT is usually equipped with different systems aimed at setup control, before and during the irradiation. As described at the end of the previous chapter, this check is even more relevant in RT with particles than with photons. Setup verification is always performed before irradiation with orthogonal kilovoltage X-ray images of diagnostic quality. Additionally, an optical localizer with marker detection and surface detection capabilities is used for real time monitoring.

2.3 Beam generation and delivery

The synchrotron accelerates proton and carbon ions to a maximum energy of 400MeV/u (corresponding to 27 cm penetration depth in water). The accelerating machine is composed by different parts, and a scheme of the units is represented in figure 2.3]

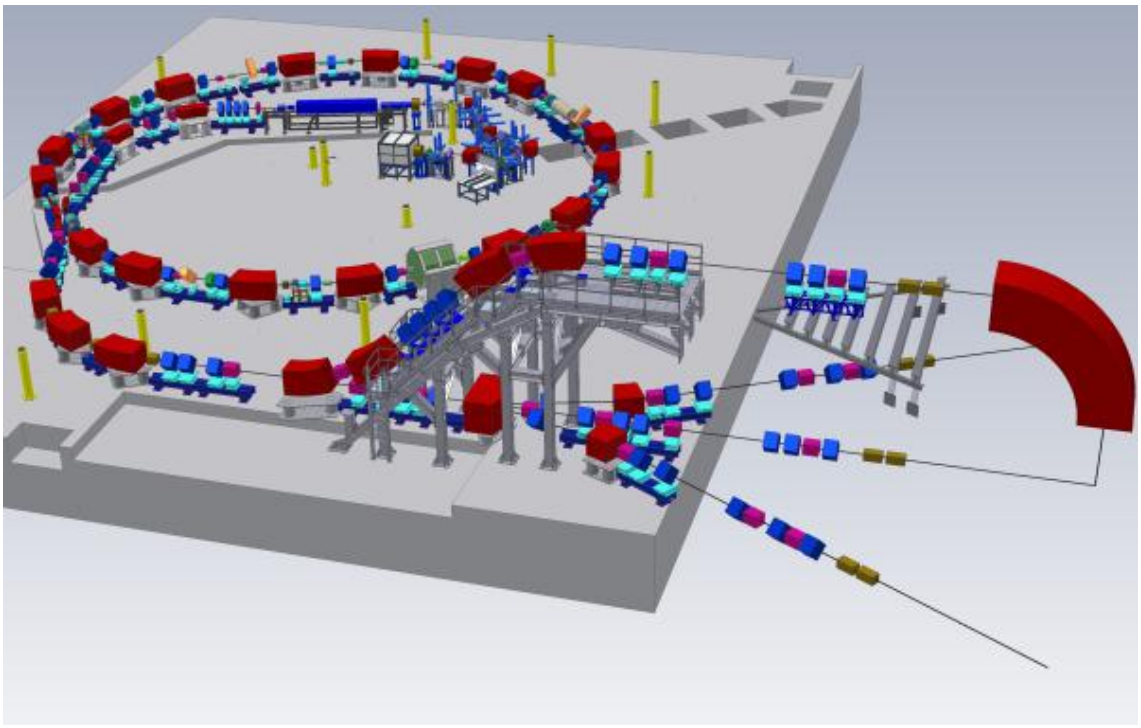

Figure 2.3. Scheme of the CNAO accelerator.

Below, the main components of the accelerator machine are described.
LEBT: the low energy beam transport (LEBT) is composed by the sources and by the first line, that connects the sources with the linear accelerator. In this track a continuous beam is generated. Energies are: 0.008 MeV/u for H^{3+} and 0.008 MeV/u for C^{4+}.
RFQ-LINAC: the radio frequency quadrupole (RFQ), running at 217 MHz, ramps up the energy to 0.4 MeV/u and injects the beam in the linear accelerator (LINAC). At the end of LINAC beam energy is up to 7 MeV/u.
MEBT: this is the section that transports pre-accelerated particles from the LINAC to the synchrotron. The middle energy beam transporter (MEBT) not only aligned the beam to the synchrotron, but it is also characterized by different high technology devices. For example the stripping foil, that scrubs away residual unwanted electrons.
SYNCHROTRON: the 24 m diameter ring accelerated particles in a range of 2-250 MeV in the case of protons and 7-400 MeV/u in the case of carbon ions. There is the betatron core. Even if, obviously, each of the components in this list is fundamental, the synchrotron represents the heart of the high technology. It was designed for a slow extraction of the beam.
HEBT: the high energy beam transporter (HEBT) connects the synchrotron with the treatment rooms. Once reached the required energy, beam is spilled out from the ring and driven in the exit line corresponding to the desired room.
A summary of the reachable energies, for each section, is reported in Table 2.2.

	Energy [MeV/u]			
	LEBT	MEBT	SYNCHROTRON	HEBT
Protons (<10^{10} per spill)	0.008	7	7-250	60-250
Carbon (<4 10^{8} per spill)	0.008	7	7-400	120-400

Table 2.2. Summary of energies achievable.

Three rooms equipped with fixed beam lines (two rooms with a horizontal beam and one room with vertical and horizontal beams) are operative for patient treatments. During first trials, CNAO treats patients only in one room, in order to accelerate the commissioning of carbon ion beam using the remaining rooms. In figure 2.4 is reported the design of the treatment rooms, while in figure 2.5 a recent picture of room 1 is shown.

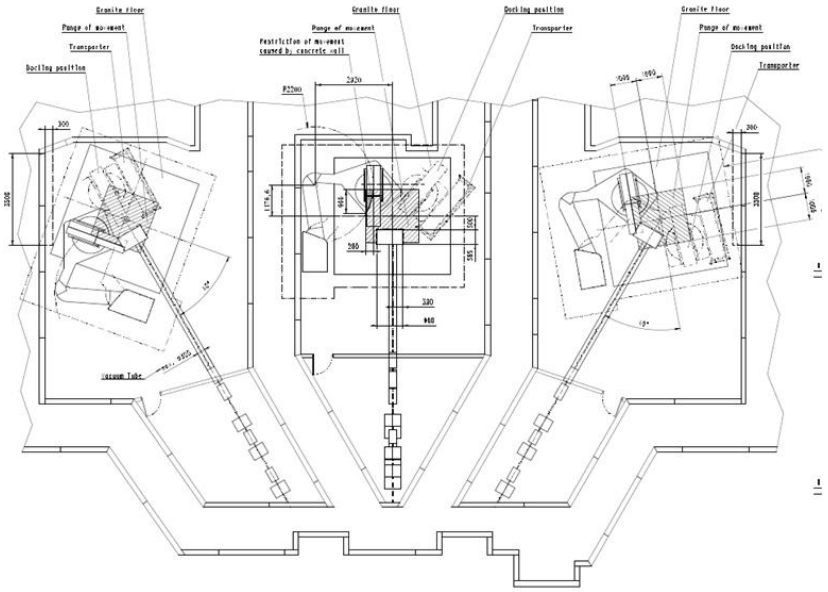

Figure 2.4.Draws of the three treatment rooms.

Figure 2.5. Treatment room 1. A carbon couch is docket to the PPS.

The facility will be upgraded in a second phase with a room equipped with a rotating gantry. It is important to point out that all the rooms are designed for proton and carbon ion therapy, and switching between protons and carbon ions on a patient by patient basis will be possible without impacts on the time schedule.

2.4 Dose delivery: Beam scanning

In chapter I readers can find a description of the characteristic profile of particles' dose distribution in depth. Bragg peak allows to release the higher energy ideally in a point, saving entrance pathways and tissues around this area. It was shown that more than one Bragg peak can be combined to obtain profiles of uniform dose distribution in the treatment volume. Summarizing, there are mainly two different methods to obtain the so called Spread Bragg peaks (SOBP): the first one is passive (that is, one energy spill, use of range shifters to compensate the depth) and the second one is active (that is, sum of different spills by tuning accelerator parameters). In the first case (passive), the beam produced by the accelerator is processed through ridge filters or rotating modulator wheels, realizing the spread out Bragg peak. Collimators are then used to conform the desired geometry. It is also necessary to include a bolus, personalized for each patient, for depth compensation. Even if this technique allows to concentrate all the geometrical operations near the end line of the beam, it is difficult to manage the residual dose in proximal area of the irradiated body. The activation of tools aimed at beam conformation should be taken also into account.
Recent facilities (CNAO is one of these), use an active system, that means that the energy and the conformation of beam is set before and during irradiation by tuning machine parameters. Target volume is irradiated according to the planned geometry and spot size. In this case there are mainly two different types of irradiation techniques: raster scanning foreseen a constant irradiation while the beam steering is in progress. Spot scanning requires to deposit the dose in each spot-size volume, and to turn off the irradiation while the beam is moved trough different spot-size subvolumes.
In order to control the steering of the beam, it is necessary to consider both depth variations and lateral corrections. To obtain different depth in dose delivery, it is necessary to spill different energies. To deflect the beam in lateral directions, a couple of orthogonal magnets are generally used (figure 2.6).

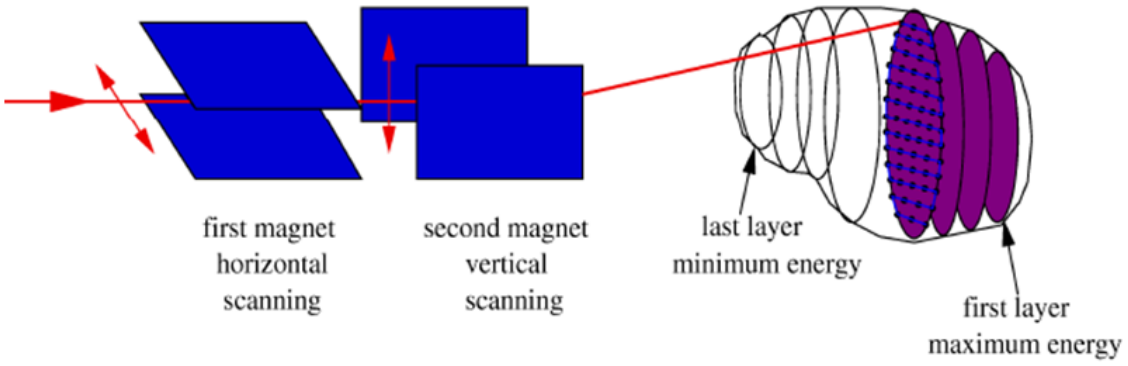

Figure 2.6. Steering magnets in an active scanning system.

CNAO employs an active spot-scanning system. Two orthogonal magnetic fields are used to scan the beam in planes parallel to its direction. Magnets are designed to allow scanning of square of 20 x 20 cm. Depth is varied directly by adjusting the beam energy. The smallest step of penetration range achievable is 0.2 mm. The synchrotron allows variation of the energy at each spill, so that every second it is possible to irradiate a layer at a different depth. Different spot size are available (with a radial size adjustable from 4 to 10 mm, in steps of 1 mm). The active scanning system and the dose rate have been designed to be able to deliver 2 Gy to a volume of 1 liter in 1-1.5 min (Orecchia *et al* 2009).
Other key features necessary to take advantage of the high spatial precision of particle therapy are an accurate identification of the target and a precise and reproducible patient setup. The facility is equipped with dedicated devices aimed at guarantee the highest accuracy in patient repositioning and set up control. These systems are described in next paragraphs.

2.5 Computer Aided Positioning in Hadrontherapy

The Politecnico di Milano collaborates with CNAO in developing all the patient setup procedures. The Institution has participated as consultant and supervisor in selection, control and installation and it was responsible for the commissioning of these systems.
One of the major issue in RT with particles is that they exhibit higher sensitivity to set up errors. This implies the need for adequate patient positioning systems to ensure the highest accuracy and control. The rationale, based on conventional RT experience, was to optimize image guidance technologies with an high accuracy positioning device in an automated procedure for real-time control. Computer Aided Positioning in Hadrontherapy (C.A.P.H.) project started with this aim.

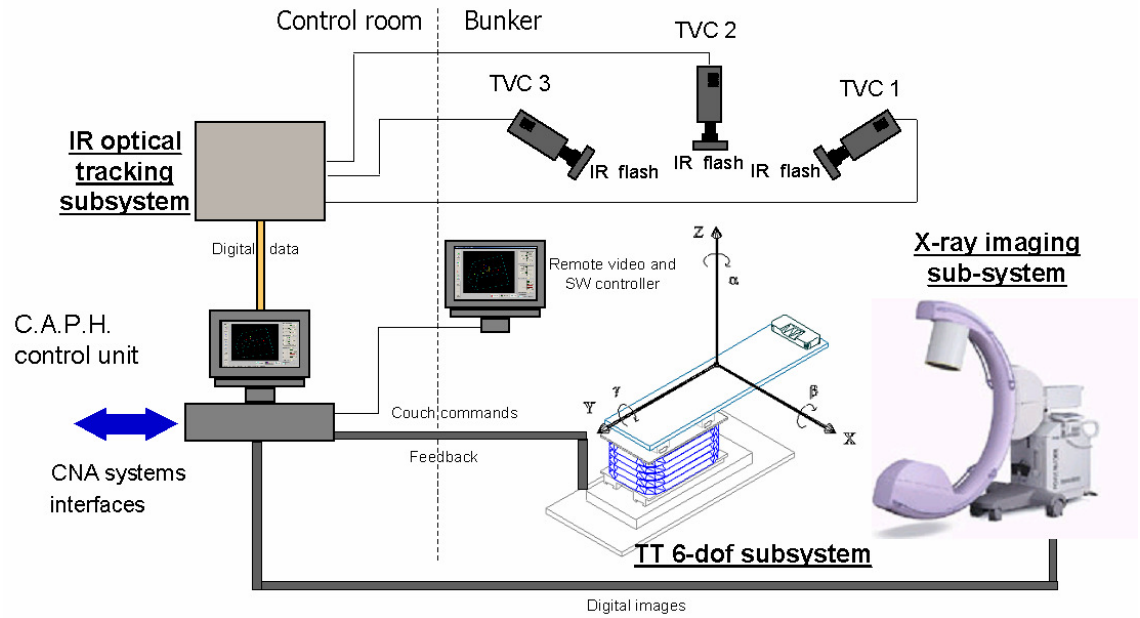

Figure 2.7. Interactions between systems of CAPH project.

At startup the project had two main goals. The first one was to provide the best accuracy and overall quality in treatment positioning procedures. The second was to optimize the efficiency of the workflow, minimizing time consumption. For these reasons, time consuming preparation activities are handled in dedicated rooms, and the procedures in treatment rooms were designed in order to reach an high level of automatization.

The selected approach is depicted in figure 2.7, and it is based on the integration of different sub systems:

- A robot for automatic patient positioning.
  Hardware was provided by Schaer Engineering, while steering and control software was designed by Odevis.
- A in-room imaging verification system.
  Also in this case hardware was provided by Schaer Engineering. The steering and control of the system was ideated by Odevis. The image registration software was provided by Medcom (Verisuite Software).
- An optical tracking system for real time setup verification.
  Hardware was provided by BTS Bioengineering. Layout and software was developed by Politecnico di Milano.

All these systems and their specifications are described in details in next paragraphs.

2.5.1 Patient positioning system

The patient positioning system (PPS) is a robotic arm featuring 6 degree of freedom. It is a pantograph laid on the floor equipped with a coupling system. The basement of the PPS moves on a granite floor where attrite effects are minimize by a layer of compressed air. The movement area of the device is defined by the granite plates. The evenness of the granite surface is $\leq$ 0.02mm for a surface with a radius of 10mm, 0.1mm for a surface with a radius of 500mm and 0.3mm for a surface with a radius of 3000mm. The required air flow for the PPS is 133.3 l/min at 10bar.
The PPS was primarily designed for fixed-beam applications. It can be coupled with a treatment couch or chair, and it provides an adequate range of patient setup possibilities.
Patients up to 200 kg can be aligned to the nominal position. Horizontal translation movements are supported by an air bearing, switched off when the final position is reached. This way, compensation of attrite large forces is not needed and a precise repositioning is allowed.
The mechanical construction has been designed so that failures of the mechanics cannot lead to patient injury, and safety systems were considered (both software and hardware).
In figure 2.8 a scheme of the PPS is reported (while in figure 2.9 translational and rotational conventions are reported).

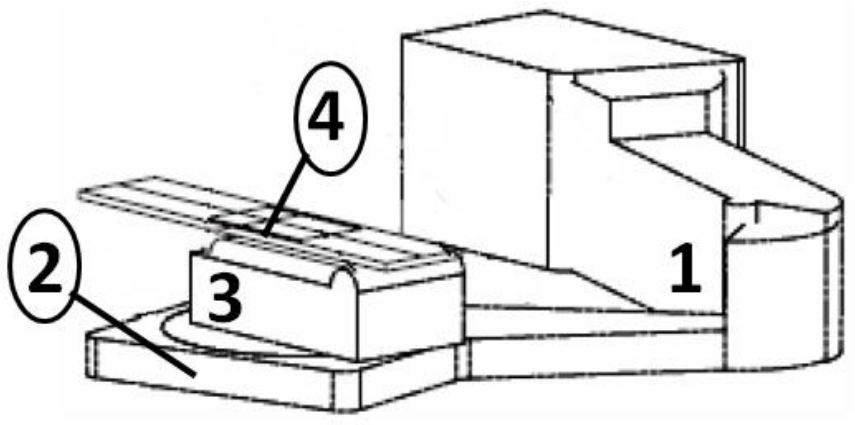

Figure 2.8. Sketch of the PPS

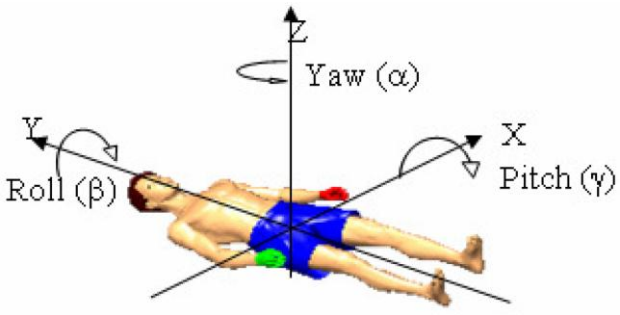

Figure 2.9. Rotational and translational conventions.

According to figure 2.8, a description of the PPS and its main components is reported below.

1. pantograph

The pantograph consists of two arms that rotate around two points. The rotation of an arm is achieved by using a spindle with a servo-motor. For the position verification two absolute encoders are directly mounted on the spindle. Additionally, the two extreme positions of each arm are verified with limit switches.

The arm rotation may not exceed 7°/s and the travel speed may not exceed 100mm/s.

The compressed air supply is verified by two sensors and regulated by one valve.

2. rotation unit

The rotation of the rotation unit is achieved by using a cogwheel and a servo-motor. The position of the rotation unit is verified by two absolute encoders and one angle measurement system.

For the pantograph to move the rotation unit needs to be slightly elevated, this is done with 16 air bearings and a supply of compressed air (regulated in the pantograph).

The rotation of the rotation unit may not exceed 7°/s and the travel speed may not exceed 100mm/s.

3.vertical lift

The vertical lift is achieved by using a spindle with a servo-motor. For the position verification two absolute encoders are directly mounted on the rotation axis. Additionally, the two extreme positions of the vertical lift are verified with limit switches.

The speed of the vertical lift may not exceed 100mm/s.

4.pitch\roll

The pitch and roll movements are achieved by using two spindles and a servo-motor for each spindle. For the position verification two absolute encoders are directly mounted on each rotation axis. Each extreme position is verified by a limit switch.

The rotation of the pitch and roll may not exceed 7°/s and the travel speed may not exceed 100mm/s.

According to technical specification provided by the manufacturer, range of motion and accuracy of PPS are:

Translations:

X: • ± 1000 mm

Y: • ± 1000 mm

Z: from 700 mm to 1300 mm above ground

Rotations:

Yaw: • ± 185° (with respect to room coordinates)
Pitch: (depending by the height, up to) ± 30°
Roll: (depending by the height, up to) ± 15°

Absolute precision of the PPS (open-loop error in point positioning in room coordinates) is ≤ ± 0.3mm in translations and ≤ ± 0.1° in rotations (Martin *et al* 2007).

2.5.2 Coupling Mechanism

Hereafter the procedures for coupling couches and treatment chairs to the PPS are reported.

2.5.2.1 Couch coupling

The transport system for the couch is manually operated and its purpose is to move the patient on the couch at a height of 800mm. The transport system consists of a frame and four wheels and a brake system for immobilization (figure 2.10).

Figure 2.10.Couch transport system.

Before the coupling procedure can start, the vertical lift of the PPS is moved to a predefined coupling height. A mechanical guiding system helps the user to position the couch correctly. Once the transport system and the couch are correctly aligned to the basement of the PPS, operators brake the transport systems and continue the docking procedure via software. Two light emitters and two receivers detect when the couch is in position, after which the vertical lift is moved to the coupling position (that is, the coupling mechanism makes contact). In this position the same light emitters and another two receivers detect if the couch is still correctly positioned. A linear actuator is then activated to couple the couch, the two positions (closed and open) are verified by limit switches. The couch is lifted for transport system removal.
The coupling mechanism detects automatically which device is mounted by using two barcode-readers. Additional information, as patient ID, can be stored in the barcode.
For patient specific adjustments four load cells are integrated in the coupling mechanism.
These sensors play an important role in compensation of the weight.

The couch is designed for a load up to 200kg, and it is made of carbon fiber and foam core, built as a sandwich construction, usable for X-ray pictures and allowing the possibility to perform treatments trough the couch.
The weight of the couch is 20kg, and its dimensions are 2300mm length, 500mm width, and 50mm thickness.

2.5.2.2 Chair coupling

The procedure for coupling and weight compensation is exactly the one described for couch. The transport system (see figure 2.11) for the chair is manually operated, as for the couch. It consists of a frame and four wheels and a brake system for immobilization.

Figure 2.11.Chair transport system.

The chair is designed for a load of up to 200 kg, and it is equipped with a head fixation for the immobilization of the patient during treatment. The inclination is verified by two potentiometers that needs dedicated external electrical connections.
The seat height and leg length of the chair can be manually adjusted to best fit patient's anatomy.

2.5.3 Patient verification system

The patient verification system (PVS) installed is a stereoscopic X-ray imaging device suspended from the ceiling, that can rotate around the vertical axis according to the treatment table position. The PVS is supported by vertical beams, and stabilized by horizontal beams fixed to the concrete. Both X-ray tubes and flat panels are deployed only during imaging, when the tubes pivot whereas the flat panels slide into position. Time consumption for deployment is lower than 30 seconds.
PVS is installed in room 1 and room 3. No PVS is installed in room 2 (the one with two beam lines) because of the presence of the vertical nozzle. A different design has to be taken into account, and feasibility studies are going on.
The function of the PVS is to provide a double projection kV X-ray with high-resolution flat panel detectors. It is intended to be used before irradiation, when the set up is verified using a dedicated software that performs image-based registration between images acquired in the treatment room through the and the corresponding DRR (Digitally Reconstructed Radiograph) extracted from the treatment planning CT. More images can be acquired during treatment, for example to check again the setup or in the case of multiple fields.

Summing up, the system has to provide:

-double projection X-ray images.
- automatic registration of images with treatment plan DDRs (mutual information) and point-based registration.
- Estimation of set-up correction on bony anatomy and/or manually selected markers

Each x-ray system has an image receptor, an X-ray generator and an X-ray tube. Based on the X-ray results, the Verisuite software calculates the correction vectors of the misalignment of the bone anatomy on basis of a high resolution CT picture acquired during planning phases. The software (Verisuite, Medcom) installed on a dedicated workstation provides several different tools for PVS operations and provides also different modes for calculation of the position verification (manual alignment, manual and automatic or fully automatic).
In figure 2.12 a scheme of the PVS is reported.

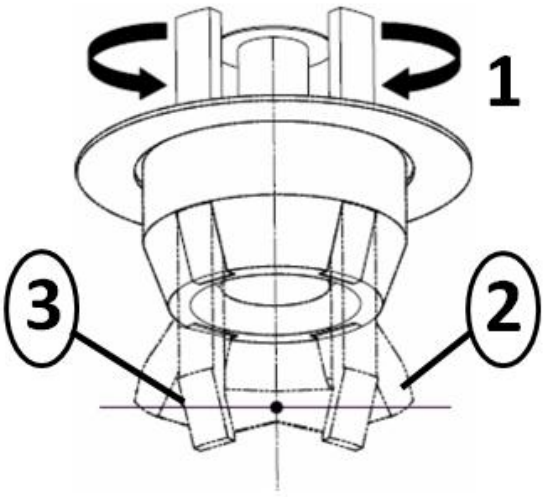

Figure 2.12. Sketch of the PVS.

According to figure 2.12, a description of the PVS is reported below.

1.Rotation

The rotation of the rotation unit is achieved by using a cogwheel and a servo-motor. The position of the rotation unit is verified by two absolute encoders.

The rotation of the rotation unit may not exceed 7°/s and the travel speed may not exceed 100mm/s.

A mechanical stop is integrated in the system at ±185°.

2.X-ray

The PVS consist of two X-ray tubes and two collimators for position verification. The X-ray tubes have two positions, extended for X-ray imaging and retracted when not in use or during irradiation.

The rotation is achieved by using an asynchronous motor. The two positions (extended and retracted) are verified by limit switches.

The rotation of the X-ray tubes may not exceed 7°/s and the travel speed may not exceed 100mm/s.

3.Flatpanels

The PVS consist of two flatpanel arms for position verification. The flatpanels have two positions, extended for X-ray imaging and retracted when not in use. The movement is achieved by using a chain and an asynchronous motor. The two positions (extended and retracted) are verified by limit switches.

The speed of each flatpanel arm may not exceed 100mm/s.

Image receptors are a Varian 4030E digital flat panels featuring a resolution of 3200x2300 pixel (~ 30 x 40 cm pixel area; 0.127mm pixel size). X-ray generators (Varian) allow to acquire an image every 3 seconds and feature 150 kVp, 640 (optional 800) mA.

Accuracy of movements, in respect to specifications, are:

- Translations of flatpanels: ≤ ± 0.15mm (diagnostic positions of the flat panels)
- Rotations of X-ray tube: ≤ ± 0.15mm (diagnostic positions of the X-ray tubes)
- Rotation of the entire system: ≤ 0.1°

2.5.4 Safety

Both PPS and PVS are equipped with an anticollision system, to guarantee the safety of operators and patients. There are two levels of alarm: the first is managed by software, while the second is hardware based. During automatic drives, a position have to be pre-edited in the GUI. If this position is not compatible with room geometry, collisions are avoided by an error box message on the control GUI, that requires the operator to stop the current drive and to enter a new one. If this message box is ignored (continue drive is sometimes allowed in manual mode), the speed of the PPS is automatically slowed down until a recovery is needed.

To avoid potential crashes, collision plates were mounted on the moving parts of the systems. (see figure 2.13).

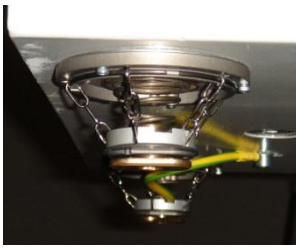

Figure 2.13. A detail of the anticollision system.

Light emitters and receivers are used to detect if a collision plate has been actuated (so if the spring is compressed by an accidental crash). The system complies with the standards for human safety.
Even if the availability of OTS gives the opportunity to track in real time the position of passive markers, and so to detect misalignments due to patient's movements, the PPS basement is equipped with weight sensors, able to provide a feed back to the control system, interrupting the operations if an over threshold change in weight load is recorded.

2.5.5 Optical Tracking System

The otpical tracking system (OTS) features three TV cameras (digital with IR illumination, ~680 nm) for stereophotogrammetric real-time 3-D localization of passive markers or laser spots (projected onto patient's surface). The system provides also a real-time visual feedback for operators and real-time detection of breathing phases.
The layout was optimized to allow the integration of functionalities under a unique control and man- machine interface, minimizing the impact on other hardware installed in treatment rooms. Cameras are mounted on a custom suspension placed on the gantry (see figure 2.14).

Figure 2.14. TVC mounted on the nozzle.

At this time, the system is ready for point-based localization with passive markers. It will be progressively updated to surface detection by integrating additional HW components, like laser scanners, and appropriate SW modules.
The synergy between in-room imaging capabilities and optical tracking in CNAO is a fundamental issue for applied clinical research as it represents one of the preferred approach for real-time tumor targeting in extra-cranial carbon-ion therapy (Seppenwoolde *et al* 2007, Brown *et al* 2007, Hoogeman *et al* 2009).
The OTS reduces time consumption during the first alignment of the patient. Moreover, it provides interlock generation in case of undesired patient motion, and would allow on-line breathing phase detection for gated irradiation. One of the drawback in this systems could be represent by the periodic need of a calibration. By the way, the position of TVCs and the rigidity of the suspension require a swift calibration only if morning QA procedures are not between specifications.

In a steady state, detection and registration of hybrid configuration of control points (laser spots, passive markers) with immobility verification (particularly suited for enhancing control points redundancy while keeping the presence of few reliable corresponding control points) will be allowed.
The optical localizer is a COTS product (commercial off-the-shelf) equipped with specific HW for data synchronization with multiple systems. The system is CE certified for clinical use, although not in RT.
Politecnico di Milano has provided a proprietary CNAO-SW module, that ensures high flexibility in using the system, providing also an ideal framework for the definition of custom setup procedures.

From the procedural point of view, the OTS is used before image -based patient position verification (for quantitative verification of patient position) and during irradiation, with continuous real-time verification of patient position and providing computation of a breathing signal for gating. In order to do that, a reference configuration of markers (or surface) have to be stored during planning phases. At this time, CT rooms are not equipped with an OTS. The approach is to use radio-opaque passive markers applied before diagnostic imaging. Thus, their reference position in reference to patient's surface can be extracted directly by the treatment plan.

Details about OTS hardware specifications are reported below.

- Field of view (FOV): 500x500x300 mm^3 around isocenter
- Peak error in 3-D fiducial localization: ≤0.5 mm
- Real-time point-based or surface based registration guarantee at 15 Hz sample rate

It is important to underline that the final result of the collaboration between the Center and the Politecnico di Milano consists of a CNAO proprietary system capable of point-based, surface based and hybrid registration for patient position correction, real-time immobility verification and respiratory gating. The system is novel with respect to all the available systems on the market, and represents a CNAO specific product.

2.5.6 Interfacing with CNAO systems

PPS, PVS and OTS have to deal and be integrated in CNAO network. The communication uses dedicated Ethernet cables. Many systems must be connected: patient archive, PACS, oncology information system, supervision system, beam delivery system are just examples. As usual (and sometimes mandatory) in clinical facilities, clinical/treatment planning information exchange is based on DICOM / DICOMRT/ DICOMRT-ION standards. Moreover, interlock signals should occur as soon as the causing effect takes place. Fast interfaces are taken into account, based on optical communication platforms with chopper and/or vertical dumpers. A comprehensive description of the interfaces, or the communication modules, does not represent one of the aims of this thesis. However, for completeness, a scheme of the communication connections of the systems described in this chapter is reported in figure 2.15.

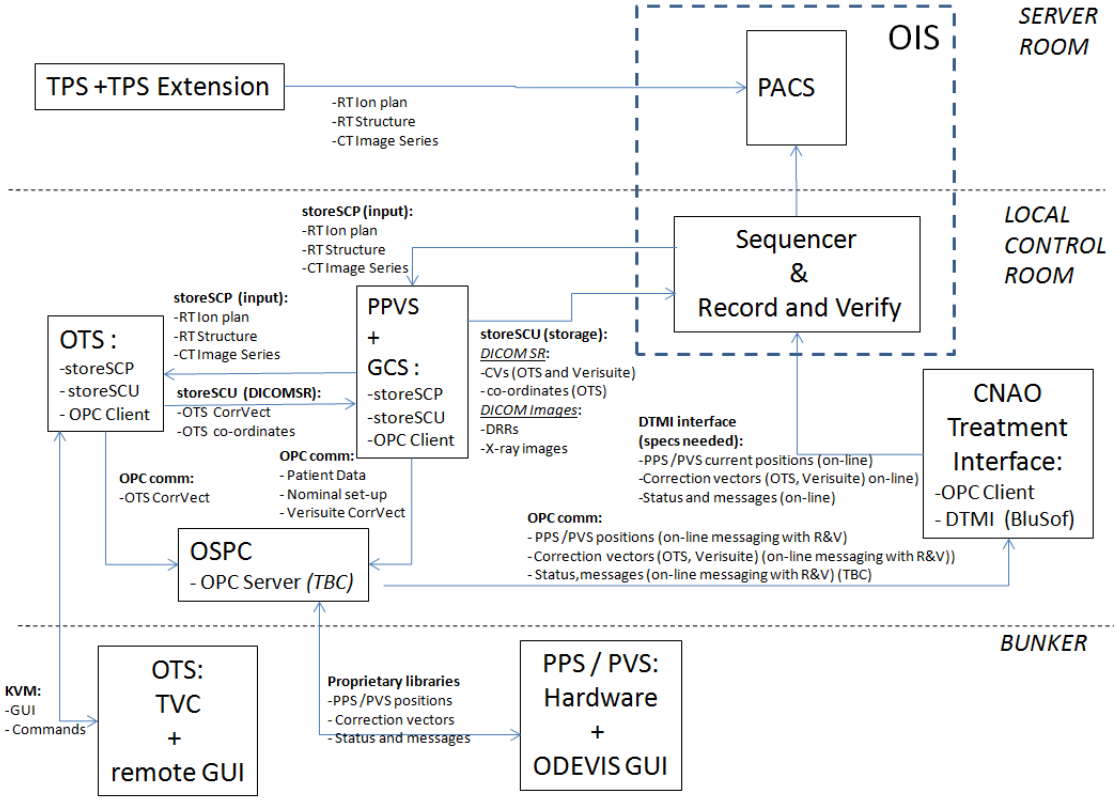

Figure 2.15. Interconnection scheme between systems

2.6 Material and methods for systems commissioning

The systems described in previous paragraphs were installed in the treatment rooms between 2009 and 2010. The reasons why an high accuracy is required in set up procedures have been discussed. In order to verify that functionalities were conformed to the expectations, CNAO required a set of measurements and evaluation reports.

Different measurement sessions were performed to test the accuracy of the PPS and the PVS, over a period of two years (2010-2011). Measurements were conducted also to optimize the procedures and check the consistency of accuracy in the largest working volume possible.

To investigate the accuracy of the PPS we used a Leica laser tracker. Both couch and chair were tested, applying sockets on their surface as control points.

Concerning the PPS, we performed measurements without and with an additional weight applied to treatment tools, to simulate the presence of a patient. We operated in this way to test two different situations: we wanted to simulate the presence of a patience and to test the correctness of compensation adopted by the PPS.

Also PVS accuracy in rotation and linear displacements of tubes and flat panels was investigated. In principle, the setup chosen was the same used for PPS testing. Several sockets were applied to the moving parts of the cylinder and registered by a Leica laser tracker (0.01 mm\m accuracy). Two sets of acquisitions were performed: the first one was intended to quantify the errors in PVS rotations, the second one to quantify the errors in repositioning of flat panels and X-ray tubes during their deployment (linear repetitions). Moreover, a last quality assurance test was performed. We firstly aligned a radio-opaque object at the isocenter. This tool is usually utilized by medical physicists for laser cross calibration

verification. Then, we acquired Xray images with the PVS. Imaging software (Verisuite, Medcom) allows to display on screen the center of the flat panels, that corresponds to the projection of the isocenter supposing tubes correctly calibrated. We evaluated the distance of this point from the top of the custom tool, to verify the consistency between different tools.

2.6.1 Leica Laser Tracker

During measurement campaigns we used a Leica Laser Tracker model LT(D)500 (figure 2.16).
This is a high accuracy measurement tool, widely used in industry. An example of application is represented by robots calibration, but this is also the tool that CNAO personnel used to align synchrotron components. It resulted particularly indicated in our case because first of all it is mobile (useful to reduce time consumption for multiple rooms campaigns). It also has an adequate automation, that allowed us to place the laser tracker in a defined position on the granite floor and to perform the required set of measurements.
This laser projector has a built-in laser interferometer, featuring a range of measurement summarized below:

- horizontal ± 235°
- vertical ± 45°
- distance 0–35 m (0–115')

The accuracy, as declared by manufacturer, is:

- Angle resolution 0.14"
- Distance resolution 1.26 µm

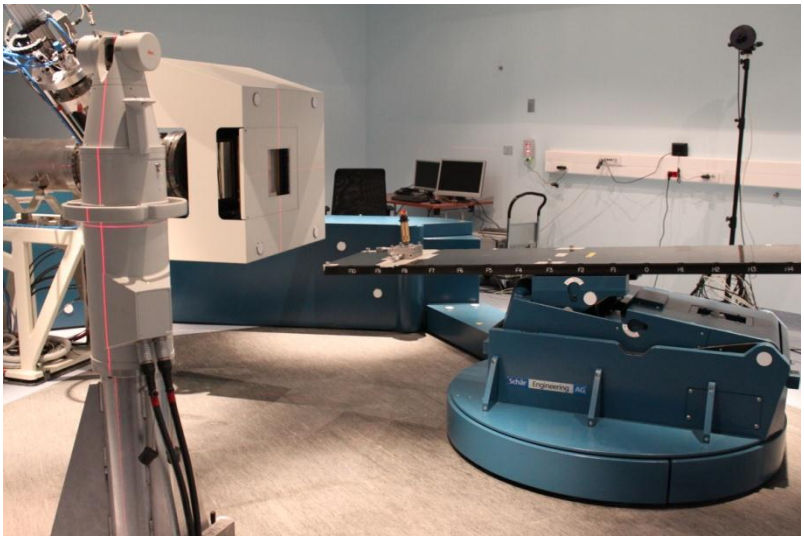
Figure 2.16. Leica laser tracker

For our purposes the best retro-reflector was a corner cube reflector (figure 2.17). A set of magnetic sockets were glued directly on the couch or on the carter of the treatment chair at the beginning of each measurement session.

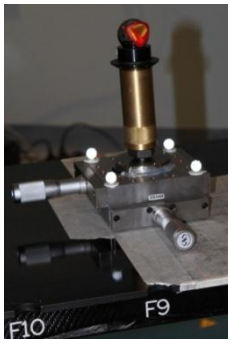

Figure 2.17. Corner cube mounted
on the measurement tool.

Data were storage into the laser tracker control computer, and then exported in text files. An offline analysis was performed with Matlab (Matlab, MathWorks Inc).

2.6.2 Data analysis

A reference position was set to the PPS controller and recorded by means of the laser tracker. The only requirements in this operation was to match one of the control points in the nominal room isocenter. Then, different operators moved the PPS, imposing different sets of rotations and translations. All markers were again recorded by means of the laser tracker. Off line data were exported in Matlab (The MathWorks, Inc), and roto-translations were applied to the reference position, according to what was performed in the bunkers. Two sets of marker coordinates were available at this point: a first one concerning a nominal, calculated position. The second one concerning a measured position, as seen by the laser tracker in treatment rooms. Differences between these two sets were evaluated and statistical analysis was performed. Results of the measurements campaign are shown in next paragraphs.

2.6.3 A custom tool for PVS quality assurance

In order to check the consistency of PVS imaging with laser cross (that is, a cross produced by laser projectors mounted on each room wall, used by medical doctors and physicists to pre-align the patient or measurement tools) a dedicated setup was needed. We placed a radio-opaque tool aligned with laser cross and we evaluated via software the discrepancies between double X-ray projections and laser cross alignment. In figure 2.18 the tool used for these tests is depicted.


Figure 2.18. picture of the custom tool used
to check the consistency between laser cross and PVS.

2.7 Results of CNAO positioning systems commissioning

This section provides results of the measurement campaigns carried out in CNAO, aimed at quantify the accuracy of the systems (PPS and PVS) installed in the treatment rooms. Measurements were carried out in the period 2010-2011. The manufacturer claimed a PPS accuracy of 0.3 mm in 3D repositioning in the treatment area, and an accuracy of 0.1 ° in PVS rotations. Reports about this requirements were included in the contract between the manufacturer and CNAO. Preliminary measurements were carried out in the manufacturer facility by a third company : GDV Ingenieurgesellschaft Holst mbH (GDV). Their results are summarized in table 2.3.

PPS testing (accuracy)	
Repeatability in XY raster (±250 mm)	0.2 mm
Accuracy of rotation axis (yaw)	0.09 mm
Accuracy of roll axis*	0.14 mm
PVS testing (accuracy)	
Continuous rotation (±180)	0.1 mm
Absolute rotational positioning (60° step)	0.01 mm
X-ray tube deployment	0.13 mm
Flat panel deployment	0.02 mm

Table 2.3. Preliminary measurements done by GDV in the manufacturer's facility.
*measured at -25° roll and 12.5 pitch with a eccentric load (144 Kg with 660 mm lever action)

The same company repeated the set of measurements after the installation of the systems in Pavia. Those measurements were performed to guarantee that the accuracy of the systems was maintained. The compliance of the systems with patient's safety, here intended as speed of the PPS, acceleration of the PPS and breaking distance after pressing the emergency buttons were investigated.
A more comprehensive set of measurements was conducted by Politecnico and CNAO personnel, aiming at testing both the isocentricity in pure rotations and the overall accuracy of the systems. On the top of all, by CNAO side, the aim was to test separately the PPS coupled with the carbon couch and the treatment chair, to simulate a clinical workflow. The instrumentation used (Leica laser tracker, 0.01 mm\m accuracy) is described in the previous paragraphs.
This section is organized as follow:

- Commissioning of the PPS
    - Report and results by GDV with random movements (4 control points)
    - Report and results of Politecnico group with random movements
        - Preliminary test of isocentric rotations
        - Couch (6 control points plus isocenter)
        - Chair (4 control points plus isocenter)
    - Benchmark between OTS and PPS
- Commissioning of the PVS
    - Report and results by GDV (accuracy of rotations and linear motion)
    - Quality assurance test by Politecnico group

Even if a great number of acquisitions were recorded during the installation and the fine tuning of the systems, only those measurements related to the last version of the software

and hardware are considered in this chapter. By then, only the measurements done during the acceptance protocols are reported. Readers can find in appendix *a* graphs of velocity and acceleration of the PPS .

2.7.1 PPS (couch). Report of GDV with random movements

GDV basically mounted on the PPS basement a device (see figure 2.19) where four control points were monitored among different positions. Then, discrepancies between nominal positions (that is, where ideally these control points should be looking at the PPS control software) and current positions (measured with laser tracker) were determined.

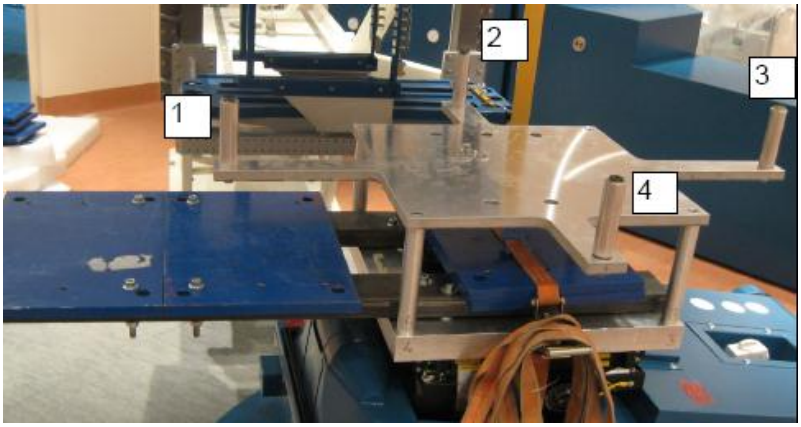

Figure 2.19. GDV measurement tool docked to the PPS for accuracy check in room 1.

GDV considered two different coordinate systems, as show in figure 2.20: the first set of measurements is expressed in reference to the measurement tool; the second in reference to the treatment area. This choice was motivated by the fact that data could be interpreted in reference of two center of rotations, that is: a point placed ideally on the robotic arm of the PPS; a point placed on the tool mounted on the PPS basement. In this last, an offset has to be taken into account in the calculations of the nominal position.

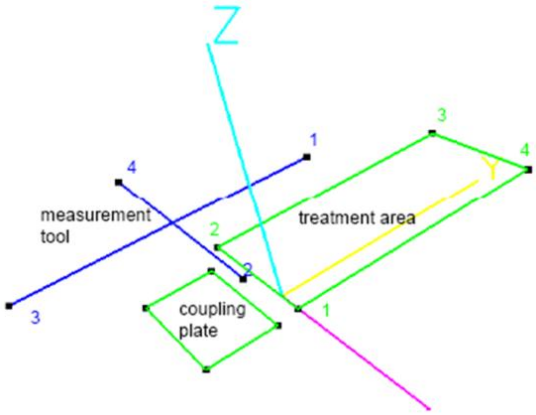

Figure 2.20. scheme provided by GDV representing the set up
and the coordinate systems used to verify the accuracy of the PPS.

Once docked the measurement tool onto the PPS, GDV moved the robotic arm in different positions, summarized in table 2.4.

GUI POSITIONS								
Position	X	Y	Z	pitch	roll	rotation	weight	torque
001_*	271	-396	-172	-8	8	26	120	370
002_*	779	188	-269	-13	-12	113	117	388
003_*	958	12	-346	-18	-8	76	118	411
004_*	573	12	-346	-23	-7	76	118	409
005_*	91	-652	-338	-13	10	8	119	387
006_*	-294	-380	-420	-18	4	-39	120	414
007_*	-766	96	-457	-12	-5	-98	122	393
009_*	150	-200	-610	-2	0	5	123	368
010_*	252	-90	-610	-17	6	63	119	408
011_*	-157	-376	-426	-21	-8	-48	117	420
012_*	-159	-376	-319	8	1	-75	122	327
013_*	-668	-123	-276	-13	-8	-87	119	392
014_*	-668	107	-151	-21	9	-107	118	418
015_*	-409	-306	-215	-15	-12	-63	117	393
016_*	-75	-610	-282	-11	-7	-24	121	387
017_*	82	-940	-316	-14	-5	-11	121	396
018_*	409	-360	-378	-18	11	39	117	404
019_*	780	-105	-506	-19	7	92	120	415
020_*	840	97	-401	-17	-8	104	117	408
Range (min\max)	-766\358	-940\188	-610\-151	-23\8	-12\11	-107\113	117\123	327\420

Table 2.4. PPS positions used in CNAO, Pavia, by GDV to check the accuracy in positioning simulating the presence of the treatment couch.

Regarding the couch, GDV proceeded with two different setups. During the first set of trials, a weight was applied to the basement of the PPS, simulating a positive torque. In a second set of trials, an additional manual torque was added. Results of these measurements in terms of 3D errors, for each control point, are reported in figure 2.21 and figure 2.22, respectively.

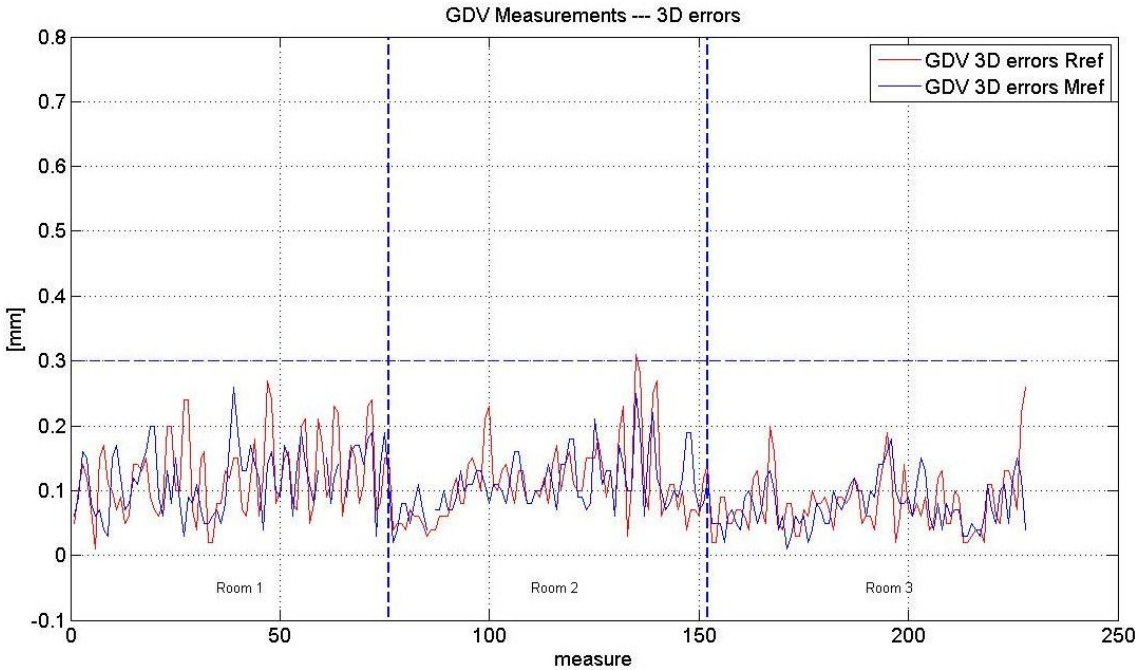

Figure 2.21. 3 D errors reported by GDV after measurement campaigns in room 1,2 and 3. All the four points of each trial are shown. Red line refers to the room coordinate system, blue line to the measurement tool coordinate system.

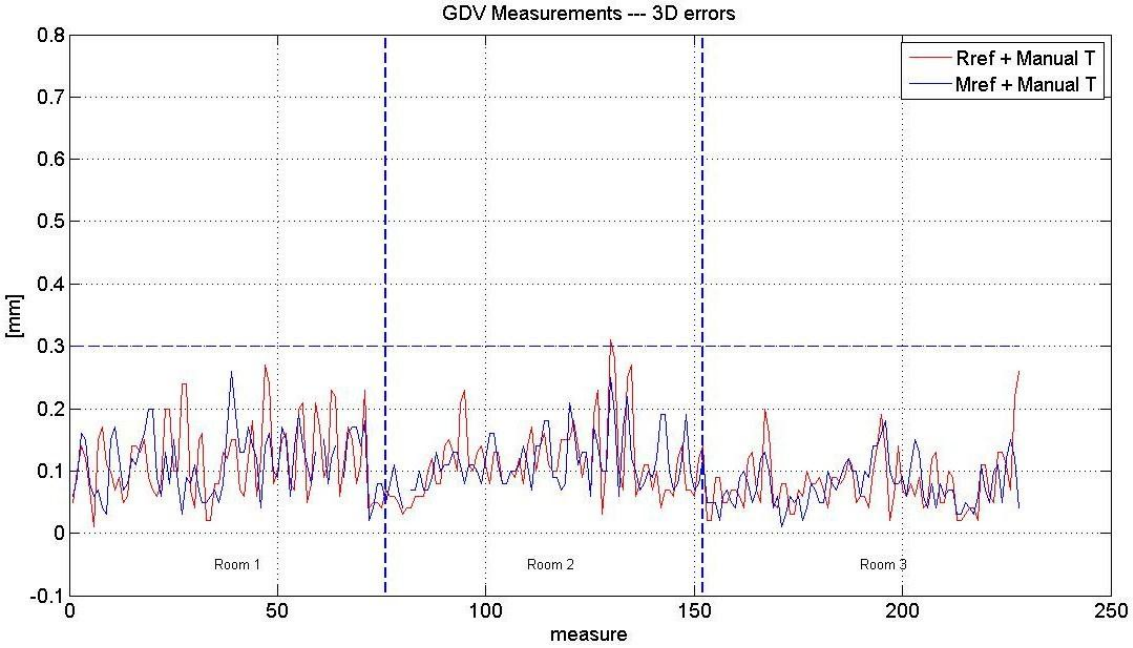

Figure 2.22. 3 D errors reported by GDV after measurement campaigns in room 1,2 and 3 and an additional manual torque applied. Again, all the four points of each trial are shown. Red line refers to the room coordinate system, blue line to the measurement tool coordinate system.

2.7.2 PPS (chair). Report by GDV with random movements

At the time GDV personnel were in Pavia both the carbon couch and the treatment chair were not already delivered to the Center. This is the main reason why they did not use these tools docked to the PPS. But if the carbon couch has a weight of 40 kilograms, the chair weights nearly 250 kilograms. To reproduce this torque effect, an additional weight was applied to the measurement tool. Weight and torque, as well as the GUI positions used to check the accuracy of the PPS in this case, are reported in table 2.5.

GUI POSITION								
Position	x	y	z	pitch	roll	rot	weight	torque
001_*	816	40	-570	-3.3	1.8	81	250	3000
002_*	479	-365	-622	-4.3	0.3	58	250	3000
003_*	-116	-778	-601	0.6	0.2	-11	250	3000
004_*	-178	-588	-586	-2.3	-1.9	-49	250	3000
005_*	-379	-381	-609	-3.3	0.6	-64	250	3000
006_*	-735	131	-579	-1.7	-1.5	-99	250	3000
Range (min\max)	-735\816	-778\131	-622\-570	-4.3\0.6	-1.9\1.8	-99\81	250\250	3000\3000

Table 2.5. PPS positions used in CNAO, Pavia, by GDV to check the accuracy in positioning simulating the presence of the treatment chair.

As for the couch, 3D displacements are reported in figure 2.23.

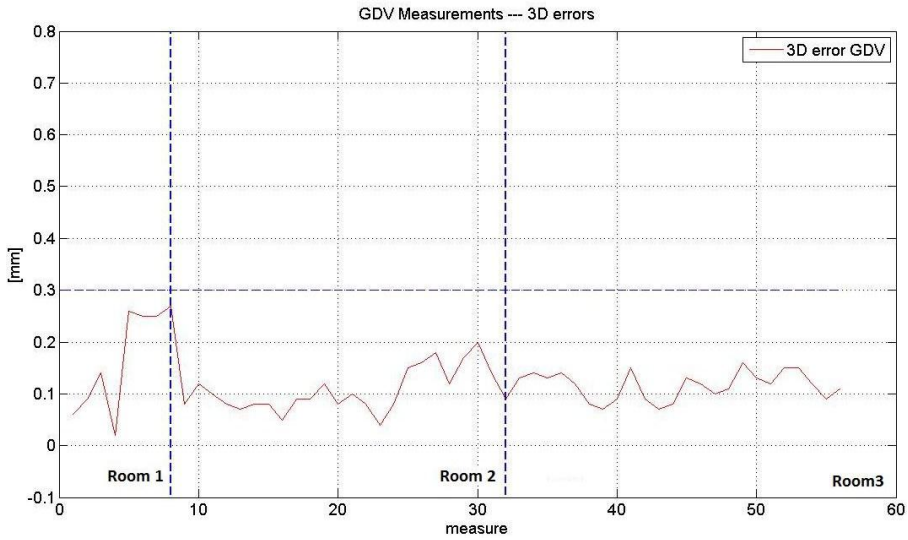

Figure 2.23. 3 D errors reported by GDV after measurement campaigns in room 1,2 and 3 and an additional load was applied during these measurements to simulate the presence of the treatment chair. Again, all the four points of each trial are shown.

2.7.3 PPS. Isocentricity in random rotations

In a treatment room the isocenter can be intended as a fixed point where the center of mass of the target, here intended as the tumor mass, should be aligned. The isocenter lies on the beam line, when no correction are applied to scanning magnets. Once the patient is aligned in this position, corrections in lateral and vertical directions are operated tuning the scanning magnets in a 20 cm square box. Depth of SOBP is changed tuning energy spill: lower energies correspond to proximal areas, while higher energies corresponds to more distal areas. The clinical workflow requires that the systems aimed at patient positioning have the ability to place a point at the isocenter with the highest accuracy available (<= 0.3 mm in our case). A correction vector of pure rotations should result in rotations around this point. By then, the number of particles released at the isocenter are more than those released in the nearby, and so errors in terms of residual dose in the tumor mass are lower than in the near tissues. The importance of an high accuracy in isocentric rotations is critical because that one is the point where the therapeutic dose is focused. An high geometrical accuracy allowed to follow medical indications and save normal tissues around the tumor mass.
During our tests in CNAO we used two different set up, comprehending a laser cross alignment (figure 2.24) and a more accurate custom tool for laser tracker measurements aligned at the nominal isocenter. During tests with laser tracker the corner cube was placed at the isocenter. Then, with a continuous acquisition, we checked in real time the trajectory and the mismatch between the current and the nominal position, previously recorded as reference. Obviously, these tests should be intended as prerequisite in respect to random combinations of linear translations and rotations presented forward in the chapter.

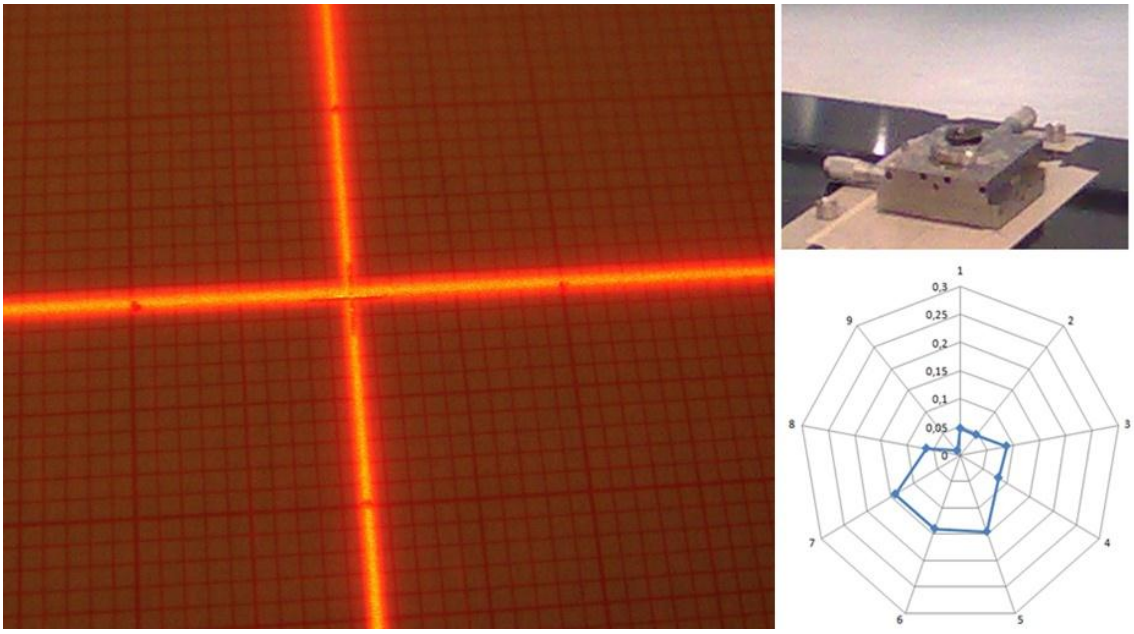

Figure 2.24. Test of PPS isocentricity in rotations. Panel (a): check with laser cross consistency; panel (b): tool used to measure the isocenter with Leica laser tracker; panel (c): accuracy of a carbon couch docked to the PPS in room 1.

Results obtained with laser tracker showed that is possible to reach an accuracy lower than 0.3 mm during isocentric rotations. As example, in figure 2.24 (right panel) are reported results of the isocentric rotations accuracy of a carbon couch, docked to the PPS of Room1.

2.7.4 PPS. Random movements

Politecnico and CNAO approach differs from GDV mainly in two aspects:

- We measured the accuracy of the PPS using a clinical carbon couch and a treatment chair, with sockets glued on their surface as control points (plus a marker at the isocenter in both cases).
- We performed measurements without and with an additional weight applied to treatment tools, to simulate the presence of a patient.

Moreover, if compared with GDV campaigns, a larger number of measurements was considered. Details about the investigated positions are reported in (Table 2.8-9) for the couch and (Table 2.14-15) for the chair.

The set up of the measurements is described in the previous chapter. Briefly, we glued six sockets on the carbon couch, plus an additional socket at the isocenter. Four control points were glued on the chair, plus, again, an additional point at the isocenter.
We acquired in each room 20 random positions with carbon couch docked to PPS and 20 positions with treatment chair. For each treatment tool 10 positions were recorded without an additional weight and 10 measurements with an additional weight. In table 2.6 are shown for the first case mean values, standard deviations and maximum values of linear displacements from nominal positions (measured – nominal position).

	Room 1						
	couch				chair		
	Mean [mm]	Std [mm]	Max [mm]		Mean [mm]	Std [mm]	Max [mm]
X	-0.02	0.14	0.20		0.08	0.23	0.47
Y	-0.01	0.07	0.13		-0.01	0.11	0.28
Z	0.02	0.09	0.21		-0.04	0.05	0.07
	Room 2						
	couch				chair		
	Mean [mm]	Std [mm]	Max [mm]		Mean [mm]	Std [mm]	Max [mm]
X	0.06	0.13	0.27		-0.01	0.09	0.13
Y	0.03	0.10	0.21		0.02	0.12	0.31
Z	-0.01	0.12	0.24		-0.06	0.06	0.04
	Room 3						
	couch				chair		
	Mean [mm]	Std [mm]	Max [mm]		Mean [mm]	Std [mm]	Max [mm]
X	-0.09	0.24	0.36		0.08	0.13	0.25
Y	-0.19	0.20	0.12		-0.11	0.09	0.07
Z	-0.01	0.08	0.20		-0.02	0.04	0.05

Table 2.6. Mean values, standard deviations and maximum values of linear displacements over 10 measurements (without additional load).

In table 2.7 are shown linear displacements of X, Y, Z coordinates (measured-nominal) when an additional weight was applied to the treatment tools.

	Room 1						
	couch				chair		
	Mean [mm]	Std [mm]	Max [mm]		Mean [mm]	Std [mm]	Max [mm]
X	-0.01	0.14	0.17		0.02	0.29	0.64
Y	-0.01	0.08	0.11		-0.03	0.31	0.73
Z	-0.04	0.06	0.10		0.02	0.04	0.10
	Room 2						
	couch				chair		
	Mean [mm]	Std [mm]	Max [mm]		Mean [mm]	Std [mm]	Max [mm]
X	0.07	0.11	0.36		0.01	0.15	0.32
Y	0.05	0.10	0.30		0.02	0.18	0.47
Z	-0.04	0.08	0.11		-0.04	0.03	0.02
	Room 3						
	couch				chair		
	Mean [mm]	Std [mm]	Max [mm]		Mean [mm]	Std [mm]	Max [mm]
X	-0.05	0.20	0.25		0.05	0.18	0.36
Y	-0.13	0.20	0.08		-0.17	0.17	0.20
Z	-0.01	0.07	0.13		-0.04	0.04	0.04

Table 2.7 Mean values, standard deviations and maximum values of linear displacements over 10 measurements (with additional load).

2.7.4.1 Commissioning of the couch

Six sockets were glued on the surface of the carbon couch. An additional control point was placed at the isocenter (see figure 2.25)

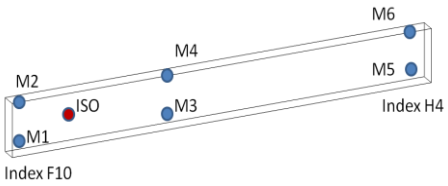

Figure 2.25. set up for couch accuracy tests

As reported in GDV results, in table 2.8 and table 2.9 are reported the values describing the position of the PPS without and with an additional extra weight of 40 Kg fixed on the surface of the couch.

GUI POSITIONS						
Position	X	Y	Z	pitch	roll	rotation
1	-50	-799	-176	-5	0	110
2	-21	-927	-193	4	2	72
3	-69	-926	-204	-1	5	-82
4	-58	-957	-73	1	4	-60
5	-241	-902	31	-1	3	-93
6	-241	-902	-150	-3	1	-92
7	0	-847	-168	1	5	-110
8	-164	-1000	-168	2	-1	22
9	-227	-873	-102	3	0	102
10	-100	-913	-231	0	0	92
Range(min\max)	-241\0	-1000\-799	-231\31	-5\4	-1\5	-110\110

Table 2.8. PPS positions used by Politecnico and CNAO personnel to check the accuracy in positioning with the treatment couch (no extra load applied).

GUI POSITIONS						
Position	X	Y	Z	pitch	roll	rotation
1	-60	-779	-126	-1	1	105
2	-31	-957	-173	-0.5	0	82
3	-207	-851	-122	0	-0.5	100
4	-130	-915	-211	1	-1	42
5	-95	-923	-201	0	0	90
6	-79	-946	-214	0	1.5	-89
7	-78	-951	-115	-2	0	-65
8	-221	-942	-100	1	2	-83
9	200	-912	-120	-1.5	0.5	-99
10	10	-857	-178	0	-1	-105
Range(min\max)	-221\200	-957\-779	-214\-100	-2\1	-1\2	-105\105

Table 2.9. PPS positions used by Politecnico and CNAO personnel to check the accuracy in positioning with the treatment couch (extra load applied).

3D errors measured by Politecnico and CNAO personnel after measurement campaigns in room 1,2 and 3 are shown in figure 2.26. All the control points are considered in the graph.

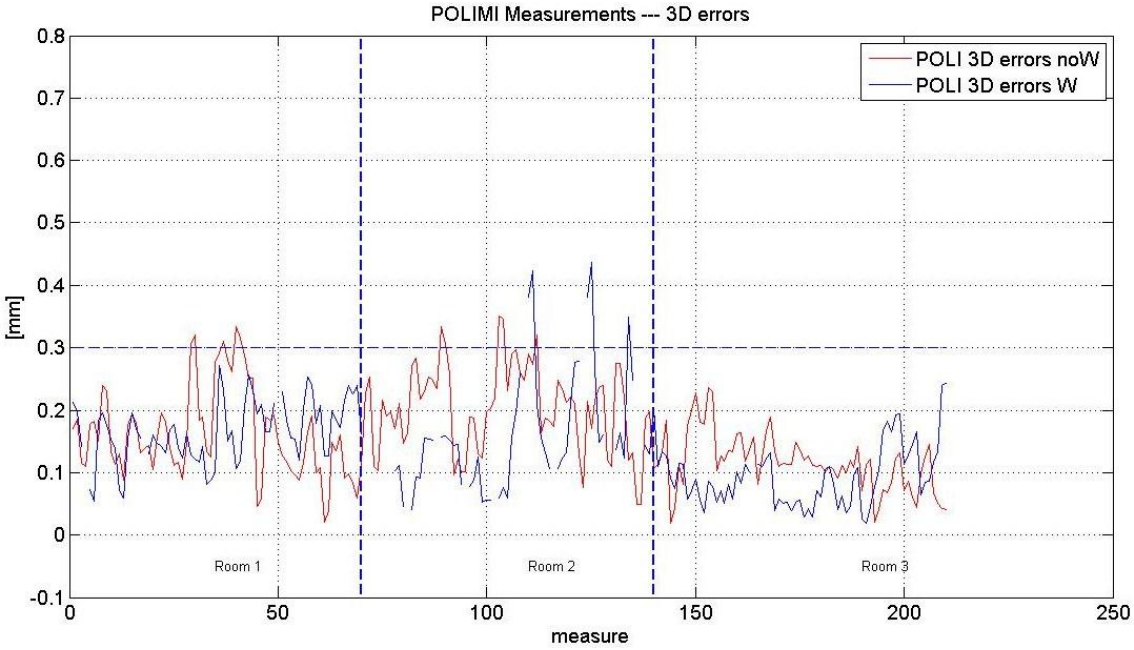

Figure 2.26. 3 D errors reported by PoliMi and CNAO personnel after measurement campaigns in room 1,2 and 3 with a carbon couch docked. All the seven points (six controls plus iso) of each trial are shown. Red line refers to the measurements without an additional weight, blue line to the ones with a load (ca 40 Kg) applied.

Our approach allowed us to investigate each control point separately. In figure2.27 and figure 2.28 results of 3D errors are reported for both the set up conditions (without and with the additional load).

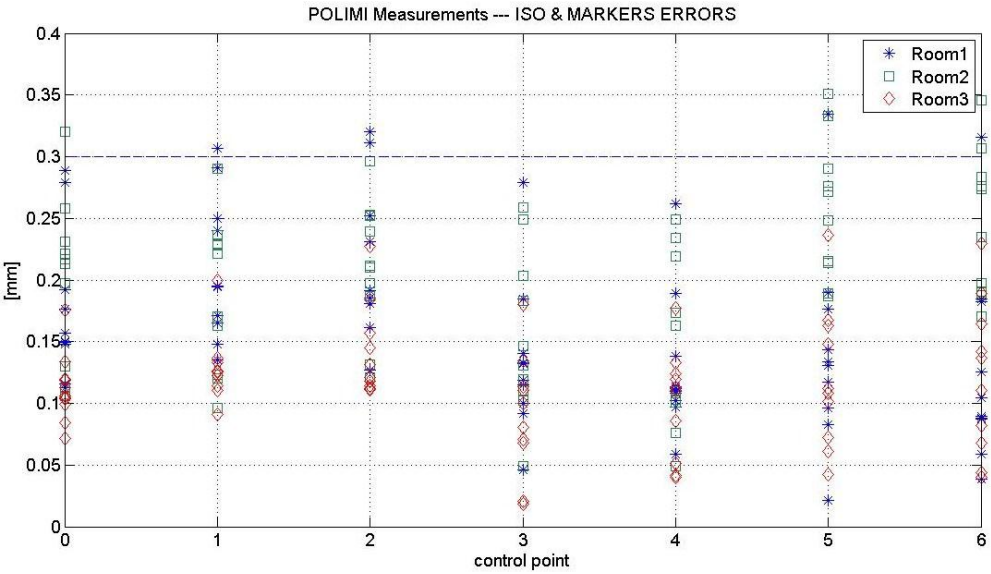

Figure 2.27. 3 D errors after measurement campaigns in room 1,2 and 3 (no additional weight). Markers are shown separately in this figure (where 6=ISO). Blue stars refers to room 1; green square to room 2 and red diamonds to room 3.

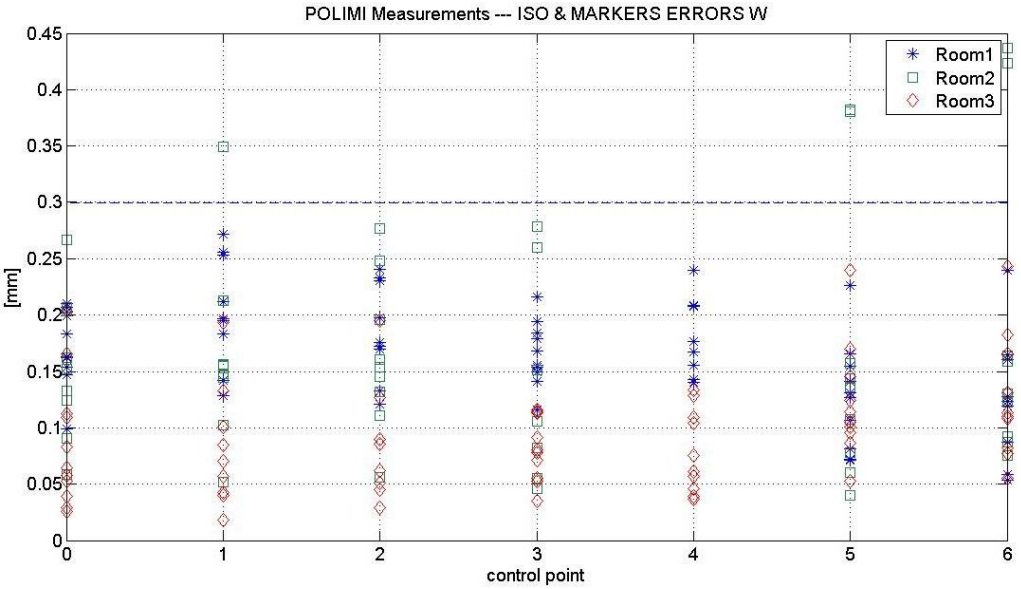

Figure 2.28. 3 D errors after measurement campaigns in room 1,2 and 3 (additional weight). Markers are shown separately in this figure (where 6=ISO). Blue stars refers to room 1; green square to room 2 and red diamonds to room 3.

A box&whisker graph for each room (1, 2 and 3) and for each set up condition is reported in figure 2.29. While median is considered in figure 2.29, details about mean values and standard deviation are reported in table 2.10.

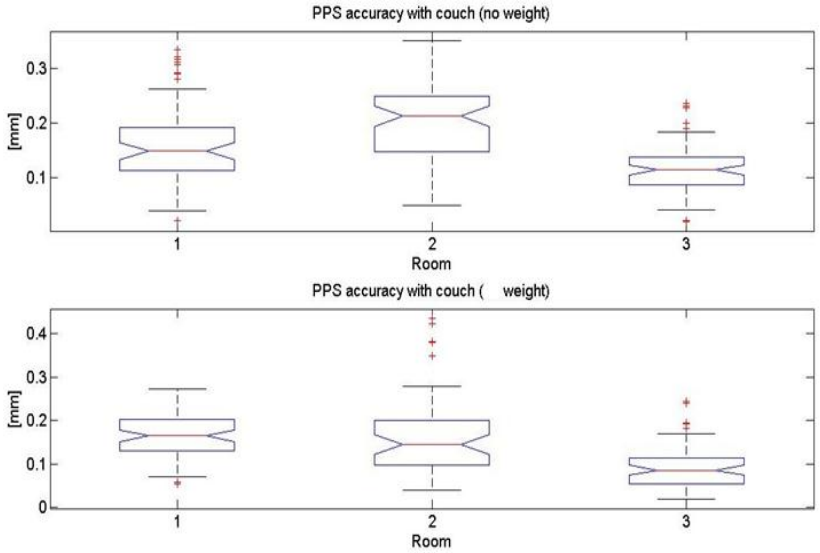

Figure 2.29. B&W plots for PPS + carbon couch accuracy. Upper panel: no additional weight. Lower panel: an additional 40 Kg weight was applied on the couch.

	No additional weight				Additional Weight		
	Mean [mm]	Std	Max [mm]		Mean [mm]	Std	Max [mm]
Room 1	0.16	0.07	0.33		0.17	0.05	0.27
Room 2	0.20	0.07	0.35		0.16	0.10	0.44
Room 3	0.12	0.05	0.24		0.09	0.05	0.24

Table 2.10.Mean values and standard deviation for room 1,2,3. On the left no additional weight was applied, on the right results concerning measurements with 40 Kg mass on the carbon couch.

Absolute errors VS number of cases are reported in figure 2.30

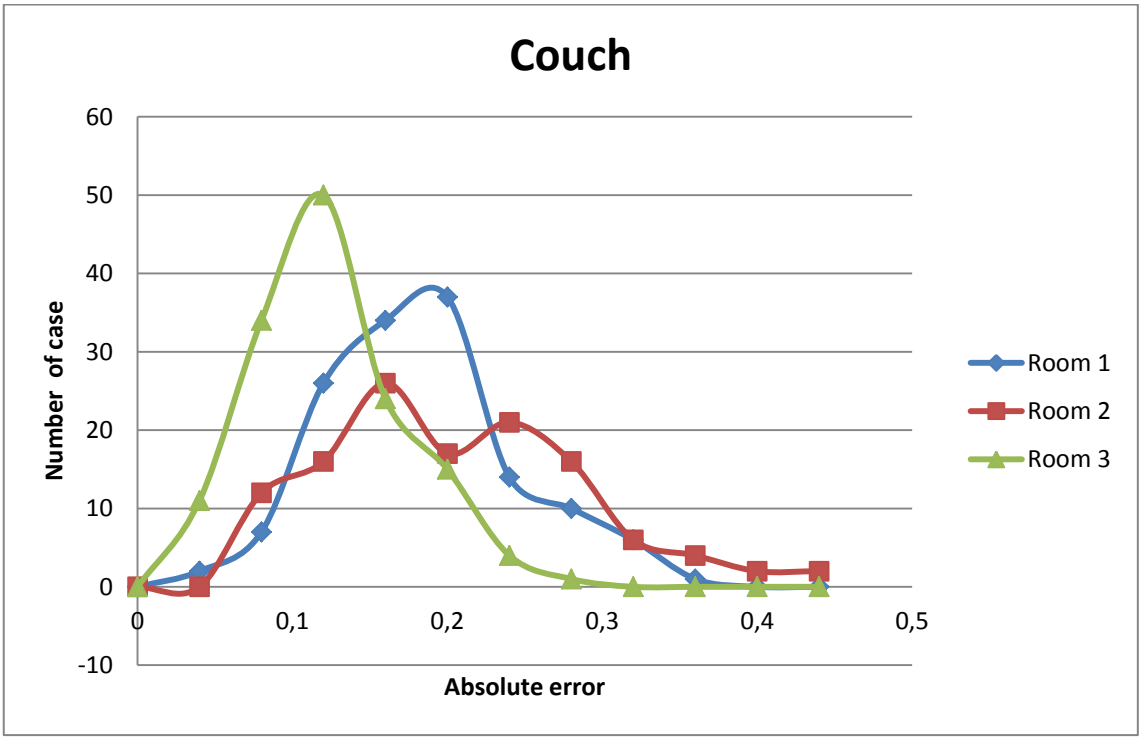

Figure 2.30. Absolute errors VS number of cases for couch accuracy test.

A Lilliefors test was performed in order to check normality distribution of data (Table 2.11).

Lilliefors	Couch (no wheight)		Couch (plus weight)	
	H	p	H	p
Room1	1	0.0070	0	0.5000
Room2	0	0.2592	1	<1.0000e-003
Room3	0	0.0524	0	0.0897

Table 2.11. Lilliefors test results for couch measurements in Room1, Room2 and Room3.

Results show that data are not normally distributed in Room1 (no additional weight) and Room2 (additional weight).
It is important to point out that results were found to be close to the threshold of 0.3 mm and to the measurement sensibility.
Statistical analysis was applied to investigate two different aspects:

- Case 1: investigate if the presence of the weight (added to simulate the presence of a patient) influenced the measurements.
- Case 2: investigate if there are differences in the three rooms, that is, if measurements recorded in a room differs statistically from the others.

Case 1.

A Lilliefors test was performed in order to check normality distribution of data (Table 2.12). In this case, data of couch without and with an additional load are collected together for the three rooms.

Lilliefors	Couch	
	H	p
NO Weight	1	<0.001
Weight	1	0.0067

Table 2.12. Lilliefors test results for couch measurements with\without weight.

Non parametric statistical analysis (Two-sample Kolmogorov-Smirnov test) applied to couch shows a significant difference among the two investigated cases (that is, absence or presence of an additional load (p-value=0.0085).
A plot of the empirical cumulative distribution function (CDF) for data is reported in figure 2.31.

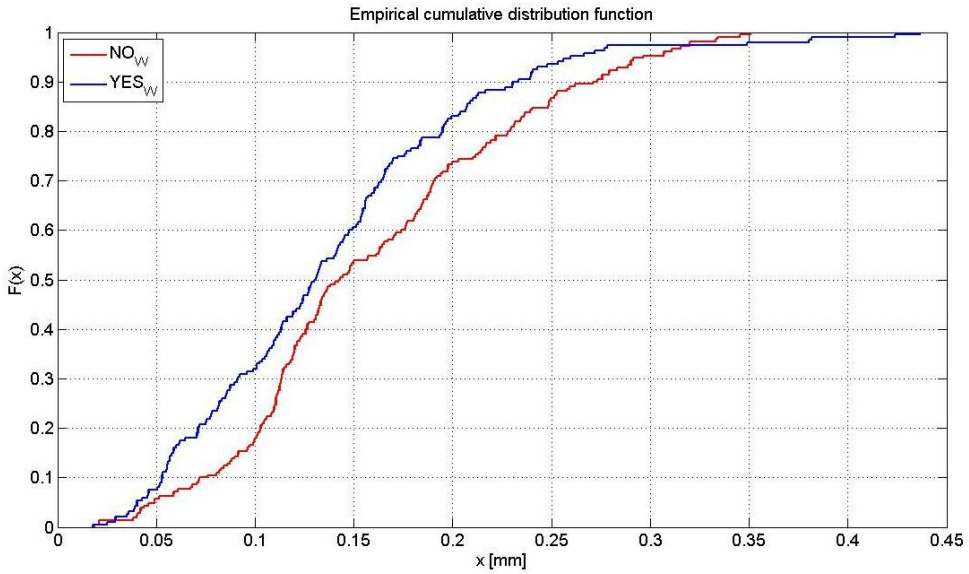

Figure 2.31. cumulative distribution function for couch with (blue line) and without an additional load (red line).

Case 2.

Again, Lilliefors test was performed for the second condition (difference in between the rooms). Results are shown in Table 2.13.

Lilliefors	Couch	
	H	p
Room1	0	0.2186
Room2	0	0.0920
Room3	1	0.0344

Table 2.13. Lilliefors test results for couch measurements in all the rooms.

Non parametric statistical analysis (Friedman test) applied to couch shows a significant difference among the three rooms (p-value=$2.6645 \cdot 10^{-15}$).
A post-hoc comparison (Tukey-Kramer test) indicates best results (lower errors) in treatment room 3, whereas room 2 and room 1 are comparable at 95% confidence. (see figure 2.32).

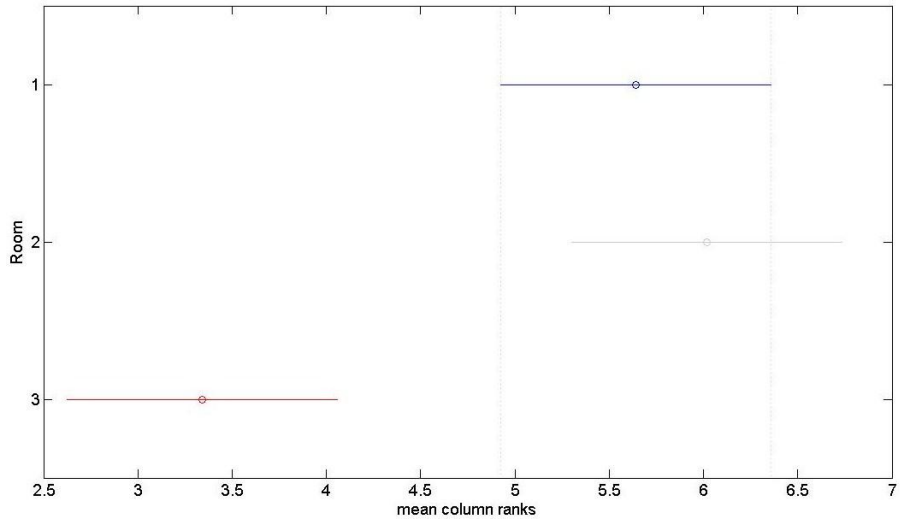

Figure 2.32. post-hoc comparison of measurements performed in room 1,2,3 with couch.

2.7.4.2 Commissioning of the chair

Four sockets were glued on the back carter of the treatment chair, and an additional control point was placed at the isocenter (see figure 2.33).

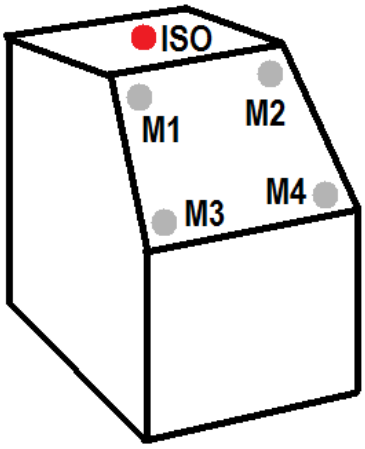

Figure 2.33. set up for chair accuracy test

In table 2.14 and table 2.15 the positions of the PPS without and with an additional extra weight of 40 Kg placed on the treatment chair are reported.

GUI POSITIONS						
Position	X	Y	Z	pitch	roll	rotation
1	5	-150	-100	0	1	95
2	-25	-200	-120	1	0	85
3	-25	-250	-130	0	-1	55
4	0	-270	-150	0.5	0	15
5	0	-290	-160	0	-0.5	-25
6	10	-280	-155	-1	1	-45
7	50	-240	-158	0	0	-75
8	60	-230	-148	0	0	-90
9	85	-200	-165	0	-1.5	-100
Range(min\max)	-25\85	-290\-150	-165\-100	-1\1	-1.5\1	-100\95

Table 2.14. PPS positions used by Politecnico and CNAO personnel to check the accuracy in positioning with the treatment chair (no extra load applied).

GUI POSITIONS						
Position	X	Y	Z	pitch	roll	rotation
1	15	-230	-150	1	0	95
2	25	-250	-150	0	0	85
3	-20	-290	-130	1	0	55
4	0	-270	-155	0.5	0	15
5	20	-300	-160	0	-1	-25
6	5	-285	-158	-1	1	-45
7	55	-230	-145	0	0	-75
8	60	-230	-148	0	0	-90
9	85	-200	-155	0	-1.5	-100
Range(min\max)	-20\85	-300\-200	-160\-130	-1\1	-1.5\1	-100\95

Table 2.15. PPS positions used by Politecnico and CNAO personnel to check the accuracy in positioning with the treatment chair (extra load applied).

3D errors measured by Politecnico and CNAO personnel after measurement campaigns in room 1,2 and 3 are shown in figure 2.34. Again, all the control points are considered in the graph.

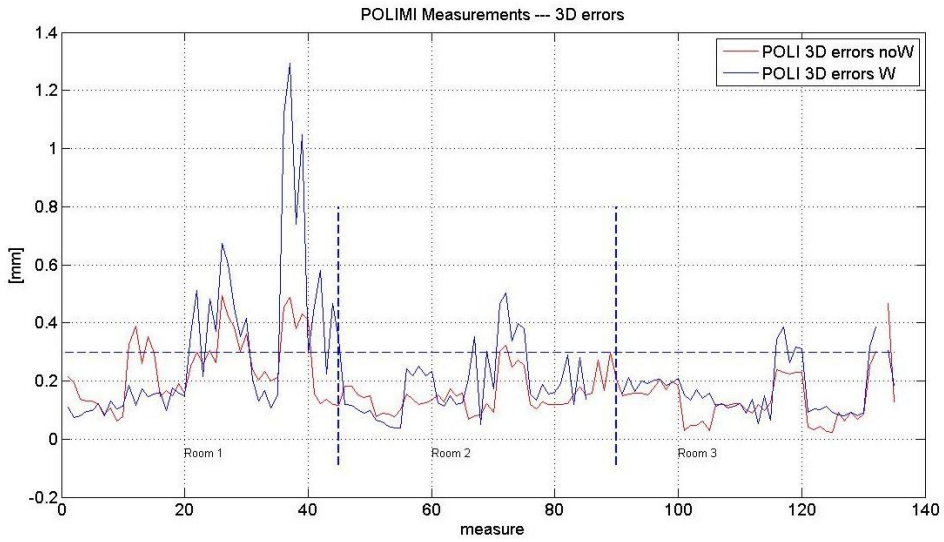

Figure 2.34. 3 D errors reported by Politecnico and CNAO personnel after measurement campaigns in room 1,2 and 3. Red line corresponds to the measurements without an additional load; blue line to those measurements acquired after an additional weight was applied to the treatment tools.

In figure 2.35 and figure 2.36 results of 3D errors are reported for each control point and for both the set up conditions.

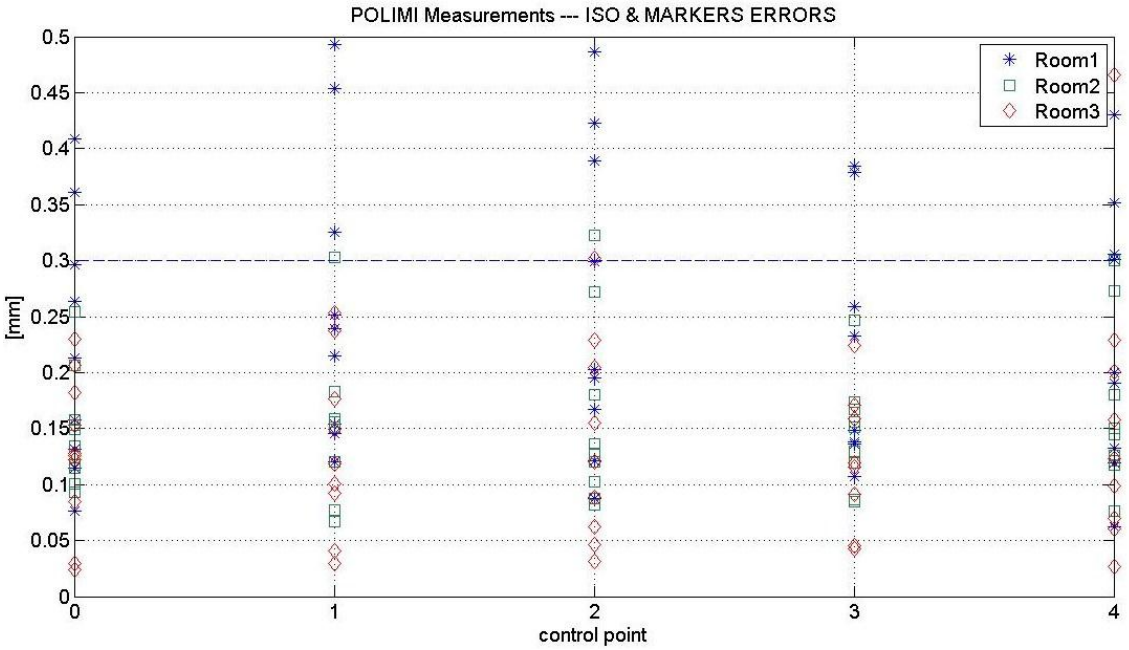

Figure 2.35. 3 D errors after measurement campaigns in room 1,2 and 3 (no additional weight). Markers are shown separately in this figure (where 0=ISO). Blue stars refers to room 1; green square to room 2 and red diamonds to room 3.

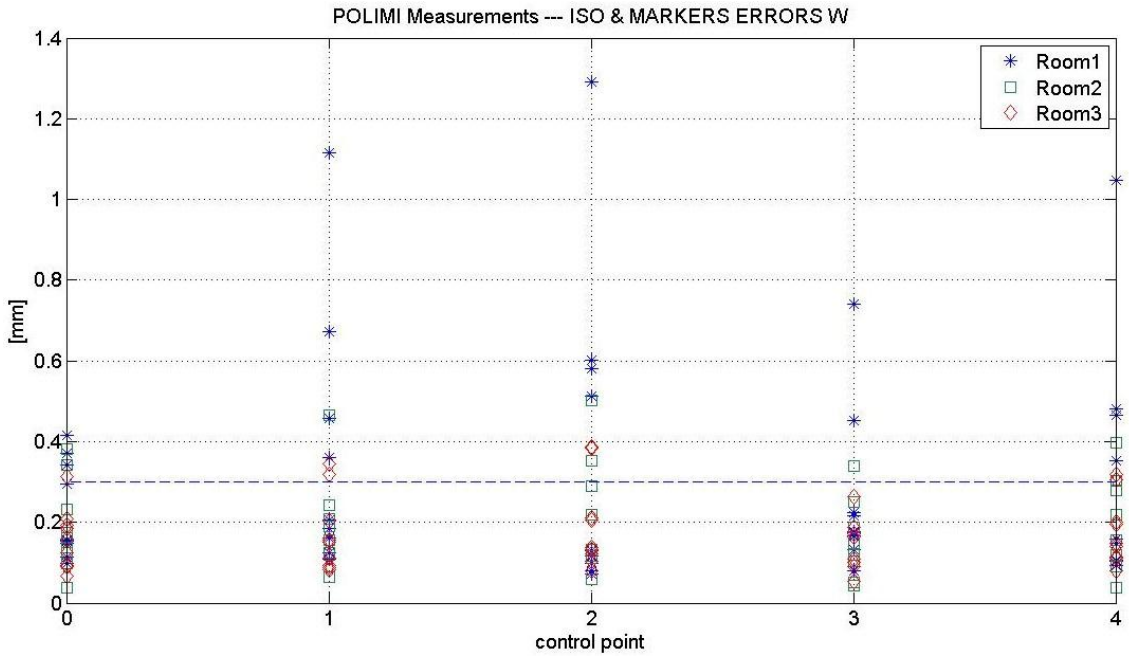

Figure 2.36. 3 D errors after measurement campaigns in room 1,2 and 3 (additional weight). Markers are shown separately in this figure (where 0=ISO). Blue stars refers to room 1; green square to room 2 and red diamonds to room 3.

In figure 2.37 a box&whisker graph concerning the chair is reported. Details about mean values and standard deviation are reported in details in table 2.16.

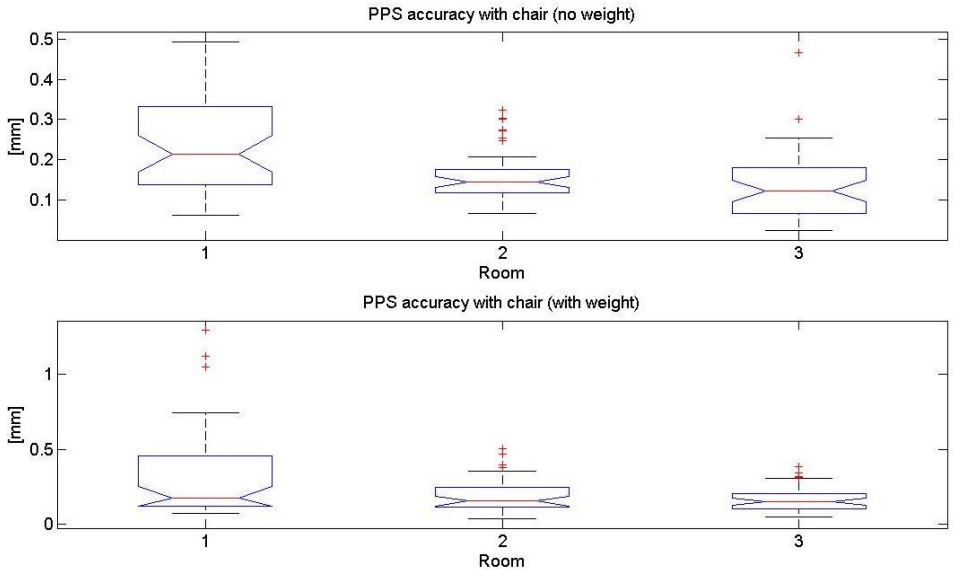

Figure 2.37. B&W plots for PPS + chair accuracy. Upper panel: no additional weight. Lower panel: an additional 40 Kg weight was applied on the chair.

	No additional weight				Additional Weight		
	Mean [mm]	Std	Max [mm]		Mean [mm]	Std	Max [mm]
Room 1	0.24	0.12	0.49		0.32	0.29	1.29
Room 2	0.15	0.06	0.32		0.19	0.12	0.50
Room 3	0.13	0.09	0.47		0.17	0.09	0.39

Table 2.16.Mean values and standard deviation for room 1,2,3. On the left no additional weight was applied, on the right results concerning measurements with 40 Kg mass on the chair.

Absolute errors VS number of cases are reported in figure 2.38.

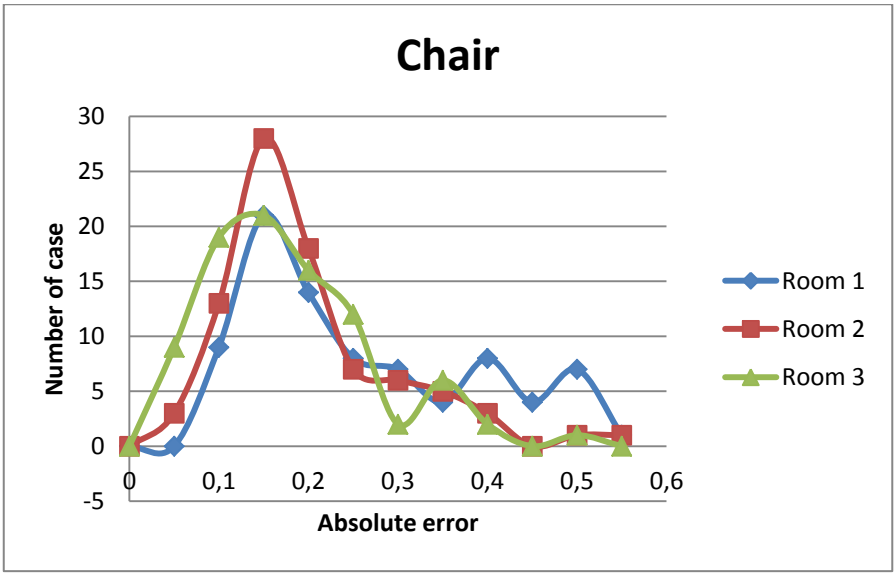

Figure 2.38. absolute errors VS number of cases for treatment chair in Room1 (blue line), Room2 (red line) and Room3 (green line). Out of nominal not reported.

A Lilliefors test was performed in order to check normality distribution of data Table 2.17.

Lilliefors	Chair (no wheight)		Chair (plus weight)	
	H	p	H	p
Room1	0	0.1172	1	<1.0000e-003
Room2	1	<1.0000e-003	1	0.0315
Room3	0	0.1127	1	0.0277

Table 2.17. Lilliefors test results for chair measurements in Room1, Room2 and Room3.

Also in this case (except few out of nominal) results were found to be closed to the threshold of 0.3 mm. the statistical analysis presented in this paragraph follow the one conducted for couch case. The first analysis aimed at investigating if the presence of an additional weight (to simulate the presence of a patient) influenced the measurements (Case 1). The second one aimed at understanding if there are differences in the three rooms, that is, if measurements recorded in a room differs statistically from the others (Case 2).

Case 1.

A Lilliefors test was performed in order to check normality distribution of data Table 2.18. In this case, data of chair without and with an additional load are collected togheter for the three rooms.

Lilliefors	Couch	
	H	p
NO Weight	1	<0.001
Weight	1	<0.001

Table 2.18. Lilliefors test results for couch measurements with\without weight.

Non parametric statistical analysis (Two-sample Kolmogorov-Smirnov test) applied to chair shows no significant difference among the two investigated cases, that is, absence or presence of an additional load (p-value=0.2131).
As for couch, also in this case a plot of the empirical cumulative distribution function (CDF) for data is reported in figure 2.39.

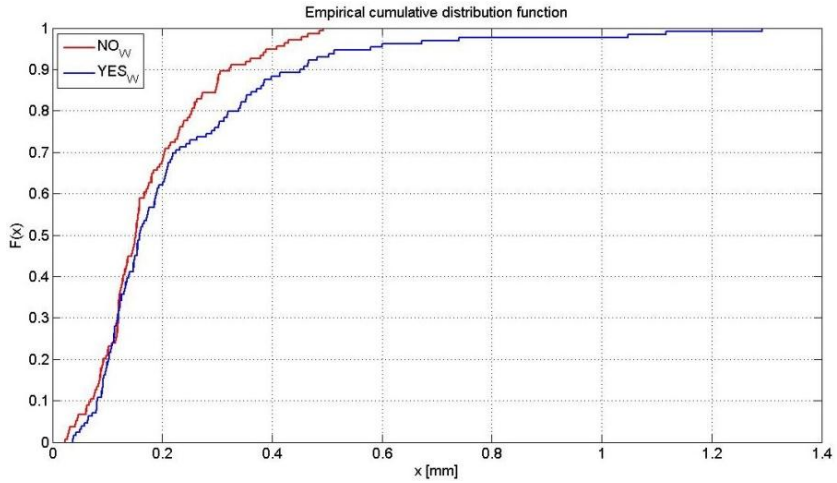

Figure 2.39. cumulative distribution function for chair with (blue line) and without an additional load (red line).

Case 2.

Lilliefors test was performed for the second condition (difference in between the rooms). Results are shown in Table 2.19.

Lilliefors	Couch	
	H	p
Room1	1	<0.001
Room2	1	<0.001
Room3	1	0.0116

Table 2.19. Lilliefors test results for couch measurements in all the rooms

Non parametric statistical analysis (Friedman test) applied to chair shows a significant difference among the three rooms (p-value=$6.9720 \cdot 10^{-7}$).
A post-hoc comparison (Tukey-Kramer test) indicates that room 1 and room 3 were significantly different, with best results (lower errors) in treatment room 3. Room 2 is not statistically different from room1 and room 3 (95% confidence) (see figure 2.40).

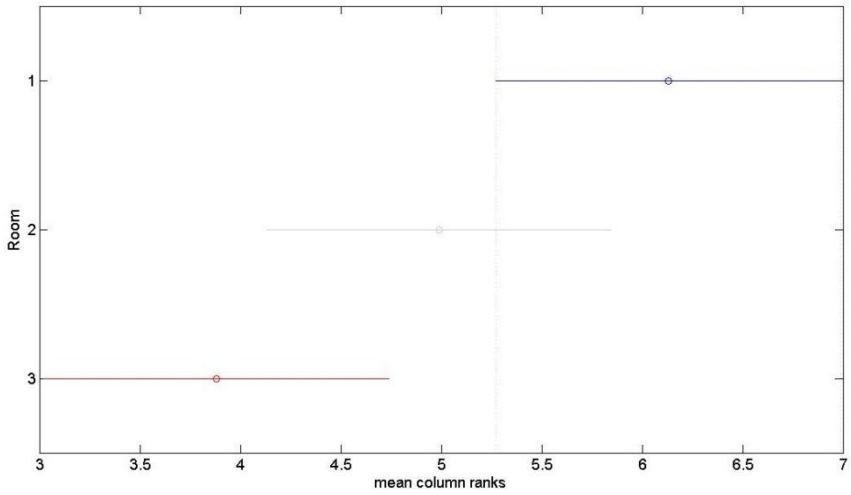

Figure 2.40. post-hoc comparison of measurements performed in room 1,2,3 with chair.

2.7.5 PPS. A benchmark between OTS and PPS

To evaluate the consistency of these two different systems, the PPS was finally benchmarked vs. the OTS on site by means of a head phantom fitted with 4 passive markers. The PPS was moved in 6DOF within a ±5 mm and ±3° range from isocenter and the final position was measured with the OTS. The head phantom study performed on site showed an agreement between PPS and OTS (mean±SD) within 0.1±0.1 mm and 0.06±0.07° in 30 repeated measurements: the error distributions for both translational and rotational errors is shown in figure 2.41.

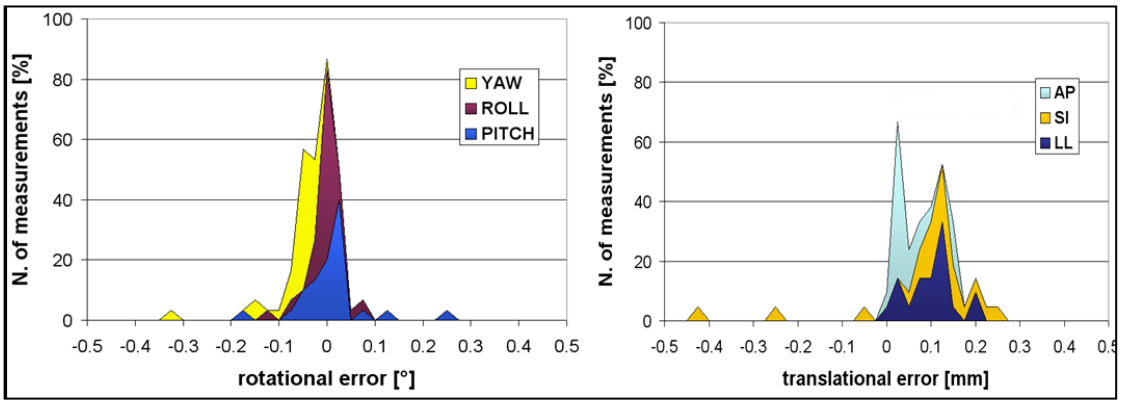

Figure 2.41. Histograms showing the statistical distribution of translational (left panel) and rotational (right panel) errors in the head phantom study (Riboldi *et al* 2009).

2.7.6 PVS. Accuracy of rotations and linear motion

Measurements of PVS accuracy were carried out by GDV. No additional measurements were done by Politecnico and CNAO group. The relevancy of PVS accuracy on a clinical workflow are less than those potentially affecting the PPS, being its structure anchored at the roof and stabilized by steel bars. Moreover, minor discrepancies are efficiently corrected through geometrical calibration of tubes and flat panels, an operation that is required to be performed once every six months.

The principle of the setup chosen by GDV was the same presented for PPS analysis. Several sockets were applied to the moving parts of the cylinder and registered by a Leica laser tracker 0.01 mm\m accuracy. Two sets of acquisitions were performed: the first one was intended to quantify the errors in PVS rotations, the second one to quantify the errors in repositioning of flat panels and X-ray tubes during their deployment (linear repetitions). To estimate these potential inaccuracies, the center of rotation have to be measured at first. The center of the cylinder is aligned at the Room isocenter, and it rotates around the vertical axes. The center of the reference system considered is the projection of the Room isocenter on the plane described by the lower surface of the cylinder (Figure 2.42).

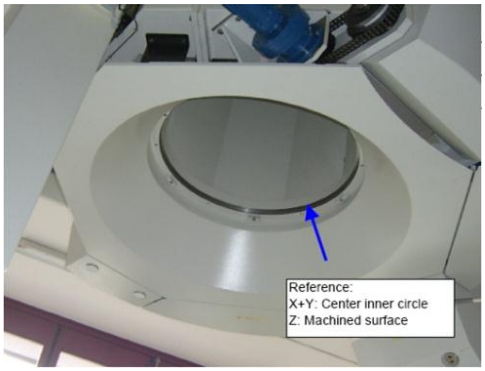

Figure 2.42.lower part of the PVS. Blue arrow indicates the nominal zero considered for accuracy in rotation measurements.

In table 2.20 results of these measurements, compared with nominal positions, are reported for room 1 and room 3.

	Global coordinate of the center for R1		
Measured [mm]	-0.23	0.21	1375.05
Nominal [mm]	0.00	0.00	1375.00
	Global coordinate of the center for R3		
Measured [mm]	0.28	0.46	1374.99
Nominal [mm]	0.00	0.00	1375.00

Table 2.20. Nominal and measured values of the reference point for PVS testing.

GDV determined a tilt of the surface equal to 0.0062° and 0.0025° in room 1 and room 3, respectively.

The first set of measurements was focused on the rotational accuracy of the PVS. In figure 2.43 results are reported for flat panels and X-ray tubes in room 1 and room 3, respectively.

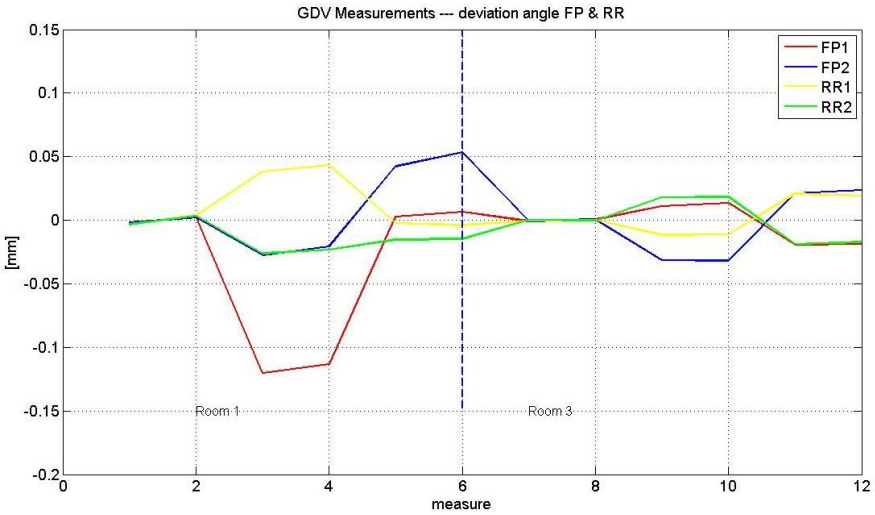

Figure 2.43. Deviation angles calculated by GDV during different rotation angles of the PVS. Flat panels, Xray tubes are reported for room1 (left part of the graph) and room3 (right part of the graph).

As described before, it was necessary to investigate the repeatability accuracy in linear movements off lat panels and X-ray tubes. By then, 12 linear repetitions were monitored and results in terms of mean values and standard deviation are summarized in table 2.21.

	FP1	FP2	RR1	RR2
	Room1			
Mean	117.64	110.00	326.03	352.14
Std	0.05	0.05	0.12	0.08
	Room3			
Mean	115.87	112.67	368.14	471.57
Std	0.05	0.09	0.09	0.19

Table 2.21. Mean values and standard deviation of 12 linear repetition of flat panels (FP1, FP2) and tubes (RR1, RR2).

To complete the analysis, the reader can find in appendix *b* extensive graphs reporting angles VS deviations for flat panels and X-ray tubes in reference to global coordinate system (nominal zero) and in reference to offset (measure zero).

2.7.7 PVS. Quality assurance: benchmark laser cross – imaging

Results of a quality assurance test are reported in this paragraph. Laser cross are periodically checked with Leica laser tracker by medical physicist. As known, laser projectors intersect at the room isocenter, and they are useful for a first alignment of the patient, or measurement tools. After a proper calibration of tubes and flat panels, in order to check the consistency of PVS imaging, we proceeded as follow:

- Alignment of a custom tool to laser cross.
- Acquisition of X-ray double projections of the measurement tool.
- Quantification (via software) of the distance between the tool and the center of flat panels.

Verisuite software (Medcom) provides the exact position of flat panels centre. Ideally, a radio opaque mass placed at the isocenter should result in a projection in this point within 1mm distance (figure 2.44).

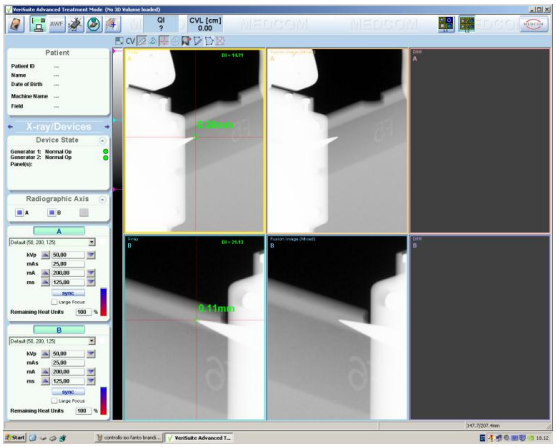

Figure 2.44.screenshot of Verisuite software. It is possible to note the red cross on the Xray images corresponding to the center of the flat panels. Tool is aligned with <1mm accuracy.

This quality check is performed every time a new calibration is needed. Moreover, CNAO personnel check this distance before each treatment.

In this chapter the solutions adopted in CNAO for patient's positioning and setup control have been presented. The manufacturer of these systems claimed an overall accuracy for PPS <0.3 mm and <0.1° in rotation of PVS. These specifications were tested during the commissioning and the acceptance protocols. Results shown, except of few out of nominal, that is possible to reach sub-millimetric accuracy in patient repositioning. The integration of systems were also successfully tested. The use of these devices minimize the time required for setup procedures and also errors or misalignments. Even if this result is relevant, some other issues remain as an open points. As example, the organ motion management. This effect requires implicitly to get used to different strategies, depending by the district to be irradiated and by the magnitude of motion. Next chapter is dedicated to organ motion mitigation, and relevance will be put on a particular case, that is the lung cancer.

Chapter III

Organ motion management

As introduced in the previous chapter, CNAO uses beam scanning, a methodology applied nowadays in the majority of the new centers. This technique allows to better conform the dose distribution, planning energy spills and operating on scanning magnets. If compared with beam scattering systems, the main advantage is that it is possible to plan the best dose distribution for each patient, without the necessity of collimators or wedges for geometry compensations (Figure 3.1).

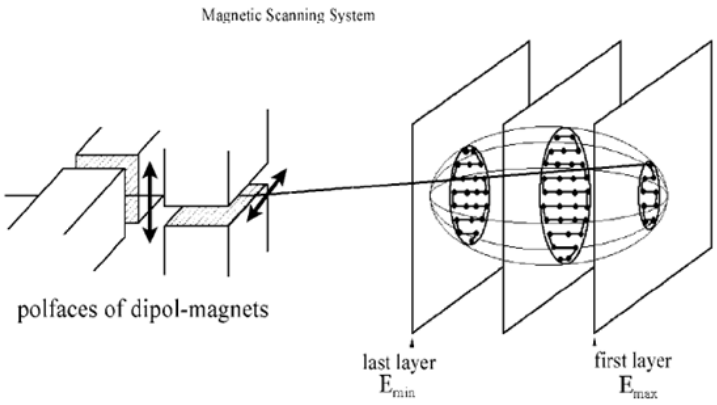

Figure 3.1. Schematic drawing of the intensity controlled magnetic scanning system (Kraft 2002).

A major issue is represented by the need of high precision in setup control and dose delivery systems. This difficulty depends mainly by geometrical inaccuracies in target definition during setup procedures. Generally, safety margins are added to the nominal target volume, in order to minimize errors. Moreover, as described before, particles therapy implicitly requires the support of accurate methods for image guidance and setup control.
This chapter is organized as follow:

- Image guided radiotherapy
- Organ motion mitigation in lung cancer
- Applications of tumor tracking

This chapter should not be intended as a review of technological and methodological aspects concerning the organ motion or organ motion mitigation in RT. For this purpose readers can refer to literature (Verellen *et al* 2008, Xing *et al* 2006, Warlick 2008, Jiang 2006, Bert and Durante 2011, Shirato *et al* 2007, Balter and Kessler 2007, Dawson and Jaffray 2007). This chapter aims at stressing the concept that advantages in the high geometrical accuracy available with new dose delivery systems could be nullified if not supported by high accuracy devices for setup verification. The general goal is to maximize therapeutic effectiveness and minimize secondary effects in healthy tissues. Moreover, tumors should not be intended as static rigid volumes, and their geometry, as the position in respect to anatomic reference point, could vary. These parameters should be taken into account while delivering therapeutic dose.

3.1 IGRT aspects

The probability of tumor control has been improved since the emergence of 3D imaging and dose delivery techniques like conformal radiotherapy or intensity modulated radiotherapy (IMRT) (Jaffray 2005). On the other hand, high precision requires more stringent requirements on the accuracy of beam targeting. Imaging is widely used during the entire process, from planning and simulation phases to radiation delivery and patient follow up.
The planning process begins with the definition of target volumes. Medical doctors and physicists optimize the treatment plan outlining on the treatment CT regions of interest. Additional information can be integrated with other imaging techniques, such as MRI, MRI spectroscopy, and PET/CT. Target volumes are distinguished between gross tumor volume (GTV) and clinical target volume (CTV). This last added some margins to the GTV to cover potential microscopic spreads. Finally, the planning target volume (PTV) is an expansion of the CTV, taking into account potential misalignments and physiological movements of organs.
In order to minimize set-up uncertainties, immobilization devices are generally used, including vacuum bags, custom molds, rigid stereotactic head frames, rectal balloons for immobilization of the prostate.
In the previous chapter, CNAO approach to in room image guidance technologies was presented in details, providing technical specifications for all the systems involved in this task. It was demonstrated that is possible to reach a sub-millimetric accuracy in patient positioning and set up control. Without the intent of providing a review on commercial devices and strategies adopted in new facilities, hereafter are reported brief descriptions of alternative strategies of other centers. The first one is American and it treats patients only with protons. The other three (two Japanese and one German) are allow to treat patients both with protons and carbon ions.

The Roberts proton therapy center is in Philadelphia (PA), USA. This center consists of up to five treatment rooms, four gantries, and one fixed-beam room. This facility also includes a separate research room. In figure a picture acquired in spring 2011 of one of the treatment rooms equipped with rotating gantry (Figure 3.2).

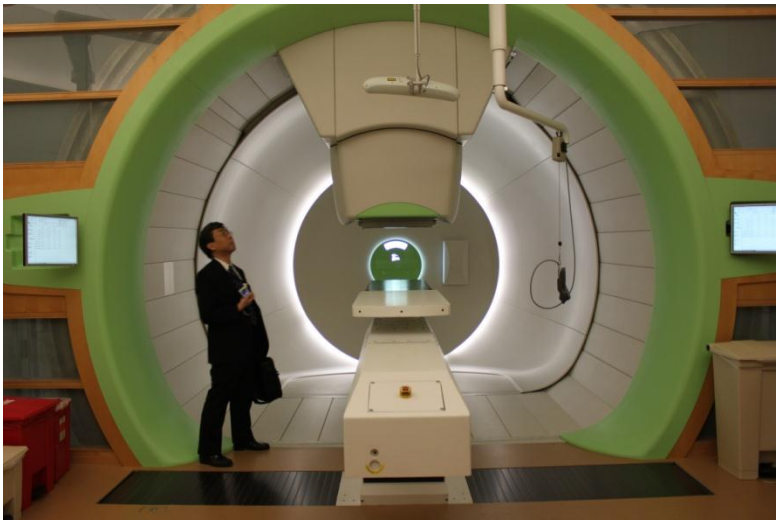

Figure 3.2. The rotating gantry at Roberts proton therapy center

Figure 3.3 shows a recent picture (spring 2010) of the treatment room of the heavy ion synchrotron complex (HIMAC project) at National Institute of Radiological Science (NIRS) in Japan. All the solutions for patient positioning and verification are evidenced in the figure.

Figure 3.3. HIMAC treatment room

A second center in Japan (Gunma University Heavy ion Medical Center,GHMC) has adopted a different approach, as depicted in figure. This facility, newer than the previous one, started its medical trials in 2010.
Again, all the solutions for patient positioning and verification are evidenced in the figure 3.4.


Figure 3.4. GHMC treatment room

The last solution presented here is the one adopted in the Heidelberg Ion-Beam Therapy Center (Heidelberg, Germany), depicted in figure 3.5. This facility is equipped with three treatment rooms. Two of them are characterized by fixed horizontal beams, while the third has a 360° rotating gantry. Since the start of clinical activities (November 2009), about 600 patients have received a treatment at HIT.


Figure 3.5. Treatment room in HIT, Heidelberg.

All the previous systems integrated a patient positioning system (PPS) and a X-ray patient verification system (PVS). Most of them are also equipped with devices devoted at providing information about patient's breathing phase. As seen in previous chapters, PPS is required for a proper immobilization of the patient and also to provide a precise alignment to the beam line. Images (PVS) are acquired to verify concordance of the patient's skeletal anatomy to a

digitally reconstructed reference radiograph (DRR) to guide translational shifts to the ideal planned isocenter. There are obviously difficulties in soft-tissue imaging. Gold marker seeds are frequently implanted near the tumor mass to help target identification, but also different methods (like ultrasonography, markerless fluoroscopy, cone beam projections and spirometry) have been explored (Xu and Hamilton 2005, Li *et al* 2009, Lin *et al* 2009, Cui *et al* 2008, Lewis *et al* 2010, Hoisak *et al* 2006, Kessler 2006, Amies *et al* 2005).
Because IGRT improves precision, it raises the possibility of hypofractionate the dose, by reducing the number of treatment sessions. Tumor targeting in external beam radiotherapy entails the confinement of the prescribed radiation dose to the target volume, thus reducing secondary damage (Sharpe and Moseley 2007). This is needed to provide maximal dose deposition in the tumor with contemporary sparing of healthy structures.
The achievement of optimal tumor targeting requires mainly:

- accurate treatment planning, aiming at the definition of the target volume from the anatomical and functional point of view;
- continuous and precise information concerning target position during treatment, that is when radiation dose is actually being delivered.

The former requirement is typically accomplished through specific imaging protocols, relying on current technologies for high definition volumetric imaging.

An important task of IGRT is to (ideally) eliminate or (more realistically) significantly reduce the margins involved in defining the clinical and planning target volume (CTV and PTV, respectively).
According to Xing *et al.* (2006), IGRT developments are focused in four major areas: (1) biological imaging tools for better definition of tumor volume; (2) time-resolved (4D) imaging techniques for modeling the intra-fraction organ motion; (3) on-board imaging system or imaging devices registered to the treatment machines for inter-fraction patient localization; and (4) new radiation treatment planning and delivery schemes incorporating the information derived from the new imaging techniques.
Regardless of the course of therapy, current standard imaging modalities such as CT and MRI do not always provide an accurate picture of the tumor extent, especially in the zone of infiltration that may be the limiting factor in an attempt of a radical treatment approach. Image fusion is often applied to combine anatomical and functional information for treatment planning, providing high resolution images for target definition (Balter and Kessler 2007). Current imaging technologies also allow time-resolved acquisition protocols to be used for those sites when target motion is an issue, such as in the lung or liver (Balderbos and Sonke 2009). For example, four-dimensional CT (4D CT) is commonly used to image anatomy variations as a function of patient breathing (Evans 2008).
In some cases, it is useful to monitor tumor motion during radiation therapy treatment. IGRT uses images of the patient at the time of treatment to determine the accuracy of setup so that corrections can be made in real time before the treatment is delivered.
Target localization during treatment requires the use of imaging technologies inside of the treatment room, to image the target or specific target surrogates when the patient is in position for treatment. When IGRT is applied to moving tumors image guidance becomes challenging, as motion leads to increased uncertainty (Dieterich *et al* 2008). Furthermore, the need of continuously monitoring tumor motion to achieve adequate targeting accuracy limits the applicability of IGRT technologies due to imaging dose constraints (Keall *et al* 2006, Murphy *et al* 2007, Walter *et al* 2007). Specifically, when ionizing radiation is applied in IGRT techniques, the imaging dose must be traded off with the required accuracy according to the ALARA principle (As Low As Reasonably Achievable) (Keall *et al* 2006).

The interest in real-time tumor targeting based on IGRT technologies is growing momentum in external beam radiotherapy because uncertainty in patient setup has long been known as a limiting factor to conformal radiation therapy. This applies both to conventional therapy, that uses photons and electrons, and to particle therapy, where protons and ions provide higher geometrical selectivity and enhanced biological effects (Durante and Loeffler 2010). In addition to the geometrical movements, particle beams show a strong dependence of the deposited dose distribution on the traversed radiological pathlength that changes with organ motion. All established techniques are thus adapted with respect to photon beam treatment to consider this important influence

Beam scanning requires accurate tumor tracking and effective motion compensation (Bert *et al* 2007, Grozinger *et al* 2008, Van de Water *et al* 2009). This is needed to make the most of the increased dose conformation and biological effect that can be achieved through dose painting techniques (Rietzel and Bert 2010).

In conclusion, new dose delivery techniques show significant potential for improving the effectiveness in treatments and can represent a step forward to reduce the number of treatment sessions and improve control in secondary diseases induced by radiations.

The increase geometric accuracy necessitate enhanced precision and accuracy in patient localization. Appropriate methodologies cannot be renounced but in most of the centers they are well integrated into the radiation therapy process.

3.2 Organ motion mitigation in lung cancer

Recent technological advances in radiation therapy, such as particle therapy, provide the capability of delivering a highly conformal radiation dose distribution to a complex static target volume. However, treatment errors related to internal organ motion may greatly degrade the effectiveness in presence of organ motion (Bert and Durante 2011).

In RT with particles, errors in target identification result in over or under dosage in planned structures. Consequently, we have to deal with two potential disadvantages: operators can release no therapeutic dose in healthy tissues but also a non uniform dose distribution inside the lesion.

Organ motion can seriously affect the outcome of the treatment and it can be difficult to manage adequately. The main cause for intra-fractionally organ motion in extra-cranial districts is respiration.

A clinical application affected by this effect is obviously represented by lung cancer case. In lung cancer treatments, normal physiological breathing induces in tissues (and consequently in the tumor mass) not negligible displacements. This results in the application of large safety margins. Consequently, motion can distort target volumes and result in positioning errors.

Several studies, conducted to examine the extent of diaphragm excursion due to normal respiration, reported the range of motion from 0.5 to 4.0 cm in the superior-inferior direction.

There have been several studies to characterize the amplitude, phase and periodicity of organ motion (Xu and Hamilton 2005, Shirato *et al* 2004, Seppenwoolde *et al* 2002).

Actually, even if adequate safety margins can minimize uncertainties caused by small movements (dealing with an unwanted inclusion of healthy tissue in the treatment volume), with larger movements additional and appropriate irradiation strategies have to be taken into account.

In an idealized treatment, tumor position should be directly monitored and the delivery of radiation is only allowed when the tumor is at the correct position.

The treatment workflow for intra-session organ motion mitigation requires a time-resolved measurement of the phase of the motion cycle, allowing operators to estimate the motion status of the tumor mass.
Treatment planning is usually based on 4D CT. The hypothesis is that the organ motion and references are reproducible and consistent with the planning set up during the entire treatment. Variation in breathing pattern could be monitored with intra session imaging. Moreover, patients relax or slightly change their position over time, so variations are common in middle and long treatment sessions. Tumor position during breathing is even more difficult to estimate when there is variation in amplitude, period, or baseline, or when the onset of end-expiration does not occur at the same point each cycle. When these inconsistencies arise, the sorted CT images may led to errors because of mismatches with planning reference.
In lung treatments different approaches have been debated. Only clinical methodologies are considered in this section. For example, the use of deep anesthesia is, in principle, a possible solution to stabilize the physiological movements. Nobody uses this technique because it results invasively, and also because a complete treatment session last usually weeks.

3.2.1 Breath hold

A first method to minimize the tumor motion is to ask the patient to hold the breathing (or force an interruption in breathing with mechanical respirators: active breathing control, ABC) during deep inspiration.
These techniques require patient compliance and active participation. This method is not suited for patients with compromised lung functions. Unluckily this eventuality often occurs in the most of lung cancer patients.
In breath hold the physiological movement is somehow freezed, allowing to irradiate in a steady setup. However, variations in pulmonary compression and tension of muscles can affect stability and reproducibility.

3.2.2 Gating

A diffuse technique is the so called gating. The patient is asked to breath normally. During the maximal expiration phases the patient is irradiated. During the other phases the irradiation is interrupted (Figure 3.6). Maximal expiration is considered as the most stable condition during breathing. It is obvious that this method requires the operators to monitor the breathing phase both during planning (a 4D CT is required) and during treatment sessions.
In order to perform gating, different dedicated tools are available. These tools are usually placed on the abdomen of the patient, providing an information of the current breathing phase. One of the disadvantages in gating is that treatment time increases. Long sessions do not represent just an issue of optimization of machine duty cycle, they can also results in unwanted effects like not negligible baseline shifts in respiratory patterns. Main reasons are related to patient's body adjustment in immobilization tools or a general relax of muscles. Irregularities in a patient's respiratory pattern can often be reduced by encouraging the patient to breathe calmly and consistently, and then relying on the patient's compliance during the scan. If this free-breathing approach is insufficient, dedicated software can provide proper signals that drive the patient in expiration \ inspiration.

The gating interval is typically centered at end-expiration because of the increased reproducibility at this point, and spans 20–30% of the breathing period to provide a reasonable duty cycle (Jiang 2006).

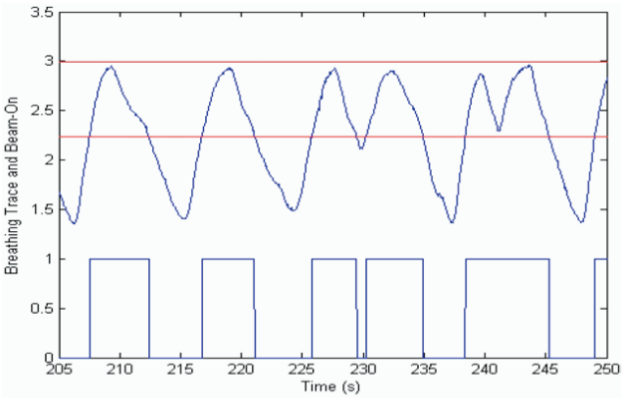

Figure 3.6. Patient breathing trace measured with the RPM system and the corresponding gating signal (Jiang 2006).

According to Jiang (Jiang 2006), in gated treatments there are two more important aspects to consider. The first is the concept of duty cycle. The second is the so called tumor residual motion. Duty cycle is a measure of the treatment efficiency and defined as the ratio of beam-on time to the total treatment time. For a non-gated 3D conformal radiation therapy (CRT) treatment, the duty cycle is 100%. For a typical gated 3DCRT treatment, the duty cycle is often about 30 –50%. Tumor residual motion is the tumor motion when the surrogate signal is in the gating window (beam on). Jiang concluded that a quality treatment is always a tradeoff between these two parameters. On a patient-specific base, operators should have to find a gating window that gives sufficient duty cycle while maintaining a small enough tumor residual motion.

3.2.3 Rescanning

If no motion mitigation technique is applied during the irradiation of a moving target with a fixed beam, dose deposition may be not homogeneously distributed. This effect is called interplay (Figure 3.7).

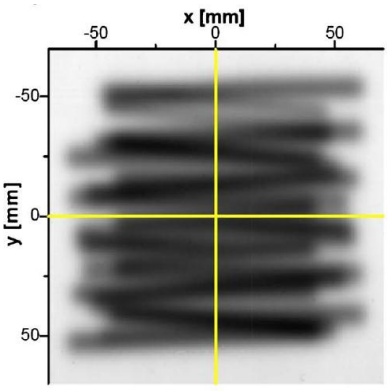

Figure 3.7. Experimental result of deterioration of the lateral dose distribution in 2D uniform scanning without motion compensation (Furukawa 2010).

Obviously, these effects reflect not only on the deposited dose, but also the geometric conformity results severely compromised.
A possible solution for interplay minimization could be to vary the number of fractions in which the therapeutic dose is subdivided, thus sparsely spread these errors in different

sessions. A more elegant solution is represented by the rescanning (or repainting). This method assumes that is possible to obtain a more homogeneous dose distribution by statistical averaging of repetitive interplay effects (Furukawa *et al* 2007, Zenklusen *et al* 2010, Seco *et al* 2009, Rietzel and Bert 2010). In fact, a smaller amount of dose is given iteratively inside the target volume, in order to statistically spread the uncertainties in its definition.
There are at least two major issues in performing rescanning:

- It is important not to synchronize the phase of dose delivery systems with target movement.
- Repetitive scanning means longer treatment sessions.

In reference to the first point, different strategies can be applied, aiming at randomize the dose delivered (Furukawa *et al* 2007, Seco *et al* 2009, Rietzel and Bert 2010). The second issue comprehend technological implications, and can be managed by using of very fast scanning hardware (Furukawa *et al* 2010).
In all the conditions, even if the dose results more homogeneously distributed into the target volume, we have to deal with a lateral deterioration of dose profiles (Figure 3.8).

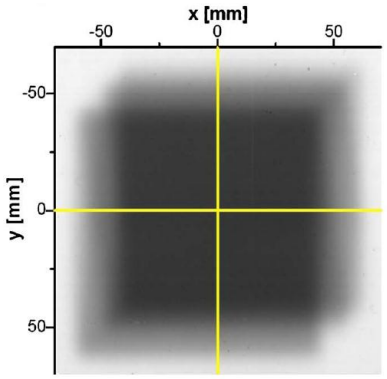

Figure 3.8. Experimental result of deterioration of the lateral dose distribution in 2D uniform scanning with ten rescans and matching of the irradiation time to twice the motion cycle (Furukawa *et al* 2010).

3.2.4 Tracking

A last solution to manage organ motion in the case of lung cancer is to compensate its effect operating on the beam line during all the respiratory phases: that is the tumor tracking. Accuracy in time as well as space is required in target tracking. Considering particle therapy, the direction of the beam, always active, is corrected phase by phase to mitigate the organ motion effect. This is an interesting approach (less beam and delivery time, high efficiency) but extremely challenging (it requires an estimation of a correction vector to follow the tumor mass, processing external signals characteristic of the surface of the patient). If we consider particle therapy, this solution does not present issues in latency of beam steering. Steering magnet system is faster than respiratory movements. One of the main issues is that throughout the whole treatment course, this consistency of patient/tumor geometry should be maintained. Beam tracking is technically feasible but will require robust planning to cover for potential changes of the underlying 4DCT data between planning and delivery. This is not the case of RT with photons, where the corrections have to be imposed directly to the accelerator.
By the way, accurate knowledge of real-time target location is challenging due to breathing motion variability during consecutive breathing cycles.

Different strategies may be applied to extract real-time target position information over time, ranging from continuous imaging (Shirato *et al* 2000, Shirato *et al* 1999, Jiang 2006, Huntzinger *et al* 2006) to the use of external surrogates (Brown *et al* 2007, Hoogeman *et al* 2009, Seppenwoolde *et al* 2007, Ernst *et al* 2011). The selection of the most appropriate approach is essentially dependent on the available technologies for in-room imaging and on the limits in imaging dose (Dieterich 2008). Therefore, minimally invasive technologies for continuous monitoring, such as optical tracking, are put forward to represent a viable solution (Baroni *et al* 2007). Such technology must be combined with prediction methods based on the correlation between external surrogates and internal tumor motion.
Instead, a possibility to reduce imaging dose is to reduce the imaging frequency. With a good predictive filter to predict tumor motion, the imaging frequency may be safely to reduce imaging dose.
Another way to reduce imaging frequency is to utilize the external markers together with the internal marker. This idea has been explored firstly on the CyberKnife® system.
One of the major disadvantages in this approach is that radio-opaque seeds have to be placed surgically into the lung, rising up the risk of pneumothorax.
Under these considerations, time prediction must take into account the latency of hardware whenever this could or not represent a problem in reacting to motion compensation information. The effective latency is a function of dose delivery systems: under this point of view particle therapy features numerous advantages, being steered by magnetic forces.

3.3 Applications of tumor tracking

Nowadays, only Cyberknife® Synchrony® performs tumor tracking. Cyberknife® is a commercial device for RT treatments with photons (Figure 3.9)

Figure 3.9. Cyberknife® system

The system is composed by a couch, two X-ray tubes (and related flat panels), an optical tracking system and a linear accelerator mounted on a robotic arm featuring 6 degrees of freedom. Once the patient is prepared and immobilized on the treatment couch, X-ray double projections are acquired, to identify metallic clips surgically placed nearby the tumor mass. In the mean time, the optical tracking system records the traces of three external surrogates placed on patient's body. These couples of external – internal coordinates are used to build a correlation model. Then, the treatment can start. The predictive model is used to provide a feedback to the robotic arm and to adjust consequently the position of the accelerator. During treatment, at predefined intervals, new X-ray images are acquired to check and update the

correlation model (Figure 3.10). The system takes into account a delay dues to mechanical inertia of the robotic arm (around 200 ms).

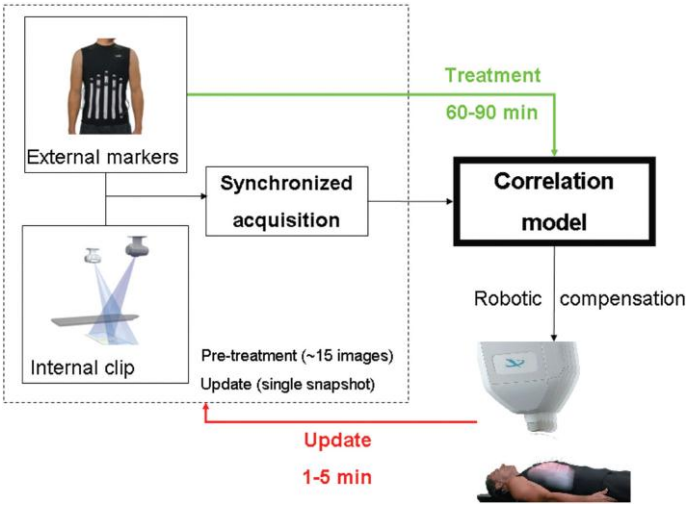

Figure 3.10. Workflow in Cyberknife® System®

The system provides tumor tracking relying on an external/internal correlation model between the motion of external infrared markers and of clips implanted near the tumor. The model is built at the beginning of each irradiation session using synchronized external/internal markers motion as training dataset. The initial model is updated as needed over the course of treatment with intermittent X-ray imaging. Infrared tracking is utilized to monitor patient breathing (at ~25 Hz) on the basis of 3 external markers placed on a vest. Implanted clips are visualized through orthogonal X-ray imaging and localized with dynamic tracking. The external/internal correlation model is exploited to adjust the position of the robotic linear accelerator according to the predicted tumor motion. The Synchrony® module models instantaneous tumor motion as a function of the external marker coordinates (Modeler) and predicts tumor motion in the near future (Predictor) to account for the system lag τ (~115 ms) (Seppenwoolde *et al* 2007). As the treatment proceeds, relevant data, including tumor motion model/prediction, the coordinates of external markers and intermittent clip localization, are logged and stored in ASCII format.

Even considering the possible limitations, the use of models able to estimate the position of a lesion, processing data from external surrogates represents a promising goal also in RT with particles . They could play an important role both during treatment planning (in order to make it more robust) and during treatment, where the use of active beam scanning allows tumor tracking in a faster way, and potentially with much more advantages, than with photons.
The next chapter is dedicated to the study of models for external – internal correlation and tumor tracking. Following the same approach of Cyberknife®, and using a database of patients irradiated with this device, alternative predictors have been investigated (Riboldi *et al* 2010, Torshabi *et al* 2010, Seregni *et al* 2011). After a first section where these models are introduced and described, results are compared with the tracking performances of the commercial device. With the intent of creating a custom dataset for models validation, a custom phantom was designed and built. The methodological approach is presented, as the integration of one of these application in the hardware of CNAO. Finally, next chapter concludes with a report about a feasibility study aimed at controlling the steering logic of scanning magnets for motion mitigation purpose during an active scanning irradiation with carbon ion beam.

3.4 Application of correlation models during an active scanning irradiation

Experimental activities for motion mitigation purpose during an active scanning irradiation with carbon ion beam were carried out in GSI Helmholtzzentrum für Schwerionenforschung GmbH (GSI). This center is situated in Darmstadt, Germany. The facility is equipped with a synchrotron and research activities are focused mainly on physics and radiobiology. Moving target group, lead by Dr. C. Bert and Dr. M. Durante, studies the effect of movement during irradiation and possible methods to compensate these effects. At the moment, this is the only group that can perform this kind of research with an active beam (Gemmel *et al* 2010, Grozinger *et al* 2008, Saito *et al* 2009). Beam delivery at GSI is performed with raster scanner technique. This methodology, together with the active energy variation provided by the synchrotron, allows completely active three-dimensional dose shaping.
In clinical, treatment planning requires the determination a priori of the necessary energies, positions and number of particles for each ion beam spots, in order to obtain an homogeneous dose distribution inside the volume. In case of particles, all the three spatial dimensions (and time if the target moves) required a planning optimization.
Cyberknife® approach can be extended, in principle, to this system. But it should be evident that errors in target identification result in a inhomogeneous dose distribution, thus variations in effective dose and biological effectiveness. The accuracy and the spot size composing the treatment volume depend from the dose delivery system. At GSI, irradiation with carbon ions allows operators to use millimetric spot sizes. That means that an error in target identification greater than this threshold produce equal erroneous deposition of particles.
For a proof-of-principle test the same optical localizer system installed in CNAO was carried at GSI, including an application for internal-external correlation (described in next chapter). Here the system was installed and connected to the therapy control system (TCS) of GSI to perform organ motion compensation by beam tracking. A custom breathing phantom was used during the irradiations, equipped with GafChromic films and 5 pinpoint ionization chamber to evaluate the concordance of tumor position estimation and beam direction. The phantom is described in next chapter but, summarizing, it is capable to mimic breathing motion, and to simulate the presence of an internal moving target.
Working in a bunker presents different issues comprehending radio-protection, available spaces (setup has to be flexible) and communication (integration of different modules and data exchange). However, controlling an active beam for treatments with accelerated particles requires at least two conditions:

- A treatment plan, and in the case of a moving target it is necessary that all the possible position of the target are coded into the treatment volume at each instance.
- A control system, able to provide a signal corresponding to the position of the target in the treatment volume.

At GSI, the system responsible of the correction of the particle beam position, in order to compensate the movements of the tumor located into organs affected by movements is called organ motion compensator (OMC). This system provides the position correction vector to the beam scanning magnets.
Usually, at the treatment planning phase, the tumor trajectory and breathing induced changes are captured in 4D by a CT scanner. In our case (phantom study) this procedure was done offline, based on a simple acquisition of the moving target with the optical localizer, so without X-ray imaging. Breathing motion was divided into multiple phases, to each of whom corresponds a position of the internal target and consequently a set of corrections for the OMC (see figure 3.11).

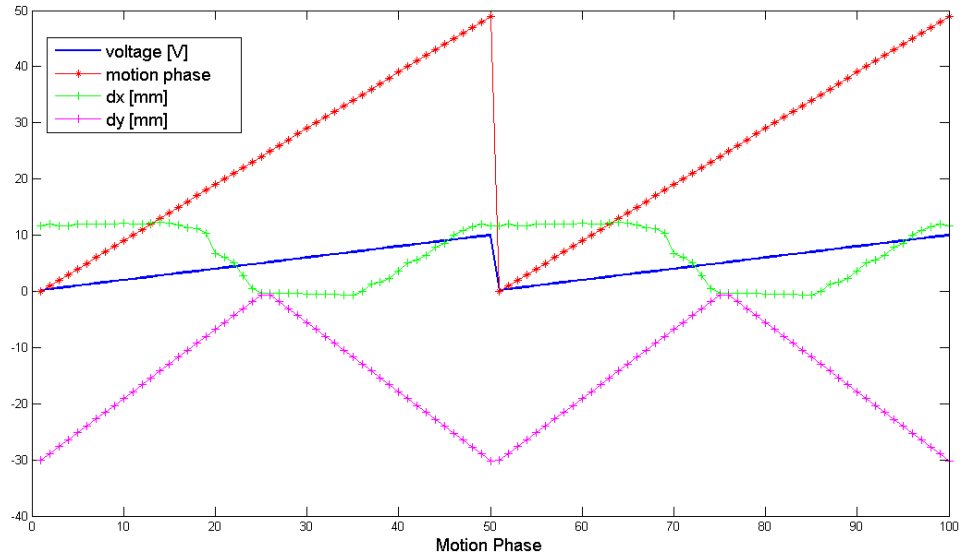

Figure 3.11. A complete breathing phase can be subdivided into windows (red line). Respiratory motion is quasi-periodic and so the signal is repetitive. The OTS is used to read the current phase, and shifts between different windows correspond to shifts in the signal sent to the OMC (blue line). Each window codes a position of the tumor in the irradiation volume, and so a correction vector is interpreted by the OMC (green and magenta lines).

The OMC selects one of the corrective vectors to be applied to the beam position, according to the respiratory phase detected by the optical system. OMC sends such vector to the steering magnets system, in order to tune the beam direction. The communication is based upon a GSI custom asynchronous serial protocol.
The OMC is connected to the IR optical system via a National Instruments USB-6501 board. This is an interface that converts the USB cable coming from the optical system (signal of breathing phase), to the GSI logic. In an alternative implementation, this correction vector can be sent to the TCS via two analogue or digital signals, for example via UDP. In this last, the process requires only to provide the correction vector to the GSI logic as a 2D vector.
During the irradiation of the phantom, the OMC receives the respiratory phase in real-time from the optical localizer. Such signal could be either the position of the internal target, on which a passive marker was applied (pure tracking), or the output of a predictive model.
Hereafter the technical specification of the system are briefly summarized:

- Sub-millimetric setup geometry verification provided by the OTS
- Mapping between local coordinate system to the room coordinate system (labeling of passive markers)
- Millisecond time scale
- Target position prediction based on:
    - Direct tracking of the target
    - Prediction with correlation model
- Amplitude based motion phase detection, according to the procedure described in this paragraph
- Communication module in input based on TTL signal (digital)
- Communication module in output based on:
    - analogic (0-10 V)
    - digital (UDP socket)

A description of the setup, here intended as the correlation models and the breathing phantom, is presented in next chapter.

Chapter IV

Methods for organ motion mitigation and tumor tracking

This chapter describes the materials and methods used to develop predictive models able to estimate the trajectory of a moving target in correspondence of patient's surface surrogates. The first section is then dedicated to the selection criteria and the description of models used. In the second section, applications are described, from a phantom study to the steering control of an active beam.
This chapter is organized as follow:

- Rationale
- Introduction
    - State model
    - Artificial neural networks
    - Fuzzy logic
- Materials and methods. Cyberknife benchmark study
    - Patient data
    - State model, artificial neural networks, fuzzy logic approaches
- Improvements in predictors
    - Improvements in fuzzy logic
    - Improvement in artificial neural networks
- Breathing phantom 1 (Aigor)
- Connections with an active beam scanning system
    - Breathing phantom 2 (Inga)
    - Connections and control software

4.1 Rationale

In radiotherapy, a successful treatment is achieved by producing high-quality target identification, and by delivering at the same time low dose to the healthy tissues surrounding the target. When tumor motion is not negligible, dose conformation may not be achieved properly, due to the uncertainties in target localization.
The use of external surrogates to predict tumor motion in real-time for extra-cranial sites requires the use of accurate correlation models. In extra-cranial treatments, accurate knowledge of real-time tumor location is challenging due to breathing motion variability during consecutive breathing cycles (Murphy *et al* 2006, Seppenwoolde *et al* 2007).
In between strategies aimed at minimize the organ motion effects, tumor tracking is the most challenging. During tumor tracking, a continuous irradiation is performed while beam and tumor motion are synchronized (Shirato *et al* 1999, Shirato *et al* 2000, Seppenwoolde *et al* 2002). This technique requires real-time accurate knowledge of tumor position in order to deliver a safe treatment. Different strategies may be applied to extract real time tumor position information over time, ranging from continuous imaging (Shirato *et al* 1999, Shirato *et al* 2000) to the use of external surrogates (Seppenwoolde *et al* 2007, Brown *et al* 2007, Hoogeman *et al* 2009). The selection of the most appropriate approach is essentially dependent on the available technologies for in-room imaging. When ionizing radiation is applied, limits on the imaging dose must be considered (Keall *et al* 2006). Therefore, prediction methods based on the correlation between external surrogates and internal tumor motion may be a valuable tool. The aim is to achieve accurate tumor position estimation while minimizing the imaging dose. A possible deal could be represent by periodic acquisitions of images for model validation or upgrade. But this requires the models to have retraining capabilities. This kind of approach is the one used by Ciberknife®, described in the previous section. We investigated different approaches, and details are reported in next paragraphs. The first test is to benchmark their performance with the commercial device, and understand if it is possible to achieved an adequate accuracy that could put forward these models as valuable tools in radiotherapy with accelerated particles.

4.2 Introduction and selection criteria for predictive models

Different models could be taken into account for tumor motion estimation processing external surrogates. There is no evidence of a gold standard model in RT applications (Murphy *et al* 2006, Seppenwoolde *et al* 2007, Hoogeman *et al* 2009, Kakar *et al* 2005, Riaz *et al* 2009, Vedam *et al* 2004, Ramrath *et al* 2007, Ruan *et al* 2008). The only device able to perform tracking is a commercial device, and by definition the correlation model used is unknown. We started our research based on these evidences, driven by the fact that medical data concerning internal external correlations is not easily available for models validation.
We used a patient database made available by the Georgetown University Medical Center (Washington, DC). Such database includes patients treated with real-time compensation of tumor motion by means of the Synchrony® respiratory tracking module, as available in the Cyberknife® system (Brown *et al* 2007). Alternative external/internal correlation models to Cyberknife® Synchrony® were at first implemented in MatLab (The MathWorks Inc., Natick, MA), using the embedded toolboxes for neural networks and fuzzy logic. The models were trained initially by using the same imaging points acquired for Synchrony® before treatment. After model parameters were estimated, all correlation models were applied to infer tumor trajectory as a function of time during treatment. The imaging points acquired during irradiation were used to check the model performance, to be compared to Synchrony®.

Following data acquisition and error calculation, the imaged tumor position was made available for model update as needed, using the same update strategy implemented in the Synchrony® module.
Briefly, we operated with different approaches based on:

- linear/quadratic correlation with implicit modeling of inhale/exhale variations (Seppenwoolde *et al* 2007, Ruan *et al* 2008). Such model is meant to represent a basic mathematical description of the regression curves that correlate the motion of external surrogates with internal tumor motion. The main advantage of this approach is the reduced computation cost, allowing near real-time model training and updating.
- artificial neural networks to correlate multiple external variables through non linear transfer functions (Sharp *et al* 2004, Robert *et al* 2002, Su *et al* 2005). Such approach features specific generalization capabilities, as neural networks are able to integrate multiple factors without the need of a priori information, and to estimate the influence of input parameters on the end result.
- fuzzy logic approach based on iterative data clustering and membership functions. The main advantage of fuzzy logic in comparison with conventional mathematical models is that the former can be developed on the basis of much less complete of precise input information (Shi *et al* 1999, Kang *et al* 2000, Lin and Wangs 1999)

Next paragraphs provide a description of these models.

4.2.1 State model approach

A possible approach to describe a dynamic model is through state variables. This approach assumes that is possible to quantify the state of a system in time. Time-dependent variations of the system can be described using mathematical associations. Moreover, state variables describe the state of a system ,at each time. Applications that require their use as a predictor have to define these variables before their application (simulation). State variables represent somehow the memory of a system, and their knowledge corresponds to a description of the system. The hypothesis is that all the variables of the system interact and are influenced one by the others. State models are used in engineering because they help to reduce complex phenomena to interactions between simpler systems. On the other hand, these last can be used to provide information of more complex systems.
Once defined the state variables, a state model is fast and it can be updated easily, every time new data are recorded.

4.2.2 Artificial Neural Network approach

The origins of studies on artificial neural networks (ANN) could be related to the idea that natural neural networks are able to provide a better interpretation of no arithmetic problems if compared with calculators. This consideration leaded first researches to find, if possible, a modelization of the natural brain using connections of basic mathematical units (Hertz *et al* 1991). This effort is at the basis of studies like ANNs, or genetic algorithms.
Nowadays the use of ANNs has assumed other dimensions than brain modelization. In facts, it is at this time impossible to reproduce an entire natural system like the human nervous system. However, ANNs are used for a wide range of problems, like signals estimation, objects classification, approximation of mathematical functions. Since their generalization capabilities,

ANNs have been proposed for medical and clinical purposes, both in decision-making problems and in extraction of unknown parameters from a group of variables (Pella *et al* 2011, Dayhoff and Deleo 2001).
From a theoretical point of view, ANNs are defined as a computational method based on non linear algorithms able to approximate the solution of a black-box problem, given a set of examples (see figure 4.1).
ANNs represent an interesting method because of their ability in generalization and their ease of use with inhomogeneous data inputs. ANNs represent a computational method for data prediction, and can be organized with an arbitrary number of interconnected layers and basic units (neurons). Each layer is ruled by a transfer function (linear, sigmoid or logarithmic are typically applied) that simulates the threshold of activation during data processing. Each node corresponds to a weight factor that describes the importance of that specific connection.
Weights are tuned to give the best interpretation of a problem during a first phase called training. In supervised learning, that is a particular situation where inputs and outputs relations are defined, a set of examples is shown to the network iteratively, and the performance of the network (typically the error committed in terms of MSE) is minimized to find the best solution. In other words, the training is the modulation of weights until (an optimal configuration of weights) the best solution is reached.

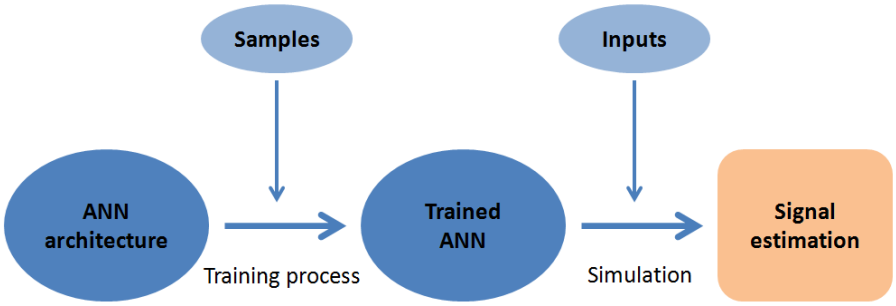

Figure 4.1. ANNs are able to process input data after a proper training process.

Compared to statistical approaches, ANNs usually produce the best performance when no significance difference is evident in how a set of inputs produce combined effects, but they suffer from initial conditions and local minima during their optimization. The performance of ANN based methods is directly correlated with the architecture, that implicitly depends on the problem to be modeled.
The majority of mathematical predictors are based on a deductive process, where a general rule is imposed to find the solution of a particular case. ANNs are based on a inductive process, where the general rule is somehow interpreted and applied case by case. This estimation can be applied every time a new set of variables is presented as input to the model.
Generalization capabilities usually produce an approximation of the solution, instead of a fixed and defined value (as it happened when a mathematical correlation is applied). ANNs could represent a reasonable approach when the problem under investigation is impossible to be described by a mathematical relation or too complex to be interpreted with an appropriate precision.

4.2.3 Fuzzy logic approach

Fuzzy logic represents a flexible tool able to model non linear functions of arbitrary complexity. This method is generally applied to classes of objects not characterized by defined boundaries, where the membership of each object is correlated to a degree of appurtenance. Fuzzy logic could represent a valuable methodology to map input data to an output space.
As in ANN approach, a set of external – internal values are used to build the clusters for data processing (Jain *et al* 1999). When a fuzzy model is built by training data, each external marker data is applied as input and the following steps are accomplished by fuzzy model to estimate the tumor motion as output.
We can divide the process in different steps.

- *Fuzzification*: This step takes the inputs and determine their participate degrees at each cluster via generated membership functions.
- *Applying AND/OR operator*: When the inputs are fuzzified, if the antecedent of a given rule has more than one part, the fuzzy operator is applied to obtain one number that represents the result of antecedent for that rule.
- *Applying implication*: Implication step in consequent part of fuzzy inference system uses a single number given by the antecedent part, and the output is a truncated fuzzy set. In the other word, the consequent is reshaped using a function associated with antecedent.
- *Applying aggregation*: This step receives all the truncated output fuzzy set of each rule and cumulate them as one fuzzy set.
- *Defuzzification*: This step acts as final step and the input is aggregated fuzzy set where the output is a single number that returns the center of the cumulated area under the curve. Defuzzification is obtained by Centroid Calculation method in our cases.

The features of fuzzy models make them quick in execution, such that the tumor position can be estimated in real-time condition.

4.3 Material and methods. Cyberknife® benchmark study

Next paragraphs provide a description of material and methods used for benchmarking state model, artificial neural networks and fuzzy logic with Cyberknife®.

4.3.1 Patient Database and Selection Criteria

A database of 130 patients, who received hypo-fractionated stereotactic body radiotherapy with CyberKnife® (Accuray Inc., Sunnyvale, CA) between 2005 and 2007, was analyzed.
Such database includes patients treated with real-time compensation of tumor motion by means of the Synchrony® respiratory tracking module, as available in the Cyberknife® system.
The available database was restricted to 86 patients (339 treatment fractions), as no indication concerning the treatment site was available for the other cases. The performance of Synchrony® respiratory tracking was analyzed in terms of residual tracking errors measured with X-ray imaging during treatment. Two groups were extracted: 10 worst cases and 10 control cases randomly selected among the population. The worst cases were defined as those fractions exhibiting the largest average tracking errors, as stored in the log files.

4.3.2 State Model

The correlation between external surrogates and tumor motion was established by means of a state model, that implicitly takes into account the hysteretic behavior of breathing motion (Ruan *et al* 2008).
The 3D movement of external markers was transformed into a mono-dimensional signal, by projecting the three dimensional coordinates in the principal component space.
Principal component analysis (PCA) was applied to marker traces acquired during the training phase, in order to extract the first principal direction of marker motion. External marker motion $m(t)$ at each timestamp t is expressed as follows:

$$m(t) = P[x(t)\ y(t)\ z(t)]$$

where P is the mathematical operator projecting the 3D coordinated onto the first principal direction, as defined in the training phase.
The state model was implemented as a linear/quadratic correlation between external marker motion $m(t)$ and internal tumor motion $\boldsymbol{T}(t)$. Hysteresis is modeled through a time lag parameter t, that is, by considering $\boldsymbol{T}(t)$ to be correlated with both $m(t)$ and $m(t - t)$. The selection of the proper time lag was limited by the sparse imaging data included in the database. We assumed the difference in breathing phase to be constant between two subsequent imaging acquisitions: therefore we selected t to be coincident with the time passing between adjacent samples. The implemented state model defines $\boldsymbol{T}(t)$ as the following matrix product:

$$T(t) = A(t)\ f(t)$$

where $\mathbf{A}(t)$ is the current state matrix, that characterizes the correlation parameters between external markers and internal tumor motion, and $\boldsymbol{f}(t)$ is defined as:

$$f(t) = \begin{bmatrix} m(t) \\ m(t-\tau) \\ 1 \end{bmatrix} \qquad f(t) = \begin{bmatrix} m^2(t) \\ m^2(t-\tau) \\ m(t) \cdot m(t-\tau) \\ m(t) \\ m(t-\tau) \\ 1 \end{bmatrix}$$

for linear and quadratic correlation, respectively.
The state matrix **A***(t)* was computed relying on the same training dataset used by Synchrony® and used to compute tumor motion for future timestamps. Least-square minimization of tracking errors was applied to compute the matrix. After each of the imaging data was acquired, **A***(t)* was updated using a first-in-first-out (FIFO) approach, with a data buffer limited to 25 imaging points. The on-line monitoring of 3D tracking errors was also implemented: when errors exceeded the 5 *mm* threshold, the PCA analysis was updated and the state matrix **A***(t)* was rebuilt as a function of the 25 most recent imaging points.
At each timestamp *t*, the selection of linear vs. quadratic correlation was made on-line according to *m(t)*: for values outside the 80% of the total range resulting from PCA analysis, the linear model was applied to limit extrapolation errors (Seppenwoolde *et al* 2007).
Separate models were developed independently for the three external markers that are available in the database: final ***T****(t)* position was computed as the average position of the three models (See Figure 4.2).

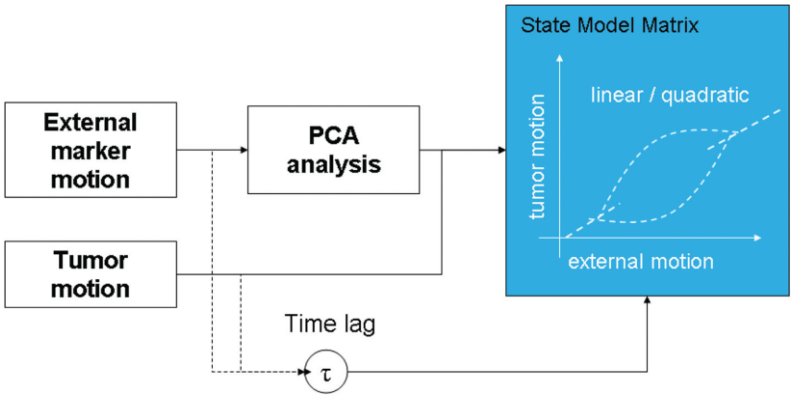

Figure 4.2. Flowchart of state model study (Torshabi *et al* 2010).

4.3.3 Artificial Neural Networks

Three independent ANNs, one for each of the external markers, were implemented for tumor tracking. Their outputs were averaged to estimate tumor position. Network architecture was designed as a single layer perceptron (Rosenblatt 1958), as depicted in figure 4.3, panel a. The X-ray images collected before irradiation was started, synchronized with the external marker motion, were considered as the initial training dataset. Out of range peaks were removed from training data in order to maximize the consistency in the definition of network parameters. Values exceeding a range of 1SD plus a 5 mm safety margin with respect to average tumor

position were defined as outliers. Training data were interpolated by a factor 1000 in order to minimize the effects due the extremely reduced dataset.
We selected a non linear and continuous transfer function equivalent to a mathematical hyperbolic tangent sigmoid:

$$Y_i = \frac{2}{1+e^{-2n_i}} - 1$$

As this function is derivable, we selected a back propagation (BP) algorithm with adaptive momentum to train the networks. We initialized the system with random weight and bias values, aiming at reducing the risk of symmetric initial conditions. The training phase in supervised learning requires that the input pattern is simulated and compared with the desired output signal. Levenberg Marquadt algorithm was selected, a fast and commonly used BP method in non linear optimization (Levenberg 1944, Marquardt 1963). We did not set any time restriction during training, but the main termination criteria were defined as follows:

- 1000 maximum iterations
- 6 maximum failures within the validation dataset
- performance goal (intended here as the mean square error between simulated and desired outputs) equal to 0.

Data acquired during the treatment session were used to control the overall performance and to re-train the networks as needed. Given the simple architecture, it was possible to retrain at every incoming X-ray image without affecting the computational speed significantly. The re-training process relied on the same data interpolation procedure described above.
The re-training strategy was implemented according to the following error-based approach:
1. If the maximum error measured on the incoming X-ray image was <0.3mm, the network was re-trained using 30% of the most recent imaging frames. Input and output data were interpolated by a factor 100.
2. If the maximum error was larger than 0.3mm, a new network was built based on 90% of the most recent imaging points for training. Input and output data were interpolated by a factor 1000.
The final output was obtained as the average of the corresponding simulations of each network along the three anatomical directions (Figure 4.3, panel b).

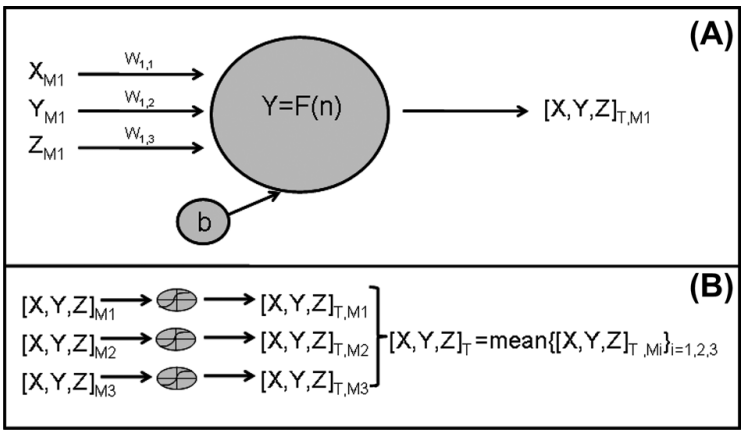

Figure 4.3. Basic unit of ANN approach (panel a); average criteria for target coordinates estimation (panel b) (Torshabi *et al* 2010).

4.3.4 Fuzzy Logic

We developed a correlation model based on a fuzzy logic inference system. This latter involves data clustering for membership function generation, logical operation and if-then rules. The end result is a nonlinear mapping from the motion data of external markers to an output which is the estimate of tumor motion, using a fuzzy logic approach. In the implemented fuzzy logic algorithm, data from all three external markers were used as inputs (figure 4.4).
Data clustering is a process of putting similar data into sub-groups and plays an important role in the construction of the fuzzy inference systems (Jain *et al* 1999). In our case, the Fuzzy C-Means (FCM) clustering algorithm was considered in initial data grouping (Dunn 1973, Bezdek 1981). In the fuzzy model the training dataset is grouped into *n* clusters using a specific influence range. A small influence range yields many small clusters in the dataset and specifying large influence range results in few large clusters. The value of such influence range was set to one third of the maximal extension of the training data space, which acts as an optimal value for defining the appropriate number of cluster for each patient. Each data point that lies close to the center of a cluster will have a high probability of belonging to that cluster (membership grade), and another data point that lies far away from the center of a cluster will have a lower grade. Our fuzzy model procedure for data grouping and membership function generation is based on the minimization of the following objective function, representing the distance from any given data point to a cluster center weighted by its membership degree:

$$J_m = \sum_{i=1}^{N}\sum_{j=1}^{C} u_{ij}^{m}\left|x_i - c_j\right|^2$$

where *m* is any real number greater than 1, u_{ij} is the degree of membership of x_i in cluster *j*, x_i is the i^{th} measured data point, and *cj* is the center of the cluster. The value of *m* was set to 2 in our objective function following preliminary tests where values in the [1.5, 2.5] range were investigated (Yu *et al* 2004, Bezdek and Pal 1998).

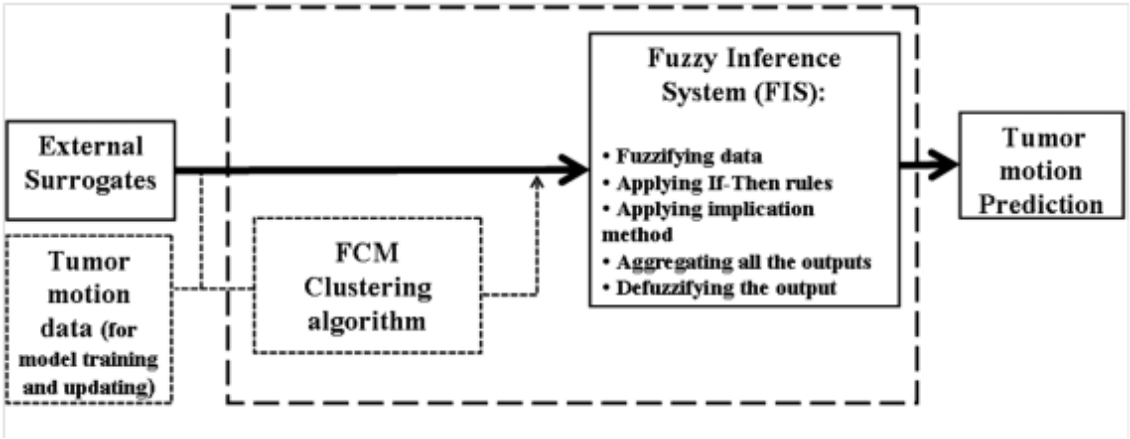

Figure 4.4. Flowchart of fuzzy logic correlation method (Torshabi *et al* 2010).

At first, FCM starts with an initial guess of cluster centers, corresponding to the mean location of each cluster. Next, the FCM algorithm assigns every data point a membership degree for each cluster, and then iteratively moves the cluster centers c_j and updates the membership degrees u_{ij}:

$$u_{ij} = \frac{1}{\sum_{k=1}^{C}\left(\frac{|x_i - c_j|}{|x_i - c_k|}\right)^{\frac{2}{m-1}}}$$

$$c_j = \frac{\sum_{i=1}^{N} u_{ij}^m \cdot x_i}{\sum_{i=1}^{N} u_{ij}^m}$$

This iteration will stop when $|U(k+1)-U(k)|<\varepsilon$, where ε is a termination criterion between 0 and 1, $U=[u_{ij}]$ matrix and k is the number of iterations. The structure of the fuzzy inference system used the model is based on Sugeno (or Takagi-Sugeno-Kang) model (Takagi and Sugeno 1985). This model is computationally more efficient and thus gives a faster response, which is critical in situations where quick decisions should be taken.
The fuzzy inference model can also be updated automatically, using X-ray imaging points during the treatment. Updating step is performed by adding the last imaging data to the previous data and then re-building the fuzzy model using all the gathered imaging data.

4.4 Improvements in model approach

Models described in previous paragraphs were benchmarked with Cyberknife Synchrony, and results are shown in next chapter. Both ANNs and fuzzy logic are a powerful tool, and their parameters can be ideally tuned in an infinitive ways. Concerning these two approaches, we performed different improvements, aimed at providing better performances and a better knowledge of their behavior. In next paragraphs, these improvements are presented. However, the goal was slightly different: in case of fuzzy logic, different clustering methods were compared. In case of ANN, a new architecture was designed and efforts were devoted to set an application that could operate in CNAO hardware. In order to do that, an application in C++ language was built.

4.4.1 Improvements in fuzzy logic

We further investigated correlation models based on fuzzy logic.
As seen, in the construction of the fuzzy inference systems data clustering plays an important role (Anil and Dubes 1988, Jain *et al* 1999). In this second approach, fuzzy model consists of two different data clustering algorithms, that results in:
1) Subtractive based fuzzy inference system
2) Fuzzy C-Means (FCM) based fuzzy inference systems (Jang 1997, Chiu 1994, Dunn 1973, Bezdek 1981).
In subtractive clustering algorithm each data point of the dataset can potentially be candidate as cluster center in proportional with the density of surrounding data points, whereas FCM algorithm uses fuzzy grouping properties in data clustering such that the given data point in a dataset belongs to several clusters with different membership degrees. Moreover, taking into account Adaptive Neuro-Fuzzy Inference System (ANFIS) (Jang 1993), there are three FIS-based systems, configured in a same time for tumor motion estimation in training step.
Since the performance of each modeler for tumor motion prediction is not necessarily the best for all cases, a model selectivity option was in the end proposed, in order to select the proper correlation model in the training step for each patient.

During training, two fuzzy inference systems based on above clustering approaches and also an Adaptive Neuro-Fuzzy Inference System, are configured for motion prediction during treatment. The properties and implementations of these inference systems are detailed in the following paragraphs. It is important to point out that all three correlation models can be updated automatically, using X-ray imaging points during the treatment. The updating step was performed by adding the last imaging data to the previous data and then re-building the correlation models using all the gathered imaging data, as in the previous case.

4.4.1.1 Fuzzy inference system using subtractive clustering

In this model, the subtractive clustering algorithm (Chiu 1994) was considered in initial data grouping and membership function generation. In subtractive clustering each data point of the dataset can potentially be candidate as cluster center, proportionally to the density of surrounding data points. Therefore based on the following equation, a calculation is performed to define the cluster center:

$$D_j = \sum_{i=1}^{N} \exp\left(- \frac{\left\| x_i - c_j \right\|^2}{\left(r/2 \right)^2} \right)$$

Where x_i is the i^{th} measured data point, c_j is the center of the cluster, and r is the neighborhood radius or influence range. By this way, a data point with high density value has a huge amount of neighboring data points.
Subtractive clustering operates as follows:

1- Selects a data point having the largest density value, candidate as first cluster center.
2- Removes all data points covered by the first cluster configured with pre-defined neighboring radius for determining the next data cluster and its center location.
3- Continues density measurements on the rest of data points until all the data points are covered by the sufficient clusters.

In this algorithm, a small influence range yields many small clusters in the dataset and specifying large influence range results in few large clusters. In the implemented model the value of such influence range was set to one third of the width of the training data space, according to the same approach followed previously.
By the end of data clustering, a set of fuzzy rules and membership functions are extracted. Each cluster represents a condition. Since the membership functions used for our fuzzy inference system are Gaussians, the cluster centers and the distance between them can be used as required parameter for membership function generation over input and output training dataset.

4.4.1.2 Fuzzy inference system using FCM clustering

In this model, the training dataset is grouped into *n* clusters and this step is performed using subtractive clustering with a specific influence range on training dataset. Then, based on FCM analyze properties, each data point in the dataset is allocated to every cluster with a certain degree according to its distance from the cluster centers. The procedure regarding this approach is presented in previous paragraphs.

4.4.1.3 Adaptive Neuro-Fuzzy Inference System

ANFIS could be intended as an adaptive network which uses neural network learning algorithms and fuzzy inference system to associate the external marker motions (input) to the tumor motion (output). In ANFIS, the membership function parameters are determined using subtractive clustering in fuzzy section and then adjusted using either a back-propagation algorithm alone or in combination with a least squares type of method.
The Gaussian and Bell-shape membership functions are increasingly popular for specifying fuzzy sets due to the smoothness and concise notation. The bell-shape membership function is defined as:

$$Bell - MF = \frac{1}{1+\left|\frac{x-c}{a}\right|^{2b}}$$

Where *a, b* and *c* are the parameters of membership functions in premise part of fuzzy if-then rules that change the shape of membership functions.

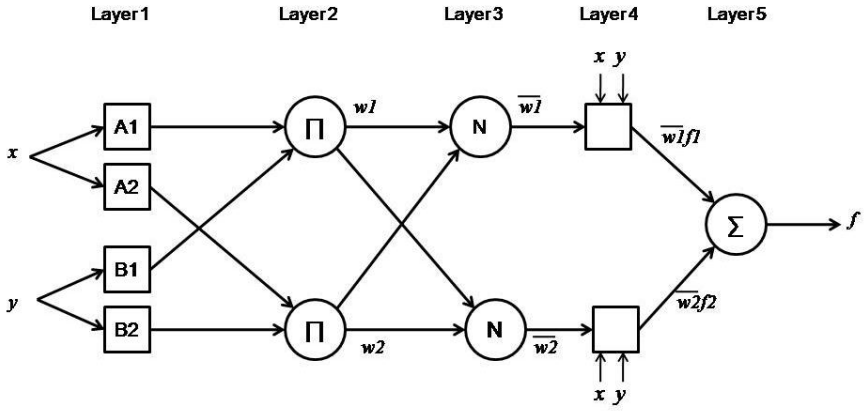

Figure 4.5. ANFIS architecture

As shown in figure 4.5, the architecture of ANFIS consists of 5 layers and the number of neurons at each layer equals to the number of rules. Layer 1 consists of input nodes. Each node generates membership grades using membership functions. In Layer 2, that includes rule nodes, the AND operator is used in order to product all incoming signals that represents the firing strength for that rule (w_i). The third layer, aimed at calculating the ratio of each i^{th} rules' firing strength to the sum of all rules' firing strength. Thus the output is called normalized firing strength. The fourth layer computes the contribution of each rule toward the total output. In layer 5 the single output node calculates the overall output by summing all incoming signals that is:

$$f = \frac{w_1 f_1 + w_2 f_2}{w_1 + w_2} = \overline{w_1} f_1 + \overline{w_2} f_2$$

In ANFIS, the non-linear premise parameters (a_i, b_i, c_i), associated with the membership functions, are tuned through the learning process iteratively. The tuning process is controlled

proportionally to the error value of the fuzzy inference system section in correlating the input/output dataset.

4.4.1.4 Model selectivity algorithm

The produced correlation models can estimate the tumor motion independently. Although all three modelers track tumor motion in accordance, they differ in their prediction accuracy due to their specifications in membership functions generation and also input/output variability. Under this consideration, selecting a patient specific adaptive fuzzy model may be useful. For this reason, a model selectivity option was proposed to be applied to final prediction algorithm in order to select the proper correlation model in the training step for each patient between three current modelers.
The available training dataset was divided into two parts with one fourth ratio. 75% of the training dataset was used as training data for three modelers configuration, whereas the 25% was exploited to check the accuracy of each modeler. The optimal modeler for each patient was selected relying on the preliminary check performed on 25% of the training dataset, assuming that optimal performance during training resulted as optimal during the rest of the treatment. Figure 4.6 represents the flowchart of our final prediction model, including the model selectivity subroutine during training. It should be considered that a large amount of training dataset contains all the necessary representative features and therefore the process of selecting the proper modeler is easier.

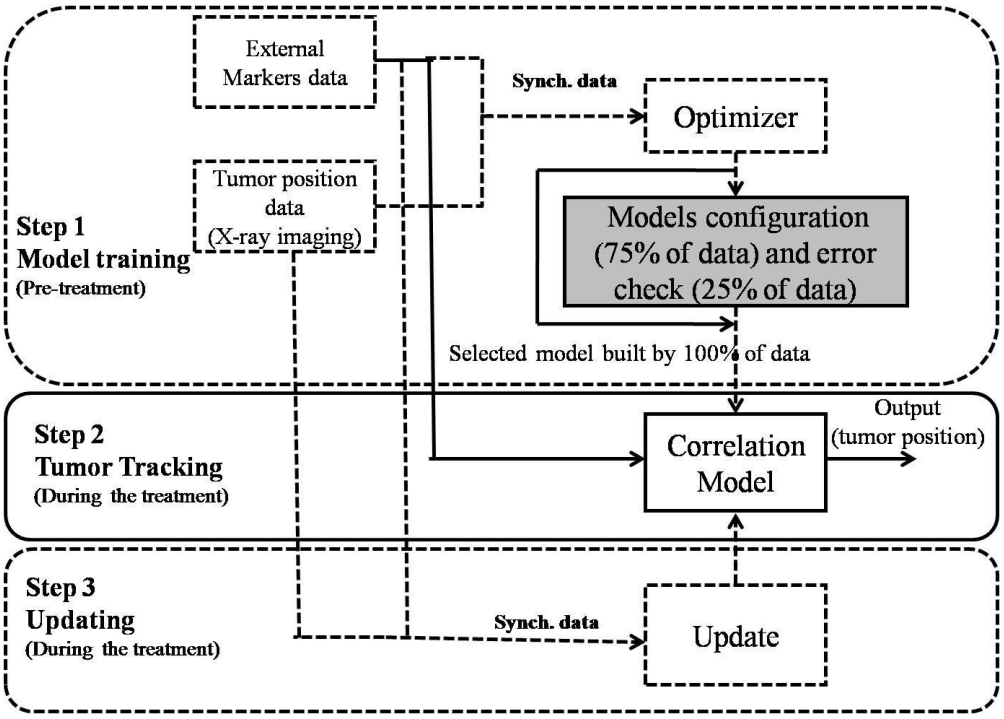

Figure 4.6.flowchart of model selectivity option.

The implemented strategies were tested and benchmarked vs. the Cyberknife® Synchrony® module in terms of residuals targeting errors.

4.4.2 Improvements in artificial neural networks

The approach described in the previous paragraph dedicated to ANN model, was improved. Changes were mainly aimed at:

- designing an algorithm to be integrated into an optical localization system used for external motion monitoring, for real time predictions.
- validating the application with a benchmark of new results vs. a clinical dataset coming from Cyberknife® Synchrony®.

ANNs have been implemented in C/C++ language. The approach was the same presented before in this chapter, providing an estimation of internal target motion as a function of external surrogate signals, and featuring some slightly modifications.
The developed method was designed to be applied in the frame of the workflow for real-time tumor tracking based on internal/external correlation, which we describe hereafter:
1. At the beginning of the treatment, a training dataset is collected, as already described. The workflow includes spline interpolation at this stage in order to obtain a training dataset containing 500 distinct examples.
2. Once the training dataset has been collected, three different neural networks, one for each of the external markers, are trained with a back-propagation algorithm. We selected a feed-forward double-layer architecture featuring a hidden layer of 10 units and a hyperbolic tangent activation function, which is applied to both the hidden and the output layer.
Termination criteria included in the algorithm were:

- Maximum number of iteration = 100
- RMS error < 0.01 mm.

3. Trained ANNs are exploited for the estimation of the target position as a function of each sample of the external signal. Again, since three independent estimations are obtained (one for each network), a unique output is calculated by averaging the outputs of the three ANNs.
4. Retraining capabilities were included in the algorithm. The retraining process was implemented as a threshold based procedure depending on the error in prediction. The estimation error is calculated for each network: if it exceeds a user-defined threshold, the neural network is retrained using a training set which is updated by including the most recent input/output data and discarding the oldest one (First In First Out, FIFO).
We defined two threshold values (α and β) both expressed in millimeters and referred to as retrain and rebuild threshold, respectively. The values of these thresholds are user-defined but β is intended to be larger than (or equal to) α: we set α = 1 mm and β = 2 mm in our implementation. According to the value of E_i, the algorithm develops as follows:

- If $E_i \leq \alpha$, the i^{th} network is not retrained.
- If $\alpha < E_i \leq \beta$, the i^{th} network is retrained starting from current inter-synaptic weights.
- If $E_i > \beta$, then the i^{th} network is retrained starting from randomly initialized inter-synaptic weights.

4.5 Breathing phantom1 (Aigor)

Experimental validation of adaptive correlation models suffers from the lack of clinical database including appropriate description of tumor motion synchronized with external markers, thus forcing to rely on simulation and / or custom phantoms (Gemmel *et al* 2010).
We designed a 4-dimensional (4D) breathing phantom (Figure 4.7), mimicking realistic respiratory motion and featuring simultaneous 3-D displacements of the external surface and of inner targets with variable phase and amplitude shifts. It should be noted that the main purpose of the phantom is to simulate internal and external signals with amplitudes and frequencies comparable to those observed in real subjects, allowing us to validate internal/external correlation algorithms. Further developments in order to obtain a more realistic breathing pattern are currently on going.
Motion in the first version of the phantom was driven by an electric motor (6-12 V, 1-4 A) with variable power supply voltage output for the tuning of breathing frequency. The mechanical coupling between the engine and the moving phantom was realized by means of a piston rod. The piston expanded a ribcage structure acting on two lateral and one frontal main ribs. The chest wall expansion was controlled by an elastic cover simulating the deformable skin surface, where external motion surrogates were attached. Motion of inner targets was provided by connecting targets to the driving piston and chest wall structures by means of variable and adjustable springs and elastic bands.

Figure 4.7. First version of the breathing phantom (Pella *et al* 2010).

We firstly tested our 4D phantom by means of CNAO OTS. We placed 3 markers (2 laterals, 1 frontal) on the surface of the phantom and one in correspondence of the inner target. External marker motion was in the 2.2-6.1 mm range with variable phase shift depending on markers

locations. 3D target displacements were up to 29.8 mm peak to peak, with significant hysteresis over multiple breathing cycles (Figure 4.8).

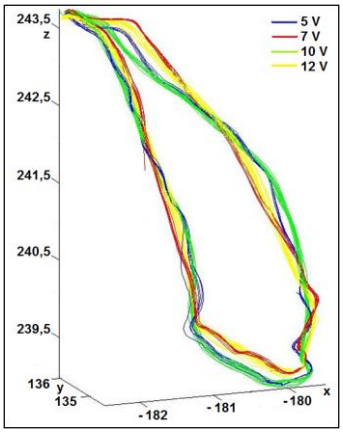

Figure 4.8. Hysteresis of target over multiple cycles (Pella *et al* 2010).

This phantom can also operates manually with an elliptic pulley. In this way, an ideally continuous rotation of the pulley is converted into a vertical harmonic motion of the piston, connected to the pulley with a belt. Moreover, the pulley features a variable cross section across its length, so that the amplitude of vertical motion can be tuned from 5 cm to 11 cm peak to peak. Faster rotations result in higher frequency, while slow rotations in slower frequency, depending by operator. The hysteretic trajectory of the inner point is maintained as in the case of motor induced movement.

In order to perform on-line acquisitions using the moving phantom, we integrated the developed correlation algorithm into the optical localization system installed in CNAO, and described in previous chapter 2.

The integration of the correlation algorithm took advantage of a software provided with the SMART-D system, whose main function is to read the 3D position of every point localized by the TVCs and to make it available to the user in real-time (60 Hz sampling rate).

In order to correctly identify the marker simulating the target and to provide a consistent input to the ANNs, an automatic labeling of the four markers is required at every acquired frame. For this reason, a dedicated algorithm was developed exploiting the a priori known distribution of the markers along the left-right direction of the phantom.

In order to mimic episodic imaging, during trial sessions the 3D position of the marker representing the target, was downsampled at 2.5 seconds of the nominal acquisition frequency). Once 15 points were available and the interpolation to reach 500 corresponding samples was completed, the algorithm proceeded with the initial training of the ANNs.

In a second stage, the target position is estimated in correspondence of each acquired frame and checked intermittently with a period of about 16.5 second (once every 1000 acquired frames). The retraining strategy was implemented exactly as previously described for the simulation of CyberKnife® treatments (α=0.1 mm; β=1 mm).

Three experimental acquisitions on the moving phantom were performed. At the beginning of the acquisition, the phantom was moved approximately from maximum inspiration (piston pushed fully down) to maximum expiration position (piston pulled fully up). In this way the initial training data set is likely to be spread on the entire range of motion of the phantom. Then, a series of regular and irregular breathings were manually imposed, changing speed and section of the pulley. The duration of these acquisitions was about 3 minutes each.

During every acquisition, the software generates a log file which contains all the real-time estimations of the target position calculated by the algorithm and the actual target position acquired simultaneously by the SMART-D system. In addition, the frame number is recorded in correspondence to each estimation for off-line analysis.
The real-time capability of the implemented application in estimating the target position was investigated by examining the sequence of the logged frames numbers: the dropping of one or more frames accounted for a missing real-time target position estimation.

4.6 Connections with an active beam scanning system

The conclusive experimental activity envisaged the integration of hardware and methods (described in the previous paragraphs) in the control logic of an active carbon ion beam. Our systems, here intended as the breathing phantom and the OTS, were moved to GSI, where two experimental sessions were conducted in collaboration with Moving Target group. A second version of the breathing phantom was built (see paragraph 4.6.1).
We perform 2 series of experimental session. The first one was carried out in July 2011, while the second in October 2011.
The first experimental series aimed at establishing the communication between the OTS and the organ motion compensator (OMC). The OMC system integrates the information provided by IR optical tracking with the dose delivery control system, providing the position correction information to the beam scanning magnets.
Natural respiration is considered quasi-periodic. Our phantom is able to simulate a breathing with high repeatability, so this hypothesis is maintained. By then, it is possible to considered a breathing period as a composition of multiple phases. Each phase interval correspond in this way to a position of the internal target. This correlation, being known during training data acquisition, is used by the model application running in the OTS to correlate the position of the tumor surrogate and so to provide a correction vector to the steering magnet system.
As mentioned in chapter 3, the OTS was connected to the GSI systems with a dedicated National Instruments USB-6501 board, an interface that converts data coming from the optical system, to the Digital Input Output (DIO) connector of GSI.
Once the phantom is moved, OTS provides a signal correlated to the current phase, as defined before. This information is sent to the organ motion compensator, that selects one of the corrective vectors to be applied to the beam position previously stored. This vector is used to change the beam direction.
The experimental series performed in July 2011 at GSI aimed at establishing the communication between the two systems.
A second experimental session, performed in October 2011, was dedicated to the active tracking of the moving target, including in the protocol ANN prediction with retraining capabilities. Even if the set up was mainly the same of July, there were several differences in the communication between systems.

4.6.1 Breathing phantom2 (Inga)

A second version of the breathing phantom was designed, aimed at being used in a treatment bunker. It was necessary for the new version to satisfy at least these specific requirements:

- It had to be controlled in remote mode. This first requirement could appear as obvious. Nobody is allow to remain near the phantom during an irradiation with carbon ions. Under another point of view, this means that all the procedures (that

is, variations in amplitude, variations in frequency, middle-long session reliability) have to be prepared before the session or controlled with a remote desktop.

- target hysteresis had to be planar. There are two main reasons because of this requirement: the first is that the OMC is able to manage only 2D displacement at the moment. The second is related to the geometry of the pinpoint holder. All the pins should face the beam, in order to maximize the effects of particles recorded by ionization chambers.
- It should be provided irregular breathing patterns. In order to stress tracking capabilities, it was necessary to tune over different hysteretic trajectories.
- Movement repeatability should be guaranteed, in order to be able to compare different tracking strategies over the same regular or irregular pattern.
- A new target holder, able to host up to 5 ionization chambers and a weight of about 200g was necessary.
- It should be avoid, or limited, the use of metals near the pinpoint holder.
- Human like dimensions or at least compatible with available space in a treatment cave (treatment couch).
- The phantom should maintain all the functionalities of the previous version (that is, possibility of an arbitrary number of markers, correlation of external/internal movement).

The second version of the phantom is depicted in figure 4.9.

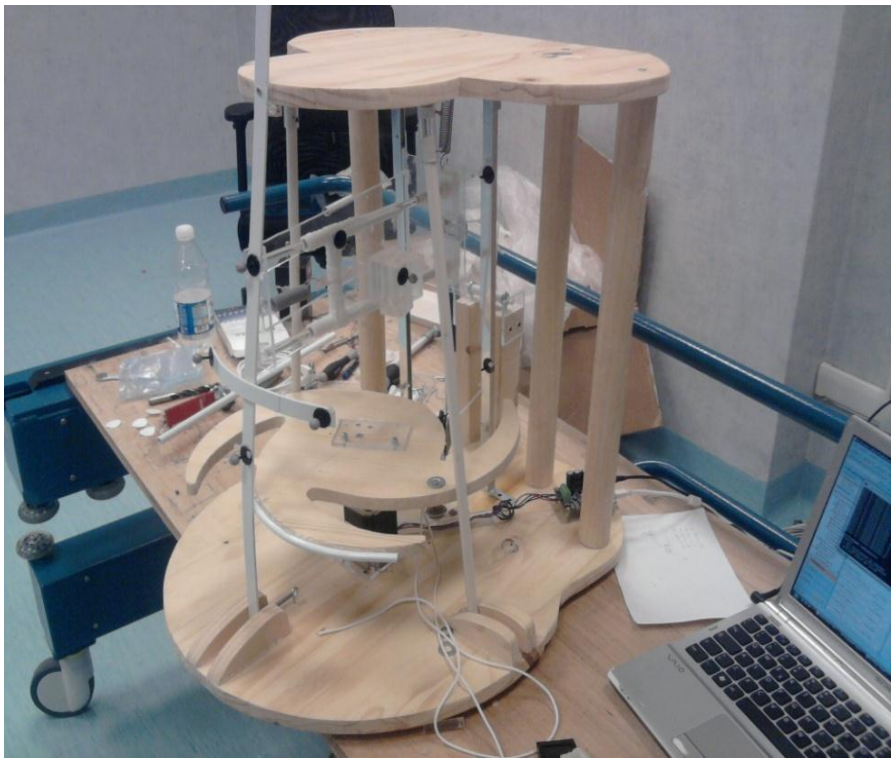

Figure 4.9. Second version of the breathing phantom.

The main components are reported hereafter:

- Rotating part. This rotating unit was designed to provide an adequate excursion to the external structures. Differently from the previous version of the phantom, the movement is a planar rotation, with a variable section length.

- External ribs. This approach is derived by the previous version. New rib-sticks were considered. The new version is characterized by light plastic ribs fixed on the top of the phantom rigidly and with springs on the bottom. The central rib has a more rigid spring, if compared with laterals, and this allowed a significant difference in trajectories of markers placed on them.
- A new structure for target motion was ideated. In order to provide a planar movement two vertical guides were used to pull up and down the pinpoint holder. Attrite was minimize by using aluminum profiles and a synthetic silicon. On the top, this structure was anchored with a spring, while on the bottom it was fixed through a rope at the rotating unit. To perform the horizontal movement, the same approach was considered. In compliance with requirements, we did not use aluminum profiles but Plexiglas/plastic components in this case.
- Pinpoint holder was designed in order to host up to 5 ionization chambers (Figure 4.10). This part is composed by a unique piece of Plexiglas, and was manufactured by GSI workshop. This particular design allowed to keep relatively low weights the highest surface of ionization chambers to beam.

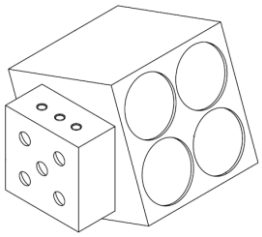

Figure 4.10. Pinpoint holder design

- A stepper motor was used to move the rotation unit. This stepper motor is USB connected to a PC by means of a dedicated control board.

Phantom repeatability of movements, as a feasibility study of the set up in terms of markers visibility were required as preliminary condition and was tested in Pavia. Results of this trials are reported in next paragraphs.

4.6.2 Connections and control software

As seen, a second version of the breathing phantom was built, according to requirements. Moreover, the new geometry of the target required implicitly to reinterpret the internal moving part of the phantom.
Major differences between the first version were also in the connections and in the control system. A general application aimed at controlling the stepper motor, the OTS and the ANN predictor was embedded in the OTS workstation. As shown in figure 4.11, this application can be intended as composed by three modules.

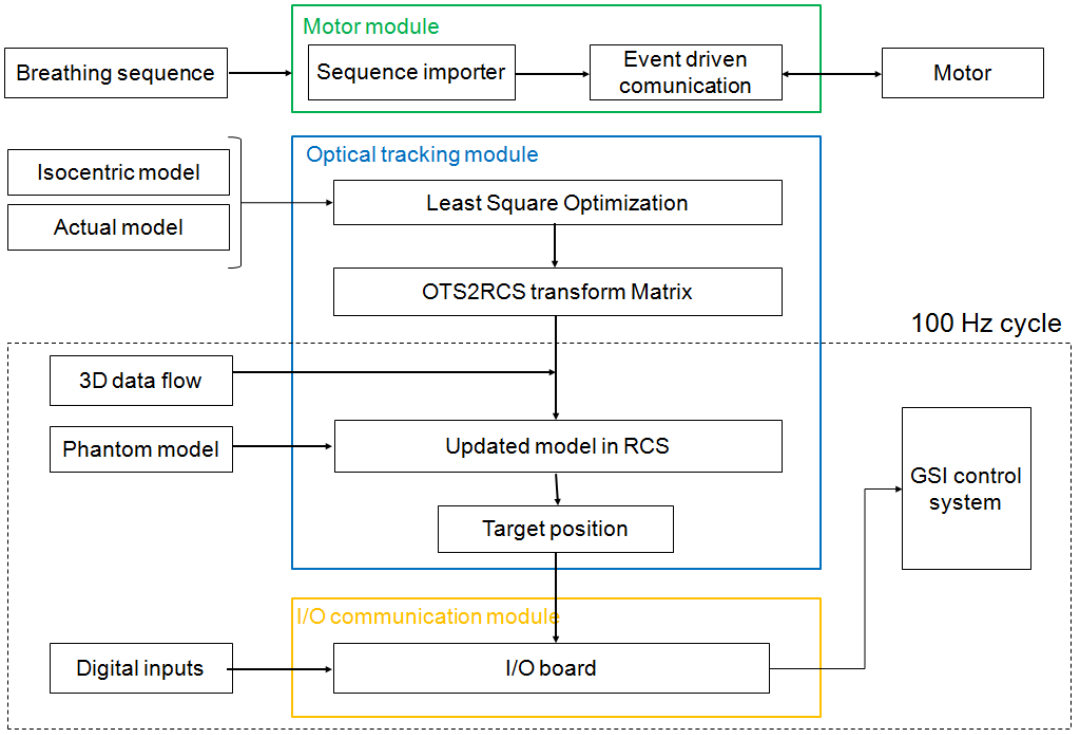

Figure 4.11. Control modules scheme.

- Motor module: this module aimed at sending the motion parameters to the stepper motor. Parameters were: speed, acceleration and destination. Tuning opportunely these parameters it was possible to provide different patterns in phantom motion. It was also possible to load pre-defined sequences from file, thus allowing operators to compile sequences and run regular or irregular patterns depending by the required set up.
- Optical tracking module: this module aimed at mapping the local coordinates as seen by the OTS in room coordinates. In this module was embedded also the ANN predictor
- I/O communication module: this module was devoted to the control of the National Instrument board (1st experimental session) or the management of the UDP communication (2nd experimental session), providing to the steering control system of GSI information about target current position.

During the first experimental session, performed in July 2011, for a proof-of-principle test the OTS were installed and connected to the therapy control system (TCS) at GSI to allow organ motion compensation by beam tracking. Phantom was equipped with GafChromic films and 4 pinpoint ionization chambers. During this first trial, the compensation parameters determined by the OTS were transmitted to the therapy control system via an analogue signal from which the motion phase was determined in the TCS. Based on an offline created look-up table (LUT) this motion phase results into the required lateral motion compensation parameters.
During tests in October, communication protocol slightly change. First of all, correction vector was sent via UDP. UDP communication is theoretically faster than digital to analog converter and there is no need for a LUT or the NI board. Also the pinpoint holder was slightly improved, hosting 5 ionization chambers instead of 4, allowing a more detailed post analysis on dose delivered to ionization chambers.
Results of Experimental sessions are reported in next paragraphs.

4.7 Model Results

The role and importance of models able to estimate the position of the tumor mass as a description of the phantoms used for experimental sessions have been widely introduced in the previous paragraphs.
This section is then organized as follow:

- Results on Cyberknife database of 20 selected patients
- Preliminary optimization of fuzzy logic and artificial neural network approaches
- Preliminary results using a custom breathing phantom
- Results of experimental sessions at GSI, Germany

The first session is dedicated to a comparative study of Cybernife Modeler with alternative predictors. A comparison of the errors between Cyberknife and alternative models are reported. The second session is focused on a first optimization of two of the approaches considered: fuzzy logic and artificial neural networks. Third session is dedicated to the scientific activities on a custom breathing phantom, to produce out own dataset for models validation and to investigate the integration of them in CNAO hardware. The last session focuses on the activities carried out at GSI, where the optical tracking system and the phantom where installed as set up for the active control of the steering of a carbon ion beam, providing in real time the position (measured or estimated) of a moving target.

4.7.1 Benchmark with Cyberknife

The cumulative probability distribution functions (PDFs) of the 3D targeting errors are depicted in figure 4.12 and figure 4.13 for worst and control cases, respectively. Each PDFs takes into account all the imaging points acquired during treatment for model validation and update.

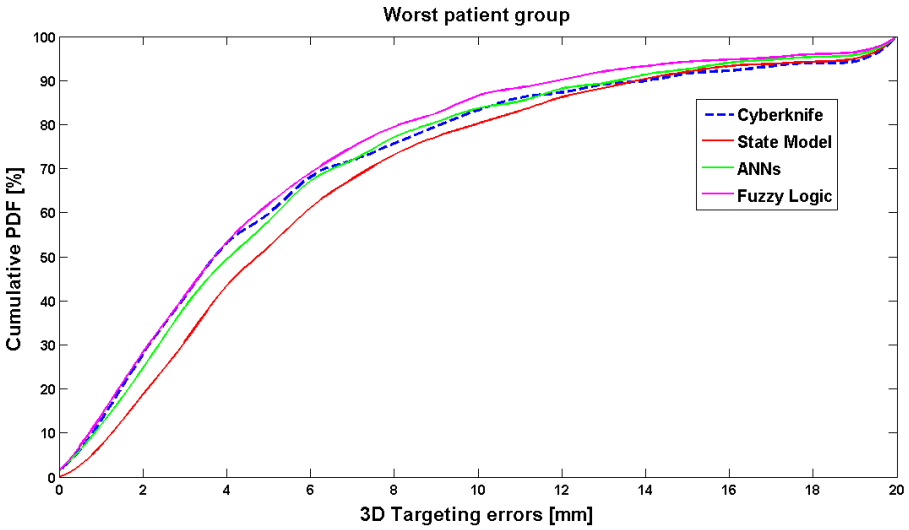

Figure 4.12.PDF of 3D targeting errors in worst case database (Torshabi *et al* 2010).

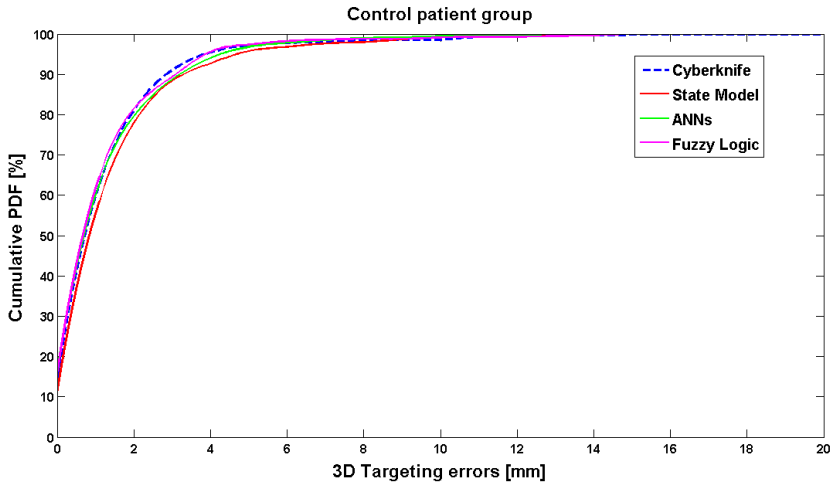

Figure 4.13. PDF of 3D targeting errors in control case database (Torshabi *et al* 2010).

Non parametric statistical analysis (Friedman test) applied to worst cases shows a significant difference among the implemented strategies (p-value <1.5·10-10). A post-hoc comparison (Dunn test) indicates that the state model has the worst performance, whereas the output of Cyberknife Synchrony®, of the ANN-based and fuzzy logic algorithms are comparable at 99% confidence. It can be noted from Figure 6 that the implemented alternative strategies ensure a reduction in the percentage of larger errors. For example, the error reduction with respect to Synchrony® at the 95% confidence level is 0.6% for the state model, 8.7% for ANNs and 10.8% for fuzzy logic. Comparable results were highlighted for all strategies on the control cases, as confirmed by statistical non parametric tests (Friedman).

Sample traces for one control and one worst case are depicted in figure 4.14, where all the implemented strategies are overlaid. As visible from figure 4.14, worst cases featured higher peak to peak tumor motion along with superior intra-fractional breathing variability. The different algorithms showed almost comparable breathing traces in control cases, whereas non negligible differences were observed in the worst cases population.

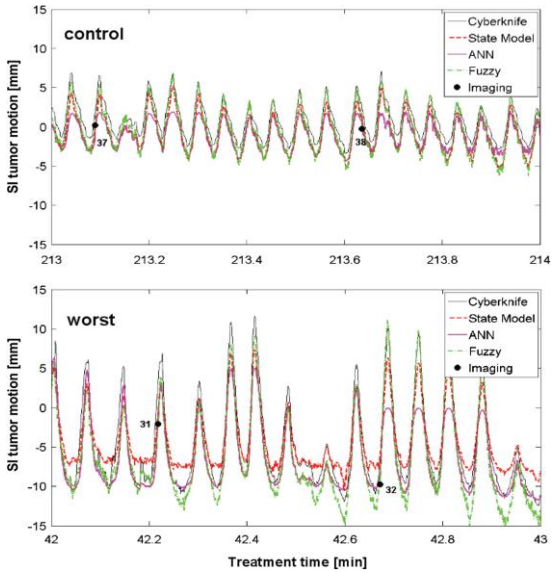

Figure 4.14.samples of traces for control and worst case, respectively (Torshabi *et al* 2010).

Concerning the dataset of worst patients, the error reduction at 95% confidence of models in respect to Syncrony® was calculated at 0.55% for the State Model, 8.69% and 13.47 for ANNs and Fuzzy logic, respectively. Comparable results were highlighted for all strategies on the control cases, as confirmed by statistical non parametric tests (Friedman).

Results suggest that is possible to obtain an overall accuracy comparable to the state of the art models. Particularly, artificial neural networks and fuzzy logic approach demonstrated to be potentially able to overcome accuracy in prediction of Cyberknife® Synchrony®. Readers should keep in mind that the use of these models is not foreseen for clinical routine in radiotherapy with ions in the next future. Moreover, the use of methods typically used in conventional image guided radiotherapy represents nowadays the frontline of research. However, both fuzzy logic and ANN are a powerful and versatile tool for data processing. Their structure and parameters can be adjusted to best fit the requirements, ideally in infinite different ways.
Under these preliminary considerations, using the same Cyberknife® database of 20 patients, additional investigations have been conducted. Results shown below cannot be intended as conclusive, but they represent a first effort in the search of an optimization criteria in fuzzy logic and artificial neural networks approaches as seen in previous paragraphs.

4.7.2 A comparison between different clustering methods in fuzzy logic

Different data clustering approaches were studied due to their substantial effects on fuzzy modeler performance. A comparative investigation was performed on two fuzzy based and one neuro-fuzzy based inference systems with respect to Cyberknife®.
Figure 4.15 represent the RMSE (Route Mean Square Error) of 3D targeting errors for 10 patients in control and worst groups, respectively.

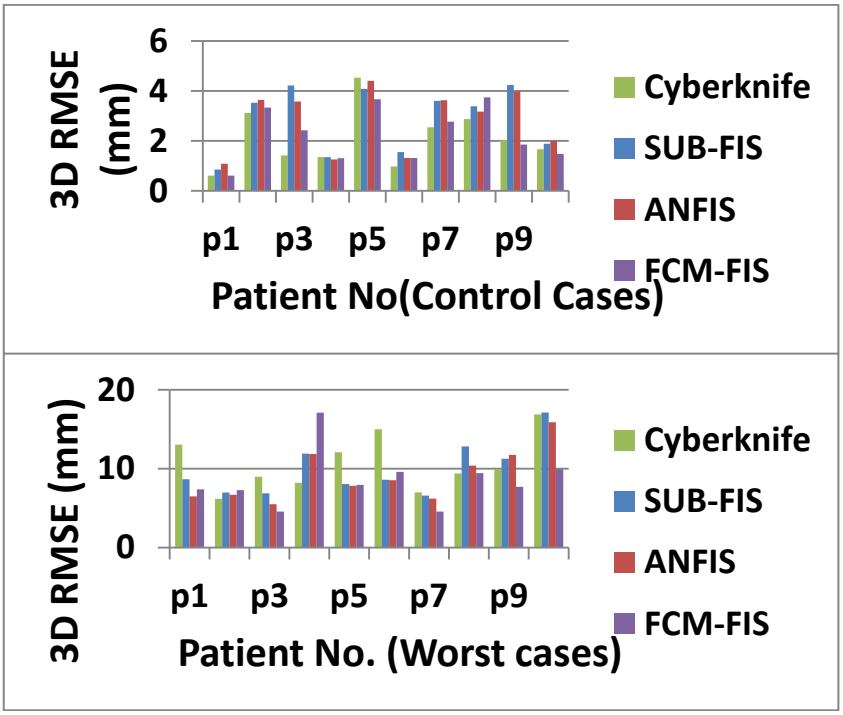

Figure 4.15. 3D root mean square errors comparison between Cyberknife® Synchrony® and fuzzy logic clustering.

The average and standard deviation of total 3D targeting errors overall 10 patients in control and worst groups are shown in Table 4.1, in order to have a comparative investigation between correlation models performance.

	Control group		Worst group	
Modeler	3D RMSE [mm]	STD	3D RMSE [mm]	STD
Cyberknife	2.113	1.176	10.666	3.490
SUB-FIS	2.869	1.310	9.879	3.361
ANFIS	2.806	1.258	9.105	3.302
FCM-FIS	2.251	1.100	8.542	3.536

Table 4.1. average and standard deviation of 3D errors overall 10 patients in different modelers in control and worst group.

As seen in Table 4.1, in control group there is no improvement in 3D error reduction versus Cyberknife® and the best performance belongs to FCM-FIS with less standard deviation among the produced modelers. In contrast, in worst group the error reduction improvement was occurred in all three modelers performance and the FCM-FIS is the best with 2.12 mm in error reduction vs. Cyberknife® modeler. In ANFIS, the motion prediction is done with the minimum fluctuation although its accuracy is worse than FCM-FIS.
As depicted in worst group of figure 4.15, for patient 4 the FCM-FIS performance is the worst while the SUB-FIS is the best for this patient and in contrast, for patient 10 the FCM performance is the best with a huge error reduction improvement while the SUB-FIS is the worst.
Due to the intrinsic inter-patient variability in fuzzy models performance, a model selectivity algorithm was proposed to select an adaptive fuzzy modeler on a case by case basis. Methods are described in the previous chapter, we reported here only the main flowchart for clustering selection figure 4.16.

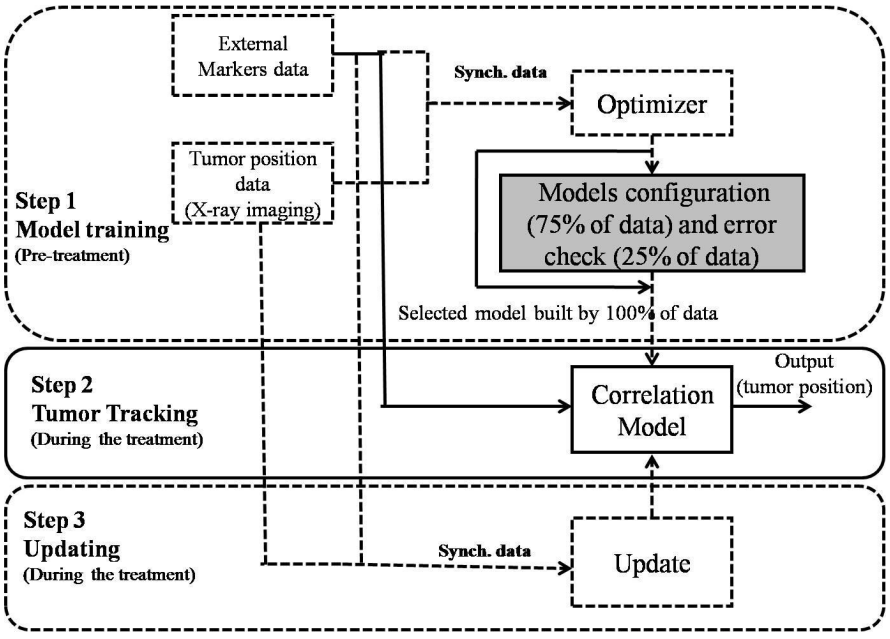

Figure 4.16.scheme of clustering selector.

The cumulative probability distribution functions (PDFs) of the 3D targeting errors are reported in figure 4.17 for control and worst patients, respectively. Average of 3D RMSE and relative standard deviation are reported in Table 4.2.

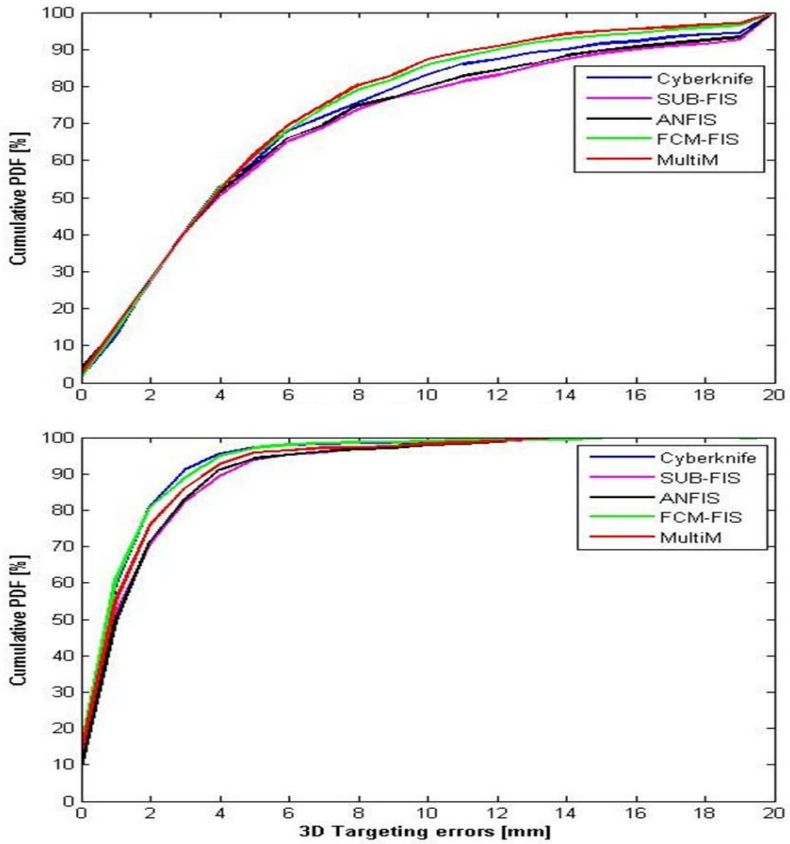

Figure 4.17.PDFs of worst and control cases

	Control group		Worst group	
Modeler	3D RMSE [mm]	STD	3D RMSE [mm]	STD
Cyberknife	2.113	1.176	10.666	3.490
Fuzzy model with selectivity option 'ON'	2.556	1.309	8.022	2.167

Table 4.2. average and standard deviation of 3D errors overall 10 patients in selectivity option mode 'ON' in control and worst group

4.7.3 Improvement in artificial neural network approach in Cyberknife® data analysis

Artificial neural network approach was optimized by means of a more complex architecture, designed in C++ language. As described in previous paragraphs, a feed-forward double-layer architecture featuring a hidden layer of 10 units and a hyperbolic tangent activation function, which is applied to both the hidden and the output layer, was selected. Briefly, trained ANNs are exploited for the estimation of the target position as a function of each sample of the external signal. Since three independent estimations are obtained (one for each network), a unique output is calculated by averaging the outputs of the three ANNs. All the procedures (building of the ANNs, training and simulating) were integrated in C++ code, in order to run the application on the same workstation of the OTS. This aspect is not crucial for the initial validation of the models, performed offline using the Cyberknife® database previously described, but it assumes importance while a real time acquisition is required.

3D targeting errors for the developed ANN-based method and for the Synchrony® tracking system were calculated. Overall median value, interquartile range and 95th percentile for the control and worst groups are reported in Table 4.3.

	Control		Worst	
	ANN	Synchrony	ANN	Synchrony
Median [mm]	0.98	1.27	3.58	4.28
Interquartile range [mm]	1.29	1.39	4.81	5.94
95^{th} percentile [mm]	3.72	4.22	14.37	21.27

Table 4.3. statistical parameters of the 3D targeting errors recorded in the control and worst group

The cumulative probability distribution functions (PDFs) of the 3D targeting errors for both the control and worst groups are shown in figure 4.18.

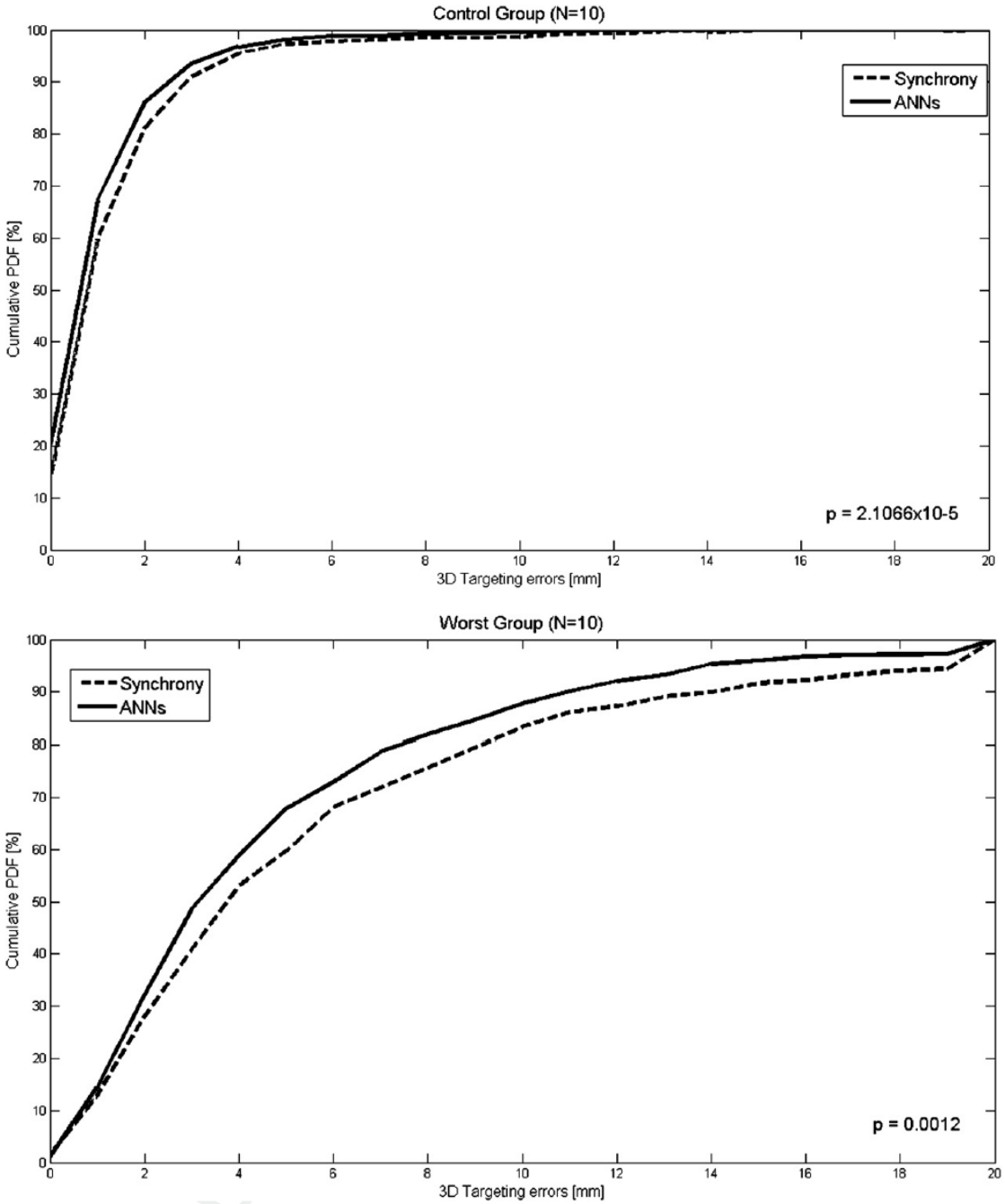

Figure 4.18. PDFs of worst and control cases (Seregni *et al* 2011).

A non parametric statistical analysis (Wilcoxon ranksum test) was applied to control and worst cases and it returned *p-values* equal to 2.1066x10-5 and 0.0012 respectively, thus proving a statistically significant error reduction for the ANN-based method relative to the Synchrony module. In conclusion, the proposed method allowed an average 3D targeting reduction (with respect to Synchrony) of 17.84 % for the control cases and 23.15 % for the worst cases.

Compared with Cyberknife Synchrony, results obtained put forward models as fuzzy logic and artificial neural networks as valuable tools to estimate the trajectory of a moving target given external surrogates. Obviously, experimental conditions and set up (such as: number and displacement of external control points, X-ray double projection during treatment for model

validation or training) are defined *a priori* in this database. At this stage of study, it is impossible to claim one of the model better than the others in all conditions, for all the treatments. However, the importance of this research lays in the search of possible advantages in the use of mathematical predictors for organ motion mitigation when its effect is not negligible. It is important to keep in mind that there are several differences in RT with photons and ions. These differences reflect also in the potential use and diffusion of models in clinic. The high geometrical selectivity, as the occurrence of secondary injuries correlated to the use of light ions, require implicitly an high precision and accuracy in tumor position estimation. Moreover, models are required to be stable and reliable in every condition in order to result in a uniform dose distribution in the tumor mass.

4.8 Use of a breathing phantom for model validation

Models such state model, and particularly fuzzy logic and artificial neural networks have been chosen due to their generalization capabilities. Their possible use as a support tool for organ motion mitigation has been in principle demonstrated.
There is no doubt that models have to be patient specific, since they have to be trained day by day at the beginning of each session. Implicitly, it becomes significant the investigation of models performance while set up conditions and parameters are changed and tuned in a controlled protocol figure 4.19. In conclusion, the use of set up where not only the predictive models but also their inputs (signal surrogates) and experimental conditions (magnitude of movements) can be controlled by operators becomes of relevant importance.

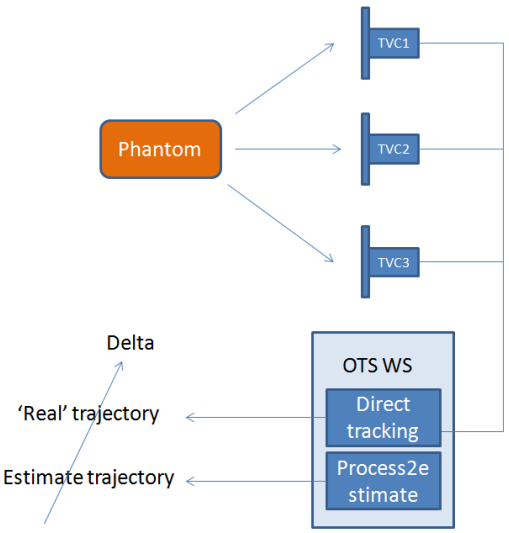

Figure 4.19. rationale of breathing phantom use and main connections

The solution adopted was to build a custom designed phantom, able to mimic a physiological breathing. The design of this phantom, has been previously described. The first version of the phantom was used for preliminary studies in CNAO. Results are presented in next paragraph.

4.9 Tracking of a moving target in real time with artificial neural networks

Neural networks architecture adopted in this study was basically the same described in the previous paragraphs, featuring a two layers feed forward with non linear transfer functions. Table 4.4 reports the size of period and amplitude variability of the phantom respiratory signal due to simulated breathing irregularities.

	Minimum	Median	Maximum
Period [s]	2.07	3.41	7.43
3D amplitude [mm]	8.46	11.53	14.38

Table 4.4. 3D motion amplitude and period observed in the acquisitions, quantified in terms of minimum, median and maximum values.

During the trials a log file was recorded, and so the complete traces of OTS and the predictor output. The log file analysis of the phantom acquisitions showed that tumor position estimation took place consistently in real-time, except during the retraining of one or more ANNs. In these cases, the retrain procedure took, on average, a period of about 34 frames, corresponding to 0.57 seconds at the nominal acquisition frequency (60 Hz).
In order to quantify the tracking accuracy during three experimental acquisitions, 3D targeting errors are computed in correspondence to each acquired frame. This is possible since the actual position of the target, although considered intermittently by the algorithm, is continuously detected by the SMART-D system. Table 4.5 reports the median ± interquartile range and 95^{th} percentile of the 3D targeting errors which were continuously calculated as the distance between the estimated and the actual position of the marked target in the phantom.

Acquisition parameters	Median [mm]	Interquartile range [mm]	95th percentile [mm]
1	1.03	0.99	2.75
2	1.01	0.72	10.72
3	1.35	0.66	2.15

Table 4.5. statistical parameters of the 3D targeting errors recorded in three acquisitions on the breathing phantom

As an example, figure 4.20 depicts a detail of the traces recorded during acquisition.

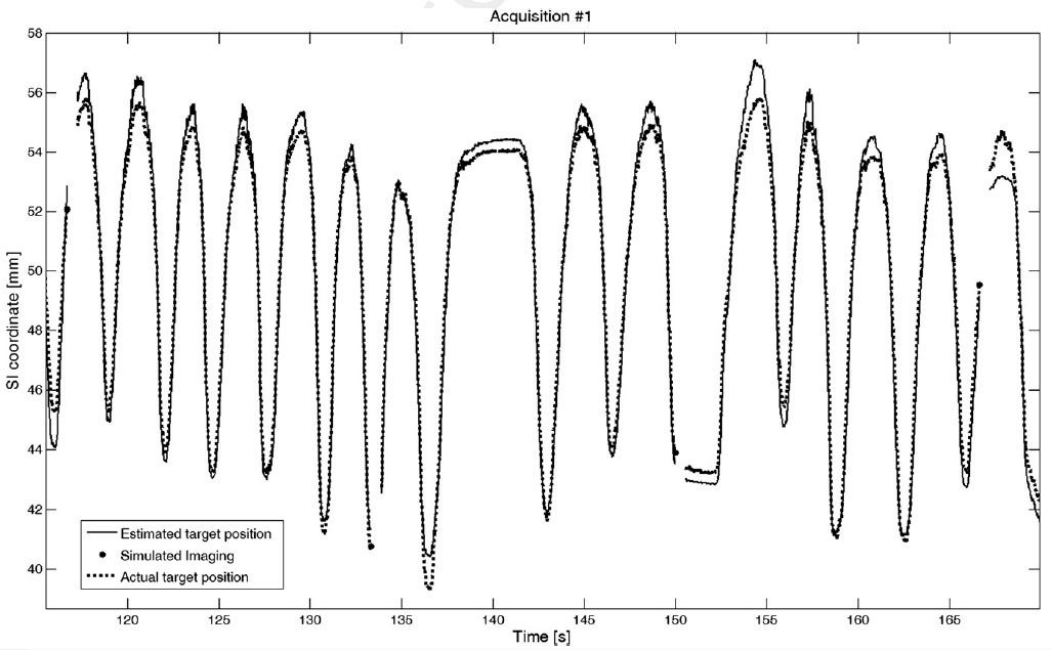

Figure 4.20.sample trace of an irregular breathing motion obtain with the breathing phantom. SI direction is reported. Dotted line correspond to the actual position as recorded by OTS, line the prediction (Seregni *et al* 2011).

In this figure, it is possible to observe the effects of frequency and amplitude variations for irregular breathing simulation. Also, the temporary suspensions of the target position estimation due to the neural networks retraining (blank trace) can be noted.

4.10 Experimental integration of optical tracking systems and 4D dose delivery systems

Results showed above demonstrate that is possible, within limitations concerning both the benchmark with Cyberknife (few control points, few patients) and the use of the breathing phantom (very simple movement and not representative of a clinical situation) to achieve an acceptable accuracy in predicting an internal trajectory processing external surrogates. It was also demonstrate that is possible, in a simple case study, to build and update predictive models with a time consumption that is compatible with clinical activities. The effort required to integrate ANN procedures in CNAO hardware was justified by one of the major aims of this research, that is basically to test a tool able to control in real time the steering of an active beam.

Research activities are strongly encouraged at CNAO, as they are intended, together with clinical, a mission. However, at this time there are no slots of beam time available to perform tests on the steering logic of deflector magnets.

In radiotherapy with particles, the use of strategies supporting the management of organ motion effects is nowadays an hot point in scientific community. Technology is in principle ready for tumor tracking, and predictive models could play an important role during treatment planning phases and during treatment sessions. Even if the steering of magnets could be reasonably intended as part of the dose delivery system, few facilities in the world are ready to test the steering in real time, given a vector of coordinates. One of this facilities is GSI. GSI is at the moment the only facility able to do research on moving targets using a carbon ion beam, acting on scanning magnets with a custom and proprietary logic.

Our systems, here intended as the breathing phantom and the optical tracking system, were then moved to GSI, where two experimental sessions were conducted in collaboration with Moving Target group. As described paragraph 4.6.1, a second version of the breathing phantom was required, according to the fact that the current version of the organ motion manager module at GSI can manage only 2D translational movements of the target (beam energy was not taken into account in these trials).
Results of the experimental activities carried out at GSI are reported in next paragraphs.

4.10.1 Preliminary activities for breathing phantom assessment and description

The main goal of the first experimental session aimed at assessing the capability of exploiting the real-time signal related to target position estimated by means of IR optical tracking coupled with internal-external correlation models (CNAO-Politecnico di Milano) and 4D dose delivery techniques (GSI). Under these considerations, the description of the set up and the motion capabilities of the second version of the breathing phantom should be intended as results. For this reason they were included in this section.
A possible set up was preliminarily tested at CNAO, where the phantom was placed on the PPS and aligned at the isocenter in one of the treatment rooms (room 3). This phantom mimics breathing motion, but differently by the first version, can simulate a 2D internal tumor motion (detector head). Repeatability of movements, as a feasibility study of the set up in terms of markers visibility were required as preliminary condition. Results and performances regarding the breathing phantom in its second version are reported in this order:

- Check of the presence of a planar hysteresis
- Repeatability of movement
    - Peak to peak analysis
    - Distance between peaks
- Repeatability of movement in between different sessions

In figure 4.21 is reported the hysteresis of a marker placed on the internal target over a 50 cycles repetitions.

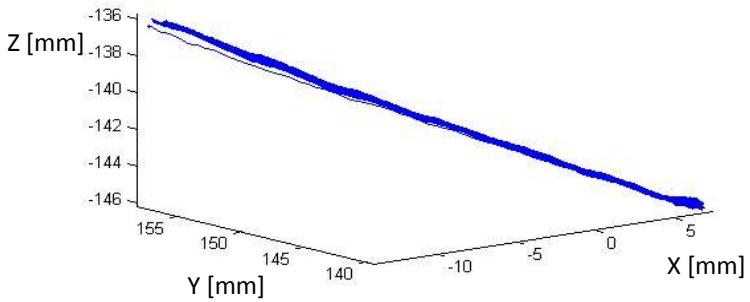

Figure 4.21. hysteresis of the second version of the breathing phantom over 50 cycles of movements.

The trajectory lies on a plane, as specifications required. The movement itself is repeatable under this point of view.

Amplitude of movements were investigated looking at lower and upper peaks. Data recorded by OTS were exported in Matlab, where maximum and minimum values were considered. In figure 4.22 box plot analysis for the three coordinates is shown.

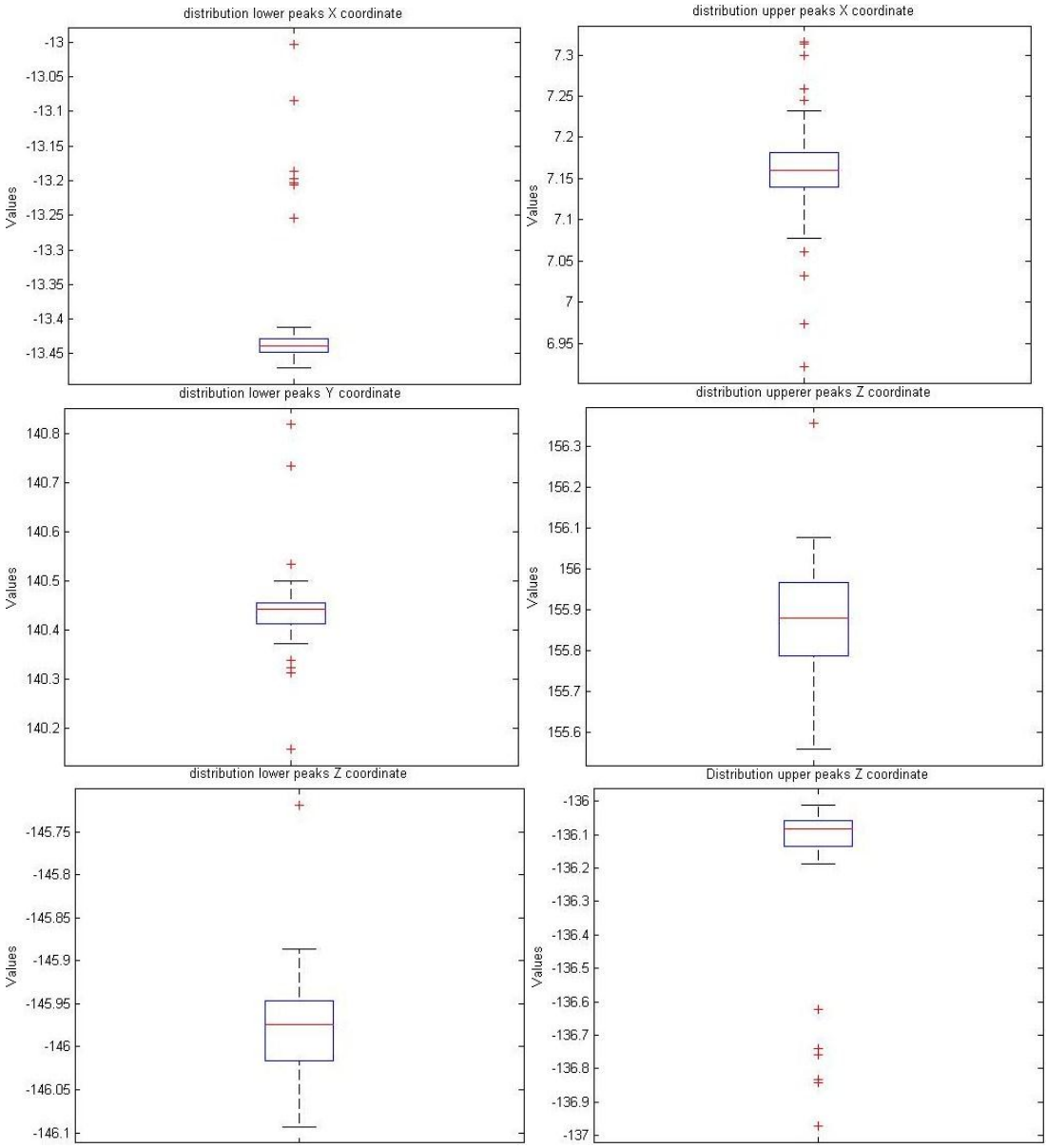

Figure 4.22. distribution of upper\lower peaks. From top to bottom: AP, SI, LL coordinates analysis is reported. Values are expressed in millimeters.

In figure 4.23 peak to peak distance versus number of sample during acquisition is reported. As expected, points are distributed on a line. Only vertical (upper-lower direction) coordinate is showed here: this direction was characterized by the maximum peak to peak distance.

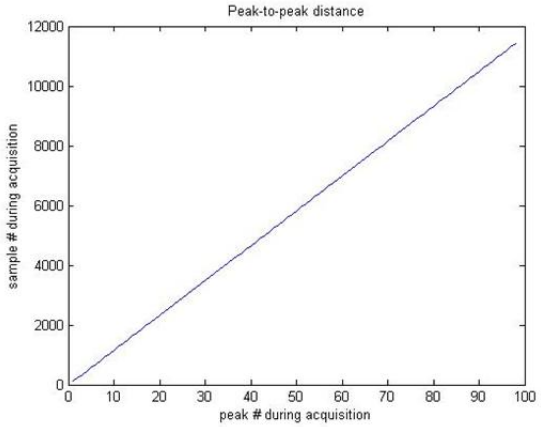

Figure 4.23. peak to peak distance vs sample number during acquisition for SI direction.

Last considerations were extracted looking at the repeatability of inner target movement. Repeatability was a specific goal of this phantom.
Mean values of differences over 5 repetitions of 50 breathings are reported in Table 4.6. Results for X,Y and Z coordinates are reported separately.

X coord	Test1	Test2	Test3	Test4	Test5
Test1	0	-0,1811	-0,2641	-0,3498	-0,455
Test2	0,1811	0	-0,083	-0,1687	-0,2739
Test3	0,2641	0,083	0	-0,0857	-0,1909
Test4	0,3498	0,1687	0,0857	0	-0,1052
Test5	0,455	0,2739	0,1909	0,1052	0
Y coord	**Test1**	**Test2**	**Test3**	**Test4**	**Test5**
Test1	0	0,1627	0,3441	0,4684	0,5357
Test2	-0,1627	0	0,1814	0,3057	0,373
Test3	-0,3441	-0,1814	0	0,1242	0,1916
Test4	-0,4684	-0,3057	-0,1242	0	0,0674
Test5	-0,5357	-0,373	-0,1916	-0,0674	0
Z coord	**Test1**	**Test2**	**Test3**	**Test4**	**Test5**
Test1	0	0,0852	0,1251	0,1694	0,2181
Test2	-0,0852	0	0,04	0,0842	0,1329
Test3	-0,1251	-0,04	0	0,0443	0,093
Test4	-0,1694	-0,0842	-0,0443	0	0,0487
Test5	-0,2181	-0,1329	-0,093	-0,0487	0

Table 4.6. Mean values of differences over 5 repetitions of 50 breathings in X, Y, Z coordinates.

4.10.2 GSI experience. First campaign of experimental session.

Feasibility studies in CNAO cave were conducted to investigate both the markers visibility and the nature of signals produced by the breathing phantom. The same set up was then replicated in the cave of GSI (figure 4.24).

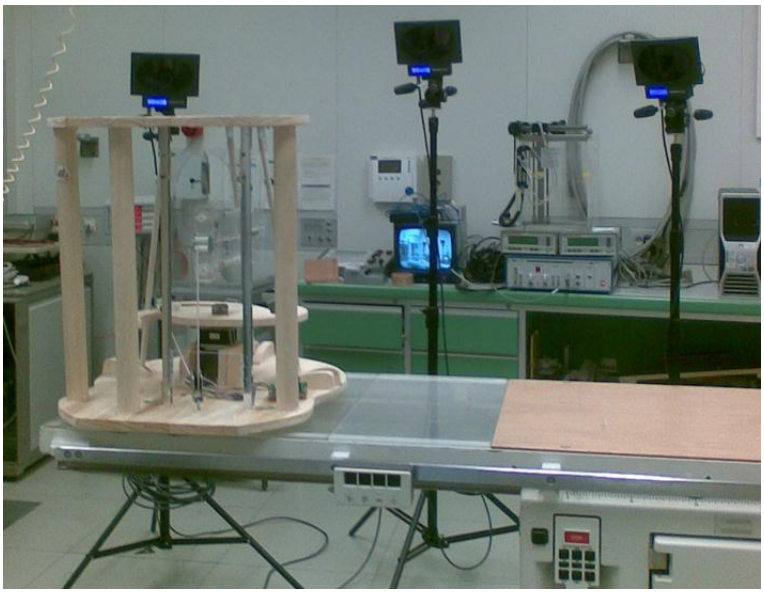

Figure 4.24. POLIMI motion phantom for beam tracking experiments installed in GSI cave.

The experimental series performed in July 2011 at GSI aimed at establishing the communication between the OTS and the organ motion compensator (OMC).
As described in chapter 3, paragraph 3.4, the OMC system integrates the information provided by IR optical tracking with the dose delivery control system, providing the position correction information to the beam scanning magnets. The main communication scheme is depicted in figure 4.11.
The optical system also computes the correction position vectors of the tumor, to correct the beam during the treatment. Such vectors (one vector for each respiratory phase) are sent to the OMC that saves them into a memory before the treatment. During irradiation, it is possible to check in real time the beam direction. Trajectory of the target is visible together with the volume of irradiation figure 4.25.

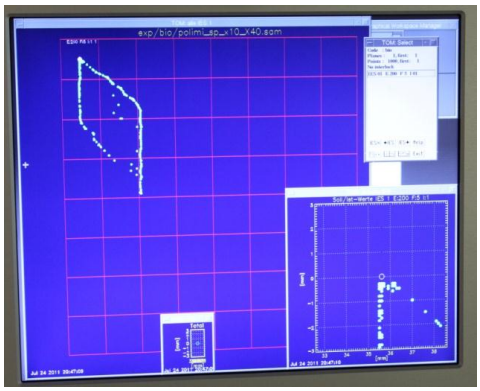

Figure 4.25. trajectory of the target superimposed to the volume of irradiation
as seen on a screen in control room. In the upper-left area the hysteresis of the moving target.

For a proof-of-principle test the IR optical tracking system (OTS) were installed and connected to the therapy control system (TCS) at GSI to allow organ motion compensation by beam tracking. Phantom was equipped with GafChromic films and 4 pinpoint ionization chambers figure 4.26. Moreover, a scintillator screen was added to visually check the coherency between correction vector and beam direction.

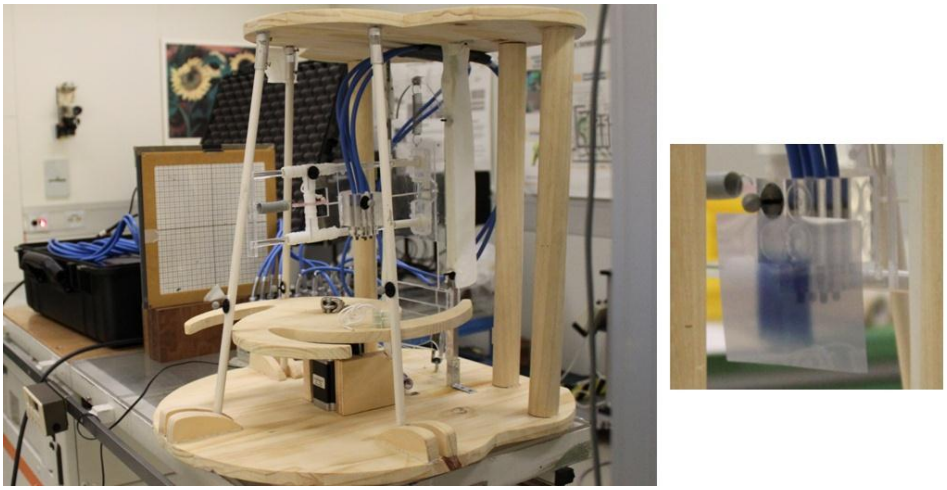

Figure 4.26. left box: the breathing phantom aligned and ready to be irradiated. Behind the phantom the scintillator screen. Right box: the pinpoint holder equipped with gafchromic film and a passive marker.

During this first trial, the compensation parameters determined by the OTS were transmitted to the TCS via an analogue signal.
The experimental series performed in July 2011 at GSI aimed at establishing the communication between the two systems and were in this respect successful. The acquired data shown in figure 4.27 show that beam tracking was successfully performed.

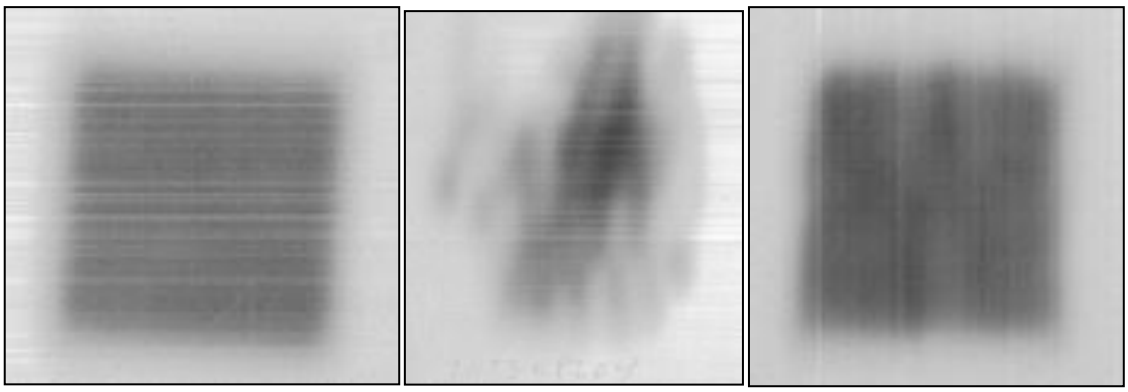

Figure 4.27. gafchromic films after irradiation. From left to right: stationary irradiation; interplay (no compensation); tracking with OTS.

4.10.3 GSI experience. Second campaign of experimental session.

A second experimental session was dedicated to the active tracking of the moving target.
Even if the set up was the same of July figure 4.28, there were several differences in the approach, mainly in the communication between systems. First of all, correction vector was sent via UDP.

Figure 4.28. Set up in GSI cave

The goal of this session was then to irradiate the moving target in two different conditions: direct tracking (providing the current position as seen by the OTS) and tracking with ANN prediction (correction vector provided by dedicated ANN).

Protocol proposal foreseen different trials:

- Acq0: irradiation of a static target (no movement). In this case, no feedback to the steering magnets was provided. This measure is useful as reference, since no effects due to errors in target tracking are included.
- Acq2: a regular motion was imposed to the phantom, setting an high speed. The CV was provided by direct tracking of a passive marker placed on the pinpoint holder.
- Acq3: a regular motion was imposed to the phantom, setting an high speed. The CV was provided by ANN predictor.
- Acq3_Slow: a regular motion was imposed to the phantom, setting a slower motor speed. The CV was provided by ANN.
- Acq11: an irregular motion (amplitude and speed variations) was imposed to the phantom. The CV was elaborated by ANN predictor.

Results of these tests are reported below.

4.10.4 Tracking with artificial neural networks

Concerning Acq3, Acq3_slow and Acq11, a direct comparison between trajectories recorded by OTS and estimated values of X and Y coordinates of the internal point are reported figure 4.29. Since it was not used during beam steering, Z coordinate is not reported because not significant.

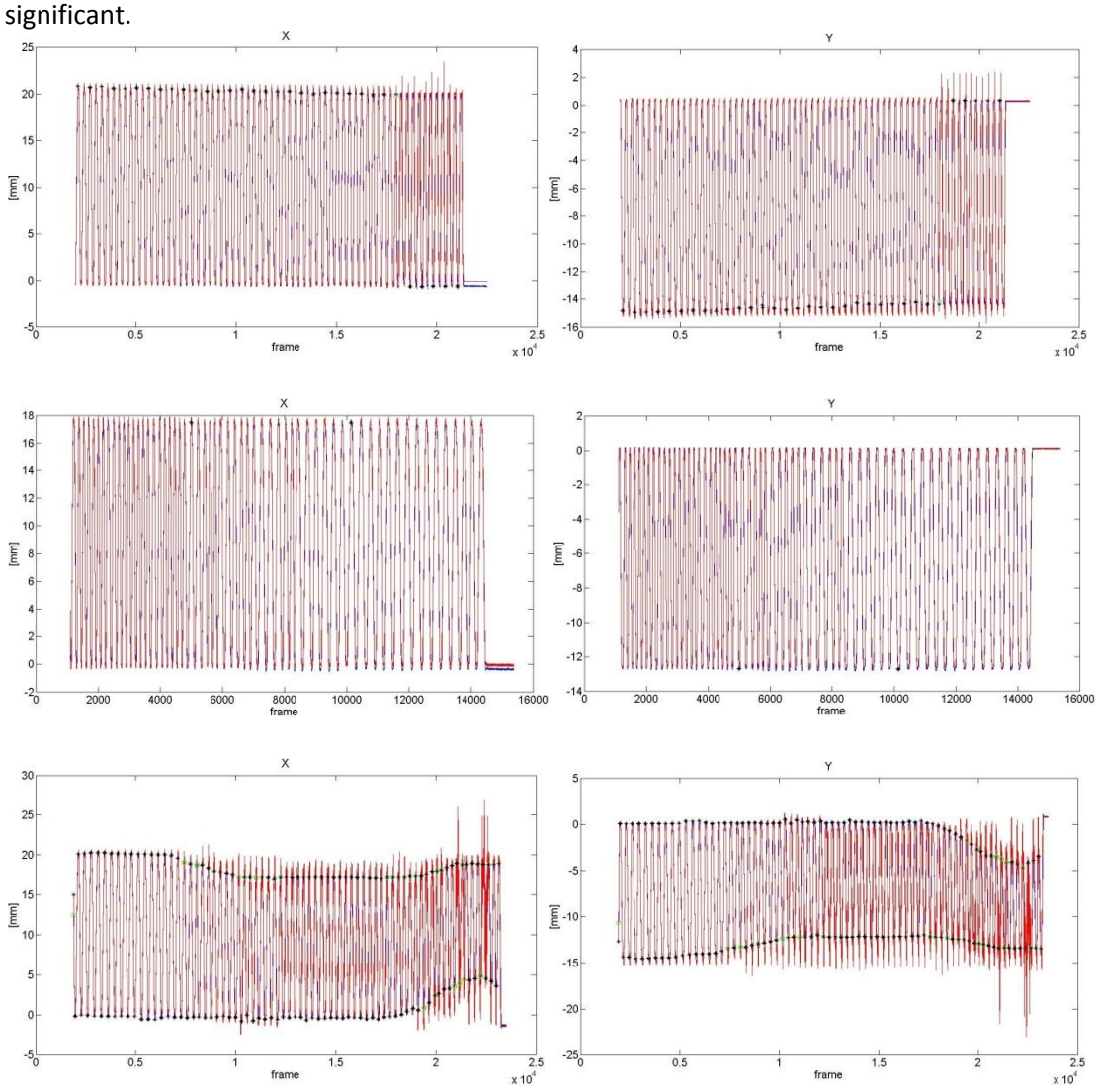

Figure 4.29. Comparison between X (left panels) and Y (right panels) coordinates of the internal point as recorded in log files. Blue lines: OTS; red lines: ANN estimation. From top to bottom: Acq3; Acq3_slow; Acq11.

Mean values, standard deviation and maximum value of errors (in terms of RMS) introduced by neural networks are reported in Table 4.7.

	Acq3		Acq3_slow		Acq11	
	X	Y	X	Y	X	Y
Mean [mm]	0.54	0.41	0.43	0.37	0.98	0.91
STD [mm]	0.71	0.52	0.38	0.39	1.10	0.99
Max [mm]	9.77	5.19	2.33	2.01	12.87	12.13

Table 4.7. RMS errors introduced by ANN. Mean, standard deviation and maximum error are reported for Acq3, Acq3_slow and Acq11

Gafchromic films for all the acquisitions are reported below figure 4.30. Even if it is not possible to advance considerations on dose effects, this measure is useful to visualize the homogeneity in dose distribution and also on the preservation of the planned geometry. The squared profile is recognizable after all the irradiations.

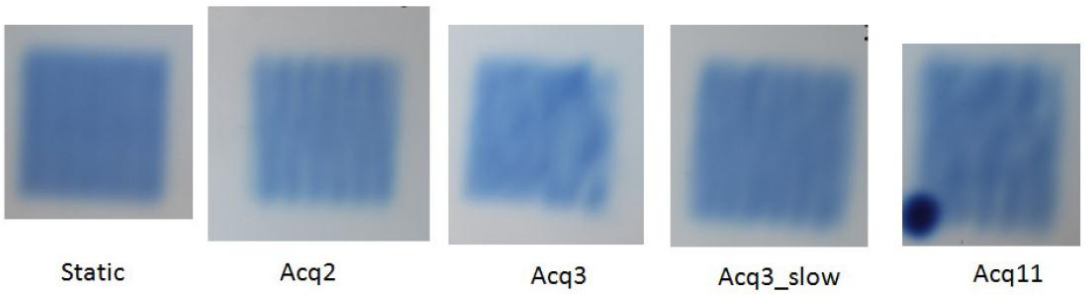

Figure 4.30. gafchromic films after irradiation. From left to right: stationary irradiation; tracking with OTS; ANN prediction (fast motor speed); ANN prediction (slow motor speed); ANN prediction of irregular breathing pattern.

Compared with static irradiation, readers can notice stripes on films correlated to all the other acquisitions. This effect could be caused mainly by two different factors: an erroneous tracking or a delay in communications. Acq2 was performed with direct tracking (that is, OTS was sending the CV to the OMC). Related film is affected by stripes as well, but it is unlikely that they are caused by an error in tracking, since residuals after calibration were <0.3 mm. Then, we put attention to delays in communication protocol. A 30 ms delay in OTS – beam steering communication was evidenced, and was assessed as the main reason in causing residual motion.
It should be evident by traces and films that it was possible to observe a good performance of ANN for position estimation when retraining was not included\required. Retraining caused ANN estimation errors (typically at the end of the acquisition, see figure 4.29, last frames).
This unwanted effects can be noticed also in pinpoint analysis Table 4.8. Table 4.8 summarized the values recorded during acquisitions by the 5 pinpoints mounted in the holder. Reference and measured values, delta and percentage in respect to the static acquisition are shown. Pinpoint number 4 was the one aligned with laser cross at the isocenter during model reference acquisition.

	VALUES					
PinPoints		Acq0	ACQ2	ACQ3	ACQ3_slow	ACQ11
	1	2.33	2.33	2.61	2.44	2.17
	2	2.47	2.43	3.01	2.47	2.11
	3	2.83	2.75	3.60	2.60	2.69
	4	2.64	2.70	3.61	2.52	2.68
	5	2.70	2.70	3.97	2.53	2.39
DELTAS vs Acq0						
PinPoints	1	0.00	0.00	0.28	0.11	-0.16
	2	0.00	-0.05	0.54	0.00	-0.36
	3	0.00	-0.08	0.78	-0.23	-0.14
	4	0.00	0.06	0.97	-0.12	0.04
	5	0.00	0.01	1.27	-0.17	-0.31
DELTAS% vs Acq0						
PinPoints	1	0.00	-0.13	11.93	4.63	-6.91
	2	0.00	-1.82	21.82	-0.12	-14.66
	3	0.00	-2.72	27.48	-8.21	-4.88
	4	0.00	2.12	36.50	-4.58	1.51
	5	0.00	0.22	47.15	-6.26	-11.49

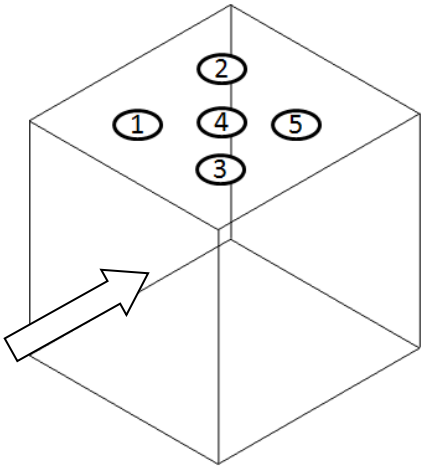

Table 4.8. values recorded during acquisitions by the 5 pinpoints. On the right the map of ionization chambers as mounted in the holder. Arrow indicates the beam eye view.

In Acq3 and Acq11 multiple retraining causes not negligible deviations with respect to real target. Pinpoint chambers measurements reflects deviations. Up to 7% deviation in pinpoint chambers measures in Acq2, Acq3_slow, acquisitions associated with residual stripes on films are caused by the later assessed delay communication (30 msec), with higher effects on Acq2 (faster motion) than on Acq3_slow (slower motion).

4.10.5 Set up validation with a different phantom

An additional test was conducted with a different phantom (Bruce Lee phantom, see figure 4.31). This phantom is property of GSI. It is composed by an external structure (thorax) moved by a motor, in order to simulate breathing motion. A second motor (KUKA robot) provides the motion of a target. Target is similar to the pinpoint holder we used with our phantom. However, differently from the one depicted in figure 4.10, Bruce Lee target can host up to 16 ionization chambers, and more than one GafChromic film.
There were two main reasons to perform this test:

- It was important to test our systems with a different set up, in order to validate the approach and the feasibility of it
- We added a kinematic predictor to provide an estimation of samples in future, to avoid delays due to communication

Unluckily it was not possible to test ANN predictor during sessions with this phantom, because of major issues with beam line after preliminary activities.
However, all the procedures for set up preparation were similar to those used for Inga phantom, requiring an alignment of the internal target (and consequently of the external surface) to the laser cross of the cave.
Because of the presence of a closed ribcage, it was not possible to put a marker directly on the pin point holder. This control point was fixed on the support harm of the holder, outside the ribcage. This choice did not affect the accuracy in estimation of tumor surrogate motion, since the correction vector is intended as delta corrections from a nominal position.

Results about dose distribution are not included in this preliminary study. The setup is shown in figure 4.31. It can be noticed the use of only two cameras, placed near the nozzle, and the presence of the wedge compensator.

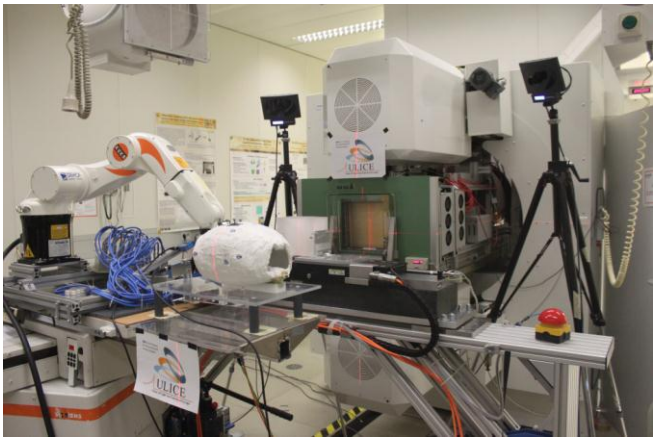

Figure 4.31. set up in GSI cave. TVCs, wedge compensator, phantom and KUKA robot placed and ready for experimental session.

Again, a comparison between trajectories recorded by OTS and 30 ms ahead values of X and Y coordinates of the internal point are reported figure 4.32. As in previous graphs, since it was not used during beam steering, Z coordinate is not reported here.

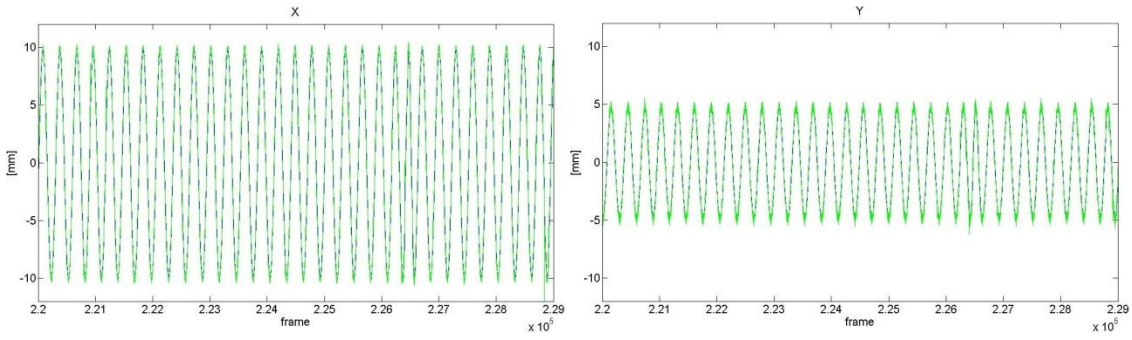

Figure 4.32. Comparison between X (left panel) and Y (right panel) coordinates of the internal point as recorded in log files. red lines: OTS; green lines: 30 ms ahead estimation.

The second session of experimental series performed in October 2011 at GSI with their phantom aimed at testing a new set up for future studies and at tracking a moving target. It was in this respect successful.

Chapter V

Conclusions

This thesis is focused on two different aspects:

- Technologies for patient setup used in radiotherapy with accelerated particles.
- Methods for organ motion mitigation and models for external-internal correlation.

Both technological solutions and models for organ motion mitigation aimed at optimizing the treatment geometry, in order to obtain a uniform profile of dose in the tumor mass, preserving in the same time healthy tissues as much as possible. To reach this result, different aspects should be considered, but it is clear that recent improvements in technology offer different methodologies for setup control and dose delivery. Even if these solutions are generally available in recent facilities, methods able to increase the tumor control, here intended as a knowledge of the position of the target, are required.

New facilities for protons and carbon ions treatments are increasing in number worldwide. Technology in this field is growing due to improvements in control and tools for setup verification before and during irradiation. Accelerators are becoming smaller and smaller, thus cheaper. Regarding dose delivery, particles can be delivered with different techniques, like active scanning or scattering, allowing clinicians to finely contour the sensible organs and critical volumes. Moreover, 4D treatment plans are utilized to include time dependent effects. This is mandatory if operators want to take into account organ motion and physiological pattern variations. A wide variety of possibilities comes from the availability of different ranges in dose and types of compensator. Scanning magnets can also be used to steer the beam line and apply corrections on beam direction. The effort requires to obtain an adequate precision in setup includes obviously those systems devoted to patients' positioning and real time monitoring during treatment sessions. It is theoretically possible to reach an high geometric accuracy in dose deposition, but we have to know exactly where the dose should be deposited.

To minimize uncertainties or errors in setup, recent facilities integrate different systems in treatment rooms, but usually a robotic patient positioner, an X-ray patient verification system and an optical localizer are required. It should be evident that image guidance systems are an important part of the scenario. Concerning the use of these systems, potentialities and disadvantages have been already investigated in RT with photons, and so the knowhow can be transferred to particles case. The attempt is represented by an optimization of the approach, in order to provide an adequate grade of accuracy, that is usually higher than in treatments with photons.
The majority of the tumors are not rigid masses anchored to rigid structures. They influence and are influenced by adjacent tissues. When the position of a tumor mass changes because of physiological movements, the setup control is even more challenging. Several methods are available to manage organ motion, ranging from immobilization tools, to the use of online imaging during treatments (image guidance), to algorithms able to estimate the position of the tumor in respect to fiducial points and\or surrogates. The combination of such models and active beam scanning allows in principle to perform tumor tracking, that is, to follow the tumor mass with an always active treatment beam. Under this point of view, nowadays technology is not seen as a limiting factor. Such models are not diffused and utilized in clinical activities. Even if different solutions are reported in this thesis, the goal here is not to provide a clinical-use tool. The final result concerning models should be intended as a feasibility study of different methodologies that could be applied in radiotherapy with particles aimed at tumor tracking. There is no reason, in facts, to claim that the proposed approaches are, univocally, the only possible choice. They represent a first step, and different techniques, as optimization strategies, remain an open point. This thesis is original because no one before tested a complete integration of different systems, comprehensive of hardware and algorithms in a steering logic of an active beam for tracking a moving target.

5.1 Discussion

This thesis was organized on three main cores. The first one has been focused on the use of accelerated particles in radiotherapy, aiming at underling the rationale of commissioning activities presented in subsequent sections, and focused on technological and methodological aspects in radiotherapy with particles. This section described the rationale of the advantages in treatments with particles compared with photons and provided an overview of technology devoted to produce treatment beam and beam delivery. Radiobiological indexes have been also presented, and again differences with photon therapy have been evidenced. During the PhD program the most of the activities were carried out in CNAO, a center able to offer treatments with protons, and in the next future the first in Italy with carbon ions. Politecnico di Milano has collaborated at designing and installing systems aimed at patients' positioning and setup verification in treatment rooms. During the last three years these systems were installed, tested and finally accepted. Clinical activities with protons are now running in one of the rooms. The first section ended by presenting the results obtained during the commissioning of these systems in CNAO.
Different technological solutions are nowadays available in radiotherapy with particles, and few examples have been shown in chapter 3. Systems dedicated to patient positioning and setup control have common features, even if not negligible differences can be noted, both in the equipments and in strategies for misalignment management or compensation. We should keep in mind that commercial companies usually provide efficient systems but with poor (or no) option for customization, thus requiring facilities to adapt their need on the offer. In this scenario CNAO chose to follow a more challenging approach, acquiring components highly

customizable, and designing the others with its manpower. This aspect leaded to the definition of a unique center. The Center owns the project designs of the majority of the high technology. In such approach, it comes evident that latest research evidences were discussed and questioned during commissioning. In order to do that, active participation of different expertise, both technical and clinical, is mandatory. Economic analysis are included in this process. Moreover, the option of further integrations should be practicable without massive reengineering processes. Under this point of view, CNAO offers a wide range of possibilities being strongly proprietary-system oriented.

The importance of setup verification and accuracy has been stressed in the second section of the thesis. This part can be intended as a link between the first and the third section, and introduced the reader to the concept of image guidance in particle therapy. In particular, when organ motion is not negligible, different strategies for motion mitigation should be considered. In this section has been put in relevance the case of lung tumor. In this case the effects of organ motion are relevant due to the respiration, and different approaches have been presented. The section concluded with a particular methodology, tumor tracking, that foreseen an on line compensation of organ motion effects while the irradiation is delivered. This is of particular relevance in the case of particle therapy because of the availability of fast and high geometrical accuracy of a charged beam. As mentioned before, this approach is not used in clinical activity nowadays, except for a commercial device used in RT with photons. This device has been described in the thesis. Even if treatment planning optimization remains an issue, dose delivery systems in radiotherapy with particles could offer enormous potentialities for tumor tracking when organ motion is not negligible. Organ motion management requires not only an accurate setup procedure, but also a description of the trajectory (magnitude of movements and phase) of the target volume. This is usually performed by means of correlation models between internal target and external surrogates. Correlation models are used to build an external (patient's surface, or surrogates) internal (tumor mass, or radio-opaque clips) correlation, able to provide a feedback signal on the dose delivery system.

Different models have been presented in the last part of the thesis. This section has been focused on the study of predictive models for tumor tracking, and their possible integration in a dose delivery system (see figure 5.1).

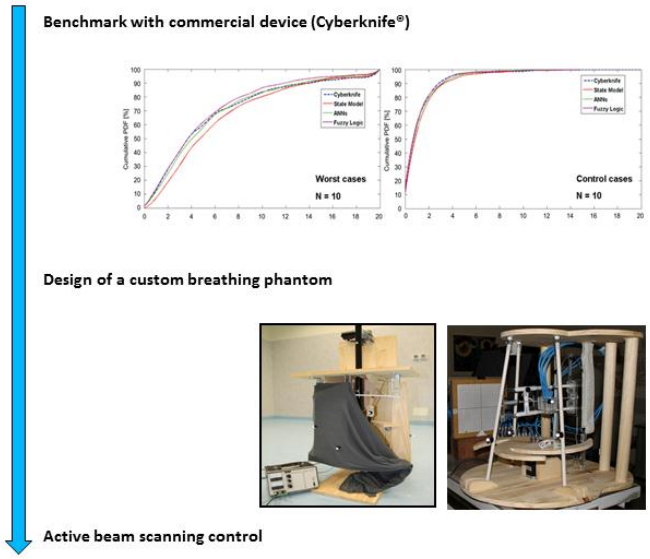

Figure 5.1. Schematic workflow of experimental activities.

Different approaches have been presented, and the algorithms comprise methods at variable complexity. Firstly, a benchmark of these algorithms vs. a commercial device has been reported. Different improvements of these models have been investigated, and then tested both on a clinical database and using a custom breathing phantom. This section concluded with a feasibility study on the integration of our approach (optical localizer, phantom and external-internal correlation models) in the control system of an active beam.

Conclusion and discussions are presented in this chapter following the same scheme. Next paragraph is dedicated to technological aspects of radiotherapy with particles, and attention will be dedicate to CNAO. The last paragraph is dedicated to the discussion of models for external-internal correlation and organ motion mitigation.

5.1.1 Technological aspects and CNAO experience

Protons and carbon ions are proved to be a valuable technique in cancer treatments. Potential advantages are represented by a high local control of the tumor and lower unwanted side effects. Moreover, this treatment is the only therapeutic solution for several types of tumors (slow progression, hypoxic deep seated tumors). High costs are the principal reason why this type of treatment is not largely diffused. Actually, in Europe only two facilities can offer this treatment. Dose distribution in depth requires an high accuracy and control in patient positioning and setup before and during irradiation. CNAO, the only facility in Italy able to perform radiotherapy with particles and carbon ions aims to provide a state of the art treatment. In this project, our team has been involved in the selection of appropriate systems for patient positioning and in room setup control. The solutions adopted have been described in the thesis. They represent the result of a selection process between different possibilities. The driving factors were the overall accuracy, the customization of the hardware design and software, and finally the costs. Installation of these systems last one year (2009). Hardware and software optimization required multiple checks and corrections. Measurements and integrations last two years (2010-2011), and they represent the result of a strong collaborations between institutions and suppliers (figure 5.2).

Figure 5.2 Installation of the systems in treatment room 1. From left to right: the pose of the granite floor, installation of PPS and PVS, a recent picture of the room acquired during accuracy tests.

Today, CNAO is starting its clinical activity. Results of commissioning activities and measurements carried out during acceptance protocols have been reported in the manuscript, supported by statistical analysis. They demonstrate that is possible to obtain sub-millimetric accuracy in patient repositioning. Integration of different systems was also successfully proved. Open issues remain in managing organ motion effects. The use of adequate immobilization

casts surely help to guarantee repeatability. All the treatment rooms, in different conditions and with different treatment tools resulted to be within the 0.3 mm accuracy, as expected. Room three seemed to reach better results in terms of 3D displacements of control points if compared with the others. This is mainly due by the fact that this room was fine tuned at the end of commissioning, and so strategies for optimizing the compensation (via software) were positively influenced by the experienced of the others. It is likely probably that during next interventions efforts will be devoted to the extension of more accurate controls also to the other rooms.
The workflow is well established, even if CNAO is treating first patients and it is not obviously at steady state. Actually, both cranial (2 patients) and extra-cranial (2 patients) treatments have been performed. The first one is now completed (head and neck Chondrosarcoma), while the others are going on (end of November 2011). All the patients are prepared following the workflow presented in chapter 2. They are immobilized on the treatment tools before PPS docking, aligned in nominal position driving the PPS in automatic mode as request by the treatment plan. Laser cross alignment is visually checked by operators. Then, correction vector provided by the OTS is applied. Last, X-rays are acquired, and new corrections are evaluated, if needed (Figure 5.3).

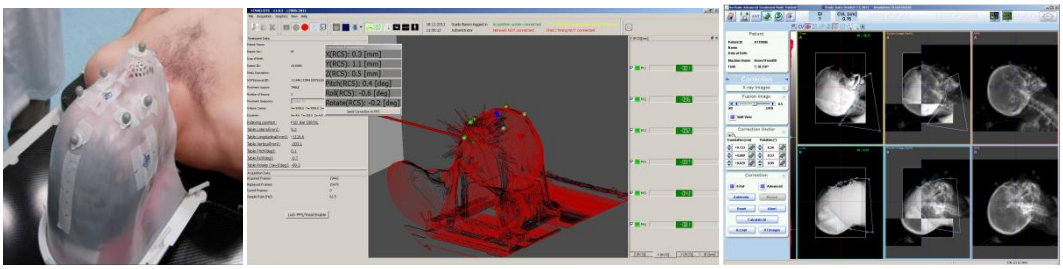

Figure 5.3. From left to right: patient immobilized on the carbon couch; first check of alignment with OTS; bone anatomy check with PVS.

In this initial experience with four patients, the most of the times no more corrections are required after the first X-ray acquisition, or they are so small that medical doctors require to compensate without the need of a second imaging. This result suggests that patient immobilization tools and positioning systems are working properly. In figure 5.4 are reported the setup errors following OTS corrections. Concordance between systems is relevant, even if larger OTS/PVS discrepancies have been noticed in extra-cranial districts.

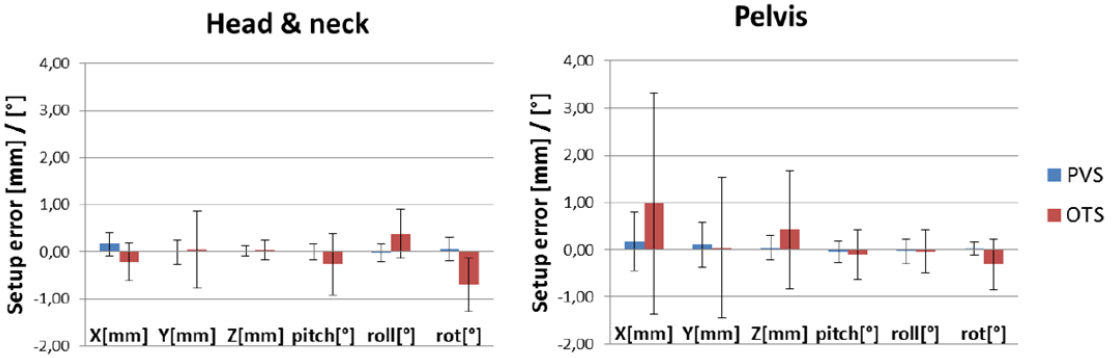

Figure 5.4 setup errors following PVS based corrections (courtesy of Dr. Maxime Desplanques).

Concerning correction vectors and displacements, data have been collected but we have to wait for an adequate number of sessions to analyze them. It is clear to operators that the selected strategies are adequate for treatments with particles. All the systems increase the

overall quality of the treatment. The use of an optical localizer helps not only in reducing time consumption during first alignment, but usually creates the conditions to renounce to the second acquisition for compensation checks. This is a major result, preserving patients from not therapeutic doses due to imaging checks. Data analysis will be included in future works as further studies are required.

5.1.2 Models for tumor tracking

First treatments in CNAO will be devoted to static tumors. Even if difficulties in treatment planning optimization remain, dose delivery systems in radiotherapy with particles could offer enormous potentialities for tumor tracking when organ motion is not negligible. Organ motion management requires not only an accurate setup procedure, but also a description of the trajectory (magnitude of movements and phase) of the target volume. This is usually performed by means of correlation models between internal target and external surrogates.
Different approaches have been described in the thesis. Firstly, a benchmark of alternative methods (based on: linear \ quadratic correlation, artificial neural networks and fuzzy logic) vs. Cyberknife® Synchrony® was performed. Results put forward these models as a potentially valuable tool for tumor position estimation, given patient's surface surrogate information. In particular, the comparative study showed that complex models are required to predict tumor motion over long time periods, showing better performances of neural networks and fuzzy logic if compared with linear \ quadratic correlation. It should be noted that the total treatment time for the considered cases was considerable (up to 118.8 minutes), by then a significant intra-session variability is expected. This last was the driving factor that required models to incorporate retraining capabilities, with continuous updating in order to achieve adequate performance. Since it is a commercial device, obviously no information was available concerning the frequency of effective model update that was used for Synchrony®, or the strategy used.
Results reported in chapter 4 showed that all models have comparable performance in control cases, whereas fuzzy logic has the best performance when worst cases have been considered. In particular, the fuzzy logic algorithm was able to improve accuracy for larger discrepancies. When considering the variability of results between different patients, the state model and ANN-based strategies exhibited a better stability. On the other hand, fuzzy logic seemed to be more sensitive to the available database for training.
The state model was built as a linear/quadratic correlation between the principal component of external marker motion and the internal tumor trajectory. In such a model, tumor hysteresis is accounted for through a time lag parameter t, so that input data across different phases of the breathing cycle have been considered. The optimization of the time lag plays a role in enhancing the performance of a state model, and optimal parameters should be established on a patient by patient basis. The intrinsic features of Cyberknife® data, where single snapshots are used for model construction, affected the effective optimization of the model time lag, thus resulting in sub-optimal results for the implemented state model.
The ANN-based approach resulted in comparable results with respect to Cyberknife® Synchrony®, pointing out similar generalization capabilities. The ANN architecture used in this study was selected as a trade-off between accuracy and the computational time for model training and re-training. These considerations mainly motivated the use of three separate networks for each of the external markers, compared to a single ANN where all marker coordinates are provided as input.
The implemented fuzzy logic algorithm proved to be superior to Cyberknife® Synchrony® in the analyzed patient database. Due to the intrinsic variability of breathing motion, a fuzzy

environment may be optimal for tumor motion estimation. The performed analysis showed that FCM data clustering is one of the key-factors which strongly affects the performance of the fuzzy inference model.
These models behaved differently. The overall comparison of breathing traces suggests a substantial overlap in most control cases among the various implemented strategies. Larger variations were found in worst cases, where each algorithm exhibited distinctive features. In the ANN-based approach the predicted traces showed occasionally reduced inhalation/exhalation peaks when compared to other strategies. On the other hand, the fuzzy logic algorithm featured a general tendency to over-estimate peaks with respect to alternative solutions. Both the fuzzy logic and ANN-based solutions revealed an increased high frequency noise in the breathing trace (especially at exhale) if compared to Synchrony® and the state model. Such effect tended to be larger following a complete model retrain.
Results are promising, but again these models are far away from clinical trials in radiotherapy with particles. Main limitations consisted for example in the lack of a proper optimization. Concerning the ANN approach, a more complex architecture can be expected to lead to better results: for example, the use of recurrent networks has been shown to be extremely efficient in other applications (Procházka and Pavelka 2007). Conversely, the time needed for model training may be not acceptable for increased levels of complexity. It should be pointed out that there is an intrinsic difficulty in achieving the optimal architecture without exploiting specific optimization algorithms. As several parameters are required to define a given architecture, optimization methods that are able to explore a great number of different combinations are needed, such as genetic optimization.
Moreover, since no evidences lead researchers to claim that one model is better than others, different approaches should not be discarded a priori. Alternative predictors or finite element modeling could be in principle utilized. First trials were conducted using a Cyberknife® database, thus processing three external surrogates and variable numbers of X-rays acquisitions. Further investigations should be devoted to the search for an optimum setup for models validation (more reference points, or placed in an optimized configuration) (Riboldi *et al* 2007), keeping in mind that a patient's specific approach is mandatory. Last, the restricted number of database does not allowed a proper validation of the proposed solutions.

A first step towards optimization of neural networks and fuzzy logic approaches was performed. The aim in this case was to obtain better performances (in terms of 3D errors reduction) and to understand if it was possible to design an application able to run in CNAO hardware. We firstly tested these improvement on the same Cyberknife® database.
Different data clustering methods were investigated, because of their obviously effect on fuzzy modeler performance. As derived from the final analyzed results, the implemented FCM technique for input/output data clustering proved to be more suitable than subtractive clustering. This was confirmed when subtractive clustering was used in the fuzzy section of ANFIS. However, it should be considered that ANFIS takes longer time for model configuration and update in comparison with the two other fuzzy modelers, owing to data processing in its neural network section. Also the adaptive selection of adequate fuzzy correlation models on a patient specific basis has been proved to be feasible, despite the limited availability of model training data.
In particular, ANN architecture was increased in complexity and the algorithm was written in C++. Concerning this approach, results obtained from both the control and the worst patient groups demonstrate that the developed algorithm, within the selected cases, yielded an effective improvement in tracking accuracy with respect to Synchrony®. This result confirms the findings of the previous approach, where ANNs proved to be able to achieve better tracking accuracy if compared with the Synchrony®. Again, no specific and particular attention

was focused on the optimization of the ANN architecture. Considering the numerous parameters required to define the neural networks architecture, a dedicated study would most probably lead to an optimal solution, both in terms of network architecture and training algorithm, with potential improvement in tumor position estimation especially in presence of breathing irregularities.

All these studies suffered for the lack of large database. In order to increase data for model testing and validation, it was implicitly required to build a custom phantom. This phantom is able to mimic a realistic breathing, and it features an internal target that moves along an hysteretic trajectory in phase with the external ribcage. Preliminary studies were conducted with ANN approach integrated in CNAO hardware. Results on phantom study demonstrate that neural networks can be not only integrated in CNAO hardware, but that they can be trained and updated with a clinical compatible time consumption.
At this time there are no phantoms in commerce able to mimic the breathing and in the same time to provide an internal trace of a moving target visible by an optical localizer. Obviously the design of our phantom can be improved, as the range of motions, that is adequate only for preliminary studies. It is evident that the motion patterns are too simplified if compared with a human like motion. Moreover, it would be interesting to add a functionality that allows to load a real respiratory pattern and to move consequently the phantom.

The use of an integrate system (phantom, optical tracking system with predictive capabilities) allowed us to test our method in GSI, Germany. There, it was possible to test the potential integration of our systems in the steering logic of dose delivery. In this respect, result was successfully reached. Even if we observed remarkable performance of predictors during the second experimental session, retraining capabilities remain at this time a major issue. More experimental sessions will be dedicated to the search of a reliable estimator, and different methodologies have to be investigated. But the main goal, that was the active control of a carbon ion beam using a signal processed by a predicting model, was reached.
Moreover, the use of models produced in pinpoint 4 (the central one in the pinpoint holder) a range of 2.12% to 36.50% in different sessions if compared with static irradiation, underlying the importance of motion compensators.
There are evident limitations in this study. Even if pattern variations are provided and motion can be easily tuned, the phantom motion cannot be considered human-like. Moreover, the performance of predictors added control in target position, but their performance was not found below acceptable thresholds. This aspect is even more evident if we consider that the motion pattern was simpler if compared with a natural, physiological, movement. Retrain capabilities should be better investigated. More studies are going on in order to optimize these aspects.

5.2 Final considerations

Radiotherapy with accelerated particles can offer a high geometric accuracy and relevant outcomes for a variety of radio-resistant tumors. Setup errors can affect severely the effectiveness of the treatment, and tools and strategies aimed at limiting setup errors must be taken into account. During the PhD program I had the chance to follow the installation of patient positioning systems and setup control in the first Italian center for radiotherapy with accelerated particles, from the first day to the first clinical trials. Focusing on tumor control and patient monitoring, the major issue is the so called organ motion. To minimize these effects, a proper immobilization of the patient is not sufficient. Research is active in developing

models for tumor tracking, even if at the moment it is not foreseen any clinical application. One of the reasons is that dose distribution is not dependent only by the tumor position, but also by the geometry of the target and the condition of surrounding tissues and structures. The presence of oxygen or density variations influence the radiobiological effectiveness of the treatment, resulting in interplay effects. Evidences suggest that more studies are needed, and also that a possible solution could be represented by the integration of different approaches. This field of research is recent, but presents at least two different difficulties. The first is that few facilities are able to offer this kind of treatments worldwide, mainly due to the cost of startup. The second is that few clinical data are made available. This lack can be partially substituted by simulators or phantoms. In order to find an alternative to clinical data, we built our own phantom. The last step was to include the application in CNAO hardware, and to run simulations with the phantom in a clinical like environment. During the last year of Doctorate, I had the possibility to perform an irradiation with an active carbon ion beam. The idea was to integrate all the systems in the steering control system of GSI, the only facility that dedicated beam time to this kind of research. This experience, made in collaboration with GSI Moving Target group, produced promising results. Most of all, it offered the chance to test all the methods prepared *offline* in a treatment cave, where technologies for tumor tracking are available and currently used for research porpoises.

Bibliography

Amaldi U 2001 Hadrontherapy in the world *proceedings of NUPECC* pp 1-18

Amies C *et al* 2006 A multi-platform approach to image guided radiation therapy (IGRT) *Medical Dosimetry* Vol. 31 No. 1 pp 12-19

Anil K J, Dubes R C 1988 Algorithms for clustering data *Prentice-Hall* New Jersey

Balderbos J, Sonke JJ 2009 State of the art lung cancer radiation therapy *Expert Rev. Anticancer Ther.* 9 1353-1363

Balter M, Kessler J, Kessler M 2007 Imaging and alignment for image-guided radiation therapy *J Clin Oncol* 25 No. 8 pp 931-937

Barendsen G W 1968 Current topics in radiation research Vol. IV North-Holland Pub. Co. pp 293-356

Baroni G *et al* 2007 Integration of enhanced optical tracking techniques and imaging in IGRT *J. Radiat. Res.* 48 Suppl. A61-A74.

Batterman JJ *et al* 1981 Observations on pulmonary metastases in patients after single doses and multiple fractions of fast neutrons and cobalt-60 gamma rays *Eur. J. Cancer* 17 pp 539-548

Belli M *et al* 1989 RBE-LET relationship for the survival of V79 cells irradiated with low energy protons *Int. J. Radiat. Biol.* 55 pp 93-104

Bert C, Durante M 2011 Motion in radiotherapy: particle therapy *Phys. Med. Biol.* 56 R113-R144

Bert C *et al* 2007 Target motion tracking with a scanned particle beam *Med. Phys.* 34 pp 4768-4771

Bezdek J C 1981 Pattern Recognition with Fuzzy Objective Function Algorithms. *Plenum Press*, New York

Bezdek J C, Pal N R 1998 Some new indexes of cluster validity. *IEEE Trans. Syst. Man. Cybern.* 23 pp 301-315

Blakely E A *et al* 1984 Heavy-ion radiobiology: cellular studies *Adv. Rad. Biol*. 11, 295-389

Bragg W, Kleemann R 1903 On the a-Particles of Radium and their Loss of Range in Passing Through Various Atoms and Molecules *Phil. Mag.* 3 pp 18-340

Brown W T *et al* 2007 CyberKnife® Radiosurgery for Stage I Lung Cancer: Results at 36 Months *Clin. Lung Cancer* 8 pp 488-492

Chiu S 1994 Fuzzy Model Identification Based on Cluster Estimation *J. Intell. Fuzzy. Syst.* 2 pp 267-278

Chu W T, Ludewigt B A, Renner T R 1993 Instrumentation for treatment of cancer using proton and light-ion beams *Rev. Sci. Instrum.* 64 pp 2055–122

Cui Y *et al* 2008 Learning methods for lung tumor markerless gating in image-guided radiotherapy *Proceedings of the 14th ACM SIGKDD international conference on Knowledge discovery and data mining*

Dawson L A, Jaffray D A 2007 Advances in image-guided radiation therapy *J. Clin. Oncol.* Vol. 25 No. 8 pp 938-946

Dayhoff JE, Deleo JM 2001 Artificial neural network, Conference on Prognostic Factors and Staging in Cancer Management: Contributions of Artificial Neural Networks and Other Statistical Methods *Cancer Supplement* 91 pp 1615-1635

Dearnaley D P *et al* 1999 Comparison of side-effects of conformal and conventional radiotherapy in prostate cancer: a randomized trial *Lancet* 353 pp 267-272

Deering R A, Rice R Jr. 1962 Heavy ion irradiation of HeLa cells *Radiat. Res.* 17 pp 774-786

Denekamp J. 1994 Neutron radiobiology revisited *Acta Oncol.* 33 pp 233-240

Dieterich S *et al* 2008 Locating and targeting moving tumors with radiation beams *Med. Phys*. 35 pp 5684-5694

Dunn J C 1973 A Fuzzy Relative of the ISODATA Process and Its Use in Detecting Compact Well-Separated Clusters *Journal of Cybernetics* 3 pp 32-57

Durante M, Loeffler J S 2010 Charged particles in radiation oncology *Nat. Rev. Clin. Oncol.* 7 pp 37-43

Ernst F, Bruder R, Schlaefer A, Schweikard A 2011 Correlation between external and internal respiratory motion: a validation study *Int. J. Comput. Assist. Radiol. Surg.* pp 1-10

Essen CF von *et al* 1985 The Piotron: II. Methods and initial results of dynamic pion therapy in phase II studies *Int. J. Radiat. Oncol. Biol. Phys.* 11 pp 217-226

Evans P M 2008 Anatomical imaging for radiotherapy *Phys. Med. Biol.* 53 R151-R191

Furukawa T *et al* 2007 Design study of a raster scanning system for moving target irradiation in heavy-ion therapy *Med. Phys.* 34 pp 1085-1097

Furusawa Y *et al* 2000 Inactivation of aerobic and hypoxic cells from three different cell lines by accelerated 3He- 12C- and20Ne-Ionbeams *Radiat. Res.* 154 pp 485-496

Gademann G 1994 Socio-economics aspects of hadrontherapy. In Amaldi U, Larsson B, eds. *Hadrontherapy in Oncology. Proceedings of the First International Symposium on Hadrontherapy, Como, Italy, 18-21 October 1993. Elsevier Excepta Medica* pp 59-66

Gemmel A *et al* 2010 Development and performance evaluation of a dynamic phantom for biological dosimetry of moving targets *Phys. Med. Biol.* 55 2997

Grözinger S O *et al* 2008 Motion compensation with a scanned ion beam: a technical feasibility study *Radiation Oncology* pp 3-34

Haberer T *et al* 1993 Magnetic scanning system for heavy ion therapy *Nucl. Instrum. Methods* A 330 pp 296-305

Hertz J, Krogh A, Palmer R G 1991 Introduction to the theory of neural computation Ch.1 *Redwood City, CA*

Hoisak J D P *et al* 2006 Prediction of lung tumour position based on spirometry and on abdominal displacement: Accuracy and reproducibility *Radiotherapy and Oncology* Vol. 78 pp 339-346

Hoogeman M *et al* 2009 Clinical accuracy of the respiratory tumor tracking system of the cyberknife: assessment by analysis of log files *Int. J. Radiat. Oncol. Biol. Phys.* 74 pp 297-303

Hug E, Debus J (2008) Oral presentation *ESTRO teaching course Heidelberg*

Huntzinger C *et al* 2006 Dynamic targeting image-guided radiotherapy *Medical Dosimetry* Vol. 31 No. 2 pp 113-125

Jaffray D A 2005 Emergent Technologies for 3-Dimensional Image-Guided Radiation Delivery *Semin. Radiat. Oncol.* 15 pp 208-216

Jain A K, Murty M N, Flynn P J 1999 Data clustering: a review *ACM Computing Surveys (CSUR)* 31 pp 264-323

Jang J 1993 ANFIS: adaptive-network-based fuzzy inference system *IEEE Trans. Syst. Man. Cybern.* 23 pp 665-685

Jang J, Chuen-Tsai S, Mizutani E 1997 Neuro fuzzy modeling and soft computing *Prentice-Hall, Englewood Cliffs*

Jiang B S 2006 Technical aspects of image-guided respiration-gated radiation therapy *Medical Dosimetry* Vol. 31 No. 2 pp 141-151

Jones B 2006 The case for particle therapy *B. J. Radiology* 79 pp 24-31

Kakar M *et al* 2005 Respiratory motion prediction by using the adaptive neuro fuzzy inference system (ANFIS) *Phys. Med. Biol.* 50 pp 4721-4728

Kang S J *et al* 2000 Evolutionary design of fuzzy rule base for nonlinear system modeling and control *IEEE Trans. Fuzzy Syst.* 8 pp 37-45
Keall P *et al* 2006 The management of respiratory motion in radiation oncology report of AAPM task group 76 *Med. Phys.* 33 pp 3874-3900

Kessler M L 2006 Image registration and data fusion in radiation therapy *British Journal of Radiology* 79, S99-S108

Koehler A M, Schneider R J, Sisterson J M 1975 Range modulators for protons and heavy ions *Nucl Instrum Methods* 131 pp 437-440.

Kraft G 2002 Radiobiological effects of highly charged ions: Their relevance for tumor therapy and radioprotection in space, The Physics of Highly and Multiply Charged Ions Ch. 10 *Ed. F. J. Currell Kluwer Academic Publisher*

Kraft G, Kraft S D 2009 Research needed for improving heavy-ion therapy *N. J. Phys. 11*

Kraft G 1987 Radiobiological Effects of Very Heavy Ions: Inactivation, Inductions of Chromosome Aberrations and Strand Breaks *Nuclear Science Applications* 3 pp 1-28

Kramer M, Scholtz M 2000 Treatment planning for heavy-ion radiotherapy: calculation and optimization of biologically effective dose *Phys. Med. Biol.* 45 pp 3319-3330

Krengli M, Orecchia R 2004 Medical aspects of the National Centre for Oncological Hadronterapy (CNAO - Centro Nazionale Adroterapia Oncologica) in Italy *Radiotherapy and Oncology* Vol. 73 pp S21-S23

Levenberg K 1944 A Method for the Solution of Certain Problems in Least Squares *Quart. Appl. Math*. 2 pp 164-168

Lewis J H *et al* 2010 Markerless lung tumor tracking and trajectory reconstruction using rotational cone-beam projections: a feasibility study *Phys. Med. Biol.* 55 pp 2505-2522

Li R *et al* 2009 A feasibility study of markerless fluoroscopic gating for lung cancer radiotherapy using 4DCT templates *Phys. Med. Biol.* 54 N489–N500

Lin T *et al* 2009 Fluoroscopic tumor tracking for image-guided lung cancer radiotherapy *Phys. Med. Biol.* 54 pp 981-992

Lin C K, Wang S D 1999 Fuzzy system identification using an adaptive learning rule with terminal attractors *J. Fuzzy Sets Syst.* 101 pp 343-352

Lodge M *et al* 2007 A systematic literature review of the clinical and cost-effectiveness of hadron therapy in cancer *Radiotherapy and Oncology* 83 pp 110-122

Marquardt D 1963 An Algorithm for Least-Squares Estimation of Nonlinear Parameters. *SIAM J. Appl. Math.* 11 pp 431-441

Martin C, Bachtold D, Schar H 2007 Specification 6DPPS & Diagnostic Device *Technical report*

Murphy M J *et al* 2007 The management of imaging dose during image-guided radiotherapy: Report of the AAPM Task Group 75 *Med. Phys.* 34 4041

Murphy, M J, Dieterich S 2006 Comparative performance of linear and nonlinear neural networks to predict irregular breathing *Phys. Med. Biol*. 51 pp 5903-5914

Murray B R *et al* 2006 The Management of Respiratory Motion in Radiation Oncology report of AAPM task group 76. *Med. Phys.* 33 pp 3874-3900

Orecchia R *et al* 1998 Particle Beam Therapy (Hadrontherapy): Basis for Interest and Clinical Experience *European Journal of Cancer* Vol. 34 pp 459-468

Orecchia R, Fossati P, Rossi S 2009 The national center for oncological hadron therapy: status of the project and future clinical use of the facility *Tumori* 95 pp 169-176

Particle Therapy Cooperative Group 2011 [online], http://ptcog.web.psi.ch

Pedroni E *et al* 1995 The 200-MeV proton therapy project at the Paul Scherrer Institute: conceptual design and practical realization *Med. Phys.* 22 pp 37-53

Pella A *et al* 2010 design of a 4D breathing phantom for motion tracking studies in extra-cranial particle therapy *Proceedings of PTCOG 49* p174

Pella A *et al* 2011 Use of machine learning methods for prediction of acute toxicity in organs at risk following prostate radiotherapy *Med. Phys.* 38 pp 2859-2867
Procházka A, Pavelka A 2007 Feed-foward and recurrent neural networks in signal prediction *Proceedings the 5th IEEE Int. Conference on Computational Cybernetics* Gammarth

Ramrath L *et al* 2007 Prediction of respiratory motion with a multi-frequency based Extended Kalman Filter *Proceedings of the 21st International Conference and Exhibition on Computer Assisted Radiology and Surgery (CARS'07)* Vol. 21

Riaz N *et al* 2009 Predicting respiratory tumor motion with Multidimensional Adaptive Filters and Support Vector Regression *Phys. Med. Biol.* 54 pp 5735-5718
Riboldi M *et al* 2007 Genetic evolutionary taboo search for optimal marker placement in infrared patient setup *Phys. Med. Biol.* 52 pp 5815-5830

Riboldi *et al* 2009 Installation and preliminary testing of a newly designed patient setup and monitoring system for particle beam therapy *Proceedings of PTCOG 48* Heidelberg p 91

Riboldi M *et al* 2010 Real-time tumor targeting in external beam radiotherapy *Brain cancer, tumor targeting and cervical cancer* Nova science publisher Elena Salvatti Editor pp 247-260

Rietzel E, Bert C 2010 Respiratory motion management in particle therapy *Med. Phys.* 37 pp 449-460

Ringborg U *et al* 2003 The Swedish Council on Technology Assessment in health care (SBU) systematic overview of radiotherapy for cancer including a prospective survey of radiotherapy practice in Sweden 2001 – summary and conclusions. *Acta Oncologica* 42 pp 357-65.

Robert C, Gaudy J F, Limoge A 2002 Electroencephalogram processing using neural networks *Clinical Neurophysiology* 113 pp 694-701

Rosenblatt F 1958 The perceptron: a probabilistic model for information storage and organization in the brain *Psychological review* 65 pp 386-408

Ruan D *et al* 2008 Inference of hysteretic respiratory tumor motion from external surrogates: a state augmentation approach *Phys. Med. Biol*. 53 pp 2923-2936

Saito N *et al* 2009 Speed and accuracy of a beam tracking system for treatment of moving targets with scanned ion beams *Phys. Med. Biol.* 54 4849

Scholtz M (2008) Oral presentation *ESTRO teaching course Heidelberg*

Schultze 2010 Technical report of PPS and PVS measurements. GDV

Schulz-Ertner D, Tsujii H 2007a Particle radiation therapy using proton and heavier ion beams *J. Clin. Oncol.* 25 pp 953-964

Schulz-Ertner D *et al* 2007b Effectiveness of carbon ion radiotherapy in the treatment of skull-base chordomas *Int. J. Radiat. Oncol. Biol. Phys.* 68 pp 449-457

Seco J *et al* 2009 Breathing interplay effects during proton beam scanning: simulation and statistical analysis *Phys. Med. Biol.* 54 N283-N294

Seppenwoolde Y *et al* 2007 Accuracy of tumor motion compensation algorithm from a robotic respiratory tracking system: a simulation study *Med. Phys.* 34 pp 2774-2784

Seppenwoolde Y *et al* 2002 Precise and real-time measurement of 3D tumor motion in lung due to breathing and heartbeat, measured during radiotherapy *Int. J. Radiat. Oncol. Biol. Phys.* 53 pp 822-834

Seregni M *et a*l Real-time tumor tracking with an artificial neural networks-based method: a feasibility study *Physica Medica* in press

Sharp G C *et al* 2004 Prediction of respiratory tumour motion for real-time image-guided radiotherapy *Phys. Med. Biol.* 49 pp 425-440

Sharpe C, Moseley D J 2007 Image guidance: treatment target localization systems Front *Radiat. Ther. Oncol.* 40 pp 72-93

Shi Y, Eberhart R, Chen Y 1999 Implementation of evolutionary fuzzy systems *IEEE Trans Fuzzy Syst* 7 pp 109-119

Shirato H *et al* 2007 Organ motion in image-guided radiotherapy: lessons from real-time tumor-tracking radiotherapy *Int. J. Clin. Oncol.* 12 pp 8-16

Shirato H *et al* 1999 real time tumour-tracking radiotherapy *Lancet* 353 pp 1331-1332

Shirato H *et al* 2000 Physical aspects of a real-time tumor-tracking system for gated radiotherapy *Int. J. Radiat. Oncol. Biol. Phys.* 48 pp 1187-1195

Shirato H *et al* 2004 Intrafractional tumor motion: Lung and liver *Semin. Radiat. Oncol.* 14 pp 10-18

Sisterson J 1999 Worldwide charged particle patient totals *Particles* 23 pp 14

Skarsgard L D *et al* 1967 Radiation Research Supplement 7 pp 208-221

Sonveaux P *et al* 2003 Irradiaton-induced angiogenesis through the upregulation of the nitric oxide pathway: implications for tumor radiotherapy *Cancer Res.* 63 pp 1012-1019

Staab A *et al* 2011 Spot-scanning-based proton therapy for extracranial chordoma *Int. J. Radiation Oncology Biol. Phys.* Vol. 81 No. 4 pp 489-496

Su M *et al* 2005 An artificial neural network for predicting the incidence of radiation pneumonitis *Med. Phys*. 32 pp 318-325

Takagi T, Sugeno M 1985 Fuzzy identification of systems and its application to modeling and control *IEEE Trans. Syst. Man. Cybern*. 15 pp 116-132

Furukawa T *et al* 2010 Moving target irradiation with fast rescanning and gating in particle therapy *Med. Phys.* 37 4874

Todd P 1964 PhD thesis Univ. California, Berkeley

Todd P 1965 Biological effects of heavy ions *Symposium on Protection against Radiation in Space*, NASA SP-71, US Govt Printing Office, A. Reetz, Editor, Washington, DC pp 105-114

Torshabi A E *et al* 2010 Targeting accuracy in real-time tumor tracking via external surrogates: a comparative study *Technol. Cancer Res. Treat.* 9 551–562

Tsujii H *et al* 2007 Clinical results of carbon ion radiotherapy at NIRS *J. Radiat. Res.* 48 A1–A13

Van de Water S *et al* 2009 Tumor tracking with scanned proton beams: assessing the accuracy and practicalities *Phys. Med. Biol.* 54 pp 6549-6563

Vedam S S *et al* 2004 Predicting respiratory motion for four-dimensional radiotherapy *Med. Phys.* 31 pp 2274-2283
Verellen D, De Ridder M, Storme G 2008 A (short) history of image-guided radiotherapy *Radiotherapy and Oncology* 86 pp 4–13

Walter C, Boda-Heggemann J, Wertz H 2007 Phantom and in-vivo measurements of dose exposure by image-guided radiotherapy (IGRT): MV portal images vs. kV portal images vs. cone-beam CT *Radiotherapy and Oncology* 85 pp 418-423

Warlick B W 2008 image-guided radiation therapy: techniques and strategies *Community Oncology* Vol. 5 No. 2 pp 86-92

Weyrather W K *et al* 1999 RBE for Track-Segment Irradiation in Cell Lines of Differing Repair Capacity *Int. J. Radiat. Biol.* 75 pp 1357-1364

Wilson R R 1946 Radiological Use of Fast Protons *Radiology* 47 pp 487-491

Xing L *et al* 2006 Overview of image-guided radiation therapy *Medical Dosimetry* Vol. 31 No. 2 pp 91-112

Xu Q, Hamilton R 2005 Novel respiratory gating method based on automated analysis of ultrasonic diaphragm motion *Med. Phys.* 32 2124

Yu J, Cheng Q, Huang H 2004 Analysis of the weighting exponent in the FCM *IEEE Trans. Syst. Man. Cybern.* 34 pp 634-639

Zanetti R *et al* 2002 Editors. Cancer in Italy 1993-1998. Incidence data from cancer registries 3rd volume, Roma: II Pensiero Scientifico Editore

Zenklusen S M, Pedroni E, Meer D 2010 A study on repainting strategies for treating moderately moving targets with proton pencil beam scanning at the new Gantry 2 at PSI *Phys. Med. Biol.* 55 pp 5103-5121

Zirkle R E, Marchbank D F, Kuck K D 1952 *Journal of Cellular Physiology* Supp. 39 pp 78-85

Appendix *a*

Patient Positioning System, Room 1 (Schultze 2010).

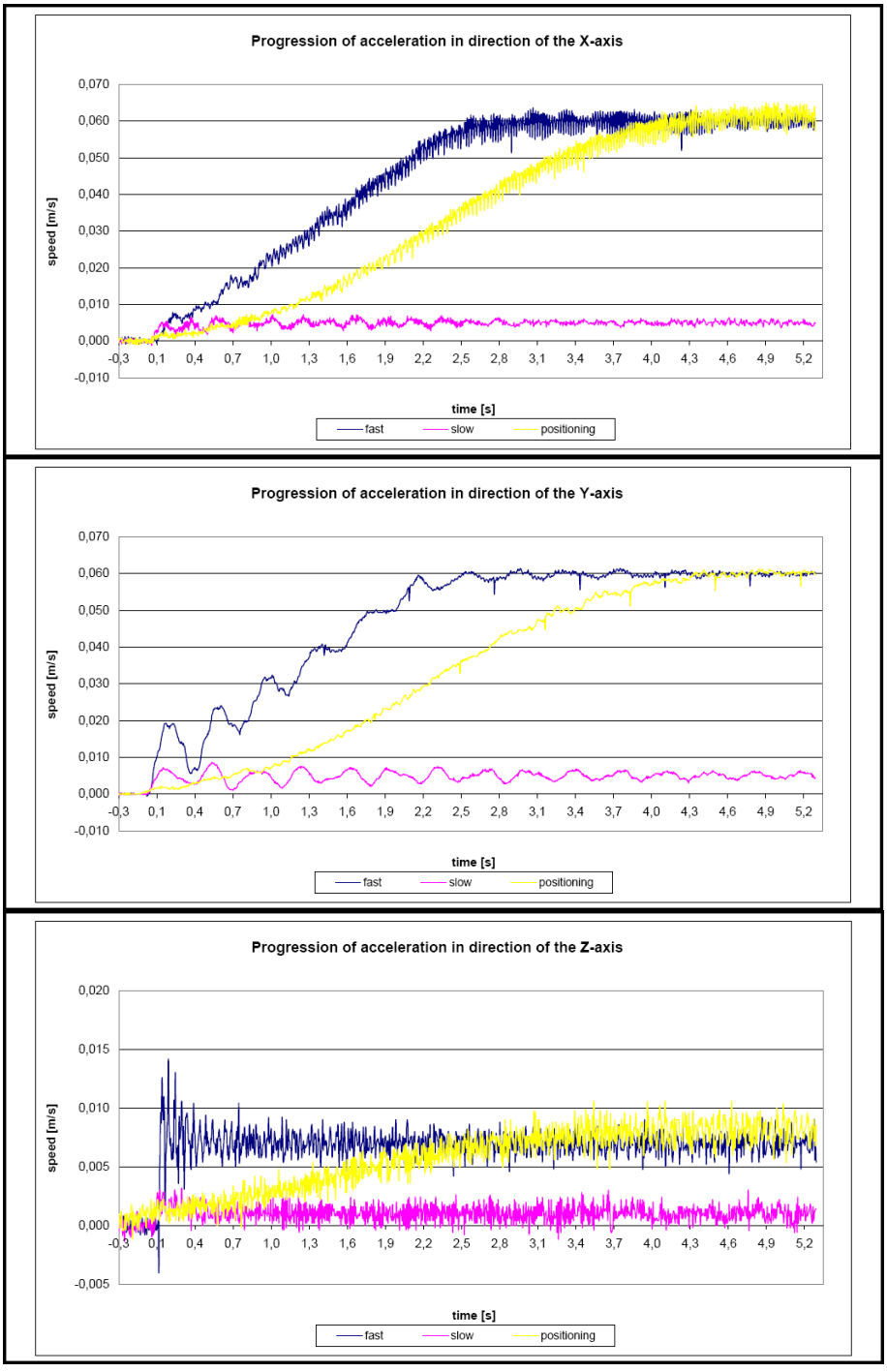

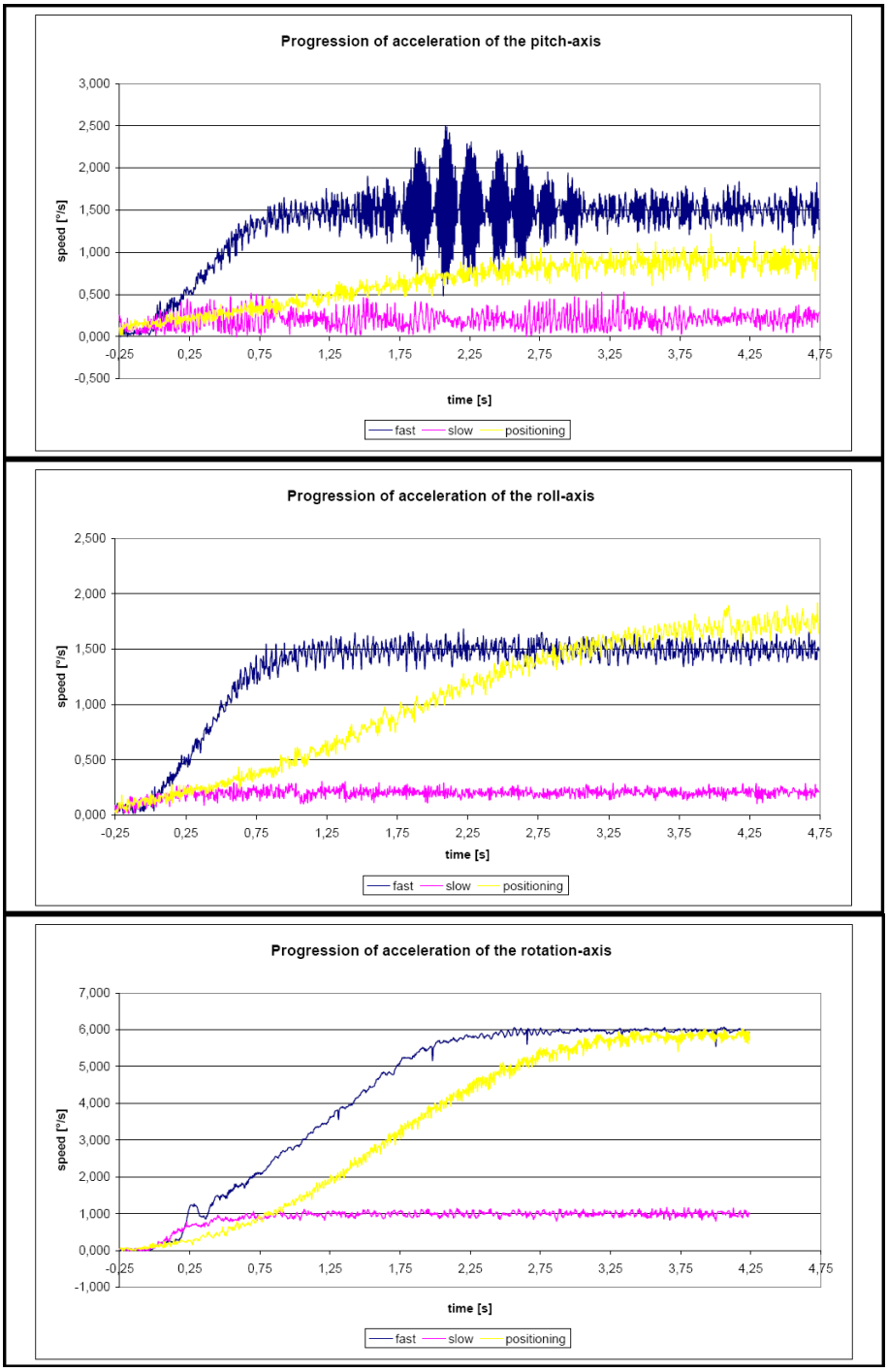
Progression of acceleration of the pitch-axis
speed [°/s]
3,000
2,500
2,000
1,500
1,000
0,500
0,000
-0,500
-0,25
0,25
0,75
1,25
1,75
2,25
2,75
3,25
3,75
4,25
4,75
time [s]
fast
slow
positioning
Progression of acceleration of the roll-axis
speed [°/s]
2,500
2,000
1,500
1,000
0,500
0,000
-0,25
0,25
0,75
1,25
1,75
2,25
2,75
3,25
3,75
4,25
4,75
time [s]
fast
slow
positioning
Progression of acceleration of the rotation-axis
speed [°/s]
7,000
6,000
5,000
4,000
3,000
2,000
1,000
0,000
-1,000
-0,25
0,25
0,75
1,25
1,75
2,25
2,75
3,25
3,75
4,25
4,75
time [s]
fast
slow
positioning

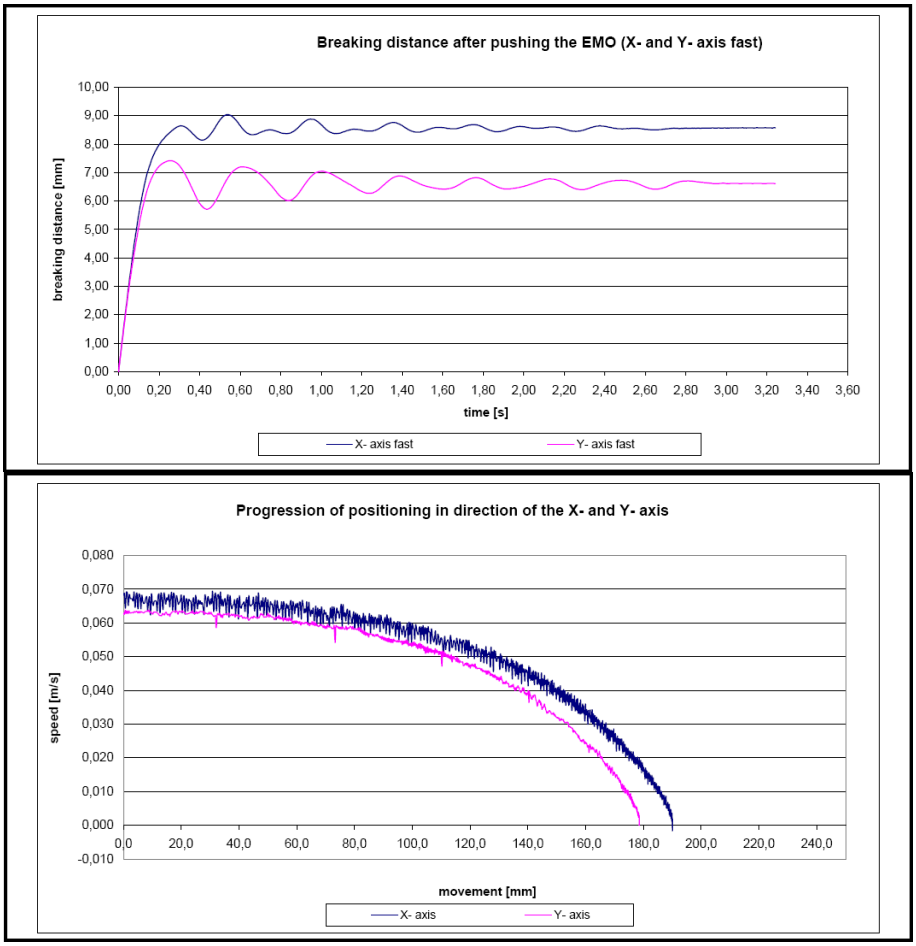
Breaking distance after pushing the EMO (X- and Y- axis fast)
breaking distance [mm]
10,00
9,00
8,00
7,00
6,00
5,00
4,00
3,00
2,00
1,00
0,00
0,00 0,20 0,40 0,60 0,80 1,00 1,20 1,40 1,60 1,80 2,00 2,20 2,40 2,60 2,80 3,00 3,20 3,40 3,60
time [s]
X- axis fast
Y- axis fast

Progression of positioning in direction of the X- and Y- axis
speed [m/s]
0,080
0,070
0,060
0,050
0,040
0,030
0,020
0,010
0,000
-0,010
0,0 20,0 40,0 60,0 80,0 100,0 120,0 140,0 160,0 180,0 200,0 220,0 240,0
movement [mm]
X- axis
Y- axis

Patient Positioning System, Room 2 (Schultze 2010).

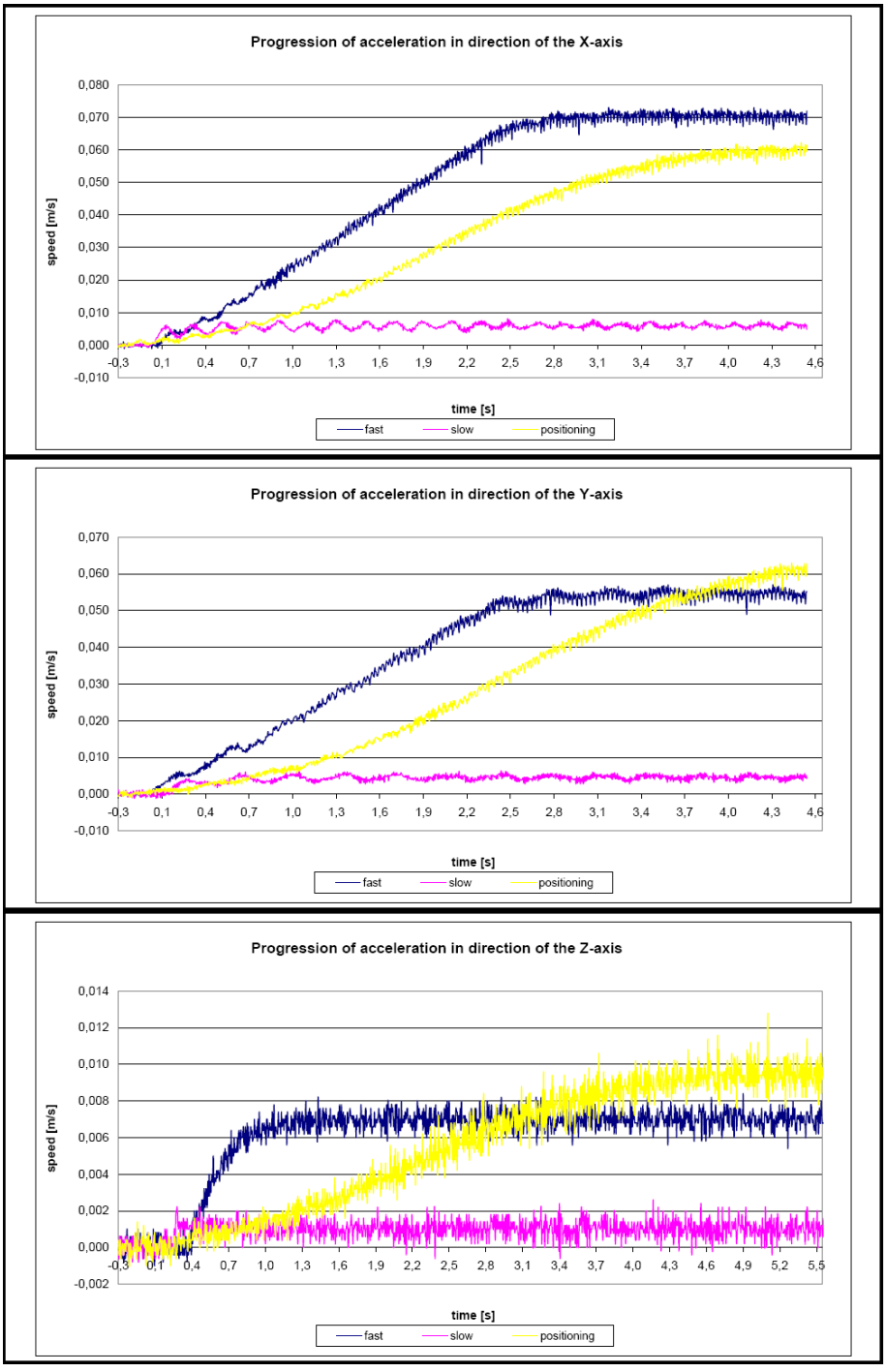

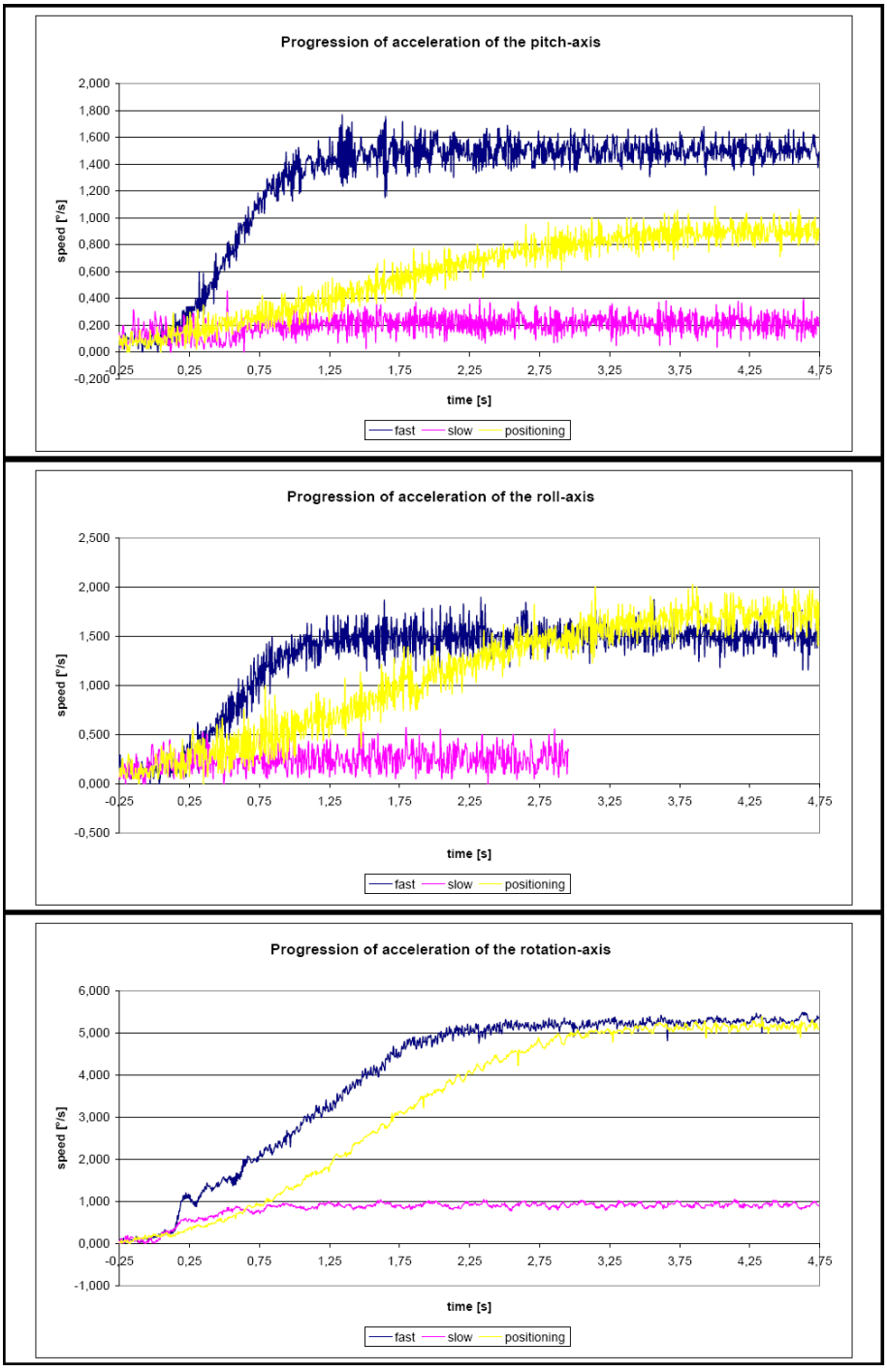
Progression of acceleration of the pitch-axis
speed [°/s]
2,000
1,800
1,600
1,400
1,200
1,000
0,800
0,600
0,400
0,200
0,000
-0,200
-0,25
0,25
0,75
1,25
1,75
2,25
2,75
3,25
3,75
4,25
4,75
time [s]
fast
slow
positioning
Progression of acceleration of the roll-axis
speed [°/s]
2,500
2,000
1,500
1,000
0,500
0,000
-0,500
-0,25
0,25
0,75
1,25
1,75
2,25
2,75
3,25
3,75
4,25
4,75
time [s]
fast
slow
positioning
Progression of acceleration of the rotation-axis
speed [°/s]
6,000
5,000
4,000
3,000
2,000
1,000
0,000
-1,000
-0,25
0,25
0,75
1,25
1,75
2,25
2,75
3,25
3,75
4,25
4,75
time [s]
fast
slow
positioning

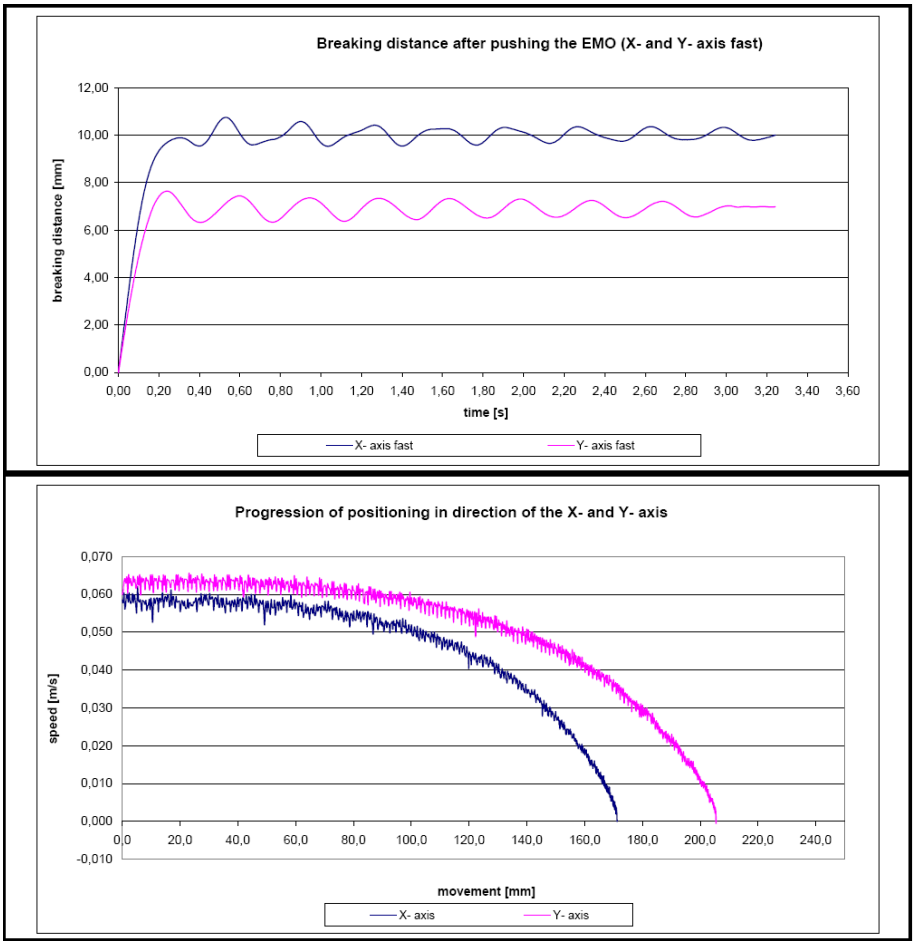
Breaking distance after pushing the EMO (X- and Y- axis fast)
breaking distance [mm]
12,00
10,00
8,00
6,00
4,00
2,00
0,00
0,00 0,20 0,40 0,60 0,80 1,00 1,20 1,40 1,60 1,80 2,00 2,20 2,40 2,60 2,80 3,00 3,20 3,40 3,60
time [s]
X- axis fast
Y- axis fast
Progression of positioning in direction of the X- and Y- axis
speed [m/s]
0,070
0,060
0,050
0,040
0,030
0,020
0,010
0,000
-0,010
0,0 20,0 40,0 60,0 80,0 100,0 120,0 140,0 160,0 180,0 200,0 220,0 240,0
movement [mm]
X- axis
Y- axis

Patient Positioning System, Room 3 (Schultze 2010).

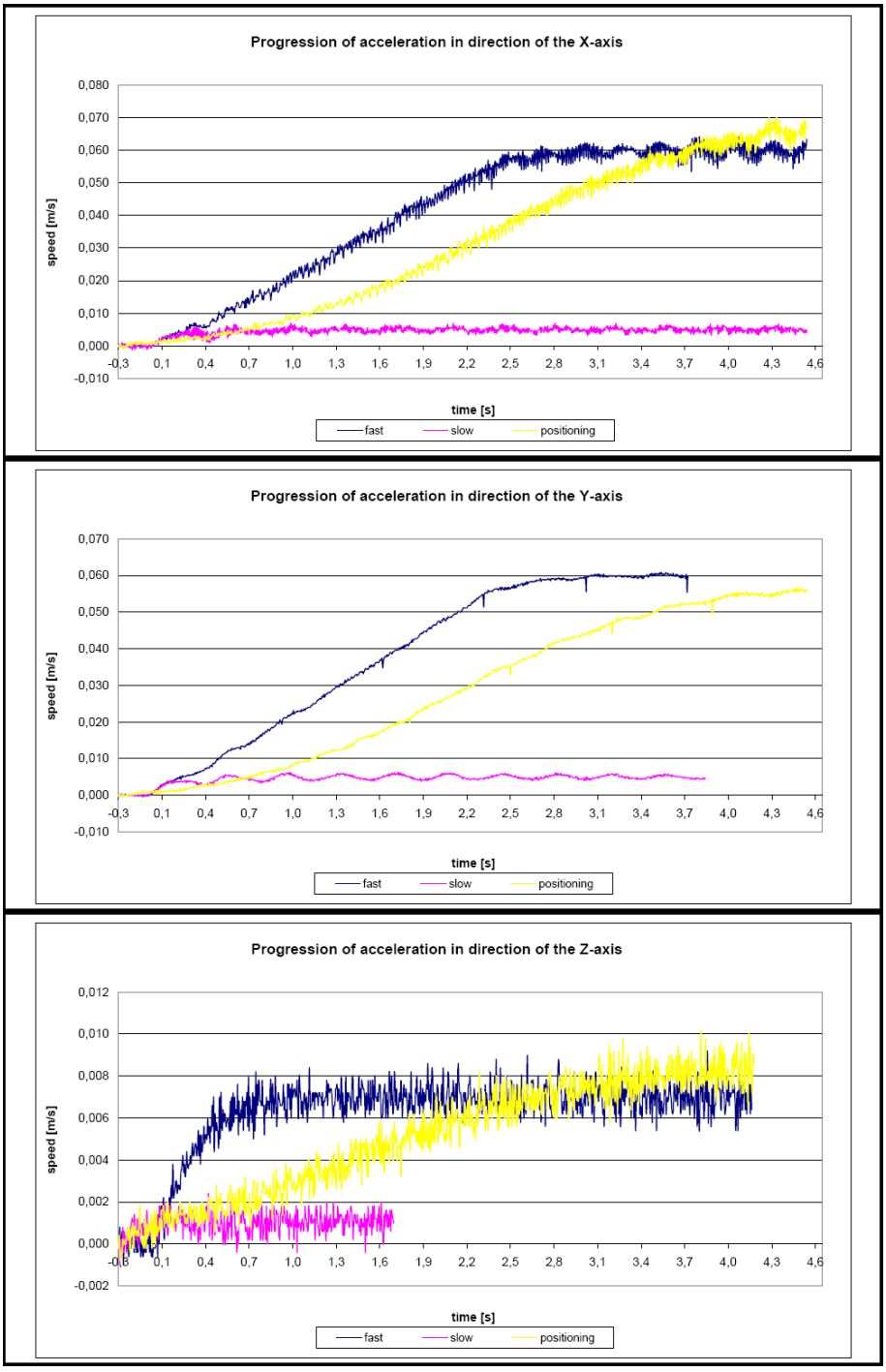

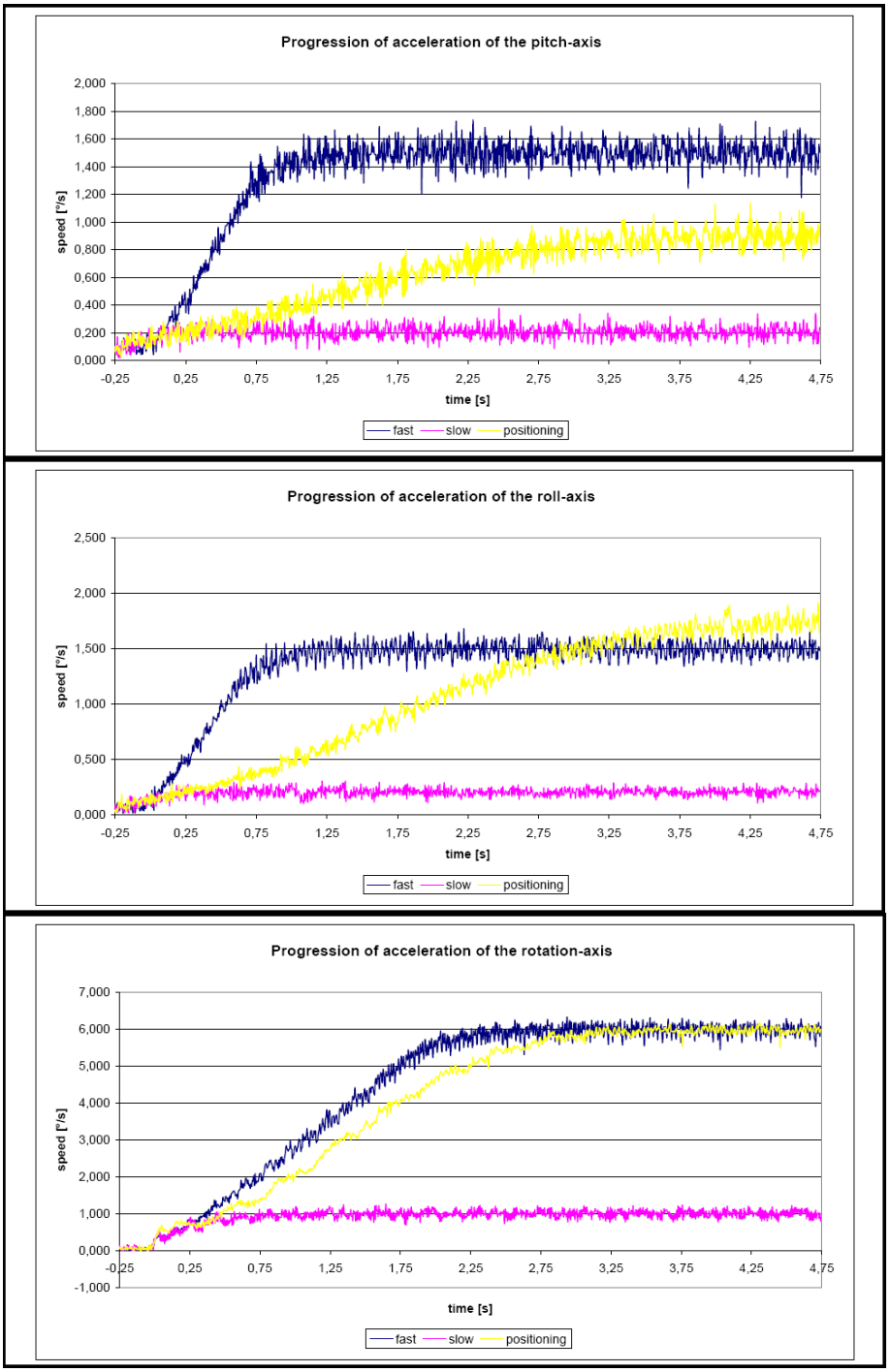
Progression of acceleration of the pitch-axis
speed [°/s]
2,000
1,800
1,600
1,400
1,200
1,000
0,800
0,600
0,400
0,200
0,000
-0,25
0,25
0,75
1,25
1,75
2,25
2,75
3,25
3,75
4,25
4,75
time [s]
fast
slow
positioning
Progression of acceleration of the roll-axis
speed [°/s]
2,500
2,000
1,500
1,000
0,500
0,000
time [s]
fast
slow
positioning
Progression of acceleration of the rotation-axis
speed [°/s]
7,000
6,000
5,000
4,000
3,000
2,000
1,000
0,000
-1,000
time [s]
fast
slow
positioning

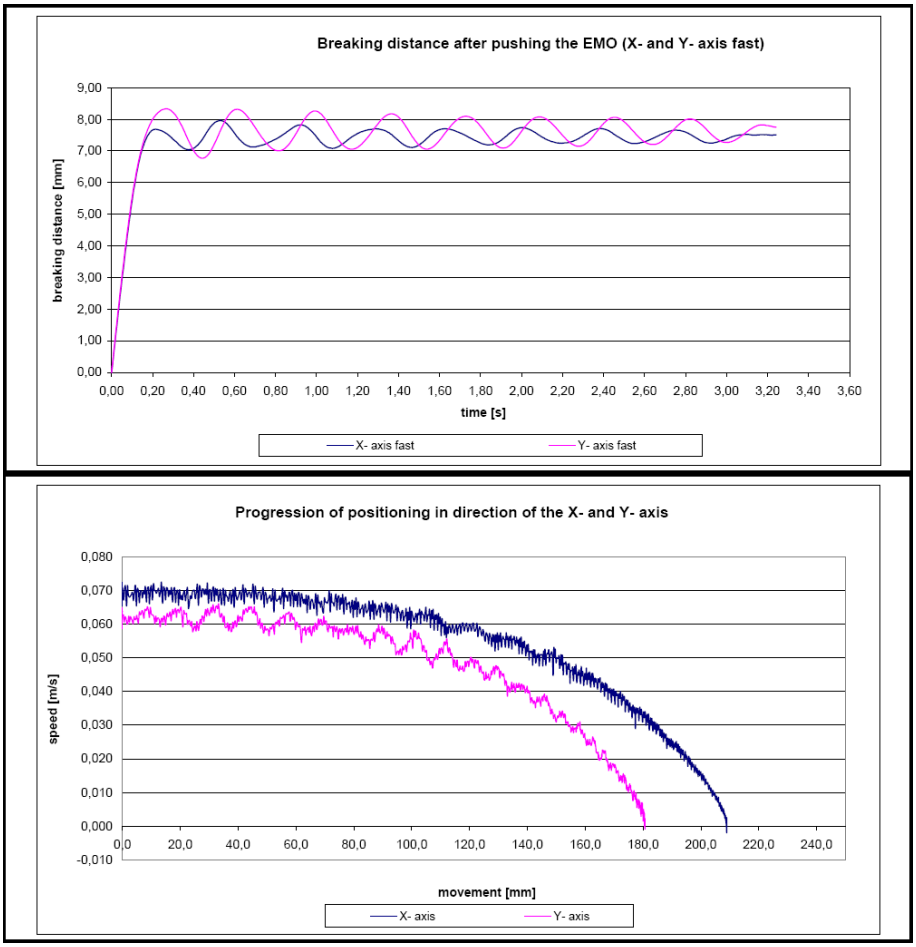
Breaking distance after pushing the EMO (X- and Y- axis fast)
breaking distance [mm]
9,00
8,00
7,00
6,00
5,00
4,00
3,00
2,00
1,00
0,00
0,00 0,20 0,40 0,60 0,80 1,00 1,20 1,40 1,60 1,80 2,00 2,20 2,40 2,60 2,80 3,00 3,20 3,40 3,60
time [s]
X- axis fast
Y- axis fast
Progression of positioning in direction of the X- and Y- axis
speed [m/s]
0,080
0,070
0,060
0,050
0,040
0,030
0,020
0,010
0,000
-0,010
0,0 20,0 40,0 60,0 80,0 100,0 120,0 140,0 160,0 180,0 200,0 220,0 240,0
movement [mm]
X- axis
Y- axis

Appendix *b*

Patient Verification System, Room 1 (Schultze 2010).

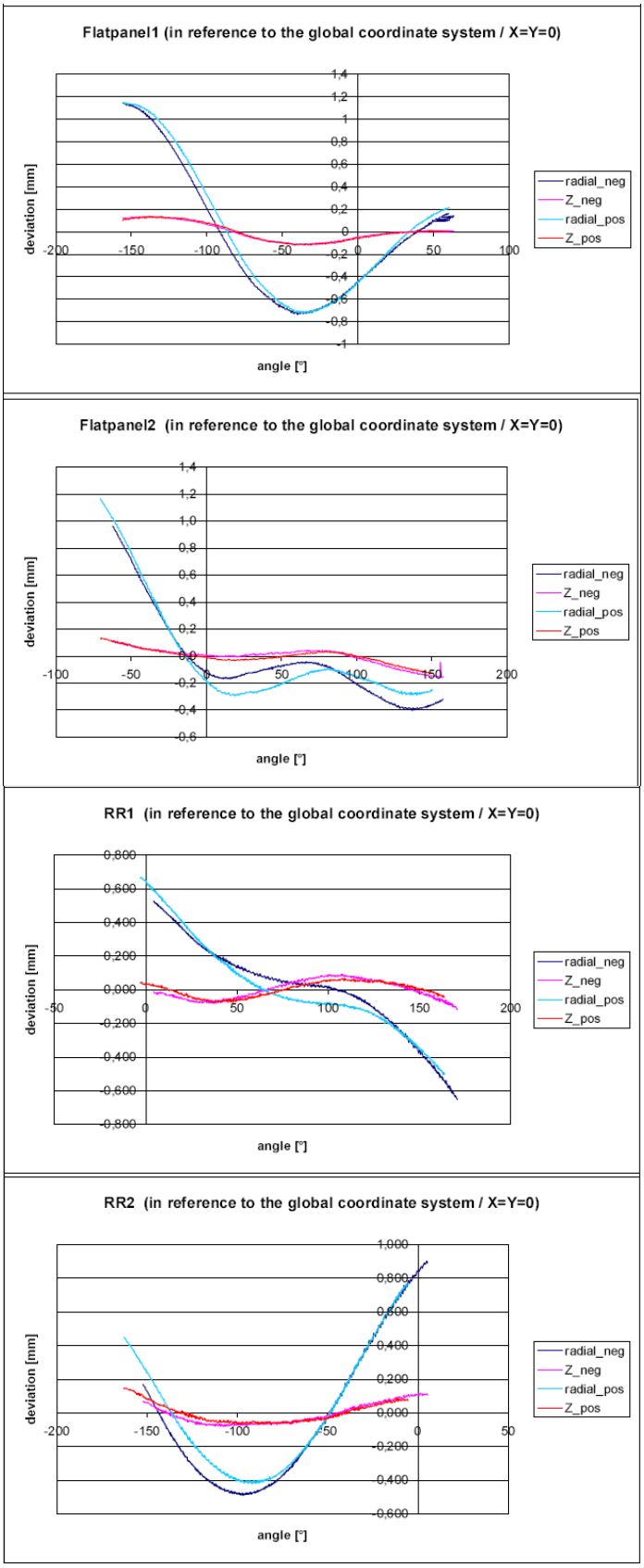

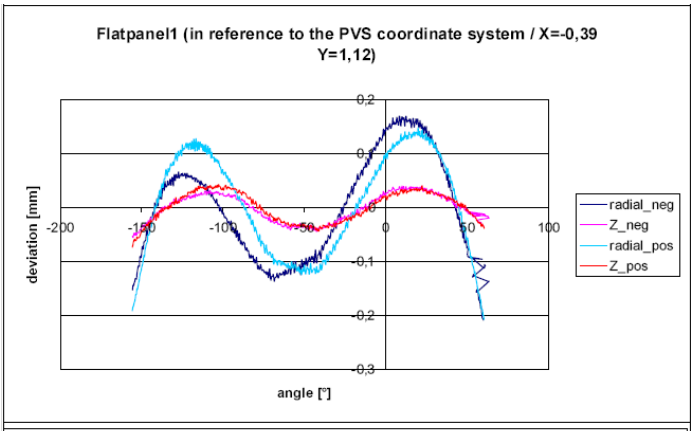
Flatpanel1 (in reference to the PVS coordinate system / X=-0,39 Y=1,12)
deviation [mm]
angle [°]
radial_neg
Z_neg
radial_pos
Z_pos

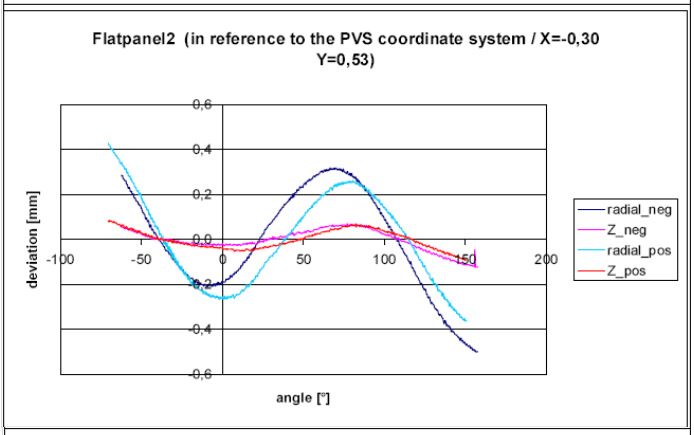
Flatpanel2 (in reference to the PVS coordinate system / X=-0,30 Y=0,53)
deviation [mm]
angle [°]
radial_neg
Z_neg
radial_pos
Z_pos

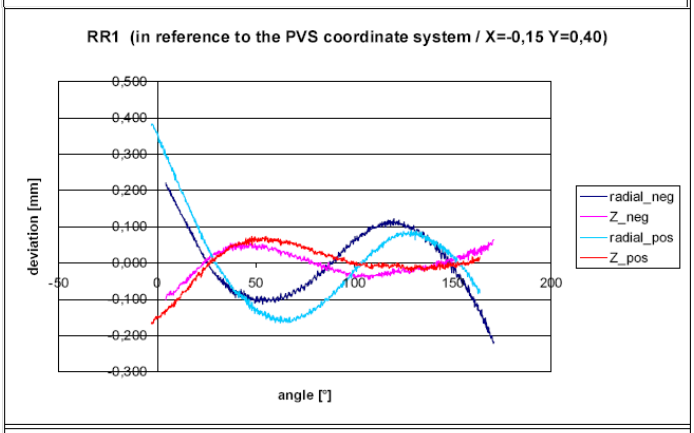
RR1 (in reference to the PVS coordinate system / X=-0,15 Y=0,40)
deviation [mm]
angle [°]
radial_neg
Z_neg
radial_pos
Z_pos

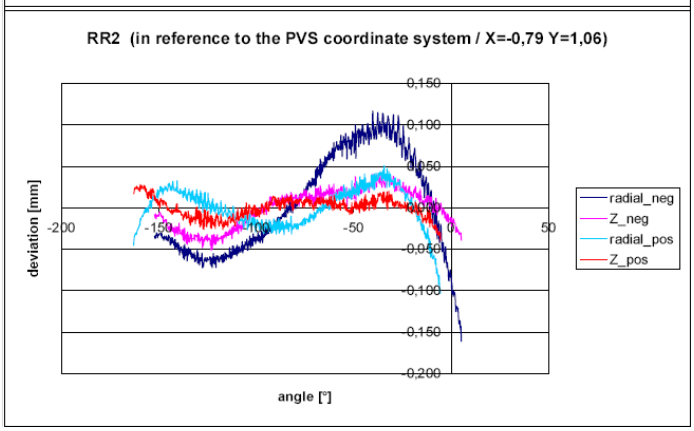
RR2 (in reference to the PVS coordinate system / X=-0,79 Y=1,06)
deviation [mm]
angle [°]
radial_neg
Z_neg
radial_pos
Z_pos

Patient Verification System, Room 3 (Schultze 2010).

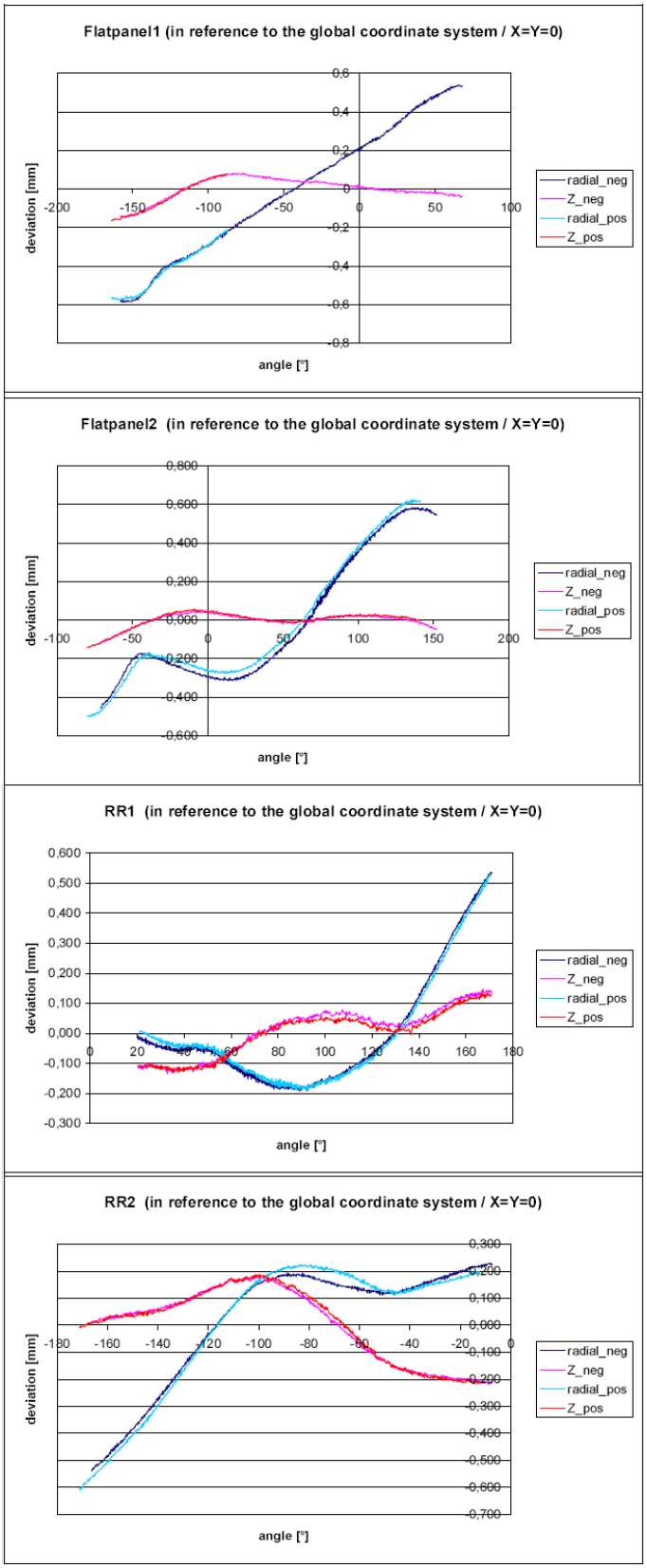

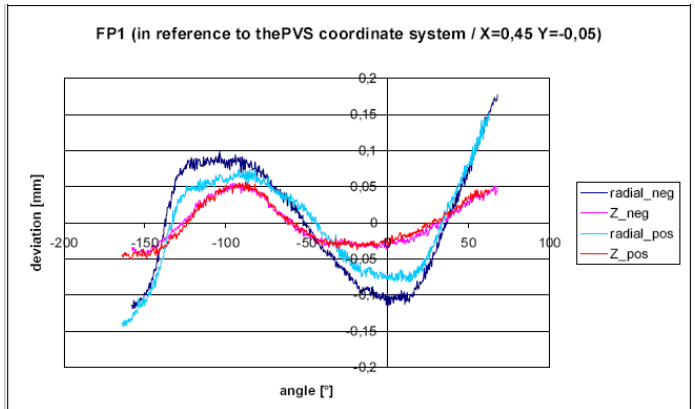
FP1 (in reference to thePVS coordinate system / X=0,45 Y=-0,05)
deviation [mm]
angle [°]
radial_neg
Z_neg
radial_pos
Z_pos

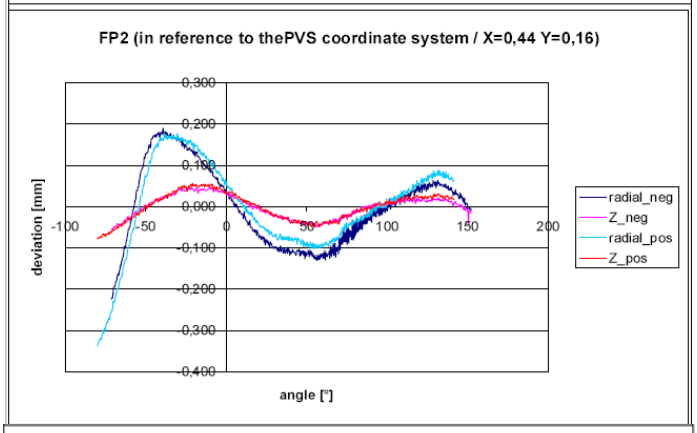
FP2 (in reference to thePVS coordinate system / X=0,44 Y=0,16)
deviation [mm]
angle [°]
radial_neg
Z_neg
radial_pos
Z_pos

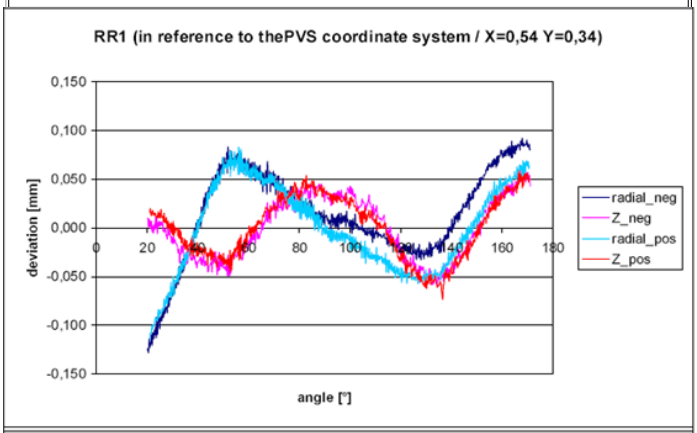
RR1 (in reference to thePVS coordinate system / X=0,54 Y=0,34)
deviation [mm]
angle [°]
radial_neg
Z_neg
radial_pos
Z_pos

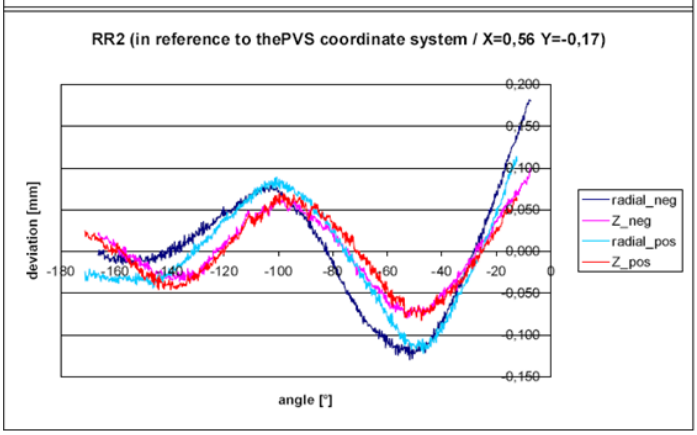
RR2 (in reference to thePVS coordinate system / X=0,56 Y=-0,17)
deviation [mm]
angle [°]
radial_neg
Z_neg
radial_pos
Z_pos